

Subduction and the genesis of mantle roots and diamonds

by

Margo Elaine Regier

A thesis submitted in partial fulfillment of the requirements for the degree of

Doctor of Philosophy

Department of Earth and Atmospheric Sciences  
University of Alberta

© Margo Elaine Regier, 2020

## Abstract

Subduction is a dominant force that has driven the evolution of Earth's atmosphere, the diversity of its crustal lithologies, and the variety of its deep mantle regimes. In this thesis, I present three separate studies that examine the importance of subduction in the creation of ancient cratonic mantle roots and in the formation of diamonds in the lithosphere, asthenosphere, and lower mantle.

The opening study, in Chapter 2, examines various models of cratonic mantle formation. The chapter begins by documenting the oxygen isotope signatures of mantle xenoliths from five different Archean cratons to determine if Ca-depleted and Si-enriched cratonic peridotites are derived from the subduction of serpentinized oceanic lithosphere. I find that orthopyroxene and olivine mineral separates, including those from Si-enriched and Ca-depleted samples, have  $\delta^{18}\text{O}$  that is equivalent to that of mid ocean ridge (MORB) source mantle. The contrast of these data to the wide range of  $\delta^{18}\text{O}$  documented in serpentinites does not support the model of recrystallized serpentinites as a protolith for cratonic peridotites. Other possible mechanisms for producing these Si-enriched peridotites are tested using isotopic and elemental modeling. This modeling suggests that the infiltration of slab melts is unlikely to produce the observed degrees of silica enrichment without also producing observable  $\delta^{18}\text{O}$  variations in the crystallized Si-rich orthopyroxene. Instead, I suggest that the infiltration of ascending mantle melts or water-fluxed depleted mantle melts may produce Si-enriched peridotite without significant modification of cratonic mantle  $\delta^{18}\text{O}$ . Subsequent collisional compression of these variably Si-enriched, cratonic mantle protoliths created the thick cratonic roots that exist today.

The third chapter is devoted to the global carbon cycle and the mechanisms and sources of diamond

formation in the lithospheric and sublithospheric mantle. Since the largest uncertainty in the carbon cycle is the depth to which carbon persists in sediments and altered oceanic crust (AOC), I examine a suite of lithospheric and sublithospheric inclusions in Kankan diamonds for the stable isotopic tracers of subduction. Oxygen isotope data on inclusions in diamond, combined with carbon and nitrogen isotopic signatures of diamond hosts, demonstrate the importance of AOC as a carbon-source at diamond-forming depths. I propose that the exceptionally elevated oxygen isotopes of asthenospheric to transition zone majoritic garnet inclusions are derived from their crystallization from carbonated slab melts. This contrasts with the lower mantle environment that is sampled by the Kankan diamonds, which appears to be isotopically identical to the convecting mantle. Since diamond is not stable in the reduced lower mantle due to the solubility of carbon in metal alloys, I propose that crystallization of diamond is driven by the mobilization of carbon after the destabilization of metals near a dehydrating subducting slab. This transition from diamond formation in carbonated slab melts in the transition zone to diamond formation in hydrated lower mantle confirms an experimentally hypothesized lower mantle barrier for carbon subduction.

Finally, the fourth chapter shifts the focus to the formation of the ultra-rare and valuable boron-bearing blue diamonds in the lower mantle. An analytical method for the first boron isotope analyses of blue diamonds is developed, which identifies a subducted-related origin for the boron impurities. An elemental and mineralogical study of the mineral inclusions and matrix impurities in blue diamonds specifies their formation in a Ca-rich melt. This production of a Ca-rich melt may be induced by the decomposition of hydrous silicate minerals (i.e. ‘post-serpentinite’ phases) that are present in peridotitic sections of the slab at high pressures and temperatures. The interaction of this oxidized Ca-rich melt with the reduced convecting mantle would induce redox-driven diamond formation. The chapter concludes with a discussion of the boron isotopic similarity

of blue diamonds, ocean island basalts (OIB), and carbonatites. Their isotopic similarity suggests that the deep mantle sources of carbonatites and OIBs may have been contaminated by the same volatile-bearing oceanic lithosphere that produced the blue diamonds in this study.

All together, these three independent studies identify the key role played by subduction in the creation of cratonic lithosphere, lithospheric diamonds, sublithospheric diamonds, and deep mantle heterogeneities. These findings help clarify our views on the evolution of volatile-bearing subducting slabs over geologic time and with depth in the Earth.

## Preface

This thesis is original work by Margo Regier. It is composed of three separate manuscripts based on the findings of the author's Ph.D. research supervised by Dr. Graham Pearson and Thomas Stachel. This project was possible with sample donations from DeBeers Industries via Dr. Jeff Harris and David Fischer, the Gemological Institute of America via Evan Smith, and Dr. Anthony Burnham. The research was funded through Canada Research Excellence Chair and Deep Carbon Observatory grants to Dr. Graham Pearson.

Chapter 1 is original work produced by the author.

Chapter 2 of this thesis is published in GEOCHEMICAL PERSPECTIVE LETTERS as: *An oxygen isotope test for the origin of Archean mantle roots*. Data are a compilation of processing and analytical work completed by M. Regier, R.B. Ickert, A. Mišković, and R.A Stern. The initial manuscript was written by M.E. Regier. Co-authors G. Pearson, T. Stachel, R. Stern, R. Ickert, A. Mišković and M. Kopylova - provided valuable contributions to the discussion of results and their implications.

Chapter 3 of this thesis is published in NATURE as: *The lithospheric to lower mantle carbon cycle recorded by superdeep diamonds*. The analytical work was completed by M.E. Regier and R.A. Stern. The initial manuscript was written by M. Regier. Co-authors D.G. Pearson, T. Stachel, R.A. Stern, and B. Luth contributed valuable information to the discussion of the results.

A modified version of Chapter 4 will be submitted to SCIENCE. The analytical work was

completed by M.E. Regier, R.A. Stern, T.B. Chalk, C. Debuhr, C. Sakar, S. Woodland, H. Goring-Hartford. Initial manuscript was written by M.E. Regier. Coauthors T.B. Chalk, R.A. Stern, K.V. Smit, E.M. Smith, T. Stachel, G.L. Foster, Y. Bussweiler, C. Debuhr, J.W. Harris, and D.G. Pearson contributed valuable ideas to the manuscript.

A modified portion of Chapter 5 will be submitted to EPSL. M.E. Regier, C. Anzolini, A. Locock and F. Nestola collected the data. M.E. Regier wrote the original manuscript. Coauthors L. Bindi, N. Tomioka, R.W. Luth, D.G. Pearson, T. Stachel, C. McCammon, M.D. Wenz, S.D. Jacobsen, C. Anzolini, J.W. Harris, and F. Nestola contributed valuable ideas to the manuscript.

## Acknowledgements

Many people are to thank for help designing these projects and bringing them to fruition. First and foremost, I would like to thank my advisors - Graham Pearson and Thomas Stachel - both of whom have taught me invaluable lessons about approaching and evaluating science. I thank Graham for encouraging me to think about the big picture and thank Thomas for reminding me to keep the conclusions rooted in solid science. Other researchers at the University of Alberta contributed greatly to this study. Richard Stern aided this work during many, many hours in the lab. His unparalleled understanding of the ion probe is responsible for much of the high-quality data in this document. Bob Luth was always willing to tackle some large (and unanswerable) questions with me. Andrew Locock not only provided me with excellent analytical services but was also willing to discuss many a mineralogical quandary. Sarah Woodland and Chiranjeeb Sarkar were always present and essential for lab-related events and emergencies – whether it be a blown varistor, or a confounding centrifuge. I also owe a great deal to my collaborators at Northwestern University, University of Southampton, and University of Padua – Fabrizio Nestola, Chiara Anzolini, Michelle Wenz, Steve Jacobsen, Gavin Foster, Tom Chalk, Chris Standish. I especially appreciate the offers of lodging and entertainment when traveling.

Also, of great importance were the constructive discussions and friendship with other students – including Janina Czas, Matt Hardman, Mandy Krebs, Nicole Meyer, Ben Gruber, Pedro Waterton, Melissa Bowerman, Tim McIntyre, Yannick Bussweiler, and more. Thanks to James and Myrtle for being the best quarantine buddies and for fulfilling my life-long ambition of training an adventure cat. Thanks to Edmonton, its beautiful river valley, beautiful “nearby” mountains, and beautiful people. And finally, thank you to my family, who is my rock and my biggest source of inspiration.

# Table of Contents

<b>Chapter 1      Introduction to subduction and its geochemical tracers .....</b>	<b>1</b>
1.1 Introduction .....	1
1.2 Samples for study.....	5
1.2.1 Cratonic mantle samples .....	5
1.2.2 Kankan diamond deposit.....	6
1.2.3 Blue diamonds .....	7
1.3 Isotope systematics .....	10
1.3.1 Oxygen isotopes.....	10
1.3.2 Carbon isotopes.....	10
1.3.3 Boron isotopes .....	11
1.4 Major objectives.....	16
<b>Chapter 2      An oxygen isotope test for the origin of Archean mantle roots .....</b>	<b>17</b>
2.1 Introduction.....	18
2.2 Approach and results.....	19
2.3 Implications for craton formation .....	21
2.4 Conclusions.....	26
2.5 Methods.....	27
<b>Chapter 3      The lithospheric to lower mantle carbon cycle in superdeep diamonds.....</b>	<b>29</b>
3.1 Introduction.....	30
3.2 Lithospheric to Transition Zone samples.....	31
3.3 Lower mantle diamonds.....	39
3.4 The lithospheric to lower mantle carbon cycle .....	40

3.5 Methods.....	42
<b>Chapter 4      Blue diamonds document the subduction of seafloor boron to the lower mantle .....</b>	<b>44</b>
4.1 Introduction.....	45
4.2 Ca-rich superdeep medium .....	46
4.3 Slab-derived isotopic signatures .....	47
4.4 Deep volatile cycles and the formation of blue diamonds.....	52
4.5 Methods.....	55
4.5.1 Quantification of N and B impurities and the C isotopic composition of blue diamonds .....	55
4.5.2 Boron isotopic analyses – method development and accuracy tests.....	56
4.5.3 Boron isotopic analyses – natural blue diamonds.....	58
4.5.4 Trace elemental analyses .....	59
4.5.5 Inclusion study .....	61
<b>Chapter 5      Conclusions.....</b>	<b>63</b>
5.1 Subduction and the formation and evolution of cratonic mantle .....	63
5.2 The relevance of subduction to the formation of diamonds: lithosphere to lower mantle ...	65
5.3 Deep volatile cycles .....	68
5.3.1 Carbon cycle .....	69
5.3.2 Boron cycle .....	70
5.3.3 Evolution of volatile cycles over time .....	71
5.4 Future directions .....	73
<b>Bibliography .....</b>	<b>77</b>
References for Chapters 1-5 and Appendices A-C .....	77
<b>Appendix A – Supplementary material for cratonic peridotites .....</b>	<b>116</b>

Supplementary figures .....	116
Supplementary tables .....	118
<b>Appendix B – Supplementary material for Kankan inclusions.....</b>	<b>164</b>
Supplementary figures .....	164
Supplementary tables .....	168
<b>Appendix C – Supplementary material for blue diamonds .....</b>	<b>232</b>
C1 Supplementary information.....	232
C1.1 Isotopic and spectroscopic zoning of blue diamonds.....	232
C1.2 Impact of laser window on trace element blank.....	232
C2 Supplementary figures.....	235
C3 Supplementary tables .....	246

## List of Tables

Table 1.1. Boron reservoirs on Earth and their isotopic composition.....	14
Table A1. $\delta^{18}\text{O}$ and major elements for cratonic olivine samples in this study. ....	118
Table A2. $\delta^{18}\text{O}$ and major elements for cratonic Opx samples in this study. ....	135
Table A3. $\delta^{18}\text{O}$ and major elements for non-cratonic fore-arc olivine samples.....	136
Table A4. pMELTS and $\delta^{18}\text{O}$ mass balance modeling for melts interacting with harzburgite....	137
Table A5. Source data for oxygen isotopes of MORB.....	139
Table A6. Source data for oxygen isotopes of eclogite xenoliths .....	145
Table A7. Source data for oxygen isotopes of serpentinite.....	157
Table B1. Mineral assemblages of analyzed Kankan diamonds.....	168
Table B2. The Mg# of bridgmanite and ferropericlase for experiments and natural inclusions in diamond.....	171
Table B3. Standards utilized for EPMA analyses .....	172
Table B4. Source data for eclogitic garnet inclusion Mg#.....	173
Table B5. Source data for peridotitic garnet inclusion Mg# .....	195
Table B6. Source data for $\delta^{18}\text{O}$ and $\delta^{13}\text{C}$ in AOC carbonate. ....	198
Table B7. Source data for mantle eclogite xenoliths $\delta^{18}\text{O}$ . ....	205
Table B8. Source data for $\delta^{18}\text{O}$ of eclogitic and majoritic garnet inclusions in diamonds .....	221
Table B9. Source data for $\delta^{13}\text{C}$ and $\delta^{15}\text{N}$ of eclogitic and superdeep diamonds. ....	223
Table C1. Results for standards, including the biogenic standards (JCp-1 and JCt-1) and synthetic diamonds .....	246
Table C2. Results on natural blue diamonds .....	247
Table C3. Electron probe analysis of recovered olivine inclusion from Blue 2a.....	250

Table C4. Trace element abundances determined for blue diamonds.....	251
Table C5. Limit of quantification (LOQ) and limit of detection (LOD).....	257
Table C6. Results of trace element analyses of silica glass ablation windows. ....	259
Table C7. Standards, analysing crystals and detection limits for EPMA analyses.....	263
Table C8. Source data for $\delta^{11}\text{B}$ of uncontaminated OIB.....	264
Table C8. continued .....	265
Table C8. continued .....	266
Table C8. continued .....	267
Table C9. Source data for $\delta^{11}\text{B}$ of uncontaminated carbonatite. ....	268
Table C10. Source data for $\delta^{11}\text{B}$ of meta-sediments and meta-AOC.....	269

## List of Figures

Figure 1.1. Elemental evidence supporting the low-pressure depletion of cratonic mantle. ....	3
Figure 1.2. Elemental evidence for Si-enrichment in cratonic mantle peridotite.....	3
Figure 1.3. Map indicating the locations of Archean and Proterozoic cratons .....	9
Figure 1.4. Boron isotope reservoirs in the subduction system.....	12
Figure 1.5. Range of slab related reservoirs and MORB for three stable isotopic tracers .....	15
Figure 2.1. Popular models of cratonic mantle formation.....	19
Figure 2.2. Elemental chemistry of xenoliths in this study. ....	20
Figure 2.3. Oxygen isotopes from this study compared to other reservoirs.....	24
Figure 2.4. pMELTS and isotopic mass balance modeling of melts reacting with surrounding harzburgite.....	26
Figure 3.1. Stable isotope compositions of diamonds and their mineral inclusions .....	33
Figure 3.2. Elemental and isotopic composition of majoritic garnet inclusions .....	34
Figure 3.3. Worldwide database of $\delta^{13}\text{C}$ and $\delta^{15}\text{N}$ for diamonds of lithospheric and superdeep origin .....	37
Figure 3.4. Model of diamond formation in the lithosphere, transition zone, and lower mantle....	41
Figure 4.1. Optical photographs and Raman spectra of inclusion-bearing blue diamonds.....	48
Figure 4.2. Rare earth element and carbon isotopic values for the blue diamond matrices.....	49
Figure 4.3. Boron isotope signature of blue diamonds and other reservoirs.....	51
Figure 4.4. Transfer and remobilization of slab-derived volatiles - B, C, and H <sub>2</sub> O - in the Mesoproterozoic and current day deep mantle.....	53
Figure 5.1. Stability of hydrous meta-peridotitic phases.....	71
Figure A1. Cumulative distribution plots of our samples and other reservoirs. ....	116
Figure A2. Oxygen isotope compositions for olivines from subcratonic and noncratonic peridotites	

Figure B1. Oxygen isotopes for majoritic garnet inclusions versus depth.....	164
Figure B2. Oxygen isotopes versus Cr/Al of Jagersfontein majoritic garnets.....	165
Figure B3. Ion probe $\delta^{18}\text{O}$ calibration for Cr-rich garnets. ....	166
Figure B4. Ion probe $\delta^{18}\text{O}$ calibration for enstatite Mg#. ....	167
Figure C1. $\mu\text{XRF}$ from GSECARS 13-IDE for diamonds Blue2 and NL247-2.....	235
Figure C2. Panchromatic CL images of diamonds in study.....	236
Figure C4. Typical ablation pits of diamonds .....	240
Figure C5. Boron and carbon isotope and concentration data for blue diamonds. ....	241
Figure C6. $^{11}\text{B}/^{10}\text{B}$ measurements for a 50 ppb SRM 951 standard over a full day of analyses...	242
Figure C7. REE patterns for blue diamonds.....	243
Figure C8. Trace element abundance of blue diamonds .....	244
Figure C9. Stability of hydrous meta-peridotitic phases.....	245

## List of Abbreviations and Symbols

Abbreviation/Symbol	Definition
‰	Parts per thousand or per mille
~	Approximately
ArF	Argon fluoride
AOC	Altered oceanic crust
CCIM	Canadian Centre for Isotopic Microanalysis
CL	Cathodoluminescence
DHMS	Dense hydrous magnesium silicates
EPMA	Electron probe micro analysis
E-type	Eclogitic type
FTIR	Fourier transform infrared
Ga	Giga annum; Billion years
GPa	Gigapascal
HREE	Heavy rare earth element
LA-ICPMS	Laser-ablation inductively coupled plasma mass spectrometry
LREE	Light rare earth element
Ma	Mega annum; Million years
Meta-	Metamorphosed (e.g. meta-sediments)
Mg#	100 x molar Mg/(Mg+Fe)
MORB	Mid-ocean ridge basalt
MREE	Middle rare earth element
N	Subscript to indicate normalised values
NIST	National Institute of Standards and Technology

---

<b>Abbreviation/Symbol</b>	<b>Definition</b>
n.a.	Not available
P-type	Peridotite type
ppm	Parts per million
ppb	Parts per billion
PT	Pressure and temperature
PUM	Primitive upper mantle
REE	Rare earth element
s	Second
SCLM	Subcontinental lithospheric mantle
SEM	Secondary electron multiplier
VPDB	Vienna-Pee-Dee-belemnite
VSMOW	Vienna-standard-mean-ocean-water
wt%	Weight percent
$\delta^{13}\text{C}$	Carbon isotopes relative to the international VPDB standard
$\delta^{18}\text{O}$	Oxygen isotopes relative to the international VSMOW standard
$\sigma$	Sigma or one standard deviation of the mean

---

# **Chapter 1**

## **Introduction to subduction and its geochemical tracers**

### **1.1 Introduction**

Of all the physical processes occurring on Earth, subduction, or the movement of one lithospheric plate beneath another into the underlying mantle, may have most profoundly affected the evolution of the Earth. Downwelling slabs represent one arm of the giant convection currents that conduct the tectonic plates about the surface of our planet. The descent of slabs also initiates various natural hazards. Enormous earthquakes are centered on these zones, and arc volcanoes tower over these regions due to slab fluid-mediated melting in the mantle wedge (Kirby et al. 1996). Additionally, many of our richest economic ore deposits are related to subduction (Richards 2003) and the very air we breathe is modulated by volcanic emissions (Fischer 2008). Thus, tracing the presence and behavior of subduction back through time is important for elucidating the history of the Earth. This dissertation focuses on subduction at its extremes – its importance during continent building at >2.5 Ga, and its presence in the deepest regions of the mantle.

Studying the ancient, Archean mantle is difficult because of later overprinting processes such as metasomatism and metamorphism. Nevertheless, the scavenging of mantle xenoliths by rapidly ascending kimberlitic melts can provide some minimally altered samples. Many of these samples represent the thick and buoyant lithosphere beneath old, stable cratons, and tell an important story about the formation and stabilization of continents in the Archean (Boyd 1973). The high Cr/Al contents of their garnet and the metasomatic-resistant, moderately incompatible element concentrations (Fig. 1.1) indicate depletion at low pressures (< 4 GPa) (Stachel et al. 1998b; Canil 2004; Brey and Shu 2018). These pressures are at odds with a model in which cratonic lithosphere is formed by deeply derived plume melts (Griffin et al. 1999). Rather, the data appear to favour subduction-related models for cratonic mantle formation - the stacking of subducted slabs (Helmstaedt and Schulze 1989; Pearson and Wittig 2008) and/or the collisional compression of island arcs to produce a thick cratonic keel (Jordan 1978; Lee et al. 2011; Wang et al. 2018b). The silica-enriched character of many cratons (Fig. 1.2) remains an enigmatic phenomenon that has been attributed to various processes – including the subduction of Si-rich serpentinite (Canil and Lee 2009) and the metasomatic infiltration of cratonic mantle by slab melts (Kelemen et al. 1998).

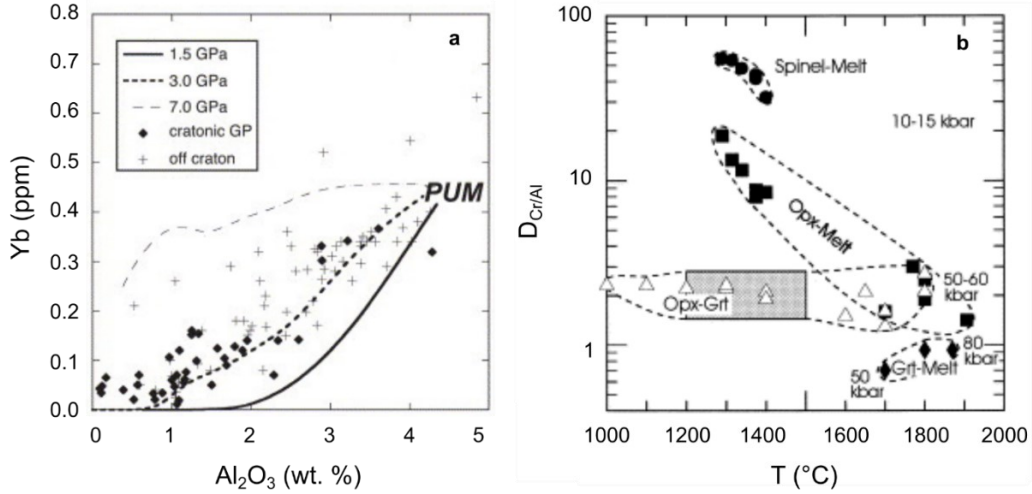


Figure 1.1. Elemental evidence supporting the low-pressure depletion of cratonic mantle. **(a)** The covariation of Yb and Al in off- and on-craton garnet peridotites is compared to partial melting trends at 1, 3, and 7 GPa. PUM is primitive upper mantle. Figure is modified from Canil (2004). **(b)** The covariation of  $D_{\text{Cr}/\text{Al}}$  and temperature for spinel, orthopyroxene (Opx), garnet (Grt), and melt at 10-15 kbar. The high  $D_{\text{Cr}/\text{Al}}$  for spinel-melt and Opx-melt suggests that residual peridotites depleted at low pressures will have high Cr/Al and will form Cr-rich garnets upon emplacement to high pressures. Figure is modified from Stachel et al. (1998).

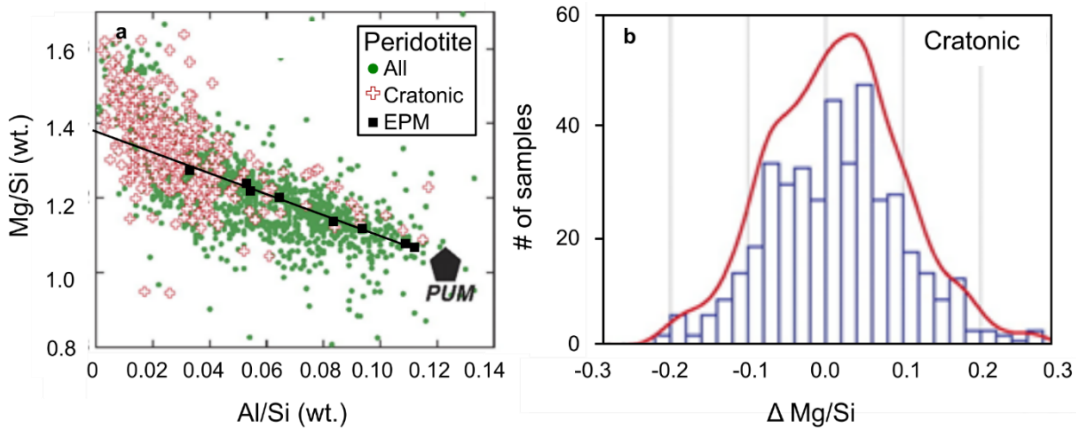


Figure 1.2. Elemental evidence for Si-enrichment in cratonic mantle peridotite. **(a)** The covariation of Al/Si and Mg/Si for peridotitic mantle xenoliths, including those from cratonic mantle regions. Also plotted are experimental partial melt (EPM) residues of primitive upper mantle (PUM) at 1.5 GPa and the best-fit curve through the data (Robinson et al. 1998). Figure is modified from Canil and Lee (2009). **(b)** The deviation of peridotitic xenoliths from the EPM curve in (a) is quantified using the parameter  $\Delta \text{Mg}/\text{Si}$ . Negative  $\Delta \text{Mg}/\text{Si}$  indicate Si-enriched xenoliths, whereas positive  $\Delta \text{Mg}/\text{Si}$  indicate Si-depleted xenoliths. Note that cratonic mantle varies to either side but is slightly skewed towards Si-enrichment. Figure is modified from Canil and Lee (2009).

Kimberlites also host diamonds, which are more resistant than xenoliths to later overprinting processes. Due to the high pressure of graphite-diamond transition, these samples are only found in regions overlying thick, cool, cratonic lithosphere (Clifford 1966). While some of these diamonds have mineral inclusion that represent peridotitic lithologies (P-type), others are basaltic/eclogitic (E-type) in composition (Meyer 1987). In addition to their basaltic chemistry, the stable isotopic character of both E-type diamonds and their inclusions bear a striking resemblance to oceanic slab oxygen and carbon isotopes (Cartigny 2005). Thus, P- and E-type diamonds are interpreted to reflect the variably depleted and subducted lithologies that are present within the cratonic mantle (Shirey and Shigley 2013). While the elemental and isotopic chemistry of diamond and diamond-included minerals is reflective of their cratonic mantle protolith, diamond crystallization is a metasomatic process. The most recent model suggests that both P- and E- type diamonds crystallize through the supersaturation of carbon in ascending CHO bearing fluids or melts (Stachel and Luth 2015).

While the vast majority of diamond deposits are found in the thick lithospheric roots beneath cratons, some diamonds are formed even deeper – from the asthenosphere to the lower mantle. There are several families of diamonds that have been assigned a superdeep genesis. These include large, inclusion-poor, irregular, and resorbed “CLIPPIR” diamonds and ultra-valuable type IIb blue diamonds, which have trace impurities of boron (Smith et al. 2016, 2018). Like their lithospheric counterparts, superdeep diamonds can be assigned a substrate based on inclusion chemistry. Recent work has shown that asthenospheric to transition zone majorite inclusions are often ‘meta-pyroxenitic’ in composition and must represent an interaction between peridotitic and eclogitic endmembers (Kiseeva et al. 2013). The literature on blue

diamonds is limited, but carbon isotopes appear to suggest meta-basaltic substrates, whereas the inclusion mineralogy was identified to include both meta-basaltic and meta-peridotitic endmembers (Smith et al. 2018). Other superdeep diamonds, including those from the Kankan deposit in Guinea, contain lower mantle assemblages that appear to be meta-peridotitic in nature (Stachel et al. 2000b).

These three sample suites – cratonic mantle minerals, lithospheric diamonds, and superdeep diamonds – are powerful tools for probing the deep history and deep roots of our Earth. Using a combination of trace element and stable isotope analyses as tracers for various reservoirs, this dissertation attempts to tease out the role subduction has had in altering the inner Earth, which in turn affects the surficial characteristics of our planet. Below I discuss the details of these three sample suites and the various isotopic systems that are utilized for their study.

## **1.2 Samples for study**

### **1.2.1 Cratonic mantle samples**

The cratonic mantle samples used for this study include peridotite xenoliths from several kimberlites within the Slave, Rae, North Atlantic, Kaapvaal, and Siberian cratons. Here, a brief geologic setting is discussed for each region.

Xenoliths from the Kaapvaal craton in southern Africa are derived from kimberlites on either side of the Colesberg lineament – the Finsch and Kimberley kimberlites on the western Kimberley Block and the Jagersfontein, Kaalvallei, Letseng, and Premier kimberlites on the eastern Witwatersrand Block (Brey and Shu 2018). Xenoliths from the Slave craton in

Northwest Territories and Nunavut provinces of northern Canada were collected from the Diavik and Jericho kimberlites, which lie in the central and northern part of the craton, respectively (Mather 2012). Xenoliths from the Rae craton, which lies within the Churchill Structural Province of the Canadian shield, are derived from the NE trending Nord, Batty Bay, JP, and Nikos kimberlites on Somerset Island (Irvine et al. 2003). The Siberian craton xenoliths are derived from the Udachnaya kimberlite in the Republic of Sakha, or Yakutia, in Eastern Russia. And finally, xenoliths from the North Atlantic craton are sourced from the NW to SW regions of Kangerlussuaq, Safartoq, Manitsoq, and Pyramidefjeld in western Greenland (Wittig et al. 2008).

These xenoliths represent a diverse sampling of Archean aged cratonic roots, as they are derived from both the spinel and garnet stability fields and include lherzolite, harzburgite, and dunite lithologies. Additionally, these samples are derived from both Si-poor cratonic roots, such as the North Atlantic craton ( $> 89$  wt. % olivine), as well as the more Si-enriched Slave and Kaapvaal cratonic roots ( $\sim 64$  wt. % olivine; Pearson and Wittig, 2014).

### **1.2.2 Kankan diamond deposit**

The Kankan diamond deposit is located on the West African craton. This craton, composed of the Reguibat Shield and Man Shield, is Archean and Paleoproterozoic-aged (Kouamelan et al. 1997). Various Cretaceous kimberlites (90-140 Ma) erupted through the Leo Uplift of the Man Shield, producing numerous alluvial diamond deposits (Haggerty 1992).

Prior studies of these diamonds documented peridotitic suites of olivine, clinopyroxene,

chromite, and garnet inclusions as well as eclogitic suites of coesite, rutile, clinopyroxene, and garnet (Stachel et al. 2000a). Asthenospheric to transition zone diamonds have yielded majoritic garnet and Ca-silicates (Stachel et al. 2000a; Brenker et al. 2005), as well as lower mantle assemblages of ferropericlase, retrogressed bridgmanite and retrogressed Ca-perovskites (Stachel et al. 2000b).

### 1.2.3 Blue diamonds

Blue diamonds have been reported from the Kollur mine in India; the Jagersfontein, Koffiefontein, and Premier/Cullinan mines in South Africa; Kalimantan in Indonesia; and the Santa Elena mine in Venezuela (King et al. 1998; Gaillou et al. 2012). All studied blue diamonds have been interpreted as superdeep, based on their similarity to the superdeep “CLIPPIR” diamonds and the mineralogy of their sublithospheric inclusions (Smith et al. 2018). Blue diamonds achieve their characteristic color from the boron impurities within the diamond matrix, which can be measured via ion probe (SIMS) or hyperspectral cathodoluminescence (CL), and range from 0.1 to 8 ppm B (Gaillou et al. 2012). Fourier transform infrared spectroscopy (FTIR), in contrast, only provides a minimum estimate, given the neutralization of boron signal by singly substituted nitrogen (Gaillou et al. 2012). Prior to this dissertation, the isotopic composition of the boron impurities in diamonds had not been measured.

While three diamonds (AB, 110208425476, DVBT) in this study are of unknown origin (donated by Drs. Evan Smith and Anthony Burnham), the rest are derived from the Cullinan (Premier) mine in South Africa. This kimberlite is located in the central part of the Kaapvaal

craton in Southern Africa and has a relatively old eruption age of ~1151 Ma (Wu et al. 2013). Re-Os isotopic data has suggested that the lithospheric mantle underneath the Kaapvaal craton was initially formed during the early Proterozoic to Archean, but a cluster of Re-depletion ages ~2 Ga supports the modification of the lithosphere by the ~2.06 Ga emplacement of the Bushveld Complex (Carlson et al. 1999). A plume-related origin of the Bushveld Complex is supported by the large number of inclusions within Cullinan diamonds that record supra-adiabatic temperatures (Korolev et al. 2018a). The same deposit also supports a large percentage of sublithospheric diamonds (~9%) that requires the infiltration of this craton by transition zone and deeper material (Korolev et al. 2018a). However, it remains unclear if these sublithospheric diamonds were translated to the cratonic mantle during the large-scale upwelling event that emplaced the Bushveld large igneous province at ~2.06 Ga, or were translated directly from the sublithospheric mantle during the eruption of the ~1151 Ma Cullinan kimberlite.

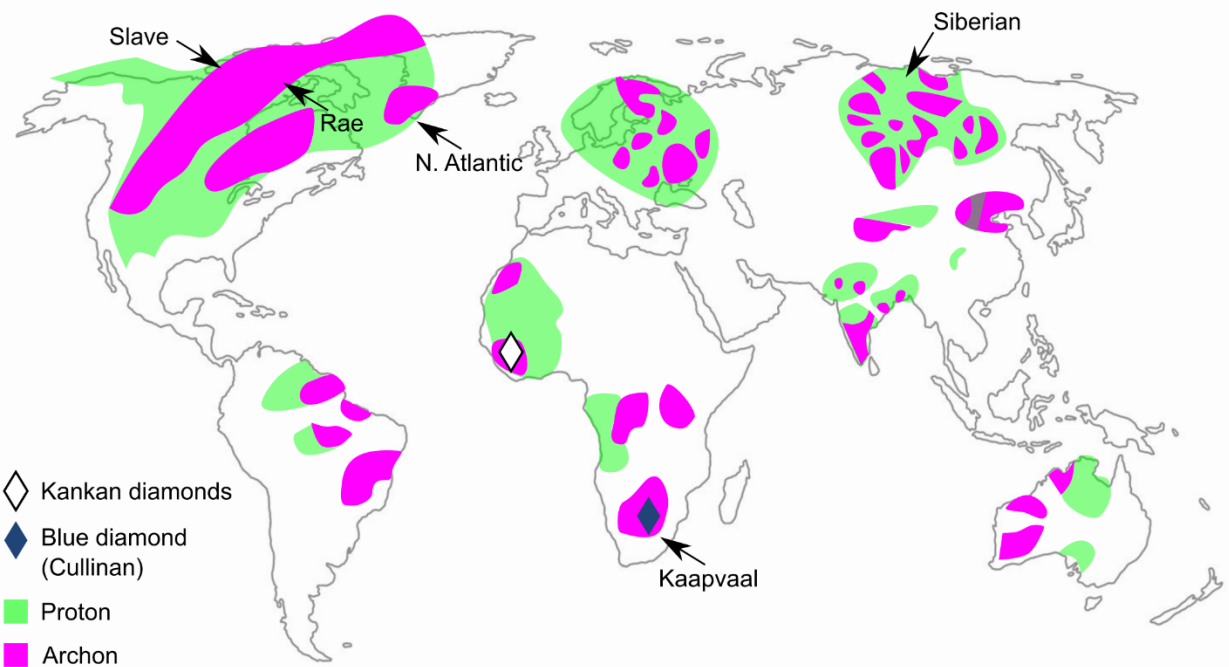


Figure 1.3. Map indicating the locations of Archean and Proterozoic cratons (Archons and Protons, respectively). Indicated on the map are the locations of the samples in this study, including the Kankan diamonds, blue diamonds from Cullinan, and mantle xenoliths from the Kaapvaal, Siberian, N. Atlantic, Rae, and Slave cratons. Figure modified from Haggerty (1999).

## 1.3 Isotope systematics

### 1.3.1 Oxygen isotopes

Oxygen isotope geochemistry is one of the most-well developed tracers of subduction processes in the mantle (Bindeman 2008). Fresh MORB falls within a narrow  $\delta^{18}\text{O}$  range of  $5.46 \pm 0.21\text{ ‰}$  (Eiler et al. 2000a; Cooper et al. 2004, 2009). This narrow range is disrupted during seawater alteration of oceanic sections, where pillow lavas and basalt become  $^{18}\text{O}$  enriched due to low-temperature alteration, and gabbros become  $^{18}\text{O}$  depleted after high-temperature hydrothermal alteration (Muehlenbachs and Clayton 1976). This same bimodal character, relative to MORB, is seen within cratonic mantle eclogites (Korolev et al. 2018b). This similarity is a major backbone of the interpretation of cratonic mantle eclogites as ancient portions subducted oceanic slabs.

### 1.3.2 Carbon isotopes

Carbon isotopes are another commonly employed tool for tracing subduction processes in mantle magmas. While carbon isotopes of MORB are well-defined at  $-5.2 \pm 0.7\text{ ‰}$  (Marty and Zimmermann 1999), carbonated altered oceanic crust (AOC) and sediments are offset to either side of MORB. This correlates well with the isotopic values measured in eclogitic diamonds, which have a much greater range in  $\delta^{13}\text{C}$  than is seen for peridotitic diamonds (Cartigny 2005). While some of this variation may be due to differences in fluid speciation (Stachel et al. 2017) and high-temperature fractionation processes (Cartigny 2005), much of it must be derived from the slab protolith (Korolev et al. 2018b). Conventionally, the prominent isotopically light signatures found within diamonds have been interpreted to reflect

subduction of organic rich matter, which is isotopically very depleted in  $^{13}\text{C}$  (Plank and Manning 2019). However, a recent study suggested that carbonated AOC, and not sediment, could produce the range of  $\delta^{13}\text{C}$  seen in eclogitic diamonds (Li et al. 2019). In this study, they identified that carbonated basaltic ( $\delta^{13}\text{C}$  of -20 to +5), gabbroic ( $\delta^{13}\text{C}$  of -25 to +5), and peridotitic ( $\delta^{13}\text{C}$  of -10 to +10) sections all contain the expected  $^{13}\text{C}$ -enriched carbonate that precipitates in equilibrium with dissolved inorganic carbonate (DIC), as well as  $^{13}\text{C}$ -depleted carbonate that precipitates from biogenically fractionated carbon (Li et al. 2019).

### 1.3.3 Boron isotopes

Boron is a moderately incompatible element with two stable isotopes -  $^{10}\text{B}$  (abundance: ~20%) and  $^{11}\text{B}$  (abundance: ~80%). Because of its incompatible nature, most boron has been removed from the mantle, with  $\leq 0.1$  ppm B remaining in the depleted mantle (Leeman and Sisson 1996). This is in stark contrast to sediments, altered oceanic crust, and serpentinized mantle, all of which can have hundreds of ppm B (Table 1.1). Recently, examination of fast-spreading regions of oceanic lithosphere has suggested that only  $< 1$  ppm B is incorporated into the deep suboceanic lithospheric mantle during subduction-related bend faulting (Fig. 1.4; McCaig et al. 2018). Instead, significant boron may only be hosted in slow-spreading serpentinized lithosphere where long-lived transform faults have allowed for the prolonged alteration of the lithospheric mantle, or where large displacement faults have exposed significant amounts of peridotite at the surface of the seafloor (McCaig et al. 2018).

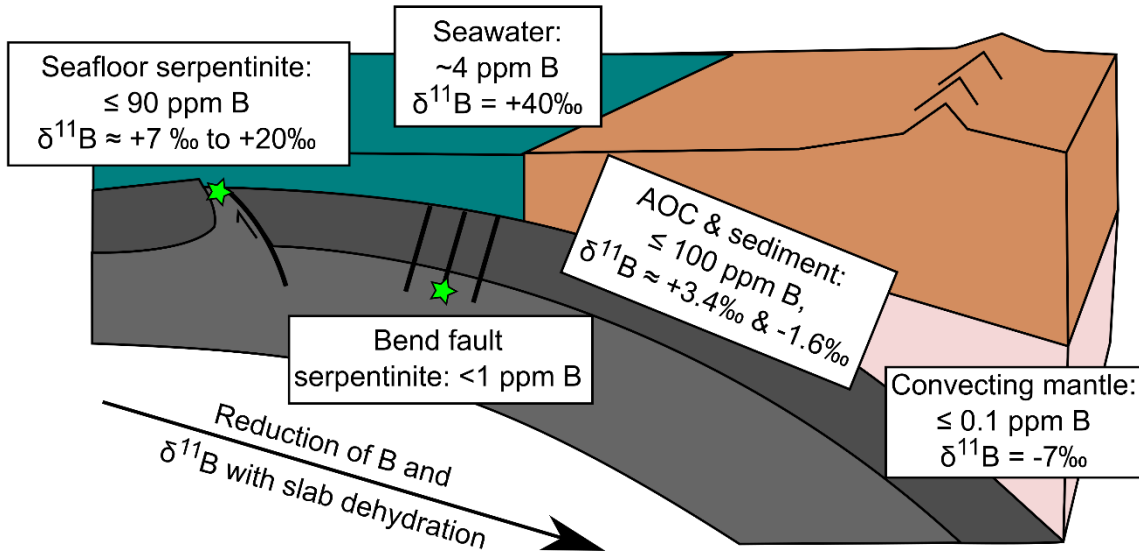


Figure 1.4. Boron isotope reservoirs in the subduction system including  $^{11}\text{B}$ -enriched serpentinite (green stars), subducting altered oceanic crust (AOC) and sediment. Peridotite that has been moved to the surface via large scale displacement faults can host substantial boron in serpentinite, but serpentization through small bend faulting does not significantly increase boron concentrations (McCaig et al. 2018). See table 1.1 for reference values.

Since boron can be trigonally or tetrahedrally coordinated to oxygen, large isotopic fractionations between different phases are common (Schmidt et al. 2005).  $^{11}\text{B}$  is preferentially incorporated into trigonal sites, such as the  $\text{B}(\text{OH})_3$  species dominant in seawater and in slab-related fluids over a wide range of pressure and temperature (Schmidt et al. 2005). In contrast,  $^{10}\text{B}$  is preferentially fractionated into tetrahedral ( $\text{BO}_4$ ) sites in smectite, carbonate, and serpentine (Schmidt et al. 2005). The partitioning of boron between seawater ( $\delta^{11}\text{B} = +39.6\text{\textperthousand}$ ; Foster et al. 2010) and these reservoirs leads to a  $\delta^{11}\text{B}$  of  $+7.0$  to  $+19.9\text{\textperthousand}$  for most serpentinites (Marschall 2018), an average seafloor sediment of  $-1.6\text{\textperthousand}$  (Leeman and Sisson 1996), and an average AOC of  $+3.4\text{\textperthousand}$  (Smith et al 1995).

During low to moderate temperature subduction ( $\leq 400^\circ\text{C}$ ), fluids that are released from the

slab and sediments are heavily enriched in fluid-mobile  $^{11}\text{B}$  (Benton et al. 2001). This dehydration and metasomatism of the overlying mantle wedge produces serpentinites with a range of boron isotope signatures ( $\delta^{11}\text{B}$  -14 to +10 ‰; Martin et al. 2020). These mantle wedge serpentinites can be pulled deeper into the mantle by subduction, and may act as fluid-sources for arc volcanoes (Tonarini et al. 2007, 2011; Scambelluri and Tonarini 2012). The residual subducting crust and sediments become progressively isotopically lighter during prograde blueschist and eclogite metamorphism and dewatering (Peacock and Hervig 1999; Nakano and Nakamura 2001). Because of the large degree of fluid-loss that they experience, sediments are unlikely to carry boron beyond sub-arc depths (De Hoog and Savov 2018). In addition, mineralogy dependent modeling suggests that altered oceanic crust at ~2.5 GPa may have a  $\delta^{11}\text{B}$  of -10 to -40 ‰ (Marschall et al. 2007). The remaining isotopically light boron in the slab is stable in phengite, until its breakdown at 10 GPa (De Hoog and Savov 2018).

Prograde metamorphism appears to have little effect on the boron isotopic composition of serpentinites in meta-peridotitic portions of the slab, perhaps due to a lack of major fluid loss (Scambelluri and Tonarini 2012; Martin et al. 2020). One recent study found that the  $\delta^{11}\text{B}$  of serpentinites is independent of the serpentine polymorph and that no major B loss is recorded across the lizardite to antigorite transition (Martin et al. 2020). Even after the antigorite-out isograd, a heavy boron isotopic composition can be carried to the deep mantle by chlorite and olivine at high temperature slab geotherms, or by dense hydrous magnesium silicates (DHMS) in cold systems (De Hoog and Savov 2018).

Table 1.1. Boron reservoirs on Earth and their isotopic composition.

Reservoir	Ave. B (ppm)	$\delta^{11}\text{B} (\text{\textperthousand})$
Ocean Water	~4 (Gaillardet and Allègre 1995)	+40 (Foster et al. 2010)
Carbonates	11-71 (Hemming and Hanson 1992)	+15 to +25 (Rae 2018)
Altered oceanic crust	7.2-104 (Smith et al. 1995)	-6.2 to +25; average of +3.4 (Smith et al. 1995)
Serpentinized oceanic lithosphere	<327 (Smith et al. 1995; Boschi et al. 2008; Martin et al. 2020)	+7 to +20 (Marschall 2018)
Marine sediments	~100 (Ishikawa and Nakamura 1993)	-6.6 to +4.8 (Ishikawa and Nakamura 1993); average of -1.6 (Leeman and Sisson 1996)
Arc volcanics	<94 (Morris et al. 1990)	-7 to +12 (Ishikawa and Nakamura 1994; Ishikawa and Tera 1997; Smith et al. 1997; Ishikawa et al. 2001; Straub and Layne 2002; Leeman et al. 2017)
MORB	0.1 (Leeman and Sisson 1996)	-7 $\pm$ 1 (Marschall 2018)
Azores OIB	<50 (Turner et al. 2007)	-12 to -3 (Marschall 2018)
Blueschist/eclogites	n.a.	-9 $\pm$ 5.4 (Peacock and Hervig 1999; Pabst et al. 2012)
Metasedimentary rocks	--	-4.2 $\pm$ 4.4 (Nakano and Nakamura 2001; Pabst et al. 2012)

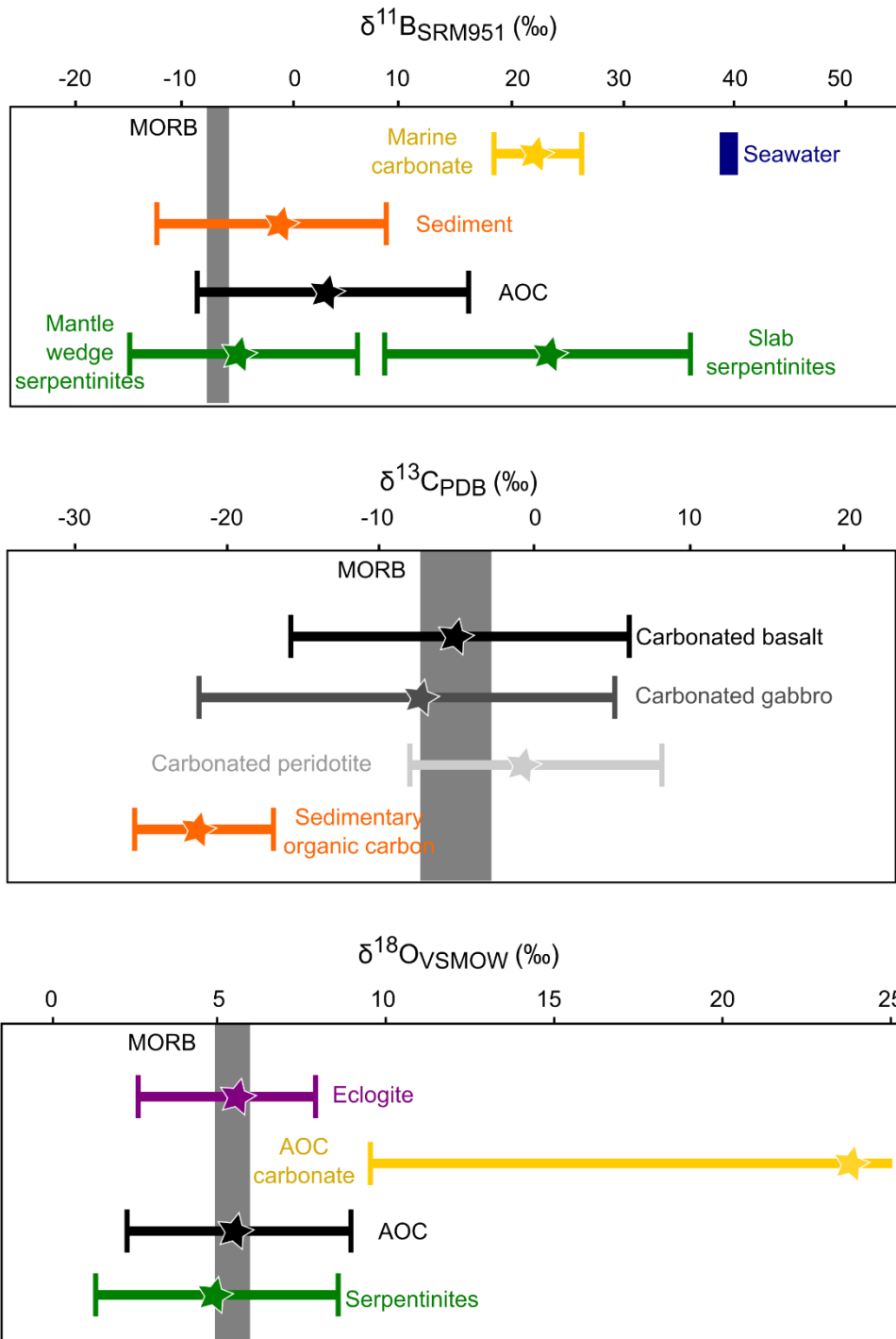


Figure 1.5. Range of slab related reservoirs and MORB for three stable isotopic tracers – boron, carbon, and oxygen. Data for carbonate (Hemming and Hanson 1992; Li et al. 2019), serpentinite (Martin et al. 2020), sediments (Ishikawa and Nakamura 1993), AOC (Smith et al. 1995), carbonated basalt, gabbro, peridotite (Li et al. 2019), sedimentary organic carbon (Galy et al. 2010), and eclogite (Korolev et al. 2018b) are 95% ( $2\sigma$ ) of all reported data. Averages of these data are indicated with a star.

## **1.4 Major objectives**

While subduction is a dominant force in shaping the natural world, its geochemical signature in deep time and in the deep Earth has remained enigmatic. In this vein, the main objectives of this dissertation are as follows:

- 1. Identify the appropriate models for lithosphere formation using tracers for subduction processes**

Characterize the elemental and oxygen isotopic characteristics of cratonic mantle xenoliths from 5 different cratons.

- 2. Identify the behavior of slab volatiles – C, N, O – at asthenospheric to lower mantle depths.**

Characterize the behavior of convecting mantle and/or slab-derived volatile elements at lithospheric, asthenospheric, transition zone, and lower mantle depths using elemental and oxygen isotope analysis of Kankan mineral inclusions.

- 3. Identify the mode of formation for superdeep blue diamonds and determine the source of boron in these samples.**

Characterize the inclusion mineralogy and the trace element and stable isotopic geochemistry of superdeep blue diamonds and determine a slab or mantle source of boron using boron isotope geochemistry.

## **Chapter 2**

### **An oxygen isotope test for the origin of Archean mantle roots**

#### **Chapter Summary**

The origin of the peridotites that form cratonic mantle roots is a central issue in understanding the history and survival of Earth's oldest continents. A long-standing hypothesis holds that the unusual bulk compositions of some cratonic peridotites stem from their origin as subducted oceanic serpentinite, dehydrated during subduction to form rigid buoyant keels (Schulze 1986; Canil and Lee 2009). We present oxygen isotope data from 93 mantle peridotites from five different Archean cratons to evaluate their possible origin as serpentinites. Cratonic mantle peridotite shows remarkably uniform  $\delta^{18}\text{O}$  values, identical to modern MORB-source mantle, that do not vary with bulk rock Si-enrichment or Ca-depletion. These data clearly conflict with any model for cratonic lithosphere that invokes serpentinite as a protolith for cratonic peridotite, and place additional constraints on cratonic mantle origins. We posit that the uniform  $\delta^{18}\text{O}$  was produced by sub-arc and/or MOR depletion processes and that the Si-enriched nature of some samples is unlikely to be related to slab melt infiltration. Instead, we suggest a peridotitic source of Si-enrichment, derived from ascending mantle melts, or a water-fluxed depleted mantle. These variably Si-enriched, cratonic mantle protoliths were then collisionally compressed into the thick cratonic roots that have protected Earth's oldest continental crust for over 2.5 Gyr.

## 2.1 Introduction

An essential element to the study of the growth and longevity of Earth's continental crust is the origin of the chemically buoyant and rigid lithospheric mantle that underpins ancient continental cratons. The vast majority of geochemical evidence for the origin of cratonic peridotites supports initial melt extraction at pressures  $\leq 5$  GPa, with most melting occurring in the spinel stability field. This depletion in a shallow, spinel-bearing environment is indicated by low concentrations of mildly incompatible elements and the Cr-rich nature of garnet in cratonic peridotites, documenting a strong increase in bulk rock Cr/Al during melt depletion (Stachel et al. 1998b; Canil 2004; Brey and Shu 2018). If a moderate to low pressure origin is accepted, then two endmember models remain. The first model (Fig. 2.1a) invokes the successive imbrication of subducted oceanic lithosphere (e.g. Helmstaedt and Schulze 1989; Pearson and Wittig 2008). The second model – collisional compression via pure shear (Fig. 2.1b) - proposes that depleted mantle protoliths from Neoarchean sub-arc settings and/or hot spreading centers are tectonically amalgamated, compressed, and gravitationally thickened during cooling (Jordan 1978; Lee et al. 2011; Wang et al. 2018b). The serpentinite-like major element signatures of some peridotites (Si-enriched bulk rock and subcalcic garnets) have been used to support the imbrication of hydrated oceanic lithosphere (Schulze 1986; Canil and Lee 2009). However, these cratonic peridotites have not been systematically tested for the distinctive oxygen isotopic ratios that are characteristic of serpentinites. Here, we search for these distinctive isotopic signatures in mantle-derived cratonic xenoliths.

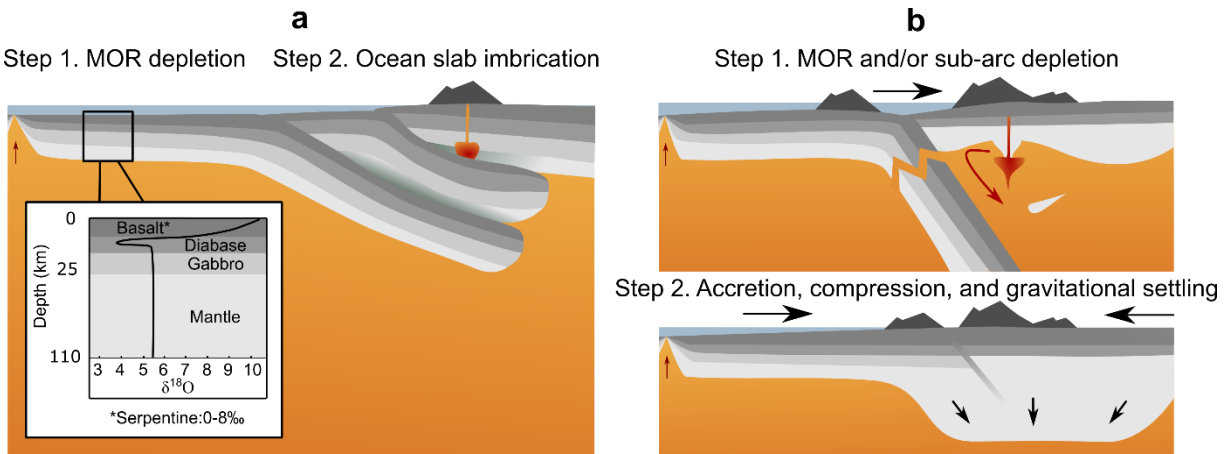


Figure 2.1. Popular models of cratonic mantle formation. (a) Imbrication of MOR sequences to form a thick lithosphere. An estimated oxygen isotope profile through Neoarchean oceanic lithosphere is inset. (b) Depleted cratonic mantle protoliths produced at MOR and in sub-arc environments are compressed via pure shear into a thick lithospheric root.

## 2.2 Approach and results

To characterize the oxygen isotopic composition of cratonic mantle peridotites we present ion microprobe analyses (see appendix A) of olivines from coarse, “low-temperature” peridotite xenoliths (Table A1), thought to represent the bulk of the cratonic lithospheric mantle. The sample suite is derived from the Slave, Rae, North Atlantic, Kaapvaal, and Siberian Archean cratons, and excludes cratonic peridotites that were modified after emplacement by high-temperature deformation and melt metasomatism. We also report precise laser fluorination and ion probe measurements on cratonic mantle orthopyroxene (Opx) as well as olivine from forearc peridotites.

Our samples span both sides of the average cratonic mantle olivine Mg# (100 x molar Mg/(Mg+Fe)) of 92.6 (Fig. 2.2a). A subset of our samples are Si-enriched, manifested as high bulk rock SiO<sub>2</sub> and elevated modal Opx contents. We adopt the  $\Delta\text{Mg/Si}$  parameter of Canil

and Lee (2009) to quantify Si-enrichment (Fig. 2.2b), where negative  $\Delta\text{Mg/Si}$  denotes Si-enriched, or a lower Mg/Si and Al/Si than can be produced by experimental partial melting of peridotite.

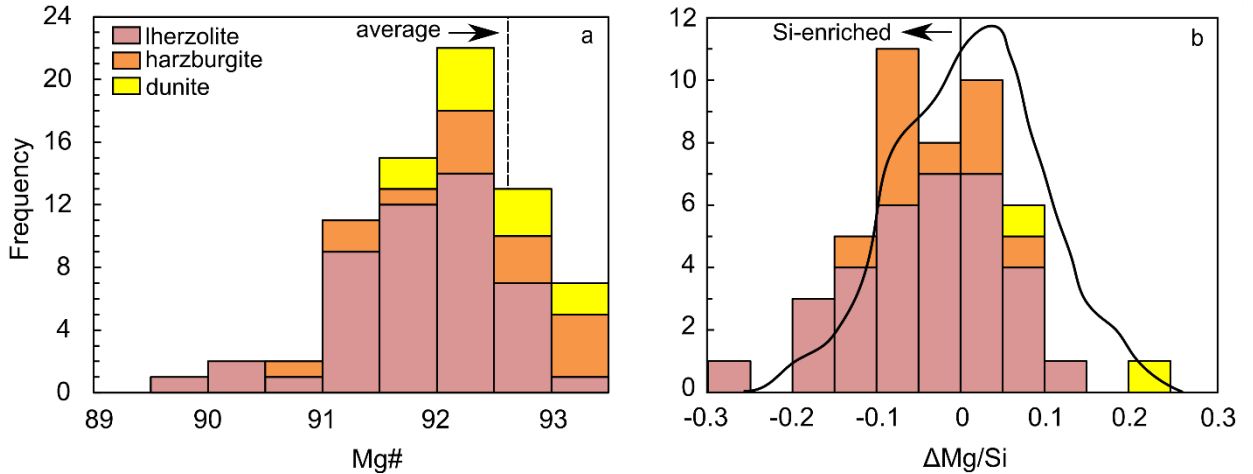


Figure 2.2. Elemental chemistry of xenoliths in this study. (a) Mg# histogram of olivines in this study. Mg#s are both more and less depleted than the worldwide average for olivine in cratonic peridotite, denoted by the dotted line (Pearson and Wittig 2008). (b)  $\Delta\text{Mg/Si}$  histogram of the studied samples compared to a vertically unscaled probability density function for worldwide cratonic mantle xenoliths from Canil and Lee (2009). Negative  $\Delta\text{Mg/Si}$  designates Si-enriched lithologies.

Our measurements reveal that cratonic mantle olivines are normally distributed (Shapiro-Wilk  $W=0.99$ ,  $p=0.52$ ) over an extremely restricted  $\delta^{18}\text{O}$  range of +5.01 to +5.53 ‰, with a mean of  $5.26 \pm 0.22$  ‰ ( $2\sigma$ ). There are no statistically significant deviations in  $\delta^{18}\text{O}$  with chemical proxies (Fig. A1). Additionally, cratonic mantle Opx from variably Si-enriched xenoliths (Table A2: mean  $\delta^{18}\text{O}$  of  $5.74 \pm 0.27$  ‰) are in isotopic equilibrium with associated olivine ( $\Delta_{\text{enstatite-olivine}} \text{ at } 1300^\circ\text{C} = \sim 0.5$  ‰; Rosenbaum et al. 1994)

In order to determine if there are crustal sources of oxygen in the cratonic mantle, we compare

our dataset to the well-defined MORB-source mantle (Fig. A1). We adjust our olivine  $\delta^{18}\text{O}$  to whole-rock peridotite values using a fractionation factor that accounts for the ultramafic composition. Oxygen isotope fractionation between an ultramafic peridotitic mantle source and olivine at high mantle temperatures has been estimated at  $\sim 0.2\ \text{\textperthousand}$  (Valley et al. 1998), based on a basalt-olivine fractionation of  $0.32\ \text{\textperthousand}$  at  $1300\ ^\circ\text{C}$  (Eiler et al. 2000b) and the positive correlation between melt  $\text{SiO}_2$  and  $D_{\text{melt-olivine}}$  (Eiler 2001). A bootstrapped, or resampled, Kolmogorov-Smirnov (K-S) statistical evaluation to test for differing probability distributions of the MORB dataset and the  $0.2\ \text{\textperthousand}$  fractionation-corrected cratonic mantle olivines indicates that they are statistically indistinguishable ( $D=0.11$ ,  $p=0.57$ ), with both populations having analytical uncertainties equal-to or larger than the population variance. In contrast, serpentinized peridotite and cratonic mantle olivine have clearly distinct distributions ( $D=0.54$ ,  $p << 0.05$ ; Fig. 2.3a).

## 2.3 Implications for craton formation

The striking similarity between oxygen isotope compositions of present-day MORB and Archean cratonic peridotites documents the stability of the  $\delta^{18}\text{O}$  of Earth's mantle over a 3-billion-year interval. Despite this, the diverse  $\delta^{18}\text{O}$  values of cratonic eclogite xenoliths demonstrate that  $\delta^{18}\text{O}$  heterogeneities in the subcontinental lithospheric mantle can persist even at the meter scale, likely due to the slow diffusion of oxygen. Since hydrothermal alteration, or the serpentinization of ultramafic rocks, is an effective method of producing highly variable  $\delta^{18}\text{O}$  (Wenner and Taylor 1971), cratonic mantle olivines derived by prograde metamorphism of serpentinite (Canil and Lee 2009) should retain both serpentinite-like major element chemistry and distinct oxygen isotopic compositions (Fig. 2.3a).

In contrast to the extreme  $\delta^{18}\text{O}$  variability of Phanerozoic serpentinite (0 to +8 ‰; Fig. 2.3a), cratonic peridotitic olivines are strikingly uniform, even over the full compositional range typical for Archean lithospheric mantle. Olivines co-existing with subcalcic garnets and from Si-enriched peridotites - proposed signatures of a serpentinite origin (Schulze 1986; Canil and Lee 2009) - have oxygen isotope compositions that are statistically indistinguishable from normal upper mantle (Fig. 2.3b). A key piece of evidence previously used in support of the meta-serpentinite hypothesis was a reported correlation between  $\delta^{18}\text{O}$  and Mg/Si from Colorado Plateau peridotitic xenoliths (Canil and Lee 2009). We note that this Proterozoic terrane is not under-pinned by an Archean cratonic root and shows clear evidence of hydrous weakening and thinning (Li et al. 2008). Furthermore, our replotting of these data resolves a positive correlation ( $r^2 = 0.89$ ) between  $\delta^{18}\text{O}$  and Mg# (Fig. 2.3c). This trend is not consistent with a metaserpentinite origin, as serpentine minerals are commonly higher in Mg# than the initial olivine and Opx that they replace (Evans 2008). Therefore, these samples likely do not represent seafloor alteration (Canil and Lee 2009), but may instead be a consequence of the water-rich metasomatism of the Colorado Plateau lithospheric mantle by Si-enriched fluids or melts from the low-angle subducting Farallon Plate at 80-35 Ma (Li et al. 2008). Finally, as the narrow variance in Archean cratonic mantle peridotite is statistically equivalent to that of MORB, there is no evidence for even small inputs of meta-serpentinite. Hence, meta-serpentinite is an unlikely protolith to the peridotitic root of the Colorado Plateau, and can be rejected as a protolith for Archean cratonic mantle.

While the Colorado Plateau lithosphere is not a good proxy for pristine cratonic mantle, it is a

geometric analogue for the Archean slab imbrication model. The low angle subduction that occurred underneath the Colorado Plateau in the Cretaceous - Eocene likely injected slab melts/fluids directly into the overlying lithospheric mantle, offsetting  $\delta^{18}\text{O}$ ,  $\Delta\text{Mg/Si}$ , and  $\text{Mg}\#$ . The similar geometry required for the Archean slab imbrication model would likely produce the same geochemical traces in cratonic mantle olivine. Since our extensive suite of cratonic mantle olivines does not show “Colorado Plateau-like” systematics (between  $\delta^{18}\text{O}$  and metasomatic proxies -  $\Delta\text{Mg/Si}$  or  $\text{Mg}\#$ ; Fig. 2.3c, Fig. A2), it is unlikely that cratonic mantle thickening occurred by slab imbrication. This lack of a crustal alteration signature would be in-line with suggestions of higher pressure melting in plumes, but such a model can be rejected from other considerations that place melt depletion in the spinel stability field (see discussion in introduction). Instead, we hypothesize that cratonic mantle protoliths were initially depleted at MOR and/or at water fluxed sub-arc mantle wedges, environments that produce material with canonical mantle-like  $\delta^{18}\text{O}$  (Table A3). These protoliths were then thickened, without significant isotopic modification, by pure shear compression to form cratonic mantle roots (Jordan 1978; McKenzie and Priestley 2016; Wang et al. 2018b).

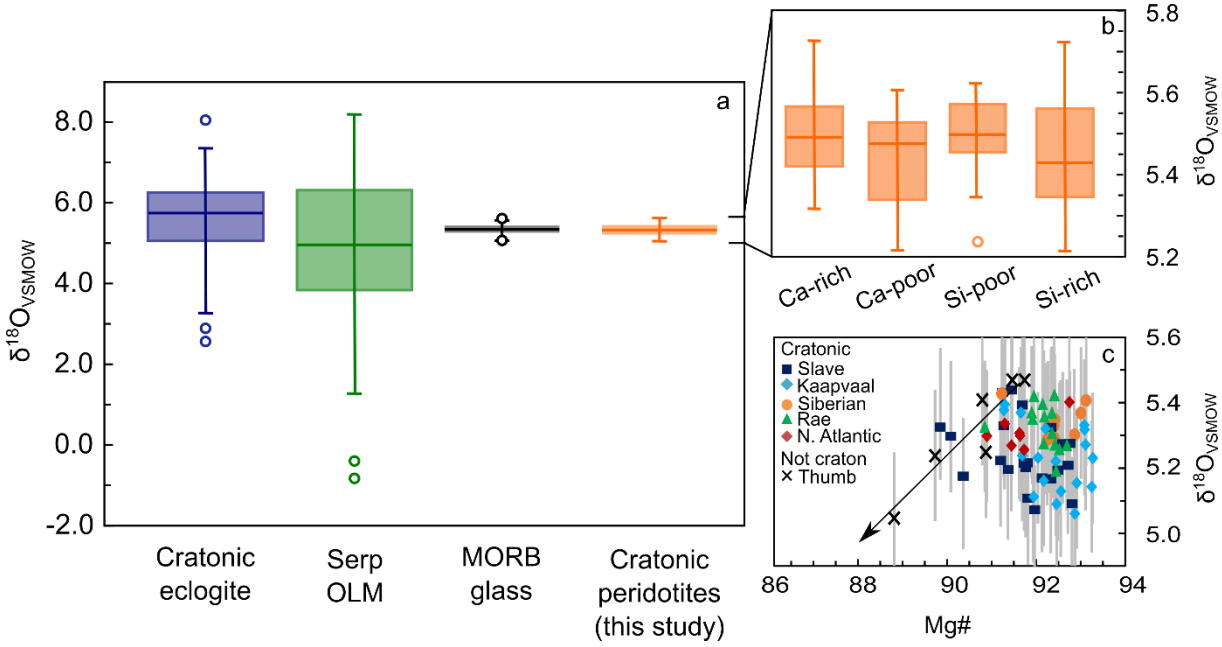


Figure 2.3. Oxygen isotopes from this study compared to other reservoirs. (a) Box-whisker plot of the oxygen isotopic composition of cratonic peridotites, calculated from olivine  $\delta^{18}\text{O}$ , compared to eclogitic xenoliths, serpentinized oceanic lithospheric mantle (OLM), and MORB glass (source data: Tables A5, A6, A7). (b) A box-whisker plot of olivine  $\delta^{18}\text{O}$ , divided into statistically insignificant chemical discriminators – Ca-rich (lherzolitic), Ca-poor (harzburgitic/dunitic) and Si-enriched ( $-\Delta\text{Mg/Si}$ ) and depleted lithologies ( $+\Delta\text{Mg/Si}$ ), demonstrates that there is no variation in the distribution of oxygen isotopes with bulk rock chemistry. (c) Scatter plot of olivine  $\delta^{18}\text{O}$  and Mg#. The lack of correlation in the cratonic mantle suite contrasts to the trendline of The Thumb xenoliths ( $r^2 = 0.86$ ; Canil and Lee 2009).

While our data is consistent with the construction of cratons by collisional compression of unaltered, depleted peridotite protoliths, we still require a means to heterogeneously enrich these regions in high-Si Opx. Many explanations for cratonic mantle Opx enrichment rely on the infiltration of slab derived melts (e.g. Rudnick 1994; Kelemen et al. 1998). However, lithosphere that has been thinned by crustal melt infiltration is marked by low Mg# and exotic  $\delta^{18}\text{O}$  (Wang et al. 2018a). Using pMELTS isenthalpic modeling (Ghiorso et al. 2002) of assimilation-fractional crystallization (AFC) of slab melt at 3 GPa, we demonstrate that these

melts fractionate garnet at slab melt/assimilated rock ratios of >5, followed by Opx (ratios of 1-5), and olivine, once the melt SiO<sub>2</sub> drops to ~50 wt. % (ratios of less than ~1). Given the low MgO and FeO of experimentally derived slab melts (Table A4), high Mg# minerals crystallize after minimal assimilation of peridotite. However, producing minerals with mantle-like δ<sup>18</sup>O is more difficult (Fig. 2.4). Mass balance calculations that include fractionation factors (Eiler 2001) and the compositional and mineralogical outputs of pMELTS (Table A4), indicate that at the required melt/rock ratios, δ<sup>18</sup>O of Opx and olivine remains higher than mantle. Even melts with modest initial δ<sup>18</sup>O (e.g., δ<sup>18</sup>O of +4.0 or +6.5 ‰) cease to crystallize Opx before mantle-like δ<sup>18</sup>O is achieved, due to low melt SiO<sub>2</sub> (<50 wt. %). Since the measured δ<sup>18</sup>O values of olivine and Opx from Si-enriched cratonic peridotites do not reflect those modeled in slab melt AFC models, we do not support the slab melt infiltration hypothesis for Si-enrichment.

Since Si-enrichment cannot be achieved by eclogite-derived melts and, as previously discussed in the introduction, cratonic lithospheric mantle does not show evidence for a high-pressure origin, we instead suggest two low-pressure mantle origins: 1) asthenospheric melts that have become Si-enriched due to the assimilation of wall rock pyroxene and fractionation of olivine during ascent (Kelemen et al. 1992), or 2) the infiltration of moderately Si-rich melts (~56 wt. %) produced from the melting of a slightly depleted mantle fluxed with ~2.5 wt. % H<sub>2</sub>O from a devolatilizing slab (Mitchell and Grove 2015). When this depleted, harzburgite-derived melt with a δ<sup>18</sup>O of +5.6 ‰ is input into our AFC model, it crystallizes Opx and olivine with cratonic mantle-like Mg# and δ<sup>18</sup>O (Fig. 2.4). The proportion of precipitating Opx, and thus, the Si-enrichment of the surrounding rock, is dependent on the evolving melt-rock ratio.

The final stage of thickening, via collisional compression of this heterogeneously Si-enriched material, therefore, leads to a cratonic mantle root with variable Opx content, but homogeneous oxygen isotopes.

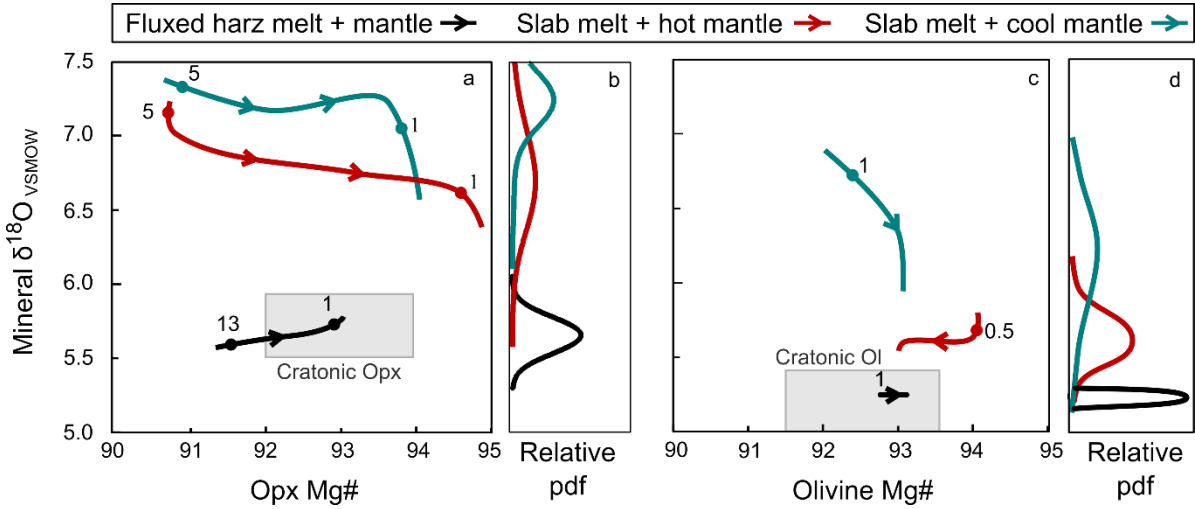


Figure 2.4. pMELTS and isotopic mass balance modeling of melts reacting with surrounding harzburgite. Slab melts ( $\delta^{18}\text{O}$  of +8 ‰) react with a 900 °C (blue) and 1500 °C (red) harzburgite, as well as a water-fluxed harzburgitic (harz) melt ( $\delta^{18}\text{O}$  of +5.6 ‰) reacting with 1300 °C harzburgite (black). The major element and isotopic evolution of crystallizing Opx (a) and olivine (c) is indicated by smoothed curves. Numbers indicate the slab melt/assimilated peridotite ratio. Typical cratonic mantle Opx and olivine (Ol) is outlined in gray fields. Kernel density estimations of the probability density functions (pdf) for Opx (b) and olivine (d)  $\delta^{18}\text{O}$  are included.

## 2.4 Conclusions

In summary, the  $\delta^{18}\text{O}$  homogeneity of a wide range of cratonic mantle peridotites demonstrates that their variably Si-enriched, sometimes subcalcic garnet-bearing nature cannot have been inherited from protoliths that experienced seafloor serpentinization (e.g. Schulze 1986; Canil and Lee 2009). Instead, these peridotites must have 1) lain at depths in the oceanic lithosphere where circulating water was minimal and 2) avoided extensive metasomatism from imbricating oceanic lithosphere. Based on these observations, we suggest that cratonic mantle

must have been depleted either in thick Archean MOR sequences (Herzberg and Rudnick 2012) or in sub-arc mantle wedges (Parman et al. 2004). The redistribution of Si with mantle-like  $\delta^{18}\text{O}$  was caused by peridotite-derived melt percolation. Finally, these buoyant, depleted proto-cratonic peridotites were thickened by collisional compression (Wang et al. 2018b) into the roots that have protected Earth's >2.5 billion-year-old crust.

## 2.5 Methods

Mount preparation and ion probe analysis is credited to the Canadian Centre for Isotopic Microanalysis (CCIM) at the University of Alberta. Minerals were arrayed on double-sided tape, cast in 25 mm epoxy disks, and then ground and polished using diamond grits. The CCIM primary reference materials (RMs) are olivine S0013D ( $\text{Mg\#} = 0.93$ ) and S0103 ( $\text{Mg\#} = 0.744$ ). The mounts were coated with 10 nm of high-purity Au prior to scanning electron microscopy (SEM) utilizing a Zeiss EVO MA15 instrument. Beam conditions were 15kV and 3 nA sample current. A further 40 nm of Au was subsequently deposited on the mount prior to SIMS analysis.

Oxygen isotopes ( $^{18}\text{O}$ ,  $^{16}\text{O}$ ) were analyzed using a Cameca IMS 1280 multicollector ion microprobe. A  $^{133}\text{Cs}^+$  primary beam was operated with an impact energy of 20keV and beam current of 1.8 – 2.2 nA. The  $\sim 10 \mu\text{m}$  diameter probe was rastered ( $20 \times 20 \mu\text{m}$ ) for 45 s prior to acquisition, and then typically reduced to  $8 \times 8 \mu\text{m}$  during acquisition, forming analyzed areas  $\sim 15 \mu\text{m}$  across and  $\sim 2 \mu\text{m}$  deep. The normal incidence electron gun was utilized for charge compensation. Negative secondary ions were extracted with 10 kV into the secondary column. Conditions included a  $122 \mu\text{m}$  entrance slit, a  $5 \times 5 \text{ mm}$  pre-ESA (field) aperture, and 100x

sample magnification at the field aperture, transmitting all regions of the sputtered area. No energy filtering was employed. The mass/charge separated oxygen ions were detected simultaneously in Faraday cups L'2 ( $^{16}\text{O}^-$ ) and H'2 ( $^{18}\text{O}^-$ ) at mass resolutions ( $m/\Delta m$  at 10 %) of 1950 and 2250, respectively. Secondary ion count rates for  $^{16}\text{O}^-$  and  $^{18}\text{O}^-$  were typically  $\sim 2 \times 10^9$  and  $4 \times 10^6$  counts/s utilizing  $10^{10} \Omega$  and  $10^{11} \Omega$  amplifier circuits, respectively. Faraday cup baselines were measured at the start of the analytical session. A single analysis took 240s, including pre-analysis rastering, automated secondary ion tuning, and 75s of continuous peak counting.

Instrumental mass fractionation (IMF) was monitored by repeated analysis of the primary olivine and enstatite standard (olivine S0013D  $\delta^{18}\text{O}_{\text{VSMOW}} = +5.26 \text{ ‰}$ ; enstatite S0170  $\delta^{18}\text{O}_{\text{VSMOW}} = +5.64 \text{ ‰}$ ; R. Stern, unpublished laser fluorination data, University of Oregon). One analysis of the primary RM was taken after every 4 unknowns. The  $^{18}\text{O}/^{16}\text{O}$ - data set for each primary RM was processed collectively for its session, yielding a standard deviation ranging from  $= 0.07 \text{ ‰}$  to  $0.12 \text{ ‰}$ , following correction for systematic within-session drift of  $\leq 0.3 \text{ ‰}$ . IMF values for olivine were corrected for EPMA-determined Mg#s by  $+ 0.038 \text{ ‰/Mg\#}$  unit relative to the IMF determined for S0013D olivine, determined on a separate mount (M0290) containing S0013D and S0103 olivine. Opx  $\delta^{18}\text{O}$  was corrected for Mg# using laser fluorination data from 94.1 Mg# sample F866 (Lowry et al. 1999) and 91.2 Mg# standard enstatite S0170 (R. Stern, unpublished laser fluorination data, University of Oregon). The 95 % confidence uncertainty estimates for  $\delta^{18}\text{O}_{\text{VSMOW}}$  average  $\pm 0.21 \text{ ‰}$ .

## **Chapter 3**

### **The lithospheric to lower mantle carbon cycle in superdeep diamonds**

#### **Chapter Summary**

The transport of material into Earth's mantle is a critical pathway in Earth's carbon cycle, affecting both climate and redox conditions of the surface and mantle. The largest unconstrained variables in this cycle are the depths to which carbon in sediments and altered oceanic crust can be subducted, and the relative roles of these mechanisms to sequester carbon in the deep mantle (Plank and Manning 2019). Mineral inclusions in sublithospheric, or "superdeep" diamonds (derived from  $\geq 250$  km), can uniquely address these questions. Here we present oxygen isotope measurements of mineral inclusions within diamonds from Kankan, Guinea that are derived from the lithosphere to the lower mantle ( $> 660$  km). These data, combined with the carbon and nitrogen isotopes of diamonds, indicate that carbonated igneous oceanic crust, not sediment, is the primary carbon-bearing reservoir in slabs subducted to deep lithospheric and transition zone depths ( $< 660$  km). Within this depth regime, sublithospheric inclusions have distinctly more positive oxygen isotope values than eclogitic lithospheric inclusions derived from crustal protoliths. The elevated values of these sublithospheric inclusions are a result of their crystallization from melts of carbonate-rich subducted oceanic crust. In contrast, lower mantle

mineral inclusions and their host diamonds (>660 km) have a narrow range of isotopic values that are typical of mantle that has experienced little or no crustal interaction. Because carbon is hosted in metals rather than diamond in the reduced, volatile-poor lower mantle (Dasgupta and Hirschmann 2010), carbon first needs to be mobilized and concentrated to form lower mantle diamonds. Our data support a model in which the hydration of the uppermost lower mantle by subducted oceanic lithosphere destabilizes carbon-bearing metals to form diamond, without disturbing the ambient mantle stable isotope signatures. This transition from carbonate slab melting in the transition zone to slab dehydration in the lower mantle supports a lower mantle barrier for carbon subduction.

### 3.1 Introduction

The first seismological images of subducted oceanic lithosphere penetrating the 660 km mantle discontinuity provided evidence for the circulation of some upper mantle material into the lower mantle (Creager and Jordan 1984). Nevertheless, the depths at which volatiles are lost from the slab as it subducts into the deep convecting mantle remain poorly understood. Diamonds are unique in that they directly sample the elements present at these depths. As high-T fractionation (Cartigny 2005) cannot account for all of the isotopic variability observed in diamonds, the  $^{13}\text{C}$ -depleted signatures of some lithospheric to transition zone diamonds are typically interpreted to reflect the deep subduction of sediments, rich in  $^{13}\text{C}$ -depleted, reduced organic carbon (Sobolev and Sobolev 1982; Kelemen and Manning 2015). This idea has garnered much attention, in part because the deep sequestration of reduced organic carbon in sediments is one hypothesized method for the production of Earth's oxidized atmosphere (Duncan and Dasgupta 2017). However, a newly expanded isotopic database implicates carbonates in altered igneous oceanic crust (AOC) as an alternative source for the  $^{13}\text{C}$ -depleted signal in many diamonds (Li et al.

2019). The stability of carbonated AOC at depth, until its partial melting in the deep asthenosphere and transition zone (Walter et al. 2008; Thomson et al. 2016), reinforces the idea that it could be the source of carbon in many superdeep diamonds (Kiseeva et al. 2013b; Thomson et al. 2016). But, thus far, no geochemical signature has clearly related these diamonds to a carbonate-rich protolith. Additionally, given the expected carbon-depleted nature of slabs after melting in the transition zone, the source of carbon for lower mantle diamonds remains unclear.

To evaluate the relative contributions of sediments, AOC, and convecting mantle to the deep mantle carbon cycle, we analyzed a suite of inclusions in superdeep diamonds for their oxygen isotope signature ( $\delta^{18}\text{O} = (^{18}\text{O}/^{16}\text{O}_{\text{sample}})/(^{18}\text{O}/^{16}\text{O}_{\text{VSMOW}}) - 1$ ), which is sensitive to the presence of recycled material. Previous measurements of  $\delta^{18}\text{O}$  in superdeep inclusions in diamond have been confined to two suites of asthenospheric and transition zone inclusions from the Jagersfontein kimberlite (South Africa) and the Collier-4, Juina-5, and Machado alluvial deposit of the Juina region in Brazil (Burnham et al. 2015; Ickert et al. 2015). Here, we report  $\delta^{18}\text{O}$  of inclusions within a diamond suite from Kankan, Guinea that contains not only lithospheric and asthenospheric/transition zone garnet inclusions, but also low- $\text{Al}_2\text{O}_3$  (<1.7 wt. %) orthopyroxene (retrogressed bridgmanite) coexisting with ferropericlase, an assemblage from the uppermost lower mantle (~700 km; Stachel et al. 2000a, b). Kankan diamonds and their silicate inclusions are thus powerful probes of the carbon cycle from lithosphere to lower mantle.

### 3.2 Lithospheric to Transition Zone samples

Lithospheric garnet inclusions in Kankan diamonds can be divided into eclogitic and peridotitic

suites based on major element chemistry (Stachel et al. 2000a). The peridotitic suite  $\delta^{18}\text{O}_{\text{VSMOW}}$  ranges from +5.3 to +5.7 ‰ ( $\pm 0.2 \text{ ‰}$ ), within error of average MORB-source mantle (+5.5 ‰; Eiler et al. 2000; Cooper et al. 2004, 2009) and in equilibrium with cratonic peridotite olivine ( $+5.3 \pm 0.2 \text{ ‰}$ ; Regier et al. 2018). The eclogitic suite has more varied  $\delta^{18}\text{O}$  values (+3.8 to +6.1 ‰), indicative of an origin from altered oceanic crust (Fig. 3.1a, c). Given the required addition of unreasonably large amounts of oxygen to change mineral  $\delta^{18}\text{O}$  values (Riches et al. 2016), these signatures are representative of the cratonic substrate and not the subsequent introduction of diamond-forming metasomatic agents.

Unlike lithospheric minerals, which can be definitively interpreted as having an eclogitic or peridotitic paragenesis using traditional major elemental classification schemes (Grütter et al. 2004), sublithospheric majoritic garnets (characterized by an excess of Si) are more difficult to assign to a specific paragenesis (Kiseeva et al. 2013b). Here, we categorize the majoritic garnets using an experimentally calibrated model, where excess  $\text{Si}^{4+}$  in the majoritic endmember is charge-balanced with  $\text{Na}^+$  in eclogitic systems, or with divalent cations in Na-poor peridotitic compositions (Kiseeva et al. 2013b). To quantify this scheme, we derive a parameter,  $\Delta_{\text{peridotite}}$ , defined as the difference in divalent cations between the mineral inclusion and a purely meta-peridotitic majoritic garnet, normalized to the difference between the two endmembers. Thus, a purely eclogitic majoritic garnet has a  $\Delta_{\text{peridotite}}$  of 1, whereas a purely meta-peridotitic majoritic garnet has a  $\Delta_{\text{peridotite}}$  of 0 (see Methods). The majority of majoritic garnet inclusions lie between these end-member trends ( $0 < \Delta_{\text{peridotite}} < 1$ ). This intermediate composition has been termed “meta-pyroxenitic” (Fig. 3.2a; Kiseeva et al. 2013b).

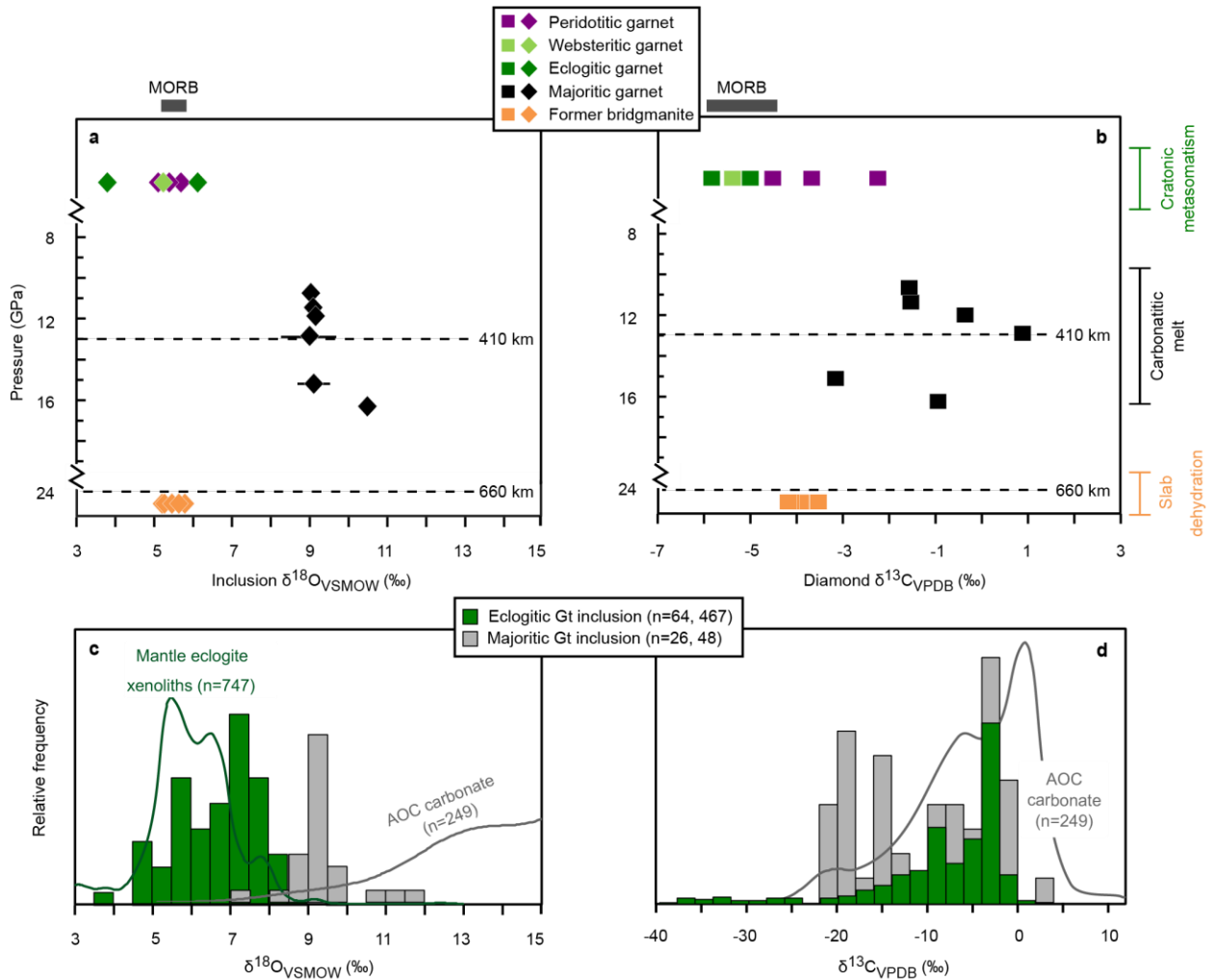


Figure 3.1. Stable isotope compositions of diamonds and their mineral inclusions. (a, b) Silicate inclusion  $\delta^{18}\text{O}$  and diamond host  $\delta^{13}\text{C}$  signatures (Stachel et al. 2002; Palot et al. 2014) versus depth for a suite of Kankan diamonds. Errors are  $2\sigma$  and smaller than the symbol. MORB isotopic ranges are indicated above panels (Marty and Zimmermann 1999; Eiler et al. 2000a; Cooper et al. 2004, 2009). Inferred environments of formation are indicated on the right. (c) Histogram of  $\delta^{18}\text{O}$  for majoritic garnet inclusions has a more positive mode than eclogitic garnet inclusions. Also plotted are probability density functions (PDF, bandwidth of 0.2 ‰) of eclogitic garnets from mantle xenoliths and AOC carbonates (bandwidth of 1.9 ‰). (d) Histograms of  $\delta^{13}\text{C}$  for eclogitic and majoritic garnet-bearing diamonds, and a PDF (bandwidth of 1.17 ‰) for AOC carbonate. Note scale differs from that of panel b. Source data and references: Tables B4, B5, B6, B7, B8.

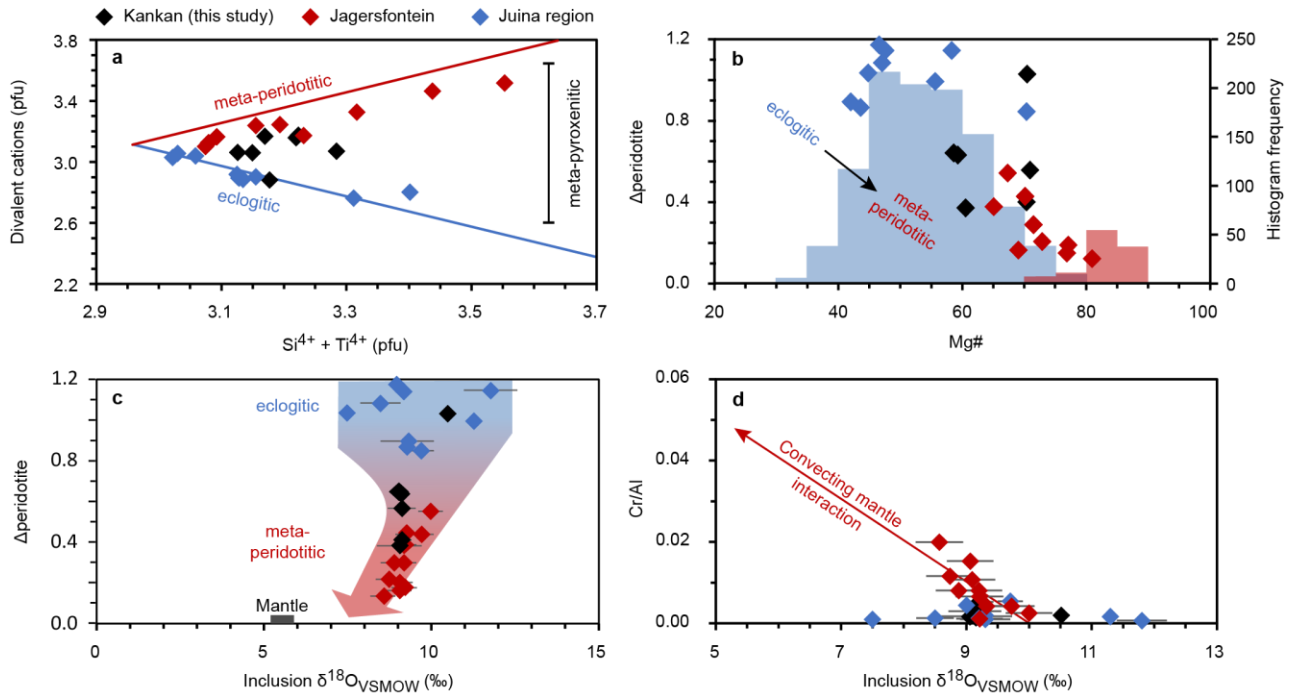


Figure 3.2. Elemental and isotopic composition of majoritic garnet inclusions. **(a)** Divalent cations ( $\text{Fe}_{\text{total}}, \text{Mg}, \text{Ca}, \text{Mn}$ ) versus  $\text{Si}$  and  $\text{Ti}$  per formula unit ( $[\text{O}] = 12$ ) in Kankan, Jagersfontein (Tappert et al. 2005a), and Juina region (Burnham et al. 2015) majoritic garnets. Red and blue lines are the substitutions typical for meta-peridotitic and eclogitic compositions, respectively, which begin at the median value for eclogitic garnets (2.96, 3.11) (Beard et al. 1996). **(b)** Majoritic garnet Mg# versus the parameter  $\Delta\text{peridotite}$ , which indicates an individual garnet's deviation from the meta-peridotitic substitution. The secondary axis histograms show the distribution of Mg# in lithospheric eclogitic and peridotitic garnet inclusions (blue and red, respectively). **(c)**  $\delta^{18}\text{O}$  versus  $\Delta\text{peridotite}$  values of majoritic garnet. **(d)** Cr/Al and  $\delta^{18}\text{O}$  in majoritic garnet. Red line is a linear regression ( $r^2 = 0.6$ ) for the Jagersfontein data, which trends from low Cr/Al eclogitic majorites to more meta-peridotitic, high Cr/Al majorites with lower  $\delta^{18}\text{O}$ . Errors for panels c, d are  $2\sigma$ , and may be smaller than symbol. Source data: Table B8.

Because these meta-pyroxenitic inclusions are intermediate in major element composition, we might also expect their  $\delta^{18}\text{O}$  to be intermediate compared to the values reported for lithospheric eclogitic and peridotitic garnets. Instead, meta-pyroxenitic majoritic garnets from Kankan have much more extreme  $\delta^{18}\text{O}$  (+9.1 to +10.5 ‰) than the Kankan eclogitic garnet inclusions of lithospheric origin (+3.8 to +6.1 ‰). Similarly, meta-pyroxenitic majoritic garnets from Juina (Brazil; Burnham et al. 2015) and Jagersfontein (S. Africa) diamonds (Ickert et al. 2015) also have a significantly higher  $\delta^{18}\text{O}$  mode than eclogitic garnet inclusions in diamonds worldwide (Fig. 3.1c), with all majoritic garnet values greater than +7.5 ‰ (n=24) and some extending to even more extreme values (+12 ‰). Only 4% of data from a composite model of oceanic lithosphere rocks approaches the average  $\delta^{18}\text{O}$  of these majoritic garnets (Ickert et al. 2013). Even more striking, < 0.05% of oceanic lithosphere bulk rocks extend to the +12 ‰ observed in some majoritic garnets (Ickert et al. 2013). Hence, we conclude that there must be a unique source for the highly elevated  $\delta^{18}\text{O}$  in meta-pyroxenitic superdeep inclusions.

The oxygen isotope compositions of asthenosphere to transition zone majoritic garnets clearly require a crustal input and hence it must be sourced somewhere in the subducting oceanic slab. Two potential reservoirs of high  $\delta^{18}\text{O}$  are the carbon-bearing constituents of sediments on top of the oceanic crust and carbonate in the AOC itself. Sediments are generally dominated by positive  $\delta^{13}\text{C}$  “marine carbonate” ( $\delta^{13}\text{C} = (^{13}\text{C}/^{12}\text{C}_{\text{sample}})/(^{13}\text{C}/^{12}\text{C}_{\text{VPDB}}) - 1$ ), but may be locally  $^{13}\text{C}$ -depleted due to the presence of “reduced organic-rich carbon”, which is comprised of organic carbon from marine and terrestrial organisms living near continental margins (Plank and Manning 2019). In comparison, much of the carbon present in AOC is  $^{13}\text{C}$ -enriched carbonate that precipitated in equilibrium with dissolved inorganic carbon (DIC), called “normal” or

“DIC-equilibrium carbonate” (Li et al. 2019). Recent studies have documented that AOC also includes  $^{13}\text{C}$ -depleted carbonate precipitated from biologically/kinetically fractionated DIC (Li et al. 2019). We label this endmember “biogenic AOC carbonate”.

The recent identification of  $^{13}\text{C}$ -depleted biogenic carbonate in AOC (Li et al. 2019) challenges the common assumption that  $^{13}\text{C}$ -depleted diamonds invariably originate from deeply subducted sediment (Sobolev and Sobolev 1982; Cartigny 2005). In order to examine the source of the  $^{13}\text{C}$ -depleted signal further, we examine the worldwide database of  $\delta^{15}\text{N}$  in diamond ( $\delta^{15}\text{N} = (\text{sample}/\text{AIR})/(\text{sample}/\text{AIR}) - 1$ ), since this isotopic system can more clearly discriminate between AOC and sediment sources. We find that ~20% of all eclogitic diamonds of lithospheric origin have lower  $\delta^{15}\text{N}$  (< -7 ‰) than the convecting mantle, and ~80% have  $\delta^{15}\text{N} < 0$ , suggesting that a portion of the subducted endmember must have strongly negative  $\delta^{15}\text{N}$  (Fig. 3.3). Organic-rich sediments cannot satisfy this requirement, as their  $\delta^{15}\text{N}$  values are almost exclusively positive (Li et al. 2014). In contrast, AOC can satisfy this condition as it spans a large range of  $\delta^{15}\text{N}$  (-12 to +12 ‰), reflecting  $^{15}\text{N}$  depletion in high-temperature clays and  $^{15}\text{N}$  enrichment in low-temperature clays (Li et al. 2007, 2014). Thus, following Li et al. (2019), we suggest that the isotopic variability defining most eclogitic diamonds can be modeled by mixing between three AOC endmembers: 1) nitrogen-bearing high-T clay with mantle-derived carbon, 2) nitrogen-bearing low-T clay with DIC-equilibrium carbonate and 3) nitrogen-bearing low-T clay with biogenic AOC carbonate (Fig. 3.3). Given the absence of a strong sedimentary  $\delta^{15}\text{N}$  signal in lithospheric eclogitic diamonds, we suggest that sediments are an even more unlikely source of carbon in the deeper mantle sampled by sublithospheric diamonds. Interestingly, we note that all published asthenospheric and transition zone diamonds have  $\delta^{15}\text{N} > 0$  (Fig. 3.3), suggesting that

diamond formation in that section of the mantle is driven strictly by the uppermost portions of AOC that are rich in carbonate, i.e. endmembers 2 and 3.

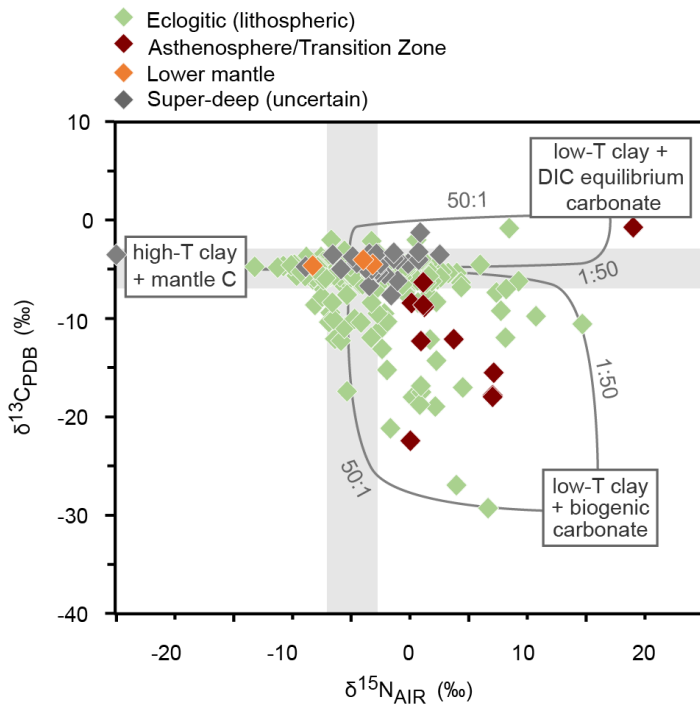


Figure 3.3. Worldwide database of  $\delta^{13}\text{C}$  and  $\delta^{15}\text{N}$  for diamonds of lithospheric and superdeep origin. MORB isotopic signatures are represented by the grey bands (Marty and Zimmermann 1999; Eiler et al. 2000a; Cooper et al. 2004, 2009). Bracketing the data are three AOC endmembers composed of nitrogen-bearing high-T clay or low-T clay, as well as carbon-bearing convecting mantle, DIC-equilibrium carbonate, or biogenic carbonate. Mixing lines between the endmembers and the mantle are N/C<sub>mantle</sub> / N/C<sub>AOC</sub> of 50:1 and 1:50 (Li et al. 2019). Superdeep diamonds include those of asthenospheric and transition zone origin (majoritic garnet and Ca-silicate inclusions), lower mantle origin (ferropericlase + MgSiO<sub>3</sub> or CaSiO<sub>3</sub> inclusions), and diamonds of uncertain super-deep origin (e.g., individual ferropericlase, ilmenite, coesite, and chromite inclusions). Note that asthenospheric/transition zone diamonds have exclusively positive  $\delta^{15}\text{N}$ , but variable  $\delta^{13}\text{C}$ .  $2\sigma$  errors are smaller than symbols. Source data and references: Table B9.

A carbonate-rich oceanic crust origin for superdeep diamonds is consistent with the majoritic garnet inclusions studied here. Not only are the inclusions offset towards the higher  $\delta^{18}\text{O}$  values recorded in oceanic crust carbonates (Fig. 3.1c), but the formation depths of majoritic garnets (7-19 GPa; Figure B1) also correlate well with the experimentally-constrained pressures at which subducted, carbonated metabasalt may melt (11-21 GPa; Kiseeva et al. 2013a). Experiments have demonstrated that slab-derived carbonatitic melt will crystallize diamond after injection into and reaction with the surrounding reduced convecting mantle, and will crystallize majoritic garnet upon cooling below the liquidus temperature (Bobrov et al. 2008; Walter et al. 2008; Thomson et al. 2016). We propose that the isotopic characteristics of these inclusions are principally derived from the AOC carbonate component, whereas the elemental characteristics are dependent on the degree of interaction with the surrounding mantle. High  $\Delta$ peridotite (more eclogitic) majoritic garnets likely crystallized from Mg-poor slab-derived carbonatitic melts ( $\text{Mg}/\text{O} \approx 0.05$ ;  $\text{Fe}/\text{O} \approx 0.04$ ;  $\text{Mg}\# \approx 55$ ; Thomson et al. 2016) that experienced little mantle contamination prior to carbonate reduction and resulting solidification and precipitation of diamond (Rohrbach and Schmidt 2011). Greater extents of interaction with the surrounding Mg-rich convecting mantle ( $\text{Mg}/\text{O} \approx 0.34$ ;  $\text{Mg}\# \approx 90$ ; Ringwood 1975) is evident in those meta-pyroxenitic majoritic garnets with elevated Mg#, but only extreme levels of interaction between melt and mantle could have produced the shift to lower  $\delta^{18}\text{O}$  that is seen in Jagersfontein majoritic garnets (Figure B2). Thus, the reaction between AOC-derived carbonatitic melt and convecting mantle created intermediate “mixed” elemental compositions, yet maintained the high  $\delta^{18}\text{O}$  values that are characteristic of extremely  $^{18}\text{O}$ -enriched AOC carbonate (Li et al. 2019).

### 3.3 Lower mantle diamonds

Whereas the strong  $^{18}\text{O}$  enrichment in majoritic garnets is related to subducted carbonated crust in the asthenosphere and transition zone, the first  $\delta^{18}\text{O}$  measurements made here of lower mantle retrogressed bridgmanites show no such  $^{18}\text{O}$  enrichment. Instead, the enstatite  $\delta^{18}\text{O}$  (+5.3 to +5.8 ‰), average Mg# of bridgmanite and ferropericlase inclusions (95.0 and 86.7, respectively), and host diamond  $\delta^{13}\text{C}$  (-3.5 to -4.1 ‰; Stachel et al. 2002; Palot et al. 2014) are all similar to estimates of fertile mantle that has not experienced significant exchange with recycled crustal material (Table B2; Katsura and Ito 1996; Wood 2000; Cartigny et al. 2014). This lack of an obvious crustal signature in sublithospheric diamonds or their inclusions is unusual (Stachel 2001), likely because slab-derived carbonate is generally required to increase carbon concentrations and stabilize diamond in the metal-bearing reduced deep mantle (> 8 GPa; Frost and McCammon 2008; Dasgupta and Hirschmann 2010; Rohrbach et al. 2014). Since the lower mantle is estimated to have 1 wt. % metal (Frost and McCammon 2008) and 16 – 500 ppm C (Hirschmann and Dasgupta 2009), iron metal and/or iron-carbides are the dominant carbon-bearing phases at these depths (Dasgupta and Hirschmann 2010; Rohrbach et al. 2014). In order to produce macrocrystalline lower mantle diamonds without carbonate input, the carbon in metal alloys needs to be mobilized and locally concentrated. One process of achieving this is via the introduction of a dehydrating slab into the lower mantle (Faccenda 2014; Schmandt et al. 2014), because carbon-bearing metal alloys are unstable in hydrated environments (Zhu et al. 2019). The local destabilization of ~1 wt.% carbon-bearing metal alloys requires limited lithosphere-derived  $\text{H}_2\text{O}$  (Zhu et al. 2019), which would not significantly affect the ambient lower mantle  $\delta^{18}\text{O}$ . Therefore, we speculate that dehydration of a carbonate-depleted subducting oceanic lithosphere can trigger the metasomatic mobilization of ambient carbon for lower mantle

diamond formation, without imposing a crustal signature on the resulting diamonds and their inclusions.

### **3.4 The lithospheric to lower mantle carbon cycle**

The contrasting stable isotope composition of diamonds and their silicate inclusions at lithospheric, transition zone, and lower mantle depths suggest profound differences in the modes of diamond formation, and the behavior of volatiles through these mantle regions. The absence of a clear sediment-derived geochemical signal at diamond-forming depths has implications for the efficiency with which carbon is recycled within Earth's mantle, and suggests that volatile elements in sediments may be efficiently recycled back to the surface during arc volcanism or stored in shallow accretionary prisms (Kelemen and Manning 2015). Instead, we document geochemical evidence for the deep cycling of carbonated AOC as a source of lithospheric to transition zone diamonds. Furthermore, diamonds from even deeper, in the uppermost lower mantle show no evidence of such subducted crustal carbon or oxygen mass flux. We suggest that these diamonds crystallized after the dehydrating slab triggered the mobilization of convecting mantle carbon from its metallic hosts. This change of the diamond-forming environment from a carbonated slab melt in the transition zone to a slab-hydrated lower mantle is consistent with experimental evidence that demonstrates major obstacles to transporting AOC carbonates to lower mantle depths along typical slab thermal trajectories (Thomson et al. 2016). Our study, therefore, supports a barrier to carbon subduction above the lower mantle (Thomson et al. 2016).

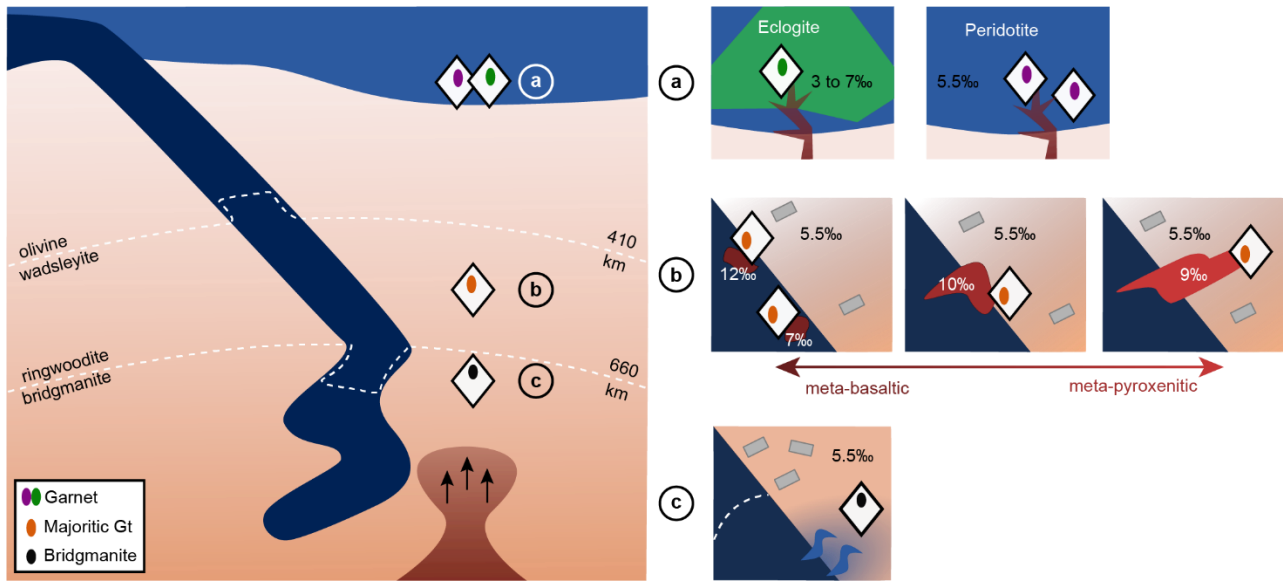


Figure 3.4. Model of diamond formation in the lithosphere, transition zone, and lower mantle. **(a)** Lithospheric diamond forms by fluid or melt metasomatism of eclogitic and peridotitic substrates (Stachel and Luth 2015), but the  $\delta^{18}\text{O}$  of the inclusions is buffered by the host lithology (Riches et al. 2016). **(b)** In the transition zone, the carbonate-rich upper portion of a subducting slab produces carbonatitic melt. Diamonds and majoritic garnets inclusions crystallize during the interaction of the carbonatitic melt with reduced, metal-bearing convecting mantle. The short melt migration path and limited interaction with convecting mantle produces majorite with eclogitic compositions and elevated  $\delta^{18}\text{O}$ , directly reflecting the local carbonated AOC melt source. Greater levels of interaction with the convecting mantle is reflected in the lower  $\delta^{18}\text{O}$  and increasingly ultrabasic, meta-pyroxenitic character of some majorites. **(c)** As the slab penetrates into the lower mantle, the negative pressure-temperature slope (i.e. Clapeyron slope) of the post-spinel transition (Irifune and Ringwood 1987) and the delayed garnet to perovskite transition in metabasaltic lithologies (Ono et al. 2001) retards the formation of lower mantle minerals (dotted white line). The transition to a lower mantle mineralogy leads to slab dehydration and the hydration of the surrounding mantle. The hydrated ambient mantle releases carbon from its metallic iron hosts to form diamond.

### 3.5 Methods

Enstatite and garnet inclusions in diamond were analyzed using a Cameca IMS 1280 multicollector ion microprobe with  $\sim 2$  nA  $^{33}\text{Cs}^+$  primary beam and 20 keV impact energy. Analytical methods and standards for garnets are previously published (Ickert and Stern 2013). The presence of high- $\text{Cr}_2\text{O}_3$  lithospheric garnets required the development of a new matrix correction. Olivine and high- $\text{Cr}_2\text{O}_3$  garnet pairs from depleted peridotite xenoliths were cast into epoxy and pressed into indium mounts along with garnet and olivine reference material. Olivine  $\delta^{18}\text{O}$  values were all within error of mantle values, suggesting that associated garnets should be also within the expected convecting mantle  $\delta^{18}\text{O}$  range. Instead, a plot of garnet  $\text{Cr}_2\text{O}_3$  vs.  $\delta^{18}\text{O}$  defines a positive slope that reaches  $\sim 1\ \text{\textperthousand}$  above the mantle range at high  $\text{Cr}_2\text{O}_3$  contents (Figure B3). A Cr-related matrix effect has been previously suggested (Wang et al. 2011), but variable laser fluorination yields of Cr-rich minerals have inhibited a robust determination of the calibration. Our method bypasses the need for laser fluorination of high Cr-garnets, being instead based on laser fluorination of a low Cr-garnet (S0068) and a reasonable assumption of mineral isotopic equilibrium at mantle temperatures. Using this calibration, the 95% confidence uncertainty estimates for  $\delta^{18}\text{O}_{\text{VSMOW}}$  for garnets averaged  $\pm 0.29\ \text{\textperthousand}$ . Enstatite  $\delta^{18}\text{O}$  measurements also required the development of a new calibration for Mg# (Figure B4) using laser fluorination results (Mattey et al. 1994) for sample F866 (94.1 Mg#) and CCIM standard S0170 (91.2 Mg#). For analyses of unknown enstatites, the 95% confidence uncertainty estimates for  $\delta^{18}\text{O}_{\text{VSMOW}}$  average  $\pm 0.21\ \text{\textperthousand}$ . Adjacent to each ion probe crater, major element data were collected on a Cameca SX100 with 5 wavelength dispersive spectrometers at 20 keV energy and 20 nA of beam current at 1  $\mu\text{m}$  diameter. The counting time was 30 seconds for all elements. Detection limits are available at the bottom of the Table B1 and standards are reported

in Table B3.

A parameter,  $\Delta_{\text{peridotite}}$ , was applied to majoritic garnets to describe the deviation from a pure meta-peridotitic endmember:

$$\Delta_{\text{peridotite}} = \frac{|(Mg+Ca+Fe+Mn)_s - (m_p(Si+Ti)_s + b_p)|}{|(m_e(Si+Ti)_s + b_e) - (m_p(Si+Ti)_s + b_p)|} \quad \text{Equation 1}$$

where  $m$  is the slope of the endmember substitution,  $b$  is the y-intercept of the endmember,  $p$  and  $e$  are the meta-peridotite and eclogitic endmembers, respectively, and  $s$  is the majoritic sample. Fe indicates total iron.

## **Chapter 4**

### **Blue diamonds document the subduction of seafloor boron to the lower mantle**

#### **Chapter Summary**

Many of the geophysical anomalies in the deep mantle can be attributed to regions of volatile-assisted melting (Ni et al. 2011; Andrault et al. 2014; Schmandt et al. 2014). The origin of these volatile-enriched domains is uncertain given the poor constraints on deep mantle composition and the depths to which volatile elements can be transported by subducting slabs. Boron-bearing blue diamonds (Type IIb) of sublithospheric origin provide snapshots of the behavior of volatile elements at great depths. Here, in this combined trace elemental, isotopic, and mineralogical study of 26 blue diamonds, we report unequivocal evidence of the presence of subducted boron and carbon in the lower mantle prior to the eruption of the Cullinan kimberlite 1.1 billion years ago. Measured carbon isotopes ( $\delta^{13}\text{C}$  of -1.8 to -20.6 ‰) match those of carbonated oceanic slabs, whereas boron isotopes ( $\delta^{11}\text{B}$  of -9 to 0 ‰) indicate a  $^{11}\text{B}$ -enriched source relative to MORB source mantle – likely derived from post-serpentinite phases found in the meta-peridotitic portions of slabs. These data, along with mineralogical and trace elemental characteristics of the diamonds and their inclusions, suggest that blue diamonds crystallized during the infiltration of carbonatitic slab melt into the reduced lower mantle and transition zone. The similar boron isotope signatures of blue diamond, oceanic island

basalts, and carbonatites suggest that the same boron-bearing phases that melted out of the slab to form the Cullinan blue diamonds in the Precambrian may have later pervaded the deepest regions of the mantle and contaminated the sources of deep-seated magmas (Hulett et al. 2016; Woodhead et al. 2019).

## 4.1 Introduction

Various mantle-derived magmas are sourced from volatile-rich regions of Earth's deep mantle (Sobolev et al. 2016; Foley et al. 2019). While the subduction of oceanic lithosphere across the 660 km seismic discontinuity provides a potential mechanism for deep volatile enrichment (Creager and Jordan 1984; Bercovici and Karato 2003), the lithologies and mineral phases that retain their volatile elements to lower mantle depths are uncertain. Boron-bearing blue diamonds provide an opportunity to examine the deep carbon and boron cycles, due to their interpreted transition zone and lower mantle origin (Smith et al. 2018). Although a recent study suggested a subducted origin for the elevated levels of boron impurities in blue diamonds (Smith et al. 2018), critical isotopic tracers of such an origin have remained elusive due to the challenges of analyzing ultra-trace impurities in these gem-quality samples.

Boron isotope geochemistry is an ideal tracer of subducted material in the deep mantle due to the highly distinctive fractionations that are generated in low-temperature crustal environments. Despite the blurring of these distinctive isotopic fractionations during the preferential loss of the fluid-mobile  $^{11}\text{B}$  isotope as a subducting slab dehydrates, the isotopic resolving power between crust and mantle environments remains strong (De Hoog and Savov 2018). Although there are numerous successful applications of boron isotopic geochemistry to volcanic arc magmatism (e.g. De Hoog and Savov 2018), few studies have attempted to apply this system to investigations of

deeper mantle processes (e.g. Chaussidon and Marty 1995; Hulett et al. 2016). This study on blue diamonds marks the first boron isotopic measurements on material sourced directly from transition zone to lower mantle depths and is coupled with mineralogical and elemental characterization of the mineral inclusions and matrix impurities of blue diamonds.

## 4.2 Ca-rich superdeep medium

In this study, we focus on a suite of 23 fragments of blue diamonds from the Cullinan mine (Kaapvaal craton, South Africa) and 3 of unknown origin (Table C2). While the vast majority of diamonds in our sample suite are inclusion-free, sample 110208425476 was previously reported to contain ferropericlase, olivine and nyerereite ( $\text{Na}_2\text{Ca}(\text{CO}_3)_2$ ) inclusions and sample DVBT was reported to contain inclusions of breyite (walstromite-structured  $\text{CaSiO}_3$ ) and an Fe-Ni-S alloy (Smith et al. 2018). Two additional samples from the Cullinan suite (Blue 2 and NL247-2) have visible inclusions of bimineralic breyite and  $\text{Ca}_2\text{SiO}_4$ -larnite and a single inclusion of enstatite, as identified by Raman spectroscopy (Fig. 4.1). X-ray fluorescence mapping of these inclusions indicates that Fe-Ni rich alloys surround both inclusion types (Fig. C1).

Given the presence of enstatite and Ca-silicate inclusions in a single diamond, the simplest interpretation is that these minerals were entrapped as bridgmanite and Ca-perovskite in the lower mantle. However, the lack of titanite-structured  $\text{CaSi}_2\text{O}_5$  in the breyite ( $\text{CaSiO}_3$ ) and larnite ( $\text{Ca}_2\text{SiO}_4$ ) bimineralic inclusions in this study and in Smith et al. (2018) indicates a bulk inclusion Ca/Si ratio of greater than 1 (Brenker et al. 2005). This bulk chemistry cannot simply represent a retrogressed Ca-perovskite ( $\text{CaSiO}_3$ ) and must instead be derived from a medium with a much higher Ca/Si ratio than pyrolite (~0.1; Ringwood, 1975). Such extreme environments are

commonly produced in experimental carbonatitic melts of carbonate-rich oceanic slab material ( $\text{Ca/Si} \sim 25$  at  $>20$  GPa; Thomson et al. 2016). The percolation of these melts into the surrounding reduced mantle has been shown to crystallize diamond through the reduction, or “freezing” of carbonate, and also produces mineral inclusions with compositions that lie between the Ca-rich carbonatitic and meta-peridotitic endmembers (Palyanov et al. 2013; Kiseeva et al. 2013b; Thomson et al. 2016; Chapter 3). In this study, the recovery of a high Mg# mineral that was associated with the retrogressed bridgmanite inclusion (discussion in Methods; Table C3), the preservation of reduced Fe-Ni rich alloys, and the modest enrichment of light rare earth elements (LREE) in the blue diamond matrix suggests that these samples must have formed after extensive interaction with the surrounding convecting mantle. Thus, I submit that the transition zone to lower mantle substrates in which these blue diamonds formed must have intermediate compositions that reflect the evolving composition of a percolating Ca-rich carbonatitic slab melt.

### 4.3 Slab-derived isotopic signatures

Further evidence in support of a slab-related crystallization environment for the blue diamonds and their inclusions is provided by boron and carbon isotopic measurements of the diamond matrix. The  $\delta^{13}\text{C}$  of blue diamond are highly variable across the sample suite (-1.8 to -20.6 ‰), similar to the  $\delta^{13}\text{C}$  of eclogitic diamonds from the lithospheric mantle (Fig. 4.2b). But unlike eclogitic diamonds, blue diamonds do not display a prominent mode at the canonical mantle value of -5 ‰ (Fig. 4.2b). This lack of a mode at -5 ‰ is typical for superdeep diamonds that crystallize from melts of the carbonate-rich upper portions of igneous oceanic lithosphere (e.g. majoritic garnet-bearing superdeep diamonds; Chapter 3; Fig. 4.2b). Moreover, the first isotopic analyses of the boron impurities in blue diamonds reveal a range of  $\delta^{11}\text{B}$  from -9 to 0 ‰ ( $n=11$ ; see Methods

for analytical procedure). These values range well above that of convecting mantle as represented by MORB-source mantle ( $-7.1 \pm 0.9\text{‰}$ ; Marschall, 2018) and strongly implicate a slab-related origin for the boron carried by these diamonds (Fig. 4.3).

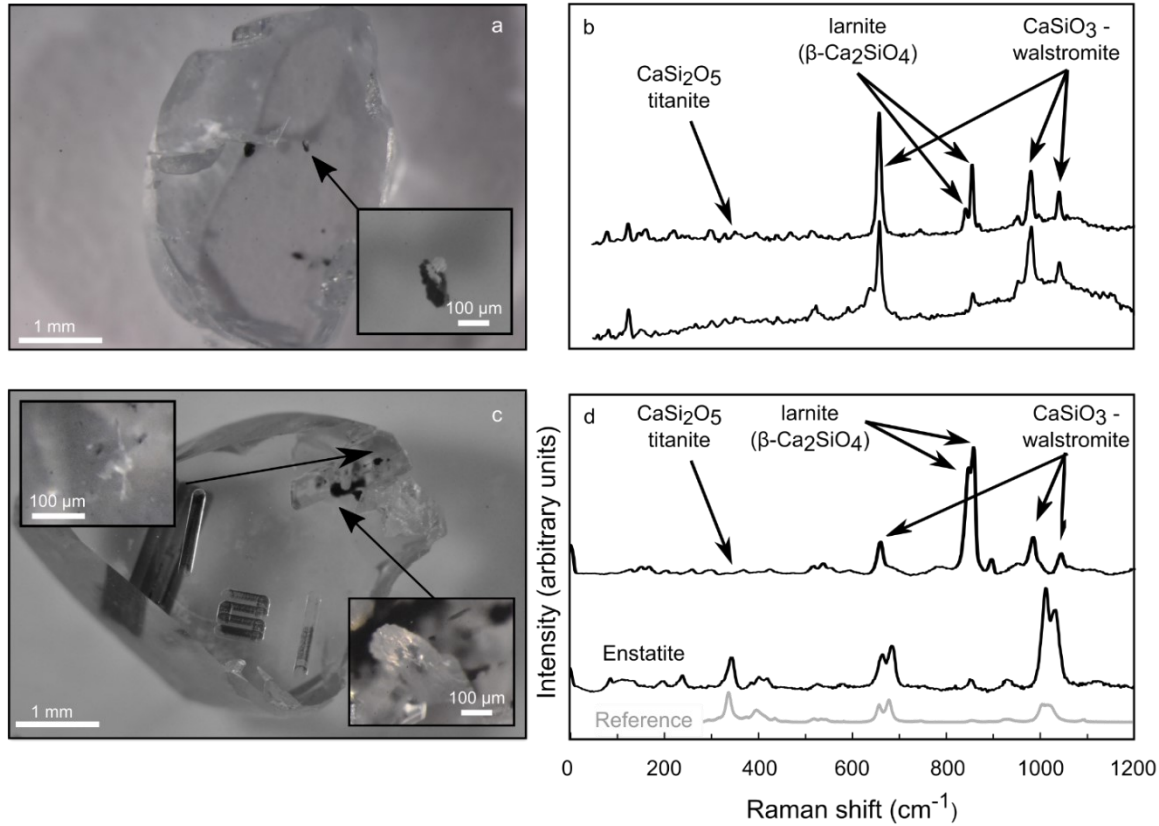


Figure 4.1. Optical photographs and Raman spectra of inclusion-bearing blue diamonds. (a) Photo of sample NL247-2 and a high magnification inset of a selected mineral inclusion. The black ring around the inclusion is composed of an Fe-Ni rich alloy as determined by  $\mu$ XRF (Fig. C1). (b) Raman spectra from two bimimetic Ca-silicate inclusions. Note that the Ca-poor CaSi<sub>2</sub>O<sub>5</sub>-titanite phase is absent in these spectra and in the Ca-silicate inclusions reported by Smith et al. (2018). (c) Optical photo of Blue 2 with an inset of an enstatite and a bimimetic Ca-silicate inclusion. Dark patterns on the surface of diamond are laser ablation rasters. (d) Selected spectra for sample Blue 2 include a bimimetic Ca-silicate inclusion, an enstatite inclusion, and a reference enstatite spectrum from the RRUFF database (Lafuente et al. 2016). The CaSi<sub>2</sub>O<sub>5</sub>-titanite phase is also absent from the Ca-silicate spectrum in this sample.

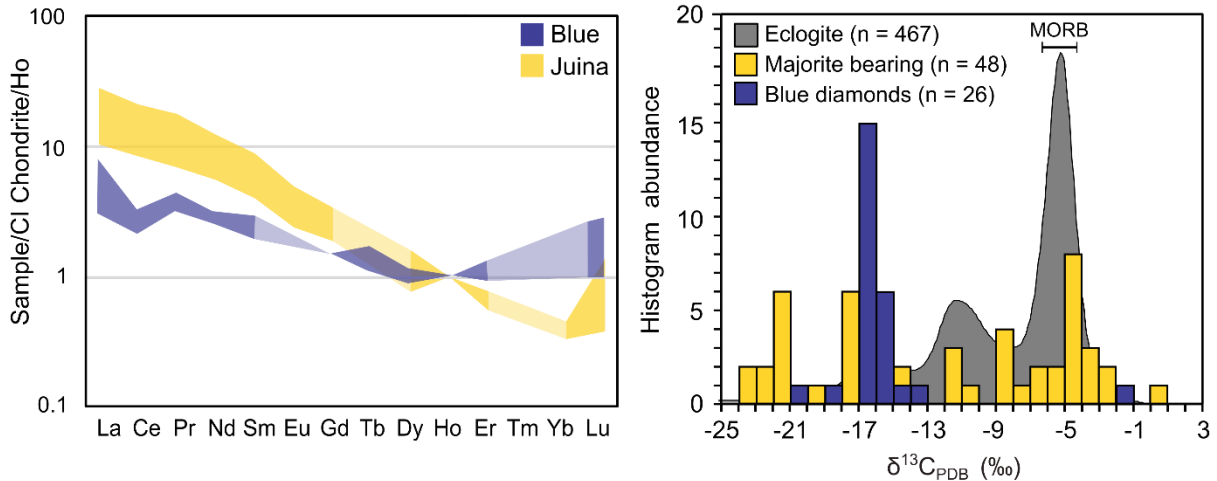


Figure 4.2. Rare earth element and carbon isotope values for the blue diamond matrices. (a) Blue diamonds have a moderate REE slope ( $\text{La}_{\text{N}}/\text{Ho}_{\text{N}} < 11$ ) compared to Juina superdeep diamonds ( $\text{La}_{\text{N}}/\text{Ho}_{\text{N}} < 35$ ; Group III; Timmerman et al. 2019). Dark colored fields indicate the interquartile range. Lighter colors (e.g. Tm) are interpolated patterns for data that lies below the limit of quantification (blank +  $7\sigma$ ). See appendix C1.2 for details on data selection and Fig. C7, Fig. C8 for individual patterns. (b) Histogram of carbon isotopic composition of blue diamonds compared to superdeep diamonds with inclusions of majoritic garnet. The background probability distribution function is the relative  $\delta^{13}\text{C}$  distribution for eclogitic diamonds from the lithosphere. Bandwidth is 0.5 ‰ and analytical precision ( $2\sigma$ ) is  $\sim 0.1$  ‰ for all samples. MORB-source mantle  $\delta^{13}\text{C}$  is indicated at top (Marty and Zimmermann 1999). Note that superdeep diamonds have a less prominent mode at -5 ‰ than eclogitic diamonds from the lithosphere. The mode at -17 ‰ may be an artifact due to the low number of analyzed blue diamonds and the oversampling of diamonds from one source. Source data in Table B8.

The measured boron and carbon isotopic values of the blue diamonds from the Cullinan mine are best described by melt-mantle mixing models that have initial melt  $\delta^{11}\text{B}$  values that range from 0 ‰ to +15 ‰ (Fig. 4.3). These values are considerably more positive than MORB-source mantle and are slightly above the range expected for boron within highly metamorphosed sediments and altered oceanic crust (AOC). Analyses of metamorphosed sediments and AOC have demonstrated that both reservoirs experience large degrees of fluid and  $^{11}\text{B}$  loss during metamorphic dehydration at low pressures and temperatures. In fact, modeling of subducting sediment and

AOC has indicated that more than half of the <100 ppm B in these components may be removed after only 7-30% fluid loss and that AOC may retain a  $\delta^{11}\text{B}$  of approximately -10 to -30 ‰ after subduction to ~2.5 GPa (Ishikawa and Nakamura 1993; Smith et al. 1995; Rose et al. 2001; Marschall et al. 2007). Thus, while the  $\delta^{11}\text{B}$  values of blue diamonds are unambiguously indicative of a slab-related origin, the boron they contain is unlikely to be sourced directly from sedimentary or crustal sections of subducting slabs.

Given the boron-poor,  $^{11}\text{B}$ -depleted nature of subducted and dehydrated AOC and sediments, additional reservoirs are required to produce blue diamonds with up to 8 ppm B (Gaillou et al. 2012) and  $\delta^{11}\text{B} \leq 0$  ‰. One possible source is slab serpentinite, which maintains elevated  $\delta^{11}\text{B}$  even under eclogite facies conditions (+12 to +34 ‰; Martin et al. 2020). Relatively  $^{11}\text{B}$ -enriched signatures may persist into the transition zone and deeper if the serpentine recrystallizes into olivine and its polymorphs (De Hoog et al., 2014), or dense hydrous magnesium silicates (DHMS; Scambelluri and Tonarini, 2012). An alternative  $^{11}\text{B}$ -enriched host phase that is stable in the deep mantle is slab carbonates, which are variably enriched in boron (e.g. 11-71 ppm B; Hemming and Hanson 1992; De Hoog and Savov 2018). While the  $\delta^{11}\text{B}$  values of metamorphosed carbonates have not yet been reported, they should maintain their initial  $^{11}\text{B}$ -enriched values (+15 to +25 ‰; (Rae 2018), as carbonates cannot experience dehydration.

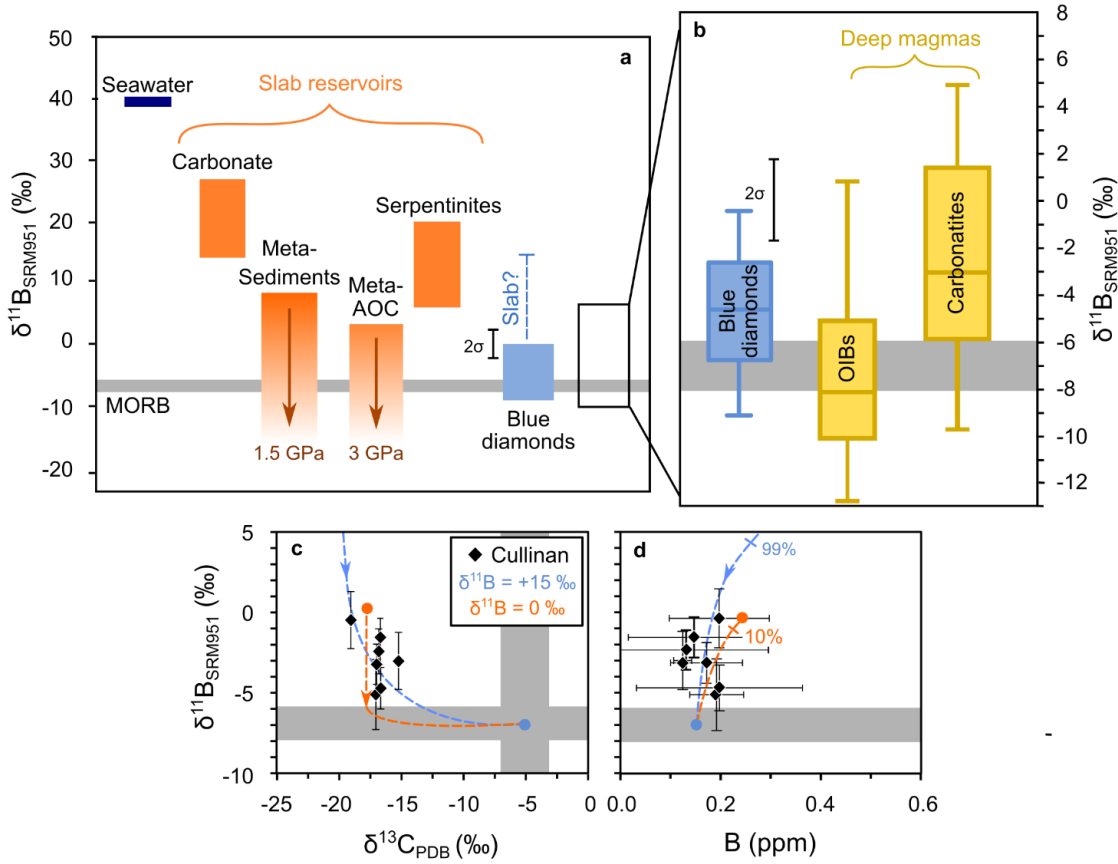


Figure 4.3. Boron isotope signature of blue diamonds and other reservoirs. (a)  $\delta^{11}\text{B}$  of blue diamonds, compared to the ranges of seawater, MORB ( $-7.1 \pm 0.9 \text{\textperthousand}$ ; Marschall, 2018), carbonate (Rae 2018), metamorphosed sediments, metamorphosed altered oceanic crust (meta-AOC; source data Table C10), and serpentinites (Marschall 2018). The typical  $2\sigma$  of blue diamonds includes repeat analysis on secondary standards. The arrows in meta-sediments and meta-AOC indicate the direction of isotope fractionation during progressive dehydration during subduction, which lowers the  $\delta^{11}\text{B}$  and boron content (decreasing color gradient). The maximum pressures experienced by the plotted meta-AOC and meta-sediments are indicated. The blue broken line indicates the possible range of initial slab melt  $\delta^{11}\text{B}$ , as determined from panels c,d. (b)  $\delta^{11}\text{B}$  of blue diamond ( $n = 11$ ; this study), ocean island basalts (OIBs;  $n = 48$ ; Table C8) and carbonatites ( $n = 23$ ; Table C9) indicated in a box and whisker plot.  $\delta^{11}\text{B}$  of MORB ( $-7 \pm 1$ ) is indicated by the gray field (Marschall 2018). (c) Possible melt-mantle mixing models for C and B isotopes of blue diamonds from Cullinan. Mantle B (0.15 ppm), C (50 ppm),  $\delta^{11}\text{B}$  ( $-7 \text{\textperthousand}$ ),  $\delta^{13}\text{C}$  ( $-5 \text{\textperthousand}$ ) and slab melt C (45 mol %; Thomson et al. 2016) are constant between models. Slab melt  $\delta^{11}\text{B}$ ,  $\delta^{13}\text{C}$ , and boron content varies between  $+15 \text{\textperthousand}$ ,  $-20 \text{\textperthousand}$ , 50 ppm B in the blue model and 0  $\text{\textperthousand}$ ,  $-18 \text{\textperthousand}$ , and 0.2 ppm B in the orange. (d) The same mixing models are fit through  $\delta^{11}\text{B}$  and CL- and SIMS-determined B content. Crosshatches indicate the percentage of convecting mantle material in the melt at that point.

#### **4.4 Deep volatile cycles and the formation of blue diamonds**

The elemental and isotopic requirements for a seafloor-altered, calcic to ultramafic medium for blue diamond formation support a model where slab-derived carbonatitic melt is reduced to diamond upon reaction with the surrounding mantle. This type of model typically relies on the melting of carbonated metabasaltic slabs after the lowering of their solidi by a Na-rich carbonate phase, and is generally invoked for the formation of majoritic garnet-bearing, low boron diamonds in the asthenosphere to upper transition zone (~7 to ~19 GPa; Chapter 3; Thomson et al. 2016). However, this boron-free, upper transition zone model may not be directly applicable to the boron-rich, lower mantle blue diamonds in this study. Instead, I suggest that carbonates in Na-poor lithologies (Na-poor eclogite or meta-peridotite), which are not depleted during slab melting in the upper transition zone, may provide an alternative source of carbon at these deeper depths.

While Na-poor carbonated lithologies may be a potential source of carbon at lower mantle depths, a reasonable model of blue diamond formation must rationalize the mobilization of this carbonate and justify the elevated levels of boron in these diamonds. These requirements can be met given the destabilization of several  $^{11}\text{B}$ -enriched hydrous post-serpentinite phases at these pressures. These phases include DHMS (Phase D and Phase B) under cold slab geotherms, and ringwoodite under hot slab geotherms (Fig. C9; Ohtani et al. 2000; Harte 2010; Nishi et al. 2014; Cannaò et al. 2020). Since serpentinites can contain significant boron (up to ~100 ppm B; Marschall, 2018), the water-induced melting of the carbonate-rich slab lithologies following the destabilization of hydrous post-serpentinite phases could produce boron-rich carbonatitic melts, which could form blue diamonds upon reaction with the reduced convecting mantle (Fig. 4.4).

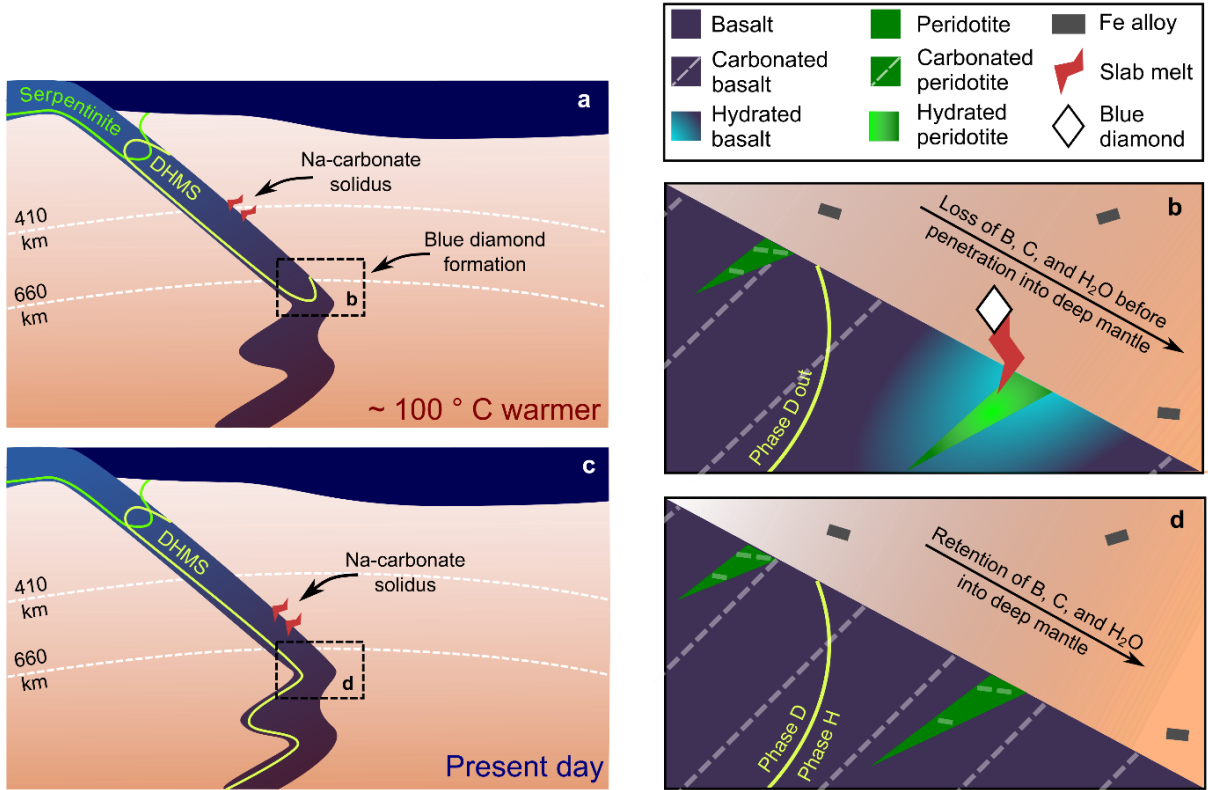


Figure 4.4. Transfer and remobilization of slab-derived volatiles - B, C, and H<sub>2</sub>O - in the Mesoproterozoic and current day deep mantle. Most subducting slabs will cross a Na-carbonate metabasaltic solidus in the transition zone but retain carbonate in Na-poor meta-basaltic and meta-peridotite portions of the slab. **(a)** The Mesoproterozoic mantle temperature is somewhat warmer (~ 100 °C; Vlaar et al. 1994). **(b)** Post-serpentinite phases, such as dense hydrous magnesium silicates (DHMS), are stable in the meta-peridotitic portion of the slab until the uppermost lower mantle, where their destabilization leads to hydrous melting of the surrounding carbonate-rich meta-peridotitic and Na-poor metabasaltic portions of the slab. Injection of the oxidized carbonatitic melt into the surrounding reduced convecting mantle produces blue diamonds via redox reactions. **(c,d)** Present-day cold slab geotherms allow for the transfer of volatiles (H<sub>2</sub>O, C and B) and incompatible elements into the deeper lower mantle within Na-poor carbonates and DHMS (e.g. Phase H; Nishi et al., 2014).

An examination of Fig. 4.3b reveals a striking similarity between the boron isotopic composition of blue diamonds and those of mantle carbonatites and ocean island basalts (OIB) that are free from crustal contamination (0.04 to 2.6 ppm B; Chaussidon and Marty 1995; Tanaka and Nakamura 2005; Hulett et al. 2016; Çimen et al. 2018, 2019). Given that these two types of magmas have long been shown to contain recycled lithospheric components in their source regions (Hofmann 1997; Hoernle et al. 2002), I suggest that deep-seated proto-carbonatite and OIB magmatism may tap a reservoir that was contaminated by the same slab components that contributed boron to the blue diamonds in this study. The Cullinan diamonds, which must have crystallized prior to kimberlite eruption at ~1.1 Ga (Wu et al. 2013), may have experienced ambient mantle temperatures ~100 °C greater than present (Vlaar et al. 1994). At these temperatures, even the coolest geotherms would likely exceed the stability of DHMS at uppermost lower mantle depths. This implies that a significant fraction of subducting slabs would have experienced both Na-rich carbonate melting in the upper mantle and dehydration-driven Na-poor carbonate melting in the uppermost lower mantle before penetration into the deep lower mantle. This extensive melt depletion may have acted as a barrier to volatile subduction and kept the deeper portions of the lower mantle relatively pristine and isolated from incompatible and volatile-rich components of the upper portions of slabs (Fig. 4.4).

Over time, the cooling of Earth's mantle may have allowed subducting slabs to remain within the stability field of DHMS - including phase H, which is stable to depths of greater than 1,250 km under cool geotherms (Fig. C9; Nishi et al., 2014). This retention of water-bearing phases would prevent Na-poor carbonate melting and blue diamond formation, even as the subducting lithosphere moved to deep lower mantle depths. Intriguingly, mantle-derived carbonatites become

systematically  $^{11}\text{B}$ -enriched only in the recent geologic past (< 250 Ma), around the same time that deep-seated kimberlites show significant incompatible element contamination in their sources (Hulett et al. 2016; Woodhead et al. 2019). I suggest that these isotopic deviations in deep-seated Mesozoic magmas may reflect the point at which sufficient cooling of the ambient mantle permitted slabs to translate their incompatible element and volatile cargo into the deep lower mantle. Therefore, this study of the deep mantle boron cycle not only illuminates strict geothermal constraints for the formation of ultra-valuable blue diamond, but also identifies the reservoirs responsible for chemically diversifying the mantle sources of Earth's deepest derived melts.

## 4.5 Methods

### 4.5.1 Quantification of N and B impurities and the C isotopic composition of blue diamonds

Diamonds were mounted in epoxy and/or indium for CL imaging and secondary ion mass spectrometry (SIMS) analysis at the Canadian Centre for Isotopic Microanalysis. CL imaging was completed using a Zeiss EVO MA15 scanning electron microscope (SEM), with a broadband photomultiplier detector, operating at 15 kV and 3 – 5 nA beam current. Carbon isotopes ( $^{13}\text{C}/^{12}\text{C}$ ) and N abundances were determined in separate ion probe sessions using methods and reference materials detailed in Stern et al. (2014). Most of the diamonds in this study have exceedingly low N contents, such that background contributions due to residual gases in the analysis chamber were the limiting factor in the detection limits. For two sessions, one with and one without a liquid nitrogen cold finger, it was determined that the backgrounds were equivalent to  $\sim 0.35$  ppm and  $\sim 0.5$  ppm, respectively, and that all but one of the blue diamonds (sample AB) had nitrogen concentrations below these values.

Boron abundances in diamonds were determined by simultaneously measuring  $^{11}\text{B}^-/\text{C}^-$  in an electron multiplier-Faraday cup (C - H1) combination over a 100 s counting interval using a  $\text{Cs}^+$  beam of 1.5 – 2.0 nA (Table C2). Mass resolution of >2000 easily resolved the isobar  $^{10}\text{BH}^-$ . Background count rates of  $^{11}\text{B}^-$  based on analysis of a particular growth zone in a Type 1, nominally boron-free diamond (NL247-23) gave repeated zero counts in the 100 s counting interval, and another with 0.01 cps, which is equivalent to a background contribution of < 0.2 ng/g B. The measurements were quantified using the boron concentration of sample NL247-20 as a primary standard, which was determined by hyperspectral cathodoluminescence (CL; Fig. C3). NL247-20 was chosen because of its extremely homogeneous nitrogen and boron abundances as determined by ion probe analyses and CL imaging. The hyperspectral CL measurements utilized a FEI Quanata 250 field emission gun SEM with a Gatan cryo-stage at the University of Calgary. The ratio of bound to free excitons at 102 K defined a calibration curve that enabled B concentration determination (Barjon et al. 2011).

#### **4.5.2 Boron isotopic analyses – method development and accuracy tests**

Laser ablations for boron isotopic analyses were conducted using an offline, 193 nm ArF Excimer laser system at the University of Alberta with the ablation product being collected in a custom-made Teflon ablation cell that was capped with a silica glass window (e.g. Krebs et al. 2019). All sample handling and cleaning took place in ULPA-filtered class 10 laminar flow hoods. Prior to the ablations, the ablation cells and sample vials were cleaned in 6 M HCl and concentrated  $\text{HNO}_3$  for more than 48 hours, and the silica glass windows were cleaned in 5% HF for 3 minutes and 6M HCl and 8M  $\text{HNO}_3$  for more than 48 hrs. In order to assess the accuracy of the analytical

method, two 1 cm pressed pellet biogenic reference materials, previously determined for their boron isotopic composition (Gutjahr, in review; Farmer et al. 2016), were ablated after cleaning in  $18.2 \Omega \cdot \text{cm} \text{ H}_2\text{O}$  and 0.5 M HNO<sub>3</sub>. The resulting ablation products, corresponding to 1.5 – 9.7 mg CaCO<sub>3</sub>, were collected in ~1 mL of  $18.2 \Omega \cdot \text{cm} \text{ H}_2\text{O}$ . Boron was separated from this solution following the method outlined in Foster (2008) and Foster et al. (2013). Briefly, this solution was loaded in a 2 M sodium acetate-0.5 M acetic acid buffer, collected using an anionic exchange resin (Amberlite IRA 743; Kiss 1988), and eluted in 0.5 M HNO<sub>3</sub>, which was necessary to remove the Ca-rich matrix and hence reduce space charge matrix effects in the plasma (Foster 2008; Foster et al. 2013). Subsequent solution-based MC-ICPMS was completed on a Thermo Neptune MC-ICPMS with a PFA spray chamber and two  $10^{12} \Omega$  amplifiers at the National Oceanographic Centre, University of Southampton using well established methods (Foster 2008; Foster et al. 2013). The sample gas was tuned daily to optimize ratio stability on NIST SRM 951, which generally resulted in a small loss of signal intensity (~0.6V per 50 ppb B at ~60 µL/min uptake rate), and ammonia gas was added to ensure an efficient B signal wash-out time and to reduce memory effects. Instrumental mass bias was corrected using rapidly bracketed 35-50 ppb NIST SRM 951 boric acid standard, as prior work has shown that it is not necessary to match concentrations within the concentrations measured here (Foster 2008). Secondary standards included ERM-AE120, and a 5 ppb solution of NIST SRM 951 was used as an internal consistency standard to check for ratio drift and accuracy of low concentration analyses. The take-up rate was approximately ~60 µL/min. Despite probable leaching effects during the H<sub>2</sub>O-based collection of the ablation products, the measurements of the ablated coral standards (JCp-1 and JCt-1) reproduced the known δ<sup>11</sup>B within 2‰ (Table C1; Gutjahr, in review; Farmer et al. 2016), suggesting that this method is accurate for B isotopic analyses at this level of precision.

Replicate ablations were also completed on synthetic, B-doped diamonds to determine the analytical precision of the method. The diamonds were cleaned in acid prior to ablation (concentrated HF, HCl, HNO<sub>3</sub>). The ablated material, corresponding to 1.1 – 2.6 mg diamond, was collected in 0.25-0.5 mL dilute nitric acid. Column chemistry for the diamond samples was not necessary, given that the matrix carbon dissipates as CO<sub>2</sub> in the ambient atmosphere of the closed ablation cell. Standard-bracketed sample measurements were corrected by repetitive measurements on the sample acid blank. Six repeat attempts over 4 different ablation sessions characterized multiple cuts of a synthetic, B-doped diamond (0.2 to 18 ppm B) and produced a reproducible δ<sup>11</sup>B of 2.6 ‰ ± 0.8 ‰ 2σ (Table C1). The analyses varied greatly in laser fluence (4-7 J/cm<sup>2</sup>), ablated material weight, dissolved B concentration, and solution volume. Thus, the precision of these synthetic diamond δ<sup>11</sup>B analyses, along with the accurate δ<sup>11</sup>B of the coral standards, suggest that our procedure produces δ<sup>11</sup>B measurements of natural diamonds within ~2 ‰, which is deemed sufficient for the purposes of this study.

#### **4.5.3 Boron isotopic analyses – natural blue diamonds**

Ablations of natural blue diamonds were completed in the same sessions as ablations on synthetic blue diamonds and utilized identical analytical procedures. Early ablations that utilized higher fluences (5-7 J/cm<sup>2</sup> measured at the site of ablation) resulted in heavy diamond fragmentation, graphitization, and viscous solutions that may have indicated contamination of the solution with melted Teflon due to the conductive nature of the diamonds. Lower fluences (~4 J/cm<sup>2</sup>) were favored during later ablations (September 2019 & February 2020) as they yielded much less graphitization, less heat, and resulted in non-viscous solutions. The ablations of the natural

diamonds corresponded to 1.5 – 8.5 mg diamond and yielded an average of 4 ppb (1 ng) B, with a range from 2-6 ppb (0.5 – 1.5 ng) B solutions (Fig. C4; Fig C5). These concentrations approximated, within 80%, the calculated total B yield, which utilized the ion-probe determined B concentrations and the weights of the diamonds before and after ablation. Two total procedural blanks (TPB) were determined for each batch of samples processed (n=6). These were prepared by placing a diamond into an ablation cell, capping the cell with a silica glass window, and utilizing the same reagents as those for the sample, even though no ablation took place. Boron concentrations of the TPB averaged 0.6 ppb (0.15 ng) and ranged from 0.3 ppb to 1.2 ppb (0.075 – 0.3 ng). TPB  $\geq$  0.7 ppb were analyzed for their  $\delta^{11}\text{B}$  for subsequent blank subtraction (average of -5 ‰).  $2\sigma$  errors associated with blank subtraction, bracketing standard jumps (Fig. C6), and reproducibility of the synthetic diamond were propagated into the final analyses reported for the natural diamonds and ranged from 1.3 to 2.24 ‰. We exclude one analysis of a blue diamond solution (AB\_2) that was analyzed in November of 2018 because it was relatively viscous and produced an extreme jump in bracketing standards of > 2 ‰, indicative of a bias induced by contamination of the sample with organics from the melted Teflon cell. None of the solutions analyzed later (September of 2019 and February of 2020) suffered from this problem due to lower ablation fluences.

#### 4.5.4 Trace elemental analyses

Closed-cell ablations of the natural blue diamonds for trace elemental analyses were carried out following the methods outlined by McNeill et al. 2009, modified for the University of Alberta ablation system as reported in Krebs et al. (2019). The ablations for samples analyzed here yielded 0.5-4.3 mg of diamond at low fluences ( $\sim$ 4 J/cm<sup>2</sup> measured at the site of ablation). Where possible,

we analyzed diamonds that were previously analyzed for boron isotopes. Following ablation, 5-6 mL of 6 M HCl was added to the cell prior to ultrasonication for 35 minutes with a Teflon lid. The solution was then transferred to a Teflon vial for drying down at 100 °C. The dried solution was then taken up in 1 mL of 0.8M HNO<sub>3</sub> solution (with 2 ppb In and Ir as internal standards) for 30 hrs at 120 °C. Four total procedural blanks (TPBs) were analyzed to determine the blank contribution. The TPB and samples were analyzed on a Thermo Scientific Element XR ICPMS. To increase sensitivity an APEX-Q high-efficiency sample introduction system was used. A 3-minute wash was run between every sample. Concentrations were calibrated using 5-point weighted regression lines derived from 25,000x, 50,000x, 100,000x, 250,000x, and 500,000x dilutions of a synthetic rock multi-element standard solution. All samples were corrected for instrument drift. We fully propagate uncertainty (Table C4), including that of the calibrated line and use a 7σ limit of quantification (LOQ) based on the TPB (Table C5). Figure 4.2a plots chondrite normalized REE patterns that are also normalized to Ho abundance. This double normalization is preferred as individual diamond REE enrichment is simply a function of micro-inclusion density (Krebs et al. 2019).

Given the extremely low concentrations of REE in these diamonds (~50 ppt to ~5 ppb La), a leaching experiment was completed following these analyses to determine the La and Ce blank produced from the silica glass ablation window that was polished in a Ce-La slurry (Appendix C1.3). La and Ce values of blue diamonds were subsequently excluded if they showed Ce/La ratios that were approximately equal to those of the window digestions. We postulate that occasional fragmentation of the diamond during ablation may have, in rare cases, “ablated” small amounts of laser window into the ablation media.

#### **4.5.5 Inclusion study**

Prior to the destructive analytical techniques outlined above, we collected Raman spectra and X-ray microfluorescence ( $\mu$ XRF) data from two diamonds (NL247-2 and Blue2). Confocal Raman spectra were collected at Northwestern University using a custom-built system with an Olympus BX microscope with a 100x or 50x objective and a Melles-Griot solid-state laser that produced  $\sim$ 8 mW power at the sample surface. Spectra were obtained for  $\sim$ 20 s and averaged over 4 or more accumulations.  $\mu$ XRF was completed at 13-IDE (GSECARS, APS, Argonne National Laboratory) using a primary beam of wavelength at 0.6199 Å. The X-ray beam was focused to  $2 \times 3 \mu\text{m}^2$ . Monochromatic x-rays were selected using a water cooled Si(1 1 1)  $\varphi = 90^\circ$  double crystal monochromator. Fluorescence maps (Fig. C1) were processed using the software package Larch v.0.9.44 (Hong et al. 2013). Since low Z elements are not detectable using this method, we cannot identify if the Fe-Ni rich rims surrounding our inclusions are carbides or sulfides, although both were documented in Smith et al. (2018).

Electron probe microanalysis was completed on a single olivine inclusion that was recovered after breaking the enstatite-bearing corner of sample Blue 2. The coexistence of olivine and other minerals (Jeffbenite, spinel) with enstatite has been well documented as features of retrogressed bridgmanite (Zedgenizov et al. 2020). The high NiO content (0.45 wt. %) of this analysed olivine inclusion and its spatial association with an unrecovered enstatite suggests that this mineral represents a retrograde product of a bimetallic high NiO ferropericlase and high Mg# bridgmanite inclusion (Stachel et al. 2000b; Smith et al. 2018). While the high Mg# of 93 suggests an ultramafic lithology (Mg# of the bridgmanite was  $> 93$ ), it cannot be used to deduce

a depleted or fertile composition, because the initial proportions of ferropericlase and bridgmanite and the final proportions of olivine and orthopyroxene are not known. The analyses utilized a JEOL JXA-8900R with 5 wavelength-dispersive spectrometers at the University of Alberta. The beam energy was 20 keV with 30 nA of beam current and 2  $\mu\text{m}$  diameter. The counting time was 20 s for Si K $\alpha$ , Fe K $\alpha$ , Mn K $\alpha$ , Ni K $\alpha$ , Zn K $\alpha$ , 30 s for V K $\alpha$ , Ti K $\alpha$ , Cr K $\alpha$ , 40 s for Na K $\alpha$ , K K $\alpha$ , Ca K $\alpha$ , Mg K $\alpha$ , and 120 s for Al K $\alpha$ . Results are reported in Table C3, and standards are reported in Table C7.

## **Chapter 5**

### **Conclusions**

In the previous three chapters of my dissertation, I have utilized cratonic mantle xenoliths, as well as lithospheric and superdeep diamonds to decipher geological processes throughout the deep mantle and deep time. In this chapter, I will conclude with a discussion regarding the role of subduction in these processes.

#### **5.1 Subduction and the formation and evolution of cratonic mantle**

As discussed in Chapter 2, there are three principal models of Archean cratonic mantle formation – plume depletion, oceanic lithosphere stacking, and the collisional compression of depleted subarc mantle. Strong evidence for depletion in a dominantly low-pressure environment was presented in Chapter 1 (Stachel et al. 1998b; Canil 2004; Brey and Shu 2018) and is grounds for rejecting the plume model for extensive cratonic mantle creation. The other two models - lithospheric stacking and collisional compression - both require operation of subduction-driven Wilson cycles in the early Earth for both cratonic mantle depletion and accretion.

Radiogenic Re-Os model ages constrain most major depletion and craton stabilization events to

the Neoarchean (e.g. model age modes for Kaapvaal, Slave, N. Atlantic are ~2.8 Ga; Pearson and Wittig, 2014). Thermal evolution models suggest that cold and stiff lithospheric plates had likely developed at this time (Labrosse and Jaupart 2007) and corresponding geochemical evidence for the initiation of plate tectonics at ~ 3 Ga includes the appearance of subduction-related paired metamorphic belts in the Neoarchean (2.8 – 2.5 Ga; Brown and Johnson 2018), a change from early TTG magmas to potassic two-mica granites in the Mesoarchean (3.2 – 2.8 Ga; Cawood et al. 2018), and Meso- to Neoarchean ages for eclogitic sulphide inclusions in diamonds and whole-rock eclogites within cratonic mantle (Shirey et al. 2001; Richardson et al. 2001). This correlation in ages for the onset of subduction and the production of cratonic mantle supports a subduction-related origin for cratonic mantle by lithospheric stacking and/or collisional compression.

Additional evidence for the subduction-related formation of cratonic mantle is the Si-enriched nature of many cratonic peridotites. While Chapter 2 argues against the formation of Opx-rich cratonic peridotites via the introduction of eclogite-derived,  $\text{SiO}_2$ -rich metasomatic melts (e.g., Kelemen et al. 1998), there are other means for a subducting slab to enrich the surrounding mantle in  $\text{SiO}_2$ . For example, the movement of aqueous slab-derived fluids through peridotitic mantle may recrystallize surrounding olivine to orthopyroxene, given that aqueous fluids can be very Si-rich at 2-3 GPa (Ryabchikov et al. 1982; Kesson and Ringwood 1989; Smith et al. 1999). The subsequent removal of this hydrous fluid via percolation would leave little evidence of  $^{18}\text{O}$ -enriched slab-derived oxygen within the peridotite. Alternatively, the melting of mildly depleted peridotite that had been fluxed by slab fluids at low pressures (Mitchell and Grove 2015) allows for the further depletion of subarc mantle, as well as the Si-enrichment of overlying depleted

mantle as the resulting Si-rich melts percolate upwards. Given that this model only requires minor involvement of slab-derived oxygen as H<sub>2</sub>O, Si-enriched regimes would not be significantly distinct in their δ<sup>18</sup>O signature. Thus, subarc environments allow for the necessary melt depletion and Si-enrichment of cratonic mantle to occur nearly simultaneously.

Despite the apparent necessity of subduction for the creation of cratonic mantle roots, subduction-related processes can also cause their destruction. The flat subduction of slabs beneath the Colorado Plateau in the Wyoming Craton, the North China Craton, and the Amazonian Craton may have destabilized and thinned their mantle roots (Li et al. 2008; Kusky et al. 2014; Wu et al. 2019). These models suggest that hot, young, low angle subducting slabs may suddenly pull away from overlying lithosphere after becoming gravitationally unstable due to the eclogitization of their crustal component. This sudden slab roll-back would lead to the influx of hot, fertile mantle into an already hydrated region, causing wide-spread melting events in both the lithosphere and asthenosphere and the eventual destruction of cratonic mantle (Li et al. 2008; Kusky et al. 2014; Wu et al. 2019). Thus, the creation and preservation of thick cratonic mantle appears to necessitate a fine balance between sufficient subduction-related metasomatism to produce Si-enriched, melt depleted peridotite, and excessive subduction-related metasomatism that can cause the destabilization of the entire cratonic mantle.

## **5.2 The relevance of subduction to the formation of diamonds: lithosphere to lower mantle**

Mechanisms of diamond formation have been a topic of discussion for many decades and have generally focused on the reduction of CO<sub>2</sub> or oxidation of CH<sub>4</sub> to produce the gemstone. This oxidation or reduction must be balanced by another redox reaction, which commonly involves

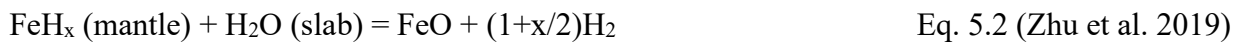
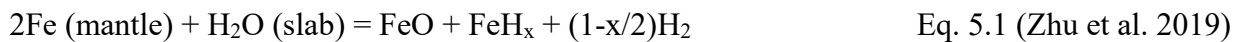
iron. Recent work, however, has questioned if iron-poor cratonic substrates have large enough buffering capacities to affect the fluid species that move through them (Stachel and Luth 2015). Instead, Stachel and Luth (2015) suggested that lithospheric mantle diamonds can precipitate from cooling, ascending fluids or melts directly, without significant redox exchange with the surrounding peridotitic mantle.

In chapter 3, I demonstrated that the oxygen isotopic signatures of mineral inclusions in eclogitic diamonds from the lithosphere are indistinguishable from eclogitic xenoliths. The isotopic signatures of eclogitic diamonds imply that the cratonic substrate must have been the dominant provider of oxygen to the ascending metasomatic melts and fluids that crystallize diamond. These limitations can be met during low fluid/rock ratio metasomatism of an eclogite substrate.

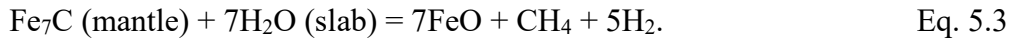
In contrast to the lithospheric signatures, asthenospheric to transition zone inclusions in diamond have extreme oxygen isotope signatures, even compared to the varied  $\delta^{18}\text{O}$  observed in eclogitic xenoliths (Fig. 3.1). Our proposed model connects these extreme signatures to the melting of the upper sections of carbonated meta-basaltic slabs. Not only is carbonated upper crust  $^{18}\text{O}$ -enriched (Fig. 3.4), the high redox capacity of the metal-bearing, fertile sublithospheric mantle (Rohrbach and Schmidt 2011) guarantees limited mantle contamination and dilution of the  $^{18}\text{O}$ -enriched isotopic signatures. As discussed in Chapter 4, blue diamonds are products of a similar reaction between a carbonated melt and the surrounding reduced mantle. However, blue diamonds rarely contain majoritic garnet and commonly include abundant retrogressed bridgmanite, which supports a greater depth of formation than is commonly invoked for majorite-bearing sublithospheric diamonds ( $\lesssim 500$  km; Beyer and Frost 2017). I connect the

formation of blue diamonds in the lower mantle to the breakdown of boron-bearing hydrous minerals, which may induce melting of carbonated meta-peridotite and Na-poor eclogite.

Finally, diamond formation in the lower mantle beneath Kankan, W. Africa, as documented by retrogressed bridgmanite-ferropericlase inclusion pairs, appears to be distinct from the other mechanisms discussed here. The isotopic signatures are indistinguishable from convecting mantle that is unmodified by crustal signatures, suggesting that these diamonds formed below the so-called “barrier to carbon subduction”, i.e. the depth at which carbonate is removed from the subducting slab (Thomson et al. 2016). These isotopic parameters call for a distinct source of carbon, preferably from a non-crustal source. Nevertheless, the suggested model in Chapter 3 still involves the presence of a subducting slab by invoking the mobilization of carbon from iron metals in the ambient lower mantle via slab dehydration. This model relies on various redox reactions that can destabilize iron metal alloys by hydration. These reactions have been observed in experiments as the following:



Similar carbon-rich redox reactions can be postulated as:



This production of methane in the uppermost lower mantle along hydration fronts allows for the

local concentration of carbon, which could facilitate the crystallization of diamond if there was an appropriate oxidizing agent. Recent work has suggested that mantle plumes could provide such an oxidizing source (Moussallam et al. 2019). Alternatively, hydrated, Fe<sub>2</sub>O<sub>3</sub>-rich bridgmanite-bearing mantle (McCammon 2005) may auto-oxidize during convective upwelling, given the lack of Fe metal to combine with Fe<sub>2</sub>O<sub>3</sub> for disproportionation to FeO. The interaction of these oxidizing agents with methane would result in the following diamond-producing redox reaction:



where FeO could plausibly be a constituent of Fe-rich ferropericlase, such as those documented in Juina diamonds (Kaminsky et al. 2001), or of a low-Fe<sub>2</sub>O<sub>3</sub>, low-Al bridgmanite from the topmost lower mantle, such as those found within Kankan diamonds (McCammon 2005).

Thus, while the commonly invoked diamond-forming redox reactions do not appear to be dominant in the cratonic mantle (Stachel and Luth 2015), they remain essential for the formation of sublithospheric diamonds. The efficacy of these redox reactions in the deep Earth are likely due to the extreme variability of oxidation states that are present at slab-mantle interfaces, as well as the greatly increased redox buffering capacity of the deep mantle due to the production of iron-metal through FeO disproportionation (Frost and McCammon 2008).

### 5.3 Deep volatile cycles

Elements that form volatile compounds influence magma genesis and convection in the deep Earth, as well as climate and atmospheric characteristics on the surface of the planet. These

elements are also key tracers of processes occurring in the deep mantle. Here, I will review the subduction-related cycling of relevant elements that form highly and moderately volatile compounds (Curtis and Gladney 1985; Lodders 2003).

### 5.3.1 Carbon cycle

Carbon is one of the most studied elements in geochemistry due to its broad impacts on various geochemical processes. The loss of its reduced organic forms to subduction may have resulted in the rise of atmospheric oxygen (Duncan and Dasgupta 2017), and its local enrichments in the mantle can control redox conditions and melting regimes (Plank and Manning 2019). Despite this interest, the estimated flux of carbon from the surface into the mantle and the oxidation state of species involved are very poorly constrained (Kelemen and Manning 2015; Plank and Manning 2019). Thus, the tracing of carbon sources through isotopic studies of diamond can play an important role in better constraining the whole-Earth carbon cycle.

Sediment is generally proposed as the source of carbon in volcanic arcs and diamonds (Plank and Manning 2019). While the presence of sediment-derived volatiles in arc volcanoes is clearly documented by high concentrations of  $^{10}\text{Be}$  and positive  $\delta^{15}\text{N}$  in arc magmas (Morris et al. 1990; Sano et al. 2001), the evidence for a sedimentary source of carbon in diamonds is much less clear. In fact, the  $^{13}\text{C}$ -depleted signatures in many diamonds that is used as evidence for a sedimentary signature (Plank and Manning 2019) is also found in altered oceanic crust (Li et al. 2019). This lack of clear evidence for sediment-derived carbon in diamonds is compounded when one considers the processes that resist the subduction of sedimentary carbon beyond sub-arc depths. These include mechanical removal of sediments into accretionary wedges,

metamorphic decarbonation, and fluid-assisted reactions and melting (Ague and Nicolescu 2014; Plank and Manning 2019). The underlying, colder, carbonated meta-basaltic, -gabbroic, and peridotitic portions of the slab are better protected from these mechanical and heat-driven processes. Chapter 3 further strengthens these arguments by favoring an AOC reservoir instead of a sedimentary reservoir to explain the carbon and nitrogen isotopic characteristics of eclogitic diamonds from the lithospheric mantle.

The apparent ability of carbonated metabasalt to transfer carbon to diamond stable depths not only results in the formation of lithospheric diamonds (Li et al. 2019), but also the sublithospheric diamonds studied in Chapter 3. These diamonds form after a subsequent drop in carbonated metabasalt solidus temperature at ~300 to ~700 km depth, due to the appearance of a Na-carbonate phase in the subducting slab (Thomson et al. 2016). This melting event may remove most of the carbon in the metabasaltic portions of the subducting slabs. However, the volatile loads of other lithological portions of the slab may remain consequential.

### **5.3.2 Boron cycle**

In contrast to carbon, boron does not substantially affect redox conditions, climate, or melting temperatures. Instead, the boron cycle is of interest because it is an effective tracer of fluid mobilization and the cycling of water. For example, boron isotope investigations have identified the progressive dehydration of slabs across arc systems (Rosner et al. 2003) and have traced the dehydration of mantle wedge serpentinites at sub-arc depths after their formation from early dewatering sediments and AOC (Harvey et al. 2014). The study of blue diamonds in Chapter 4 demonstrates that slabs can retain significant amounts of volatiles into the lower mantle, where boron - and its water and carbon-rich fluid hosts - are eventually liberated. The source of these

boron-bearing fluids is likely meta-peridotitic portions of the subducting slab that did not undergo volatile depletion during the Na-carbonate driven melting in the transition zone (Thomson et al. 2016). Possible hosts of the boron and associated water are transition zone-stable ringwoodite, or the dense hydrous magnesium silicates (DHMS) Phase D and Superhydrous Phase B, which are stable in meta-peridotitic portions of the slab until 660–1,000 km depths (Fig. 5.1; Nishi et al., 2014).

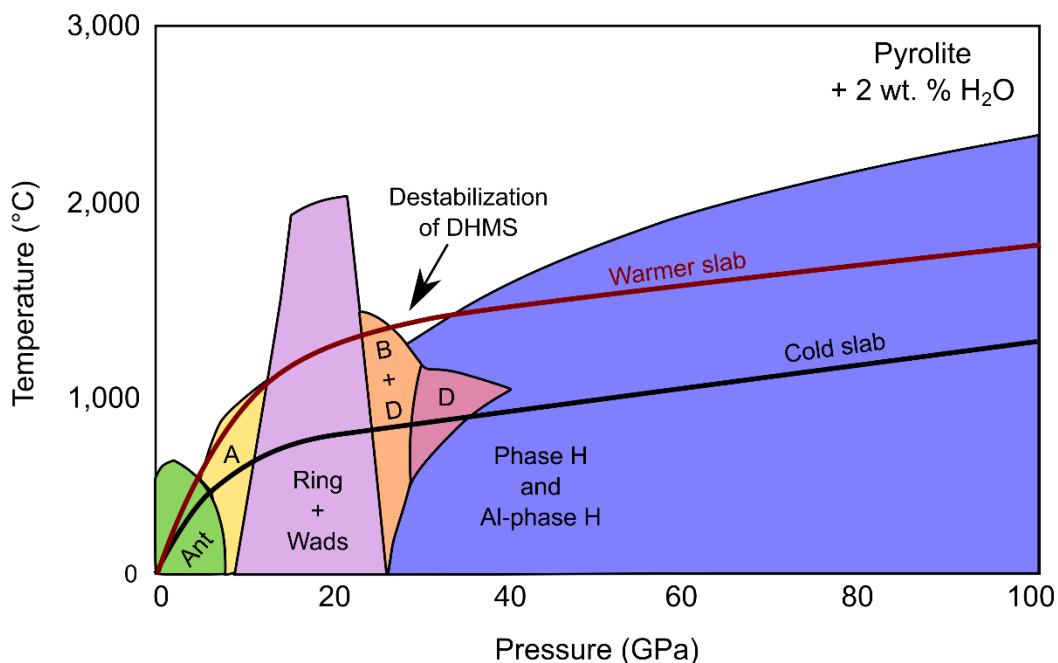


Figure 5.1. Stability of hydrous meta-peridotitic phases including antigorite (Ant), ringwoodite (Ring), wadsleyite (Wads), dense hydrous phases A, B, D, H, and aluminous phase H (Al-phase H). Overlaid on this phase diagram is the projection of a cold slab geotherm that would translate volatiles into the deep lower mantle and a warmer slab geotherm that would allow for DHMS destabilization in the uppermost lower mantle. Figure is modified from Nishi et al. (2014).

### 5.3.3 Evolution of volatile cycles over time

The gradual secular cooling of Earth's mantle has affected not only the trajectory and final location of subducting plates, but their final volatile and incompatible element load.

Geodynamical models of modern-day subduction are more likely to result in slab stagnation at the base of the transition zone if the slab is relatively cold, which results in large degrees of slab buoyancy due to the delayed transition of ringwoodite to bridgmanite, and if the slab is relatively old, which increases trench retreat (Goes et al. 2017). However, applying these variables to a hot, early Earth, with thicker and more buoyant crust, has produced conflicting models. For example, some models have estimated that the early Earth was dominated by two-layer convection split by the stagnation of slabs at the base of the transition zone (Allègre 1997; Wolstencroft and Davies 2011), whereas others have suggested more efficient whole-earth convection with limited slab stagnation (Agrusta et al. 2018).

Despite these contradictory geodynamic modeling results, geochemical consideration of hot, early Earth subduction would clearly favor more efficient dehydration and greater volume of slab melting. For example, hotter slab geotherms would decrease the stability of DHMS, and in particular, reduce the probability of the formation of Phase H, which can transport boron and water into the deepest portions of the lower mantle (Nishi et al., 2014). This destabilization of hydrous phases, and any associated carbonated melting would ensure that any slabs that did make it to the deep lower mantle were extensively depleted in incompatible and volatile elements.

The depletion of slabs in incompatible and volatile elements before penetration into the deep lower mantle would have maintained the chemical isolation of the lower mantle, in terms of volatile and some incompatible elements. Evidence for pristine lower mantle reservoirs is indicated by the radiogenic isotopes of pre-Cretaceous kimberlites (>200 Ma; Woodhead et al. 2019). Later contamination of these deep mantle regimes by volatile and incompatible elements

are documented by a decrease in the Nd and Hf isotope ratios of kimberlites, as well as an increase in the B isotope composition of deep-seated carbonatites (Hulett et al. 2016; Woodhead et al. 2019). Thus, while it remains unclear if one-layer or two-layer convection dominated in early Earth, it is likely that slabs have only recently been able to translate significant concentrations of incompatible and volatile elements into the deep mantle to form the “zoo” of mantle reservoirs that we see today (Stracke et al. 2005).

## 5.4 Future directions

The ideas presented here have opened various avenues of research that could not be addressed in this thesis. Here I present several suggested future studies.

1. Establish the oxygen isotopic composition of ferropericlase in superdeep diamonds
  - a. Ferropericlase is the most common inclusion in superdeep diamonds. The Mg# of these minerals range from ~40 to 90 (Thomson et al. 2016). Thus, it is likely that some of these inclusions do not reflect convecting mantle bulk compositions and may instead be crystallization products of slab melts. Others have suggested that the elevated Fe may come from core mantle interaction (Harte et al. 2018). At the moment, it remains impossible to unambiguously identify those ferropericlase from convective mantle and those from carbonatitic melt or core mantle interaction. Isotopic signatures of carbonatitic slab melt-derived crystals should be highly  $^{18}\text{O}$ -enriched compared to those of convective mantle origin. Work on this project is ongoing and requires calibrations of both chemical and orientation-dependent matrix effects.
2. Determine the boron concentrations and boron isotopic composition of other (non-Type IIb)

diamonds

- a. While the concentrations of boron in blue diamonds has been documented at up to 8 ppm (Gaillou et al. 2012), the concentrations of this element in N-bearing diamonds (Type I) has not been established. This absence of data is likely because high nitrogen concentrations can “compensate” or conceal the B signatures in FTIR spectra (Howell et al. 2019). However, as part of this thesis, a SIMS standard was produced for boron in diamond. Further data of the boron contents of fibrous and type I diamonds should be collected using this method. These studies will help identify if Type IIb blue diamonds are truly unique in their boron impurities, or rather simply unique in their lack of nitrogen impurities. The very low boron content of one Type I diamond studied here (NL247-23) indicates the former, although much broader testing is required. Subsequent studies may also probe B-bearing samples (e.g. fibrous stones) for their boron isotopic composition.
3. Determine the composition of melts produced from slab at variable depths and with different carbonate compositions
  - a. Chapter 4 and Smith et al (2018) both demonstrate that Raman spectra of the Ca-silicate inclusions in blue diamonds document the presence of breyite ( $\text{CaSiO}_3$ ) and larnite ( $\text{Ca}_2\text{SiO}_4$ ), but do not indicate the presence of Ca-titanite ( $\text{CaSi}_2\text{O}_5$ ). This indicates that the bulk chemistry of the inclusion has a Ca/Si ratio  $> 1$ , suggesting that this mineralogy cannot reflect solely a Ca-perovskite ( $\text{CaSiO}_3$ ) retrogression product, and instead is indicative of Ca-rich carbonatitic melts, such as those produced during experimental melting of  $\text{Mg}_{0.9}\text{Ca}_{0.1}\text{CO}_3$  (Palyanov et al. 2013). These melts can therefore explain the Ca-rich mineralogy documented in blue

diamonds and in other superdeep diamonds (e.g. Brenker et al. 2002). However, majoritic garnet-bearing diamonds, also demonstrated to be reaction products of carbonatitic melt (Chapter 3) do not show similar Ca-enrichments. Thus, possible variations of melt chemistry with depth, initial carbonate composition, melt volume, and reaction with peridotite needs to be further explored via high pressure experiments.

4. Determine the oxygen isotopic composition of inclusions within blue diamonds
  - a. Given the interpretation of blue diamonds as a product of carbonatitic slab melt, it would be expected that their mineral inclusions should have  $^{18}\text{O}$ -enriched oxygen isotopic signatures, similar to those found in the majoritic inclusions at Kankan. Thus, following the collection of sufficient numbers of inclusions from blue diamonds, their oxygen isotopic signatures should be probed to confirm the model presented here.
5. Determine the redox conditions documented by the majoritic garnet and ferropericlase inclusions at Kankan
  - a. Majoritic garnet and ferropericlase  $\text{Fe}^{3+}/\text{Fe}_{\text{total}}$  has been quantifiably linked to mantle redox (McCammon et al. 2004; Kisieva et al. 2018). These measurements have documented  $f_{\text{O}_2}$  conditions between the IW buffer and 4 log units above the IW buffer (McCammon et al. 2004; Otsuka et al. 2013). This extreme range of mantle  $f_{\text{O}_2}$  over relatively small regions of the deep mantle is a possible driving force for the remobilization of diamond- or metal-hosted carbon, and for the production of carbon-rich deeply derived, low-melt fraction magmatic rocks such as kimberlites. However, a greater number of analyses are required to determine crystal-chemical

effects on  $\text{Fe}^{3+}/\text{Fe}_{\text{total}}$ , as well as the full variation found within the transition zone and lower mantle.

6. Determine if slab melting and dehydration is a true barrier for volatile subduction
  - a. The idea of slab melting as a barrier for carbon subduction was postulated by Thomson et al. (2016) and has been expanded in this dissertation. Nevertheless, Thomson et al. (2016) only demonstrated the loss of carbonate until the exhaustion of a Na-carbonate phase. Further experimental work needs to be completed to determine to what depth carbonate in Na-poor meta-basalt and other Na-poor lithologies (e.g. gabbro, peridotite) remain stable. This experimental work should include hydrated experiments that reflect the destabilization of water bearing DHMS and should be accompanied by improved thermal models of oceanic slabs undergoing subduction.

## Bibliography

### References for Chapters 1-5 and Appendices A-C

Agrinier P, Javoy M, Girardeau J (1988) Hydrothermal activity in a peculiar oceanic ridge: Oxygen and hydrogen isotope evidence in the Xigaze ophiolite (Tibet, China). *Chem Geol* 71:313–335. [https://doi.org/10.1016/0009-2541\(88\)90057-5](https://doi.org/10.1016/0009-2541(88)90057-5)

Agrusta R, Van Hunen J, Goes S (2018) Strong plates enhance mantle mixing in early Earth. *Nat Commun* 9:1–10. <https://doi.org/10.1038/s41467-018-05194-5>

Ague JJ, Niculescu S (2014) Carbon dioxide released from subduction zones by fluid-mediated reactions. *Nat Geosci* 7:355–360. <https://doi.org/10.1038/ngeo2143>

Allègre CJ (1997) Limitation on the mass exchange between the upper and lower mantle: The evolving convection regime of the Earth. *Earth Planet Sci Lett* 150:1–6.

[https://doi.org/10.1016/s0012-821x\(97\)00072-1](https://doi.org/10.1016/s0012-821x(97)00072-1)

Alt JC, France-Lanord C, Floyd PA, et al (1992) Low-temperature hydrothermal alteration of Jurassic ocean crust, Site 801. *Proc Ocean Drill Progr* 129:415–427.

<https://doi.org/10.2973/odp.proc.sr.129.132.1992>

Alt JC, Shanks WC, Bach W, et al (2007) Hydrothermal alteration and microbial sulfate reduction in peridotite and gabbro exposed by detachment faulting at the Mid-Atlantic Ridge, 15°20'N (ODP Leg 209): A sulfur and oxygen isotope study. *Geochemistry, Geophys Geosystems* 8:. <https://doi.org/10.1029/2007GC001617>

Alt JC, Teagle DAH (2003) Hydrothermal alteration of upper oceanic crust formed at a fast-spreading ridge: Mineral, chemical, and isotopic evidence from ODP Site 801. *Chem Geol* 201:191–211. [https://doi.org/10.1016/S0009-2541\(03\)00201-8](https://doi.org/10.1016/S0009-2541(03)00201-8)

Anand M, Taylor LA, Misra KC, et al (2004) Nature of diamonds in Yakutian eclogites: Views from eclogite tomography and mineral inclusions in diamonds. *Lithos* 77:333–348.

<https://doi.org/10.1016/j.lithos.2004.03.026>

Andrault D, Pesce G, Bouhifd MA, et al (2014) Melting of subducted basalt at the core-mantle boundary. *Science* 344:892–895. <https://doi.org/10.1126/science.1250466>

Appleyard CM, Bell DR, le Roex AP (2007) Petrology and geochemistry of eclogite xenoliths from the Rietfontein kimberlite, Northern Cape, South Africa. *Contrib to Mineral Petrol* 154:309–333. <https://doi.org/10.1007/s00410-007-0195-7>

Appleyard CM (2019) The geochemistry of a suite of eclogite xenoliths from the Rietfontein kimberlite, South Africa. University of Cape Town

Appleyard CM, Viljoen KS, Dobbe R (2004) A study of eclogitic diamonds and their inclusions from the Finsch kimberlite pipe, South Africa. *Lithos* 77:317–332.  
<https://doi.org/10.1016/j.lithos.2004.04.023>

Aulbach S, Jacob DE, Cartigny P, et al (2017) Eclogite xenoliths from Orapa: Ocean crust recycling, mantle metasomatism and carbon cycling at the western Zimbabwe craton margin. *Geochim Cosmochim Acta* 213:574–592. <https://doi.org/10.1016/j.gca.2017.06.038>

Aulbach S (1999) The chemistry of syngenetic mineral inclusions in diamonds from Venetia and the stable isotope composition of diamonds from Mwadui and the Kankan district. Universitat Frankfurt

Banas A (2006) Diamonds and their formation: Characterization of diamonds from the Buffalo Head Hills, Alberta, and, Metasomatism recorded by garnet inclusions from the De Beers Pool, South Africa. University of Alberta

Barashkov YP, Zudin NG (1997) Composition of garnets with diamond inclusions from krasnopresnenskaya kimberlite pipe (Yakutia). *Geol i Geofiz* 353–357.  
<https://doi.org/10.29173/ikc1770>

Barjon J, Tillocher T, Habka N, et al (2011) Boron acceptor concentration in diamond from excitonic recombination intensities. *Phys Rev B Condens Matter* 83:73201.

<https://doi.org/10.1103/PhysRevB.83.073201>

Barnes JD, Paulick H, Sharp ZD, et al (2009) Stable isotope ( $\delta^{18}\text{O}$ ,  $\delta\text{D}$ ,  $\delta^{37}\text{Cl}$ ) evidence for multiple fluid histories in mid-Atlantic abyssal peridotites (ODP Leg 209). *Lithos* 110:83–94.

<https://doi.org/10.1016/j.lithos.2008.12.004>

Barth MG, Rudnick RL, Carlson RW, et al (2002) Re-Os and U-Pb geochronological constraints on the eclogite-tonalite connection in the Archean Man Shield, West Africa. *Precambrian Res* 118:267–283. [https://doi.org/10.1016/S0301-9268\(02\)00111-0](https://doi.org/10.1016/S0301-9268(02)00111-0)

Barth MG, Rudnick RL, Horn I, et al (2001) Geochemistry of xenolithic eclogites from West Africa, part I: A link between low MgO eclogites and archean crust formation. *Geochim Cosmochim Acta* 65:1499–1527. [https://doi.org/10.1016/S0016-7037\(00\)00626-8](https://doi.org/10.1016/S0016-7037(00)00626-8)

Beard BL, Fraracci KN, Clayton RA, et al (1996) Petrography and geochemistry of eclogites from the Mir kimberlite, Yakutia, Russia. *Contrib Miner Pet* 125:293–310.

<https://doi.org/10.1007/s004100050223>

Benton LD, Ryan JG, Tera F (2001) Boron isotope systematics of slab fluids as inferred from a serpentine seamount, Mariana forearc. *Earth Planet Sci Lett* 187:273–282

Bercovici D, Karato S-I (2003) Whole-mantle convection and the transition-zone water filter. *Nature* 425:39–44. <https://doi.org/10.1038/nature01918>

Beyer C, Frost DJ (2017) The depth of sub-lithospheric diamond formation and the redistribution of carbon in the deep mantle. *Earth Planet Sci Lett* 461:30–39.

<https://doi.org/10.1016/j.epsl.2016.12.017>

Bindeman I (2008) Oxygen isotopes in mantle and crustal magmas as revealed by single crystal

- analysis. *Rev Mineral Geochemistry* 69:445–478. <https://doi.org/10.2138/rmg.2008.69.12>
- Bobrov A V, Litvin YA, Bindi L, Dymshits AM (2008) Phase relations and formation of sodium-rich majoritic garnet in the system Mg<sub>3</sub>Al<sub>2</sub>Si<sub>3</sub>O<sub>12</sub>–Na<sub>2</sub>MgSi<sub>5</sub>O<sub>12</sub> at 7.0 and 8.5 GPa. *Contrib Miner Pet* 156:243–257. <https://doi.org/10.1007/s00410-008-0283-3>
- Boschi C, Dini A, Fru GL, et al (2008) Isotopic and element exchange during serpentinization and metasomatism at the Atlantis Massif (MAR 30°N): Insights from B and Sr isotope data. *Geochim Cosmochim Acta* 72:1801–1823. <https://doi.org/10.1016/j.gca.2008.01.013>
- Boyd FR (1973) A pyroxene geotherm. *Geochim Cosmochim Acta* 37:2533–2546.  
[https://doi.org/10.1016/0016-7037\(73\)90263-9](https://doi.org/10.1016/0016-7037(73)90263-9)
- Boyd FR, Finnerty AA (1980) Conditions of origin of natural diamonds of peridotite affinity. *J Geophys Res* 85:6911–6918. <https://doi.org/10.1029/JB085iB12p06911>
- Brenker FE, Vincze L, Vekemans B, et al (2005) Detection of a Ca-rich lithology in the Earth's deep (> 300 km) convecting mantle. *Earth Planet Sci Lett* 236:579–587.  
<https://doi.org/10.1016/j.epsl.2005.05.021>
- Brenker FE, Stachel T, Harris JW (2002) Exhumation of lower mantle inclusions in diamond: A TEM investigation of retrograde phase transitions, reactions and exsolution. *Earth Planet Sci Lett* 198:1–9. [https://doi.org/10.1016/S0012-821X\(02\)00514-9](https://doi.org/10.1016/S0012-821X(02)00514-9)
- Brey GP, Shu Q (2018) The birth, growth and ageing of the Kaapvaal subcratonic mantle. *Miner Pet.* <https://doi.org/10.1007/s00710-018-0577-8>
- Brown M, Johnson T (2018) Secular change in metamorphism and the onset of global plate tectonics. *Am Mineral* 103:181–196. <https://doi.org/10.2138/am-2018-6166>
- Bulanova GP (1995) The formation of diamond. *J Geochemical Explor* 53:1–23.  
[https://doi.org/10.1016/0375-6742\(94\)00016-5](https://doi.org/10.1016/0375-6742(94)00016-5)

Burnham AD, Thomson AR, Bulanova GP, et al (2015) Stable isotope evidence for crustal recycling as recorded by superdeep diamonds. *Earth Planet Sci Lett* 432:374–380.

<https://doi.org/10.1016/j.epsl.2015.10.023>

Canil D, O'Neill HSC, Pearson DG, et al (1994) Ferric iron in peridotites and mantle oxidation states. *Earth Planet Sci Lett* 123:205–220. [https://doi.org/10.1016/0012-821X\(94\)90268-2](https://doi.org/10.1016/0012-821X(94)90268-2)

Canil D (2004) Mildly incompatible elements in peridotites and the origins of mantle lithosphere. *Lithos* 77:375–393. <https://doi.org/10.1016/j.lithos.2004.04.014>

Canil D, Lee C-TA (2009) Were deep cratonic mantle roots hydrated in Archean oceans? *Geology* 37:667–670. <https://doi.org/10.1130/G25610A.1>

Cannaò E, Tiepolo M, Bebout GE, Scambelluri M (2020) Into the deep and beyond: Carbon and nitrogen subduction recycling in secondary peridotites. *Earth Planet Sci Lett* 543:116328. <https://doi.org/10.1016/j.epsl.2020.116328>

Caporuscio FA (1990) Oxygen isotope systematics of eclogite mineral phases from South Africa. *Lithos* 25:203–210. [https://doi.org/10.1016/0024-4937\(90\)90015-S](https://doi.org/10.1016/0024-4937(90)90015-S)

Carlson RW, Pearson DG, Boyd FR, et al (1999) Re–Os systematics of lithospheric peridotites: implications for lithosphere formation and preservation. *Proc. 7th Int. Kimberl. Conf.* 1:99–108

Cartigny P (2005) Stable Isotopes and the Origin of Diamond. *Elements* 1:79–84. <https://doi.org/10.2113/gselements.1.2.79>

Cartigny P, Farquhar J, Thomassot E, et al (2009) A mantle origin for Paleoarchean peridotitic diamonds from the Panda kimberlite, Slave Craton: Evidence from  $^{13}\text{C}$ -,  $^{15}\text{N}$ - and  $^{33,34}\text{S}$ -stable isotope systematics. *Lithos* 112:852–864

Cartigny P, Boyd S, Harris J, Javoy M (1997) Nitrogen isotopes in peridotitic diamonds from

Fuxian, China: the mantle signature. *Terra Nov* 9:175–179. <https://doi.org/10.1046/j.1365-3121.1997.d01-26.x>

Cartigny P, Harris JW, Javoy M (1998) Eclogitic diamond formation at Jwaneng: No room for a recycled component. *Science* 280:1421–1424. <https://doi.org/10.1126/science.280.5368.1421>

Cartigny P, Palot M, Thomassot E, Harris JW (2014) Diamond formation: A stable isotope perspective. *Annu Rev Earth Planet Sci* 42:699–732. <https://doi.org/10.1146/annurev-earth-042711-105259>

Cartigny P, Stachel T, Harris JW, Javoy M (2004) Constraining diamond metasomatic growth using C- and N-stable isotopes: Examples from Namibia. *Lithos* 77:359–373.  
<https://doi.org/10.1016/j.lithos.2004.03.024>

Cawood PA, Hawkesworth CJ, Pisarevsky SA, et al (2018) Geological archive of the onset of plate tectonics. In: *Philosophical Transactions of the Royal Society A: Mathematical, Physical and Engineering Sciences*. Royal Society Publishing, p 20170405

Chaussidon M, Marty B (1995) Primitive boron isotope composition of the mantle. *Science* 269:383–386. <https://doi.org/10.1126/science.269.5222.383>

Chinn IL (1995) A study of unusual diamonds from the George Creek K1 kimberlite dyke, Colorado. University of Cape Town

Çimen O, Kuebler C, Monaco B, et al (2018) Boron, carbon, oxygen and radiogenic isotope investigation of carbonatite from the Miaoya complex, central China: Evidences for late-stage REE hydrothermal event and mantle source heterogeneity. *Lithos* 322:225–237.  
<https://doi.org/10.1016/j.lithos.2018.10.018>

Çimen O, Kuebler C, Simonetti SS, et al (2019) Combined boron, radiogenic (Nd, Pb, Sr), stable (C, O) isotopic and geochemical investigations of carbonatites from the Blue River Region,

- British Columbia (Canada): Implications for mantle sources and recycling of crustal carbon. *Chem Geol* 529:119240. <https://doi.org/10.1016/j.chemgeo.2019.07.015>
- Clifford TN (1966) Tectono-metallogenic units and metallogenic provinces of Africa. *Earth Planet Sci Lett* 1:421–434. [https://doi.org/10.1016/0012-821X\(66\)90039-2](https://doi.org/10.1016/0012-821X(66)90039-2)
- Cocker JD, Griffin BJ, Muehlenbachs K (1982) Oxygen and carbon isotope evidence for seawater-hydrothermal alteration of the Macquarie Island ophiolite. *Earth Planet Sci Lett* 61:112–122. [https://doi.org/10.1016/0012-821X\(82\)90043-7](https://doi.org/10.1016/0012-821X(82)90043-7)
- Collins AT, Williams AWS (1971) The nature of the acceptor centre in semiconducting diamond. *J Phys C Solid State Phys* 4:1789. <https://doi.org/10.1088/0022-3719/1/6/137>
- Cooper KM, Eiler JM, Asimow PD, Langmuir CH (2004) Oxygen isotope evidence for the origin of enriched mantle beneath the mid-Atlantic ridge. *Earth Planet Sci Lett* 220:297–316. [https://doi.org/10.1016/S0012-821X\(04\)00058-5](https://doi.org/10.1016/S0012-821X(04)00058-5)
- Cooper KM, Eiler JM, Sims KWW, Langmuir CH (2009) Distribution of recycled crust within the upper mantle: Insights from the oxygen isotope composition of MORB from the Australian-Antarctic Discordance. *Geochem Geophys Geosyst* 10:Q12004. <https://doi.org/10.1029/2009GC002728>
- Creager KC, Jordan TH (1984) Slab penetration into the lower mantle. *J Geophys Res* 89:3031–3049. <https://doi.org/10.1029/JB089iB05p03031>
- Curtis DB, Gladney ES (1985) Boron cosmochemistry. *Earth Planet Sci Lett* 75:311–320. [https://doi.org/10.1016/0012-821X\(85\)90175-X](https://doi.org/10.1016/0012-821X(85)90175-X)
- Daniels LRM, Gurney JJ (1989) The chemistry of the garnets, chromites and diamond inclusions from the Dokolwayo kimberlite, Kingdom of Swaziland. *Kimberlites Relat Rocks* 2:1012–1021. <https://doi.org/https://doi.org/10.1016/j.tecto.2013.12.020>

Daniels LRM, Gurney JJ (1999) Diamond Inclusions from the Dokolwayo Kimberlite, Swaziland.

Proc 7th int Kimberl Conf 1:134–139

Dasgupta R, Hirschmann MM (2010) The deep carbon cycle and melting in Earth's interior. *Earth*

*Planet Sci Lett* 298:1–13. <https://doi.org/10.1016/j.epsl.2010.06.039>

Davies R, Griffin W, Pearson N, et al (1999) Diamonds from the deep: Pipe DO-27, Slave craton, Canada. In: International Kimberlite Conference: Extended Abstracts (Vol. 7). pp 170–172

Davies RM, Griffin WL, O'Reilly SY, Doyle BJ (2004a) Mineral inclusions and geochemical characteristics of microdiamonds from the DO27, A154, A21, A418, DO18, DD17 and Ranch Lake kimberlites at Lac de Gras, Slave Craton, Canada. *Lithos* 77:39–55.

<https://doi.org/10.1016/j.lithos.2004.04.016>

Davies RM, Griffin WL, O'Reilly SY, McCandless TE (2004b) Inclusions in diamonds from the K14 and K10 kimberlites, Buffalo Hills, Alberta, Canada: Diamond growth in a plume? *Lithos* 77:99–111. <https://doi.org/10.1016/j.lithos.2004.04.008>

De Hoog JCM, Hattori K, Jung H (2014) Titanium- and water-rich metamorphic olivine in high-pressure serpentinites from the Voltri Massif (Ligurian Alps, Italy): Evidence for deep subduction of high-field strength and fluid-mobile elements. *Contrib to Mineral Petrol* 167:1–15. <https://doi.org/10.1007/s00410-014-0990-x>

De Hoog JCM, Savov IP (2018) Boron isotopes as a tracer of subduction zone processes. In: *Boron Isotopes*. Springer, pp 217–247

De Stefano A, Kopylova MG, Cartigny P, Afanasiev V (2009) Diamonds and eclogites of the Jericho kimberlite (Northern Canada). *Contrib to Mineral Petrol* 158:295–315.  
<https://doi.org/10.1007/s00410-009-0384-7>

Deines P, Harris JW (2004) New insights into the occurrence of 13C-depleted carbon in the mantle

from two closely associated kimberlites: Letlhakane and Orapa, Botswana. *Lithos* 77:125–142. <https://doi.org/10.1016/J.LITHOS.2004.04.015>

Deines P, Harris JW, Robinson DN, et al (1991) Carbon and oxygen isotope variations in diamond and graphite eclogites from Orapa, Botswana, and the nitrogen content of their diamonds. *Geochim Cosmochim Acta* 55:515–524. [https://doi.org/10.1016/0016-7037\(91\)90009-T](https://doi.org/10.1016/0016-7037(91)90009-T)

Dongre AN, Jacob DE, Stern RA (2015) Subduction-related origin of eclogite xenoliths from the Wajrakarur kimberlite field, Eastern Dharwar craton, Southern India: Constraints from petrology and geochemistry. *Geochim Cosmochim Acta* 166:165–188.  
<https://doi.org/10.1016/j.gca.2015.06.023>

Donnelly C (2006) The characterization of diamonds and their mineral inclusions from the Diavik Diamond Mine, Lac de Gras, Northwest Territories, Canada. University of Alberta

Duncan MS, Dasgupta R (2017) Rise of Earth's atmospheric oxygen controlled by efficient subduction of organic carbon. *Nat Geosci* 10:387–392. <https://doi.org/10.1038/ngeo2939>

Eiler JM, Schiano P, Kitchen N, Stolper EM (2000a) Oxygen-isotope evidence for recycled crust in the sources of mid-ocean-ridge basalts. *Nature* 403:530–534.  
<https://doi.org/10.1038/35000553>

Eiler JM, Crawford A, Elliott T, et al (2000b) Oxygen Isotope Geochemistry of Oceanic-Arc Lavas. *J Pet* 41:229–256. <https://doi.org/10.1093/petrology/41.2.229>

Eiler JM (2001) Oxygen Isotope Variations of Basaltic Lavas and Upper Mantle Rocks. *Rev Miner Geochem* 43:319–364. <https://doi.org/10.2138/gsrmg.43.1.319>

Evans BW (2008) Control of the Products of Serpentinization by the Fe<sup>2+</sup>Mg–1 Exchange Potential of Olivine and Orthopyroxene. *J Pet* 49:1873–1887.  
<https://doi.org/10.1093/petrology/egn050>

- Faccenda M (2014) Water in the slab: A trilogy. *Tectonophysics* 614:1–30
- Farmer JR, Höönic B, Uchikawa J (2016) Single laboratory comparison of MC-ICP-MS and N-TIMS boron isotope analyses in marine carbonates. *Chem Geol* 447:173–182.  
<https://doi.org/10.1016/j.chemgeo.2016.11.008>
- Fischer TP (2008) Fluxes of volatiles (H<sub>2</sub>O, CO<sub>2</sub>, N<sub>2</sub>, Cl, F) from arc volcanoes. *Geochem. J.* 42:21–38
- Foley SF, Yaxley GM, Kjarsgaard BA (2019) Kimberlites from source to surface: Insights from experiments. *Elements* 15:393–398. <https://doi.org/10.2138/gselements.15.6.393>
- Foster GL, Pogge Von Strandmann PAE, Rae JWB (2010) Boron and magnesium isotopic composition of seawater. *Geochemistry, Geophys Geosystems* 11:..  
<https://doi.org/10.1029/2010GC003201>
- Foster GL (2008) Seawater pH, pCO<sub>2</sub> and [CO<sub>2</sub>–3] variations in the Caribbean Sea over the last 130 kyr: A boron isotope and B/Ca study of planktic foraminifera. *Earth Planet Sci Lett* 271:254–266. <https://doi.org/10.1016/j.epsl.2008.04.015>
- Foster GL, Höönic B, Paris G, et al (2013) Interlaboratory comparison of boron isotope analyses of boric acid, seawater and marine CaCO<sub>3</sub> by MC-ICPMS and NTIMS. *Chem Geol* 358:1–14.  
<https://doi.org/10.1016/j.chemgeo.2013.08.027>
- Frost DJ, McCammon CA (2008) The redox state of Earth’s mantle. *Annu Rev Earth Planet Sci* 36:389–420. <https://doi.org/10.1146/annurev.earth.36.031207.124322>
- Früh-Green GL, Scambelluri M, Vallis F (2001) O–H isotope ratios of high pressure ultramafic rocks: implications for fluid sources and mobility in the subducted hydrous mantle. *Contrib Miner Pet* 141:145–159. <https://doi.org/10.1007/s004100000228>
- Furnes H, Muehlenbachs K, Tumyr O, et al (1999) Depth of active bio-alteration in the ocean crust:

Costa Rica Rift (Hole 504B). *Terra Nov* 11:228–233. <https://doi.org/10.1046/j.1365-3121.1999.00251.x>

Furnes H, Staudigel H, Thorseth IH, et al (2001) Bioalteration of basaltic glass in the oceanic crust. *Geochemistry, Geophys Geosystems* 2:. <https://doi.org/10.1029/2000gc000150>

Gaillardet J, Allègre CJ (1995) Boron isotopic compositions of corals: Seawater or diagenesis record? *Earth Planet Sci Lett* 136:665–676. [https://doi.org/10.1016/0012-821X\(95\)00180-K](https://doi.org/10.1016/0012-821X(95)00180-K)

Gaillou EE, Post JE, Rost D, Butler JE (2012) Boron in natural type IIb blue diamonds: Chemical and spectroscopic measurements. *Am Mineral* 97:1–18. <https://doi.org/10.2138/am.2012.3925>

Galy V, France-Lanord C, Peucker-Ehrenbrink B, Huyghe P (2010) Sr-Nd-Os evidence for a stable erosion regime in the Himalaya during the past 12 Myr. *Earth Planet Sci Lett* 290:474–480. <https://doi.org/10.1016/j.epsl.2010.01.004>

Garlick GD, Macgregor ID, Vogel DE (1971) Oxygen isotope ratios in eclogites from kimberlites. *Science* 172:1025–1027. <https://doi.org/10.1126/science.172.3987.1025>

Gatanzaro EJ, Ghampion GE, Garner EL, et al (1970) Standard reference materials: Boric acid; isotopic and assay standard reference materials. *Natl Bur Stand Spec Publ* 260:1–70

Ghiorso MS, Hirschmann MM, Reiners PW, Kress VC (2002) The pMELTS: A revision of MELTS for improved calculation of phase relations and major element partitioning related to partial melting of the mantle to 3 GPa. *Geochemistry, Geophys Geosystems* 3:1–35. <https://doi.org/10.1029/2001gc000217>

Goes S, Agrusta R, van Hunen J, Garel F (2017) Subduction-transition zone interaction: A review. *Geosphere* 13:644–664. <https://doi.org/10.1130/GES01476.1>

Gréau Y, Huang JX, Griffin WL, et al (2011) Type I eclogites from Roberts Victor kimberlites: Products of extensive mantle metasomatism. *Geochim Cosmochim Acta* 75:6927–6954.

<https://doi.org/10.1016/j.gca.2011.08.035>

Griffin WL, O'Reilly SY, Ryan CG (1999) The composition and origin of sub-continental lithospheric mantle. *Mantle Petrology: Field Observations and High Pressure Experimentation: A Tribute to Francis R (Joe) Boyd*

Grütter HS, Gurney JJ, Menzies AH, Winter F (2004) An updated classification scheme for mantle-derived garnet, for use by diamond explorers. *Lithos* 77:841–857.

<https://doi.org/10.1016/j.lithos.2004.04.012>

Gutjahr M Sub-permil interlaboratory consistency for solution- based boron isotope analyses on marine carbonates *Geostandards and Geoanalytical Research*, in review. *Geostand Geoanalytical Res*

Haggerty SE (1992) Diamonds in West Africa: Tectonic setting and kimberlite productivity. *Russ Geol Geophys* 33:35–49

Haggerty SE (1999) A diamond trilogy: Superplumes, supercontinents, and supernovae. *Science* 285:851–860

Harris JW (1994) The Physical Characteristics and Syngenetic Inclusion Geochemistry of Diamonds from Pipe 50, Liaoning Province, People's Republic of China. *Proc Int Kimberl Conf* 2:106–115. <https://doi.org/10.29173/ikc2498>

Harte B, Hutchison MT, Lee M, Harris JW (2018) Inclusions of (Mg,Fe)O in mantle diamonds. In: International Kimberlite Conference: Extended Abstracts. pp 308–310

Harte B (2010) Diamond formation in the deep mantle: the record of mineral inclusions and their distribution in relation to mantle dehydration zones. *Miner Mag* 74:189–215.

<https://doi.org/10.1180/minmag.2010.074.2.189>

Harvey J, Garrido CJ, Savov I, et al (2014) 11B-rich fluids in subduction zones: The role of

antigorite dehydration in subducting slabs and boron isotope heterogeneity in the mantle.

Chem Geol 376:20–30. <https://doi.org/10.1016/j.chemgeo.2014.03.015>

Helmstaedt H, Schulze DJ (1989) Southern African kimberlites and their mantle sample: implications for Archean tectonics and lithosphere evolution. In: Ross J, Ferguson J (eds) Kimberlites and Related Rocks—Proceedings of the 4th International Kimberlite Conference. Geological Society of Australia by Blackwell Scientific Publications, pp 358–368

Hemming NG, Hanson GN (1992) Boron isotopic composition and concentration in modern marine carbonates. Geochim Cosmochim Acta 56:537–543. [https://doi.org/10.1016/0016-7037\(92\)90151-8](https://doi.org/10.1016/0016-7037(92)90151-8)

Herzberg C, Rudnick R (2012) Formation of cratonic lithosphere: An integrated thermal and petrological model. Lithos 149:4–15. <https://doi.org/10.1016/j.lithos.2012.01.010>

Hirschmann MM, Dasgupta R (2009) The H/C ratios of Earth’s near-surface and deep reservoirs, and consequences for deep Earth volatile cycles. Chem Geol 262:4–16.  
<https://doi.org/10.1016/j.chemgeo.2009.02.008>

Hoernle K, Tilton G, Le Bas MJ, et al (2002) Geochemistry of oceanic carbonatites compared with continental carbonatites: Mantle recycling of oceanic crustal carbonate. Contrib to Mineral Petrol 142:520–542. <https://doi.org/10.1007/s004100100308>

Hofmann AW (1997) Mantle geochemistry: the message from oceanic volcanism. Nature 385:219.  
<https://doi.org/10.1038/385219a0>

Howell D, Collins AT, Loudin LC, et al (2019) Automated FTIR mapping of boron distribution in diamond. Diam Relat Mater 96:207–215. <https://doi.org/10.1016/j.diamond.2019.02.029>

Howell D, Stachel T, Stern RA, et al (2020) Deep carbon through time: Earth’s diamond record and its implications for carbon cycling and fluid speciation in the mantle. Geochim

Cosmochim Acta 275:99–122. <https://doi.org/10.1016/j.gca.2020.02.011>

Huang JX, Griffin WL, Gréau Y, et al (2013) Unmasking xenolithic eclogites: Progressive metasomatism of a key Roberts Victor sample. *Chem Geol* 364:56–65.  
<https://doi.org/10.1016/j.chemgeo.2013.11.025>

Huang JX, Xiang YX, An Y, et al (2016) Magnesium and oxygen isotopes in Roberts Victor eclogites. *Chem Geol* 438:73–83. <https://doi.org/10.1016/j.chemgeo.2016.05.030>

Hulett S, Simonetti A, Rasbury ET, Hemming NG (2016) Recycling of subducted crustal components into carbonatite melts revealed by boron isotopes. *Nat Geosci* 9:904–908.  
<https://doi.org/10.1038/NGEO2831>

Ickert RB, Stachel T, Stern RA, Harris JW (2013) Diamond from recycled crustal carbon documented by coupled  $\delta^{18}\text{O}$ - $\delta^{13}\text{C}$  measurements of diamonds and their inclusions. *Earth Planet Sci Lett* 364:85–97. <https://doi.org/10.1016/j.epsl.2013.01.008>

Ickert RB, Stachel T, Stern RA, Harris JW (2015) Extreme  $^{18}\text{O}$ -enrichment in majorite constrains a crustal origin of transition zone diamonds. *Geochemical Perspect Lett* 1:65–74.

<https://doi.org/http://dx.doi.org/10.7185/geochemlet.1507>

Ickert RB, Stern RA (2013) Matrix corrections and error analysis in high-precision SIMS  $^{18}\text{O}/^{16}\text{O}$  measurements of Ca–Mg–Fe Garnet. *Geostand Geoanal Res* 37:429–448.

<https://doi.org/10.1111/j.1751-908X.2013.00222.x>

Irifune T, Ringwood AE (1987) Phase transformations in a harzburgite composition to 26 GPa: implications for dynamical behaviour of the subducting slab. *Earth Planet Sci Lett* 86:365–376. [https://doi.org/10.1016/0012-821X\(87\)90233-0](https://doi.org/10.1016/0012-821X(87)90233-0)

Irvine GJ, Pearson DG, Kjarsgaard BA, et al (2003) A Re–Os isotope and PGE study of kimberlite-derived peridotite xenoliths from Somerset Island and a comparison to the Slave and Kaapvaal

cratons. *Lithos* 71:461–488. [https://doi.org/10.1016/S0024-4937\(03\)00126-9](https://doi.org/10.1016/S0024-4937(03)00126-9)

Ishikawa T, Nakamura E (1993) Boron isotope systematics of marine sediments. *Earth Planet Sci Lett* 117:567–580

Ishikawa T, Nakamura E (1994) Origin of the slab component in arc lavas from across-arc variation of B and Pb isotopes. *Nature* 370:205–208.

<https://doi.org/https://doi.org/10.1038/370205a0>

Ishikawa T, Tera F (1997) Source, composition and distribution of the fluid in the Kurile mantle wedge: constraints from across-arc variations of B/Nb and B isotopes. *Earth Planet Sci Lett* 152:123–138. [https://doi.org/https://doi.org/10.1016/S0012-821X\(97\)00144-1](https://doi.org/https://doi.org/10.1016/S0012-821X(97)00144-1)

Ishikawa T, Tera F, Nakazawa T (2001) Boron isotope and trace element systematics of the three volcanic zones in the Kamchatka arc. *Geochim Cosmochim Acta* 65:4523–4537.

[https://doi.org/https://doi.org/10.1016/S0016-7037\(01\)00765-7](https://doi.org/https://doi.org/10.1016/S0016-7037(01)00765-7)

Jacob DE, Bizimis M, Salters VJ (2005) Lu-Hf and geochemical systematics of recycled ancient oceanic crust: Evidence from Roberts Victor eclogites. *Contrib to Mineral Petrol* 148:707–720. <https://doi.org/10.1007/s00410-004-0631-x>

Jacob DE, Viljoen KS, Grassineau N V. (2009) Eclogite xenoliths from Kimberley, South Africa - A case study of mantle metasomatism in eclogites. *Lithos* 112:1002–1013.

<https://doi.org/10.1016/j.lithos.2009.03.034>

Jacob D, Jagoutz E, Lowry D, et al (1994) Diamondiferous eclogites from Siberia: Remnants of Archean oceanic crust. *Geochim Cosmochim Acta* 58:5191–5207.

[https://doi.org/10.1016/0016-7037\(94\)90304-2](https://doi.org/10.1016/0016-7037(94)90304-2)

Jagoutz E, Dawson J, Hoernes S, et al (1984) Anorthositic oceanic crust in the archean earth. *Lunar Planet Sci* 15:395–396

Jaques AL, Hall AE, Sheraton JW, et al (2019) Composition of crystalline inclusions and C-isotopic composition of Argyle and Ellendale diamonds. *Kimberlites Relat Rocks* 2:966–989.  
<https://doi.org/10.29173/ikc1192>

Jordan TH (1978) Composition and development of the continental tectosphere. *Nature* 274:544.  
<https://doi.org/10.1038/274544a0>

Kaminsky F V., Zakharchenko O, Davies RM, et al (2001) Superdeep diamonds from the Juina area, Mato Grosso State, Brazil. *Contrib Miner Pet* 140:734–753.  
<https://doi.org/10.1007/s004100000221>

Kaminsky F V., Zakharchenko OD, Griffin WL, et al (2000) Diamond from the Guaniamo area, Venezuela. *Can Mineral* 38:1347–1370. <https://doi.org/10.2113/gscanmin.38.6.1347>

Katsura T, Ito E (1996) Determination of Fe-Mg partitioning between perovskite and magnesiowüstite. *Geophys Res Lett* 23:2005–2008. <https://doi.org/10.1029/96GL02086>  
Kelemen PB, Dick HJB, Quick JE (1992) Formation of harzburgite by pervasive melt/rock reaction in the upper mantle. *Nature* 358:635. <https://doi.org/10.1038/358635a0>

Kelemen PB, Hart SR, Bernstein S (1998) Silica enrichment in the continental upper mantle via melt/rock reaction. *Earth Planet Sci Lett* 164:387–406. [https://doi.org/10.1016/S0012-821X\(98\)00233-7](https://doi.org/10.1016/S0012-821X(98)00233-7)

Kelemen PB, Manning CE (2015) Reevaluating carbon fluxes in subduction zones, what goes down, mostly comes up. *PNAS* 112:. <https://doi.org/10.1073/pnas.1507889112>

Kesson SE, Ringwood AE (1989) Slab-mantle interactions. 2. The formation of diamonds. *Chem Geol* 78:97–118. [https://doi.org/10.1016/0009-2541\(89\)90110-1](https://doi.org/10.1016/0009-2541(89)90110-1)

King JM, Moses TM, Shigley JE, et al (1998) Characterizing natural-color type IIb blue diamonds. *Gems Gemol* 34:246–268

- Kirby S, Engdahl ER, Denlinger R (1996) Intermediate-depth intraslab earthquakes and arc volcanism as physical expressions of crustal and uppermost mantle metamorphism in subducting slabs. In: Subduction: Top to Bottom. Blackwell Publishing Ltd, pp 195–214
- Kiseeva ES, Litasov KD, Yaxley GM, et al (2013a) Melting and phase relations of carbonated eclogite at 9–21 gpa and the petrogenesis of alkali-rich melts in the deep mantle. *J Petrol* 54:1555–1583. <https://doi.org/10.1093/petrology/egt023>
- Kiseeva ES, Yaxley GM, Stepanov AS, et al (2013b) Metapyroxenite in the mantle transition zone revealed from majorite inclusions in diamonds. *Geology* 41:883–886.  
<https://doi.org/10.1130/G34311.1>
- Kiseeva ES, Vasiukov DM, Wood BJ, et al (2018) Oxidized iron in garnets from the mantle transition zone. *Nat Geosci* 11:144–147. <https://doi.org/10.1038/s41561-017-0055-7>
- Kiss E (1988) Ion-exchange separation and spectrophotometric determination of boron in geological materials. *Anal Chim Acta* 211:243–256. [https://doi.org/10.1016/S0003-2670\(00\)83684-3](https://doi.org/10.1016/S0003-2670(00)83684-3)
- Koga KT, Van Orman JA, Walter MJ (2003) Diffusive relaxation of carbon and nitrogen isotope heterogeneity in diamond: a new thermochronometer. *Phys Earth Planet Inter* 139:35–43.  
[https://doi.org/10.1016/S0031-9201\(03\)00141-9](https://doi.org/10.1016/S0031-9201(03)00141-9)
- Kopylova MG, Russell JK, Cookenboo H (1999) Petrology of peridotite and pyroxenite xenoliths from the Jericho Kimberlite: Implications for the thermal state of the mantle beneath the Slave Craton, Northern Canada. *J Petrol* 40:79–104. <https://doi.org/10.1093/petroj/40.1.79>
- Korolev NM, Kopylova M, Bussweiler Y, et al (2018a) The uniquely high-temperature character of Cullinan diamonds: A signature of the Bushveld mantle plume? *Lithos* 304–307:362–373.  
<https://doi.org/10.1016/j.lithos.2018.02.011>

Korolev NM, Melnik AE, Li XH, Skublov SG (2018b) The oxygen isotope composition of mantle eclogites as a proxy of their origin and evolution: A review. *Earth-Science Rev* 185:288–300. <https://doi.org/10.1016/j.earscirev.2018.06.007>

Kouamelan AN, Delor C, Peucat J (1997) Geochronological evidence for reworking of Archean terrains during the Early Proterozoic (2.1 Ga) in the western Côte d'Ivoire (Man Rise-West African Craton). *Precambrian Res* 86:177–199. [https://doi.org/10.1016/S0301-9268\(97\)00043-0](https://doi.org/10.1016/S0301-9268(97)00043-0)

Krebs MY, Pearson DG, Stachel T, et al (2019) A common parentage-low abundance trace element data of gem diamonds reveals similar fluids to fibrous diamonds. *Lithos* 324–325:356–370. <https://doi.org/10.1016/j.lithos.2018.11.025>

Kusky TM, Windley BF, Wang L, et al (2014) Flat slab subduction, trench suction, and craton destruction: Comparison of the North China, Wyoming, and Brazilian cratons. *Tectonophysics* 630:208–221. <https://doi.org/10.1016/j.tecto.2014.05.028>

Labrosse S, Jaupart C (2007) Thermal evolution of the Earth: Secular changes and fluctuations of plate characteristics. *Earth Planet Sci Lett* 260:465–481. <https://doi.org/10.1016/j.epsl.2007.05.046>

Lafuente B, Downs RT, Yang H, Stone N (2016) The power of databases: The RRUFF project. In: *Highlights in Mineralogical Crystallography*. Walter de Gruyter, pp 1–29

Laiginhas FATP (2008) Diamonds from the Ural Mountains : their characteristics and the mineralogy and geochemistry of their inclusions. PhD Thesis, University of Glasgow

Lee C-TA, Luffi P, Chin EJ (2011) Building and destroying continental mantle. *Annu Rev Earth Planet Sci* 39:59–90. <https://doi.org/10.1146/annurev-earth-040610-133505>

Leeman WP, Sisson VB (1996) Geochemistry of boron and its implications for crustal and mantle

processes. *Rev Miner Geochem* 33:645–707

Leeman WP, Tonarini S, Turner S (2017) Boron isotope variations in Tonga-Kermadec-New Zealand arc lavas: Implications for the origin of subduction components and mantle influences. *Geochemistry, Geophys Geosystems* 18:1126–1162.

<https://doi.org/10.1002/2016GC006523>

Leost I, Stachel T, Brey GP, et al (2003) Diamond formation and source carbonation: mineral associations in diamonds from Namibia. *Contrib to Mineral Petrol* 145:15–24.

<https://doi.org/10.1007/s00410-003-0442-5>

Li K, Li L, Pearson DG, Stachel T (2019) Diamond isotope compositions indicate altered igneous oceanic crust dominates deep carbon recycling. *Earth Planet Sci Lett* 516:190–201.

<https://doi.org/10.1016/j.epsl.2019.03.041>

Li L, Bebout GE, Idleman BD (2007) Nitrogen concentration and  $\delta^{15}\text{N}$  of altered oceanic crust obtained on ODP Legs 129 and 185: Insights into alteration-related nitrogen enrichment and the nitrogen subduction budget. *Geochim Cosmochim Acta* 71:2344–2360.

<https://doi.org/10.1016/j.gca.2007.02.001>

Li L, Zheng YF, Cartigny P, Li J (2014) Anomalous nitrogen isotopes in ultrahigh-pressure metamorphic rocks from the Sulu orogenic belt: Effect of abiotic nitrogen reduction during fluid-rock interaction. *Earth Planet Sci Lett* 403:67–78.

<https://doi.org/10.1016/j.epsl.2014.06.029>

Li ZX, Lee CTA, Peslier AH, et al (2008) Water contents in mantle xenoliths from the Colorado Plateau and vicinity: Implications for the mantle rheology and hydration-induced thinning of continental lithosphere. *J Geophys Res Solid Earth* 113:.

<https://doi.org/10.1029/2007JB005540>

Lodders K (2003) Solar System Abundances and Condensation Temperatures of the Elements.

Astrophys J 591:1220–1247. <https://doi.org/10.1086/375492>

Logvinova AM, Taylor LA, Floss C, Sobolev N V (2005) Geochemistry of multiple diamond

inclusions of harzburgitic garnets as examined in situ. Int Geol Rev 47:1223–1233.

<https://doi.org/10.2747/0020-6814.47.12.1223>

Lowry D, Mattey DP, Harris JW (1999) Oxygen isotope composition of syngenetic inclusions in

diamond from the Finsch Mine, RSA. Geochim Cosmochim Acta 63:1825–1836.

[https://doi.org/10.1016/S0016-7037\(99\)00120-9](https://doi.org/10.1016/S0016-7037(99)00120-9)

Luth RW, Virgo D, Boyd FR, Wood BJ (1990) Ferric iron in mantle-derived garnets - Implications

for thermobarometry and for the oxidation state of the mantle. Contrib to Mineral Petrol

104:56–72. <https://doi.org/10.1007/BF00310646>

MacGregor ID, Manton WI (1986) Roberts victor eclogites: Ancient oceanic crust. J Geophys Res

91:14063. <https://doi.org/10.1029/jb091ib14p14063>

Malkovets V, Taylor LA, Griffin WL, et al (2003) Eclogites from the Grib kimberlite pipe,

Arkhangelsk, Russia. In: International Kimberlite Conference: Extended Abstracts, Vol. 8

Marschall HR (2018) Boron isotopes in the ocean floor realm and the mantle. In: Marschall H,

Foster G (eds) Boron Isotopes. Springer, Cham, pp 189–215

Marschall HR, Altherr R, Rüpké L (2007) Squeezing out the slab - modelling the release of Li, Be

and B during progressive high-pressure metamorphism. Chem Geol 239:323–335.

<https://doi.org/10.1016/j.chemgeo.2006.08.008>

Martin C, Flores KE, Vitale-Brovarone A, et al (2020) Deep mantle serpentinization in subduction

zones: Insight from in situ B isotopes in slab and mantle wedge serpentinites. Chem Geol

119637. <https://doi.org/10.1016/j.chemgeo.2020.119637>

Marty B, Zimmermann L (1999) Volatiles (He, C, N, Ar) in mid-ocean ridge basalts: Assessment of shallow-level fractionation and characterization of source composition. *Geochim Cosmochim Acta* 63:3619–3633. [https://doi.org/10.1016/S0016-7037\(99\)00169-6](https://doi.org/10.1016/S0016-7037(99)00169-6)

Mather KA (2012) A xenolith-based lithospheric transect of the Slave craton, N.W.T., Canada. Durham University

Mattey D, Lowry D, Macpherson C (1994) Oxygen isotope composition of mantle peridotite. *Earth Planet Sci Lett* 128:231–241. [https://doi.org/10.1016/0012-821X\(94\)90147-3](https://doi.org/10.1016/0012-821X(94)90147-3)

Mc Kenna N, Gurney JJ, Klump J, Davidson JM (2004) Aspect of diamond mineralisation and distribution at the Helam Mine, South Africa. *Lithos* 77:193–208.  
<https://doi.org/10.1016/j.lithos.2004.04.004>

McCaig AM, Titarenko SS, Savov IP, et al (2018) No significant boron in the hydrated mantle of most subducting slabs. *Nat Commun* 9:1–10. <https://doi.org/10.1038/s41467-018-07064-6>

McCammon CA, Stachel T, Harris JW (2004) Iron oxidation state in lower mantle mineral assemblages II. Inclusions in diamonds from Kankan, Guinea. *Earth Planet Sci Lett* 222:423–434. <https://doi.org/10.1016/j.epsl.2004.03.019>

McCammon CA (2005) Mantle oxidation state and oxygen fugacity: Constraints on mantle chemistry, structure, and dynamics. In: Earth's deep mantle: Structure, composition, and evolution. pp 219–240

McDade P, Harris JW (1998) Syngenetic inclusion bearing diamonds from Letseng-la-Terai, Lesotho. In: International Kimberlite Conference: Extended Abstracts. Vol 7. pp 561–563

McDonough WF, Rudnick RL (1998) Mineralogy and composition of the upper mantle. *Rev Miner Geochem* 37:139–164

McDonough WF, Sun S-S (1995) The composition of the Earth. *Chem Geol* 120:223–253.

[https://doi.org/https://doi.org/10.1016/0009-2541\(94\)00140-4](https://doi.org/https://doi.org/10.1016/0009-2541(94)00140-4)

McKenzie D, Priestley K (2016) Speculations on the formation of cratons and cratonic basins.

Earth Planet Sci Lett 435:94–104. <https://doi.org/10.1016/j.epsl.2015.12.010>

McNeill J, Pearson DG, Klein-Bendavid O, et al (2009) Quantitative analysis of trace element concentrations in some gem-quality diamonds. *J Phys Condens Matter* 21:13.

<https://doi.org/10.1088/0953-8984/21/36/364207>

Melton GL, Stachel T, Stern RA, et al (2013) Infrared spectral and carbon isotopic characteristics of micro- and macro-diamonds from the Panda kimberlite (Central Slave Craton, Canada).

Lithos 177:110–119. <https://doi.org/10.1016/j.lithos.2013.06.019>

Meyer HO (1987) Inclusions in diamonds. In: Mantle xenoliths. John Wiley and Sons, pp 501–522

Mitchell AL, Grove TL (2015) Melting the hydrous, subarc mantle: the origin of primitive andesites. *Contrib Miner Pet* 170:13. <https://doi.org/10.1007/s00410-015-1161-4>

Moore RO, Gurney JJ (1989) Mineral inclusions in diamond from Monastery kimberlite, South Africa. In: Kimberlites and related rocks. p 1041

Moore RO, Gurney JJ, Griffin WL, Shimizu N (1991) Ultra-high pressure garnet inclusions in Monastery diamonds: trace element abundance patterns and conditions of origin. *Eur J Mineral* 3:213–230. <https://doi.org/10.1127/ejm/3/2/0213>

Morris JD, Leeman WP, Tera F (1990) The subducted component in island arc lavas: constraints from Be isotopes and B-Be systematics. *Nature* 344:31–36. <https://doi.org/10.1038/344031a0>

Motsamai T (2019) The composition of the lithospheric mantle beneath the Karowe Mine and its associated diamond sources in north-eastern Botswana. University of Alberta

Moussallam Y, Longpré M-AA, McCammon C, et al (2019) Mantle plumes are oxidised. *Earth Planet Sci Lett* 527:115798. <https://doi.org/10.1016/J.EPSL.2019.115798>

- Muehlenbachs K, Clayton RN (1976) Oxygen isotope composition of the oceanic crust and its bearing on seawater. *J Geophys Res* 81:4365–4369. <https://doi.org/10.1029/JB081i023p04365>
- Nakano T, Nakamura E (2001) Boron isotope geochemistry of metasedimentary rocks and tourmalines in a subduction zone metamorphic suite. *Phys Earth Planet Inter* 127:233–252
- Neal CR, Taylor LA, Davidson JP, et al (1990) Eclogites with oceanic crustal and mantle signatures from the Bellsbank kimberlite, South Africa, part 2: Sr, Nd, and O isotope geochemistry. *Earth Planet Sci Lett* 99:362–379. [https://doi.org/10.1016/0012-821X\(90\)90140-S](https://doi.org/10.1016/0012-821X(90)90140-S)
- Newville M (2013) Larch: An analysis package for XAFS and related spectroscopies. In: *Journal of Physics: Conference Series*. p 12007
- Ni H, Keppler H, Behrens H (2011) Electrical conductivity of hydrous basaltic melts: Implications for partial melting in the upper mantle. *Contrib to Mineral Petrol* 162:637–650.  
<https://doi.org/10.1007/s00410-011-0617-4>
- Nishi M, Irifune T, Tsuchiya J, et al (2014) Stability of hydrous silicate at high pressures and water transport to the deep lower mantle. *Nat Geosci London* 7:224–227.  
<https://doi.org/10.1038/ngeo2074>
- Ohtani E, Mizobata H, Yurimoto H (2000) Stability of dense hydrous magnesium silicate phases in the systems Mg<sub>2</sub>SiO<sub>4</sub>-H<sub>2</sub>O and MgSiO<sub>3</sub>-H<sub>2</sub>O at pressures up to 27 GPa. *Phys Chem Miner* 27:533–544. <https://doi.org/10.1007/s002690000097>
- Ongley JS, Basu AR, Kurtis Kyser T (1987) Oxygen isotopes in coexisting garnets, clinopyroxenes and phlogopites of Roberts Victor eclogites: implications for petrogenesis and mantle metasomatism. *Earth Planet Sci Lett* 83:80–84. [https://doi.org/10.1016/0012-821X\(87\)90052-5](https://doi.org/10.1016/0012-821X(87)90052-5)

- Ono S, Ito E, Katsura T (2001) Mineralogy of subducted basaltic crust (MORB) from 25 to 37 GPa, and chemical heterogeneity of the lower mantle. *Earth Planet Sci Lett* 190:57–63.  
[https://doi.org/10.1016/S0012-821X\(01\)00375-2](https://doi.org/10.1016/S0012-821X(01)00375-2)
- Otsuka K, Longo M, Mccammon CA, Karato S (2013) Ferric iron content of ferropericlase as a function of composition , oxygen fugacity , temperature and pressure : Implications for redox conditions during diamond formation in the lower mantle. *Earth Planet Sci Lett* 365:7–16.  
<https://doi.org/10.1016/j.epsl.2012.11.030>
- Otter ML, Gurney JJ (1989) Mineral inclusions in diamonds from the Sloan diatremes, Colorado-Wyoming State Line kimberlite district. North America. In: Kimberlites and related rocks. pp 1042–1053
- Pabst S, Zack T, Savov IP, et al (2012) The fate of subducted oceanic slabs in the shallow mantle: Insights from boron isotopes and light element composition of metasomatized blueschists from the Mariana forearc. *Lithos* 132:162–179
- Palot M, Cartigny P, Harris JW, et al (2012) Evidence for deep mantle convection and primordial heterogeneity from nitrogen and carbon stable isotopes in diamond. *Earth Planet Sci Lett* 357–358:179–193. <https://doi.org/10.1016/j.epsl.2012.09.015>
- Palot M, Pearson DG, Stern RA, et al (2014) Isotopic constraints on the nature and circulation of deep mantle C-H-O-N fluids: Carbon and nitrogen systematics within ultra-deep diamonds from Kankan (Guinea). *Geochim Cosmochim Acta* 139:26–46.  
<https://doi.org/10.1016/j.gca.2014.04.027>
- Palot M, Cartigny P, Viljoen F (2009) Diamond origin and genesis: A C and N stable isotope study on diamonds from a single eclogitic xenolith (Kaalvallei, South Africa). *Lithos* 112:758–766.  
<https://doi.org/10.1016/j.lithos.2009.04.013>

Palyanov YN, Bataleva Y V, Sokol AG, et al (2013) Mantle-slab interaction and redox mechanism of diamond formation. *Proc Natl Acad Sci* 110:20408–20413.

<https://doi.org/10.1073/pnas.1313340110>

Parman SW, Grove TL, Dann JC, de Wit MJ (2004) A subduction origin for komatiites and cratonic lithospheric mantle. *South Afr J Geol* 107:107–118. <https://doi.org/10.2113/107.1-2.107>

Peacock SM, Hervig RL (1999) Boron isotopic composition of subduction-zone metamorphic rocks. *Chem Geol* 160:281–290. [https://doi.org/https://doi.org/10.1016/S0009-2541\(99\)00103-5](https://doi.org/10.1016/S0009-2541(99)00103-5)

Pearson DG, Irvine GJ, Ionov DA, et al (2004) Re-Os isotope systematics and platinum group element fractionation during mantle melt extraction: A study of massif and xenolith peridotite suites. *Chem Geol* 208:29–59. <https://doi.org/10.1016/j.chemgeo.2004.04.005>

Pearson DG, Wittig N (2008) Formation of Archaean continental lithosphere and its diamonds: The root of the problem. *J Geol Soc London* 165:895–914. <https://doi.org/10.1144/0016-76492008-003>

Pearson DGG, Wittig N (2014) The formation and evolution of craton mantle lithosphere - Evidence from mantle xenoliths. *Treatise Geochemistry Second Ed* 3:255–292

Pernet-Fisher JF, Howarth GH, Liu Y, et al (2014) Komsomolskaya diamondiferous eclogites: Evidence for oceanic crustal protoliths. *Contrib to Mineral Petrol* 167:1–17. <https://doi.org/10.1007/s00410-014-0981-y>

Phillips D, Harris JW, Viljoen KS (2004) Mineral chemistry and thermobarometry of inclusions from De Beers Pool diamonds, Kimberley, South Africa. *Lithos* 77:155–179. <https://doi.org/10.1016/j.lithos.2004.04.005>

Plank T, Manning CE (2019) Subducting carbon. *Nature* 574:343–352.

<https://doi.org/10.1038/s41586-019-1643-z>

Pokhilenko NP, Sobolev N V., Reutsky VN, et al (2004) Crystalline inclusions and C isotope ratios in diamonds from the Snap Lake/King Lake kimberlite dyke system: Evidence of ultradeep and enriched lithospheric mantle. *Lithos* 77:57–67.

<https://doi.org/10.1016/j.lithos.2004.04.019>

Rae JWB (2018) Boron isotopes in foraminifera: Systematics, biomineralisation, and CO<sub>2</sub> reconstruction. In: *Advances in Isotope Geochemistry*. Springer, pp 107–143

Regier ME, Miškovi A, Ickert RB, et al (2018) An oxygen isotope test for the origin of Archean mantle roots. *Geochemical Perspect Lett* 9:6–10. <https://doi.org/10.7185/geochemlet.1830>

Richards JP (2003) Tectono-magmatic precursors for porphyry Cu-(Mo-Au) deposit formation. *Econ Geol* 98:1515–1533. <https://doi.org/10.2113/gsecongeo.98.8.1515>

Richardson SH, Shirey SB, Harris JW, Carlson RW (2001) Archean subduction recorded by Re-Os isotopes in eclogitic sulfide inclusions in Kimberley diamonds. *Earth Planet Sci Lett* 191:257–266. [https://doi.org/10.1016/S0012-821X\(01\)00419-8](https://doi.org/10.1016/S0012-821X(01)00419-8)

Richardson SH, Shirey SB, Harris JW (2004) Episodic diamond genesis at Jwaneng, Botswana, and implications for Kaapvaal craton evolution. *Lithos* 77:143–154.

<https://doi.org/10.1016/J.LITHOS.2004.04.027>

Richardson S, Chinn I, Harris J (1998) Age and origin of eclogitic diamonds from the Jwaneng kimberlite, Botswana. In: *International Kimberlite Conference: Extended Abstracts*. Vol. 7. pp 734–736

Riches AJV, Liu Y, Day JMD, et al (2010) Subducted oceanic crust as diamond hosts revealed by garnets of mantle xenoliths from Nyurbinskaya, Siberia. *Lithos* 120:368–378.

<https://doi.org/10.1016/j.lithos.2010.09.006>

Riches AJ V, Ickert RB, Pearson DG, et al (2016) In situ oxygen-isotope, major-, and trace-element constraints on the metasomatic modification and crustal origin of a diamondiferous eclogite from Roberts Victor, Kaapvaal Craton. *Geochim Cosmochim Acta* 174:345–359.

<https://doi.org/10.1016/j.gca.2015.11.028>

Ringwood AE (1975) Composition of the upper mantle. In: *Composition and petrology of the Earth's mantle*. p 431

Robinson J, Wood BJ, Blundy JD (1998) The beginning of melting of fertile and depleted peridotite at 1.5 GPa. *Earth Planet Sci Lett* 155:97–111

Rohrbach A, Ghosh S, Schmidt MW, et al (2014) The stability of Fe-Ni carbides in the Earth's mantle: Evidence for a low Fe-Ni-C melt fraction in the deep mantle. *Earth Planet Sci Lett* 388:211–221. <https://doi.org/10.1016/j.epsl.2013.12.007>

Rohrbach A, Schmidt MW (2011) Redox freezing and melting in the Earth's deep mantle resulting from carbon–iron redox coupling. *Nature* 472:209. <https://doi.org/10.1038/nature09899>

Rose EF, Shimizu N, Layne GD, Grove TL (2001) Melt production beneath Mt. Shasta from boron data in primitive melt inclusions. *Science* 293:281–283.

<https://doi.org/10.1126/science.1059663>

Rosenbaum JM, Kyser TK, Walker D (1994) High temperature oxygen isotope fractionation in the enstatite-olivine-BaCO<sub>3</sub> system. *Geochim Cosmochim Acta* 58:2653–2660.

[https://doi.org/10.1016/0016-7037\(94\)90135-X](https://doi.org/10.1016/0016-7037(94)90135-X)

Rosner M, Erzinger J, Franz G, Trumbull RB (2003) Slab-derived boron isotope signatures in arc volcanic rocks from the Central Andes and evidence for boron isotope fractionation during progressive slab dehydration. *Geochemistry, Geophys Geosystems* 4:

[https://doi.org/10.1029/2002GC000438@10.1002/\(ISSN\)1525-2027.FLUX1](https://doi.org/10.1029/2002GC000438@10.1002/(ISSN)1525-2027.FLUX1)

Rudnick RL (1994) Northern Tanzanian peridotite xenolith: a comparison with Kaapvaal peridotites and evidence for carbonatite interaction with ultra-refractory residues. Proc 5th Int'l Kimberl Conf 336–353

Ryabchikov ID, Schreyer W, Abraham K (1982) Compositions of aqueous fluids in equilibrium with pyroxenes and olivines at mantle pressures and temperatures. Contrib to Mineral Petrol 79:80–84. <https://doi.org/10.1007/BF00376964>

Sano Y, Takahata N, Nishio Y, et al (2001) Volcanic flux of nitrogen from the Earth. Chem Geol 171:263–271. [https://doi.org/10.1016/S0009-2541\(00\)00252-7](https://doi.org/10.1016/S0009-2541(00)00252-7)

Scambelluri M, Tonarini S (2012) Boron isotope evidence for shallow fluid transfer across subduction zones by serpentinized mantle. Geology 40:907–910.  
<https://doi.org/10.1130/G33233.1>

Schmandt B, Jacobsen SD, Becker TW, et al (2014) Dehydration melting at the top of the lower mantle. Science 344:1265–1268. <https://doi.org/10.1126/science.1253358>

Schmickler B, Jacob DE, Foley SF (2004) Eclogite xenoliths from the Kuruman kimberlites, South Africa: geochemical fingerprinting of deep subduction and cumulate processes. Lithos 75:173–207. <https://doi.org/10.1016/j.lithos.2003.12.012>

Schmidt C, Thomas R, Heinrich W (2005) Boron speciation in aqueous fluids at 22 to 600°C and 0.1 MPa to 2 GPa. Geochim Cosmochim Acta 69:275–281.  
<https://doi.org/10.1016/j.gca.2004.06.018>

Schulze DJ, Harte B, Zeb Page F, et al (2013) Anticorrelation between low  $\delta^{13}\text{C}$  of eclogitic diamonds and high  $\delta^{18}\text{O}$  of their coesite and garnet inclusions requires a subduction origin. Geology 41:455–458. <https://doi.org/10.1130/G33839.1>

Schulze DJ, Coopersmith HG, Harte B, Pizzolato L-A (2008) Mineral inclusions in diamonds from the Kelsey Lake Mine, Colorado, USA: Depleted Archean mantle beneath the Proterozoic Yavapai province. *Geochim Cosmochim Acta* 72:1685–1695.

<https://doi.org/10.1016/J.GCA.2007.09.037>

Schulze DJ, Valley JW, Spicuzza MJ (2000) Coesite eclogites from the Roberts Victor kimberlite, South Africa. *Lithos* 54:23–32. [https://doi.org/10.1016/S0024-4937\(00\)00031-1](https://doi.org/10.1016/S0024-4937(00)00031-1)

Schulze DJ (1986) Calcium anomalies in the mantle and a subducted metaserpentinite origin for diamonds. *Nature* 319:483–485

Schulze DJ, Valley JW, Spicuzza MJ, et al (2003) Oxygen isotope composition of eclogitic and peridotitic garnet xenocrysts from the La Ceniza kimberlite, Guaniamo, Venezuela. *Int Geol Rev* 45:968–975. <https://doi.org/10.2747/0020-6814.45.11.968>

Schwarzenbach EM, Früh-Green GL, Bernasconi SM, et al (2013) Serpentinization and carbon sequestration: A study of two ancient peridotite-hosted hydrothermal systems. *Chem Geol* 351:115–133. <https://doi.org/10.1016/j.chemgeo.2013.05.016>

Shatsky VS, Zedgenizov DA, Ragozin AL (2016) Evidence for a subduction component in the diamond-bearing mantle of the Siberian craton. *Russ Geol Geophys* 57:111–126. <https://doi.org/10.1016/j.rgg.2016.01.008>

Shatsky VS, Zedgenizov DA, Ragozin AL, Kalinina V V. (2015) Diamondiferous subcontinental lithospheric mantle of the northeastern Siberian Craton: Evidence from mineral inclusions in alluvial diamonds. *Gondwana Res* 28:106–120. <https://doi.org/10.1016/j.gr.2014.03.018>

Shirey SB, Carlson RW, Richardson SH, et al (2001) Archean emplacement of eclogitic components into the lithospheric mantle during formation of the Kaapvaal Craton. *Geophys Res Lett* 28:2509–2512. <https://doi.org/10.1029/2000GL012589>

- Shirey SB, Shigley JE (2013) Recent advances in understanding the geology of diamonds. *Gems Gemol* 49:188–264. <https://doi.org/10.5741/GEMS.49.4.246>
- Shu Q, Brey GP, Hoefer HE, et al (2016) Kyanite/corundum eclogites from the Kaapvaal Craton: subducted troctolites and layered gabbros from the Mid- to Early Archean. *Contrib to Mineral Petrol* 171:1–24. <https://doi.org/10.1007/s00410-015-1225-5>
- Simon NSC, Irvine GJ, Davies GR, et al (2003) The origin of garnet and clinopyroxene in “depleted” Kaapvaal peridotites. *Lithos* 71:289–322. [https://doi.org/10.1016/S0024-4937\(03\)00118-X](https://doi.org/10.1016/S0024-4937(03)00118-X)
- Smart KA, Chacko T, Simonetti A, et al (2014) A record of Paleoproterozoic subduction preserved in the Northern Slave cratonic mantle: Sr–Pb–O isotope and trace-element investigations of eclogite xenoliths from the Jericho and Muskox kimberlites. *J Petrol* 55:549–583.  
<https://doi.org/10.1093/petrology/egt077>
- Smit K V., Stachel T, Creaser RA, et al (2014) Origin of eclogite and pyroxenite xenoliths from the Victor kimberlite, Canada, and implications for Superior craton formation. *Geochim Cosmochim Acta* 125:308–337. <https://doi.org/10.1016/j.gca.2013.10.019>
- Smith D, Alexis Riter JC, Mertzman SA (1999) Water–rock interactions, orthopyroxene growth, and Si-enrichment in the mantle: evidence in xenoliths from the Colorado Plateau, southwestern United States. *Earth Planet Sci Lett* 165:45–54. [https://doi.org/10.1016/S0012-821X\(98\)00251-9](https://doi.org/10.1016/S0012-821X(98)00251-9)
- Smith EM, Shirey SB, Nestola F, et al (2016) Large gem diamonds from metallic liquid in Earth’s deep mantle. *Science* 354:1403–1405. <https://doi.org/10.1126/science.aal1303>
- Smith EM, Shirey SB, Richardson SH, et al (2018) Blue boron-bearing diamonds from Earth’s lower mantle. *Nature* 560:84–87. <https://doi.org/10.1038/s41586-018-0334-5>

Smith HJ, Leeman WP, Davidson J, Spivack AJ (1997) The B isotopic composition of arc lavas from Martinique, Lesser Antilles. *Earth Planet Sci Lett* 146:303–314

Smith HJ, Spivack AJ, Staudigel H, Hart SR (1995) The boron isotopic composition of altered oceanic crust. *Chem Geol* 126:119–135

Snyder GA (1995) Archean mantle heterogeneity and the origin of diamondiferous eclogites, Siberia: evidence from stable isotopes and hydroxyl in garnet. *Am Mineral* 80:799–809.  
<https://doi.org/10.2138/am-1995-7-816>

Sobolev NV, Logvinova AM, Zedgenizov DA, et al (2004) Mineral inclusions in microdiamonds and macrodiamonds from kimberlites of Yakutia: a comparative study. *Lithos* 77:225–242.  
<https://doi.org/10.1016/J.LITHOS.2004.04.001>

Sobolev NV, Logvinova AM, Zedgenizov DA, et al (2009) Petrogenetic significance of minor elements in olivines from diamonds and peridotite xenoliths from kimberlites of Yakutia. *Lithos* 112:701–713. <https://doi.org/10.1016/J.LITHOS.2009.06.038>

Sobolev A V., Asafov E V., Gurenko AA, et al (2016) Komatiites reveal a hydrous Archaean deep-mantle reservoir. *Nature* 531:628–632. <https://doi.org/10.1038/nature17152>

Sobolev N V., Galimov EM, Smith CB, et al (1989) Morphology, inclusions and carbon isotopic composition of diamonds from the King George alluvial deposit and the Argyle lamproitic pipe, Western Australia. *Russ Geol Geophys* 12:3–18

Sobolev N V., Yefimova ES, Reimers LF, et al (1997) Mineral inclusions in the diamonds of arkhangelsk kimberlite province. *Geol i Geofiz* 358–370

Sobolev N V., Yefimova ES, Channer DMDR, et al (1998a) Unusual upper mantle beneath Guaniamo, Guyana shield, Venezuela: Evidence from diamond inclusions. *Geology* 26:971–974. [https://doi.org/10.1130/0091-7613\(1998\)026<0971:UUMBGG>2.3.CO;2](https://doi.org/10.1130/0091-7613(1998)026<0971:UUMBGG>2.3.CO;2)

Sobolev N V., Sobolev VN, Snyder GA, et al (1999) Significance of eclogitic and related parageneses of natural diamonds. *Int Geol Rev* 41:129–140.

<https://doi.org/10.1080/00206819909465135>

Sobolev N V., Snyder GA, Taylor LA, et al (1998b) Extreme chemical diversity in the mantle during eclogitic diamond formation: Evidence from 35 garnet and 5 pyroxene inclusions in a single diamond. *Int Geol Rev* 40:567–578. <https://doi.org/10.1080/00206819809465225>

Sobolev VS, Sobolev N V. (1982) New proof on very deep subsidence of eclogitized crustal rocks. *Dokl Acad Sci USSR, Earth Sci Sect* 250:88–90

Spetsius Z V, Taylor LA, Valley JW, et al (2008) Diamondiferous xenoliths from crustal subduction: garnet oxygen isotopes from the Nyurbinskaya pipe, Yakutia. *Eur J Mineral* 20:375–385

Stachel T (2001) Diamonds from the asthenosphere and the transiton zone. *Eur J Miner* 13:883–892. <https://doi.org/10.1127/0935-1221/>

Stachel T, Harris JW (1997) Syngenetic inclusions in diamond from the Birim field (Ghana) - a deep peridotitic profile with a history of depletion and re-enrichment. *Contrib to Mineral Petrol* 127:336–352. <https://doi.org/10.1007/s004100050284>

Stachel T, Viljoen KS, McDade P, Harris JW (2004) Diamondiferous lithospheric roots along the western margin of the Kalahari Craton - The peridotitic inclusion suite in diamonds from Orapa and Jwaneng. *Contrib to Mineral Petrol* 147:32–47. <https://doi.org/10.1007/s00410-003-0535-1>

Stachel T, Chacko T, Luth RW (2017) Carbon isotope fractionation during diamond growth in depleted peridotite: Counterintuitive insights from modelling water-maximum CHO fluids as multi-component systems. *Earth Planet Sci Lett* 473:44–51

Stachel T, Luth RW (2015) Diamond formation — Where , when and how ? Lithos 223:200–220

Stachel T, Brey GP, Harris JW (2000a) Kankan diamonds (Guinea) I: from the lithosphere down to the transition zone. Contrib to Mineral Petrol 140:1–15.

<https://doi.org/10.1007/s004100000173>

Stachel T, Harris JW, Brey GP (1998a) Rare and unusual mineral inclusions in diamonds from Mwadui, Tanzania. Contrib Miner Pet 132:34–47. <https://doi.org/10.1007/s004100050403>

Stachel T, Harris JW, Tappert R, Brey GP (2003) Peridotitic diamonds from the Slave and the Kaapvaal cratons - similarities and differences based on a preliminary data set. Lithos 71:489–503. [https://doi.org/10.1016/S0024-4937\(03\)00127-0](https://doi.org/10.1016/S0024-4937(03)00127-0)

Stachel T, Harris JW, Aulbach S, Deines P (2002) Kankan diamonds (Guinea) III: δ13C and nitrogen characteristics of deep diamonds. Contrib to Mineral Petrol 142:465–475.

<https://doi.org/10.1007/s004100100297>

Stachel T, Harris JW, Brey GP, Joswig W (2000b) Kankan diamonds (Guinea) II: lower mantle inclusion parageneses. Contrib to Mineral Petrol 140:16–27.

<https://doi.org/10.1007/s004100000174>

Stachel T, Viljoen KS, Brey G, Harris JW (1998b) Metasomatic processes in lherzolitic and harzburgitic domains of diamondiferous lithospheric mantle: REE in garnets from xenoliths and inclusions in diamonds. Earth Planet Sci Lett 159:1–12. [https://doi.org/10.1016/S0012-821X\(98\)00064-8](https://doi.org/10.1016/S0012-821X(98)00064-8)

Stern R., Palot M, Howell D, et al (2014) Methods and reference materials for sims diamond C- and N- isotope analysis. Canadian Centre Isotopic Microanalysis Research Report 14–01: <https://doi.org/10.13140/RG.2.1.1680.9689>

Stracke A, Hofmann AW, Hart SR (2005) FOZO, HIMU, and the rest of the mantle zoo.

Geochemistry, Geophys Geosystems 6:. <https://doi.org/10.1029/2004GC000824>

Straub SM, Layne GD (2002) The systematics of boron isotopes in Izu arc front volcanic rocks.

Earth Planet Sci Lett 198:25–39. [https://doi.org/10.1016/S0012-821X\(02\)00517-4](https://doi.org/10.1016/S0012-821X(02)00517-4)

Tanaka R, Nakamura E (2005) Boron isotopic constraints on the source of Hawaiian shield lavas.

Geochim Cosmochim Acta 69:3385–3399. <https://doi.org/10.1016/j.gca.2005.03.009>

Tappe S, Smart KA, Pearson DG, et al (2011) Craton formation in Late Archean subduction zones revealed by first Greenland eclogites. Geology 39:1103–1106.

<https://doi.org/10.1130/G32348.1>

Tappert R, Stachel T, Harris JW, et al (2005a) Diamonds from Jagersfontein (South Africa):

Messengers from the sublithospheric mantle. Contrib to Mineral Petrol 150:505–522.

<https://doi.org/10.1007/s00410-005-0035-6>

Tappert R, Stachel T, Harris JW, et al (2005b) Mineral inclusions in diamonds from the Panda kimberlite, Slave province, Canada. Eur J Miner 17:423–440. <https://doi.org/10.1127/0935-1221/2005/0017-0423>

Tappert R, Stachel T, Harris JW, et al (2006) Placer diamonds from Brazil: Indicators of the composition of the earth's mantle and the distance to their kimberlitic sources. Econ Geol 101:453–470. <https://doi.org/10.2113/gsecongeo.101.2.453>

Tappert R, Foden J, Stachel T, et al (2009) The diamonds of South Australia. Lithos 112:806–821.  
<https://doi.org/10.1016/j.lithos.2009.04.029>

Taylor LA, Snyder GA, Crozaz G, et al (1996) Eclogitic inclusions in diamonds: Evidence of complex mantle processes over time. Earth Planet Sci Lett 142:535–551.  
[https://doi.org/10.1016/0012-821X\(96\)00106-9](https://doi.org/10.1016/0012-821X(96)00106-9)

Taylor LA, Snyder GA, Keller R, et al (2003) Petrogenesis of group A eclogites and websterites:

Evidence from the Obnazhennaya kimberlite, Yakutia. *Contrib to Mineral Petrol* 145:424–443. <https://doi.org/10.1007/s00410-003-0465-y>

Thomassot E, Cartigny P, Harris JW, et al (2009) Metasomatic diamond growth: A multi-isotope study ( $^{13}\text{C}$ ,  $^{15}\text{N}$ ,  $^{33}\text{S}$ ,  $^{34}\text{S}$ ) of sulphide inclusions and their host diamonds from Jwaneng (Botswana). *Earth Planet Sci Lett* 282:79–90. <https://doi.org/10.1016/j.epsl.2009.03.001>

Thomson AR, Walter MJ, Kohn SC, Brooker RA (2016) Slab melting as a barrier to deep carbon subduction. *Nature* 529:76–79. <https://doi.org/10.1038/nature16174>

Timmerman S, Honda M, Burnham AD, et al (2019) Primordial and recycled helium isotope signatures in the mantle transition zone. *Science* 365:692–694.  
<https://doi.org/10.1126/science.aax5293>

Tonarini S, Agostini S, Doglioni C, et al (2007) Evidence for serpentinite fluid in convergent margin systems: The example of El Salvador (Central America) arc lavas. *Geochem Geophys Geosyst* 8:. <https://doi.org/10.1029/2006GC001508>

Tonarini S, Leeman WP, Leat PT (2011) Subduction erosion of forearc mantle wedge implicated in the genesis of the South Sandwich Island (SSI) arc: Evidence from boron isotope systematics. *Earth Planet Sci Lett* 301:275–284. <https://doi.org/https://doi.org/10.1016/j.epsl.2010.11.008>

Torsvik T, Furnes H, Muehlenbachs K, et al (1998) Evidence for microbial activity at the glass-alteration interface in oceanic basalts. *Earth Planet Sci Lett* 162:165–176.  
[https://doi.org/10.1016/S0012-821X\(98\)00164-2](https://doi.org/10.1016/S0012-821X(98)00164-2)

Turner S, Tonarini S, Bindeman I, et al (2007) Boron and oxygen isotope evidence for recycling of subducted components over the past 2.5 Gyr. *Nature* 447:702–705.  
<https://doi.org/10.1038/nature05898>

Ustinov V, Ukhanov A, Grinenko V, Gavrilov E (1987) Isotopic composition of oxygen in

eclogites from the kimberlite pipes Udachnaia and Obnazhennaia. Geokhimiia 1637–1641

Valley JW, Kinny PD, Schulze DJ, Spicuzza MJ (1998) Zircon megacrysts from kimberlite:

oxygen isotope variability among mantle melts. *Contrib Miner Pet* 133:1–11.

<https://doi.org/10.1007/s004100050432>

Viberti NJ, Kerrich R, Fyfe WS (1989) Oxygen and carbon isotope studies of hydrothermal alteration in the Troodos ophiolite complex, Cyprus. *Cyprus Crustal Study Proj Initial Report, Hole CY 4:88–89*

Viljoen F, Dobbe R, Harris J, Smit B (2010) Trace element chemistry of mineral inclusions in eclogitic diamonds from the Premier (Cullinan) and Finsch kimberlites, South Africa: Implications for the evolution of their mantle source. *Lithos* 118:156–168.

<https://doi.org/10.1016/j.lithos.2010.04.011>

Viljoen KS, Harris JW, Ivanic T, et al (2014) Trace element chemistry of peridotitic garnets in diamonds from the Premier (Cullinan) and Finsch kimberlites, South Africa: Contrasting styles of mantle metasomatism. *Lithos* 208:1–15. <https://doi.org/10.1016/j.lithos.2014.08.010>

Viljoen KS, Schulze DJ, Quadling AG (2005) Contrasting Group I and Group II eclogite xenolith petrogenesis: Petrological, trace element and isotopic evidence from eclogite, garnet-websterite and alkremite xenoliths in the Kaalvallei Kimberlite, South Africa. *J. Petrol.* 46:2059–2090

Viljoen KS, Smith CB, Sharp ZD (1996) Stable and radiogenic isotope study of eclogite xenoliths from the Orapa kimberlite, Botswana. *Chem Geol* 131:235–255. [https://doi.org/10.1016/0009-2541\(96\)00018-6](https://doi.org/10.1016/0009-2541(96)00018-6)

Vlaar NJ, van Keken PE, van den Berg AP (1994) Cooling of the earth in the Archaean:

Consequences of pressure-release melting in a hotter mantle

Walowski KJ, Kirstein LA, De Hoog JCM, et al (2019) Investigating ocean island mantle source heterogeneity with boron isotopes in melt inclusions. *Earth Planet Sci Lett* 508:97–108.  
<https://doi.org/10.1016/j.epsl.2018.12.005>

Walter MJ, Bulanova GP, Armstrong LS, et al (2008) Primary carbonatite melt from deeply subducted oceanic crust. *Nature* 454:622–625. <https://doi.org/10.1038/nature07132>

Wang C-G, Xu W-L, Yang D-B, et al (2018a) Olivine Oxygen Isotope Evidence for Intracontinental Recycling of Delaminated Continental Crust. *Geochem Geophys Geosyst.*  
<https://doi.org/10.1029/2017GC007284>

Wang H, van Hunen J, Pearson DG (2018b) Making Archean cratonic roots by lateral compression: A two-stage thickening and stabilization model. *Tectonophysics* 746:562–571.  
<https://doi.org/10.1016/j.tecto.2016.12.001>

Wang W, Sueño S, Takahashi E, et al (2000) Enrichment processes at the base of the Archean lithospheric mantle: Observations from trace element characteristics of pyropic garnet inclusions in diamonds. *Contrib to Mineral Petrol* 139:720–733.  
<https://doi.org/10.1007/s004100000163>

Wang Z, Bucholz C, Skinner B, et al (2011) Oxygen isotope constraints on the origin of high-Cr garnets from kimberlites. *Earth Planet Sci Lett* 312:337–347.  
<https://doi.org/10.1016/j.epsl.2011.09.061>

Wenner DB, Taylor HP (1971) Temperatures of serpentinization of ultramafic rocks based on O<sub>18</sub>/O<sub>16</sub> fractionation between coexisting serpentine and magnetite. *Contrib Miner Pet* 32:165–185. <https://doi.org/10.1007/BF00643332>

Westerlund KJ, Gurney JJ (2004) Silicate and oxide inclusion characteristics and infra-red absorption analysis of diamonds from the Klipspringer kimberlites, South Africa. *South*

African J Geol 107:131–146. <https://doi.org/10.2113/107.1-2.131>

Wilding MC, Harte B, Fallick AE, Harris JW (1994) Inclusion chemistry, carbon isotopes and nitrogen distribution in diamonds from the Bultfontein Mine, South Africa. Int Kimberl Conf Ext Abstr 5:459

Wilding MC (1990) Study of diamonds syngenetic inclusions. University of Edinburgh

Wittig N, Pearson DG, Webb M, et al (2008) Origin of cratonic lithospheric mantle roots: A geochemical study of peridotites from the North Atlantic Craton, West Greenland. Earth Planet Sci Lett 274:24–33. <https://doi.org/10.1016/j.epsl.2008.06.034>

Wolstencroft M, Davies JH (2011) Influence of the ringwoodite-perovskite transition on mantle convection in spherical geometry as a function of Clapeyron slope and Rayleigh number. Solid Earth Discuss 3:713–741. <https://doi.org/10.5194/sed-3-713-2011>

Wood BJ (2000) Phase transformations and partitioning relations in peridotite under lower mantle conditions. Earth Planet Sci Lett 174:341–354. [https://doi.org/10.1016/S0012-821X\(99\)00273-3](https://doi.org/10.1016/S0012-821X(99)00273-3)

Woodhead J, Hergt J, Giuliani A, et al (2019) Kimberlites reveal 2.5-billion-year evolution of a deep, isolated mantle reservoir. Nature 573:578–581. <https://doi.org/10.1038/s41586-019-1574-8>

Wu F-Y, Yang J-H, Xu Y-G, et al (2019) Destruction of the North China Craton in the Mesozoic. Annu Rev Earth Planet Sci 47:173–195. <https://doi.org/10.1146/annurev-earth-053018-060342>

Wu FY, Mitchell RH, Li QL, et al (2013) In situ UPb age determination and SrNd isotopic analysis of perovskite from the Premier (Cullinan) kimberlite, South Africa. Chem Geol 353:83–95. <https://doi.org/10.1016/j.chemgeo.2012.06.002>

Xia X (2018) Mineral inclusions in diamonds from Chidliak (Nunavut, Canada): constraining the diamond substrates. University of Alberta

Zedgenizov D, Rubatto D, Shatsky V, et al (2016) Eclogitic diamonds from variable crustal protoliths in the northeastern Siberian craton: Trace elements and coupled  $\delta^{13}\text{C}$ – $\delta^{18}\text{O}$  signatures in diamonds and garnet inclusions. *Chem Geol* 422:46–59.

<https://doi.org/10.1016/j.chemgeo.2015.12.018>

Zedgenizov D, Kagi H, Ohtani E, et al (2020) Retrograde phases of former bridgmanite inclusions in superdeep diamonds. *Lithos* 370–371:105659. <https://doi.org/10.1016/j.lithos.2020.105659>

Zhu F, Li J, Liu J, et al (2019) Metallic iron limits silicate hydration in Earth's transition zone. *Proc Natl Acad Sci* 116:22526–22530. <https://doi.org/10.1073/pnas.1908716116>

## Appendix A – Supplementary material for cratonic peridotites

### Supplementary figures

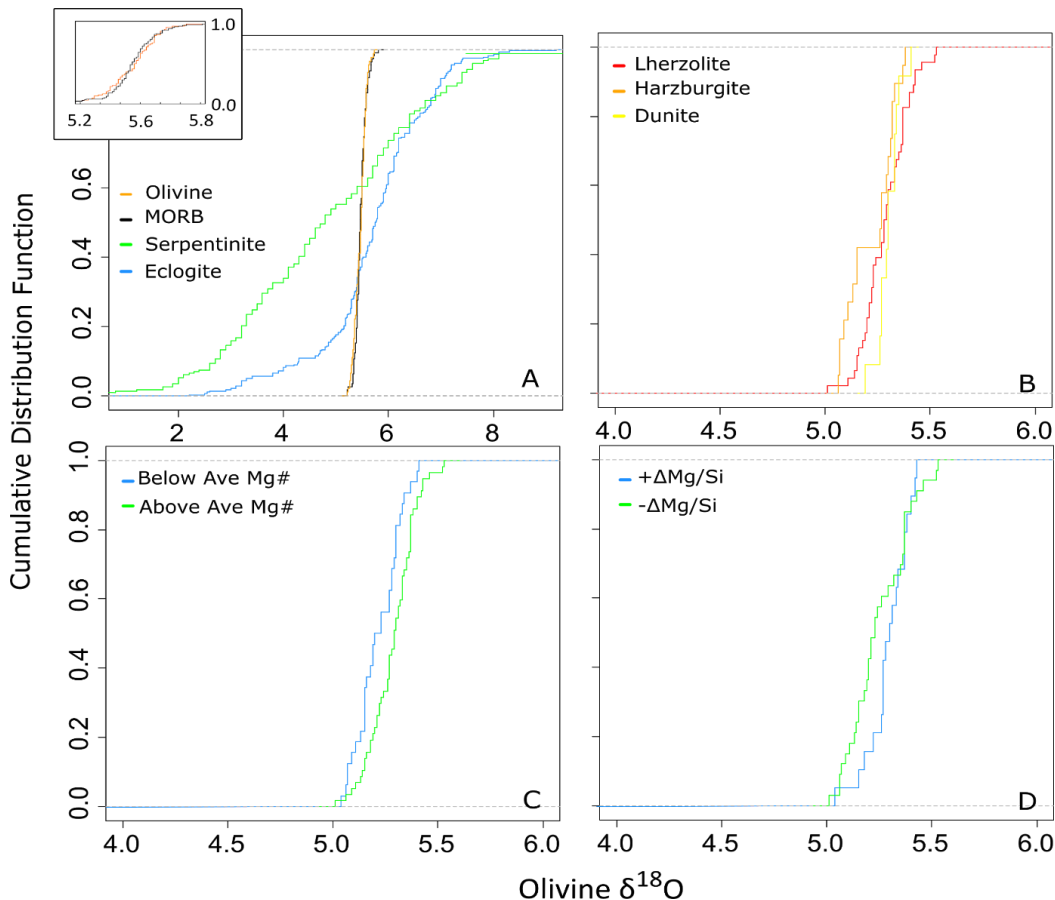


Figure A1. Cumulative distribution plots of our samples and other reservoirs. (a) Various mantle rocks are compared. MORB and olivine have statistically identical oxygen isotopes (K-S bootstrap test:  $D = 0.09$ ,  $p = 0.86$ ). Variances of MORB and cratonic olivines are statistically equal (F test:  $F_{111,73} = 0.8486$ ,  $p$ -value = 0.4314). This can be seen in the inset. (b) Lherzolitic, low-Ca harzburgitic, and dunitic peridotites have statistically identical oxygen isotopes. (Dunite-harzburgite K-S bootstrap test:  $D = 0.42$ ,  $p = 0.14$ . Dunite -lherzolite K-S bootstrap test:  $D = 0.31$ ,  $p = 0.33$ . Harzburgite-lherzolite K-S bootstrap test:  $D = 0.31$ ,  $p = 0.15$ ) (c) Below average Mg# olivines and above average Mg# olivines have statistically identical oxygen isotopes (K-S bootstrap test:  $D = 0.27$ ,  $p$ -value = 0.1). Non-statistically significant systematic offset may be due to error in Mg# ion probe matrix correction. (d) Si-enriched whole rock lithologies ( $-\Delta\text{Mg/Si}$ ) and Si-depleted whole rock lithologies ( $+\Delta\text{Mg/Si}$ ) have statistically identical oxygen isotopes (K-S bootstrap test:  $D = 0.37$ ,  $p$ -value = 0.08). Source data in Tables A1, A5, A6, and A7.

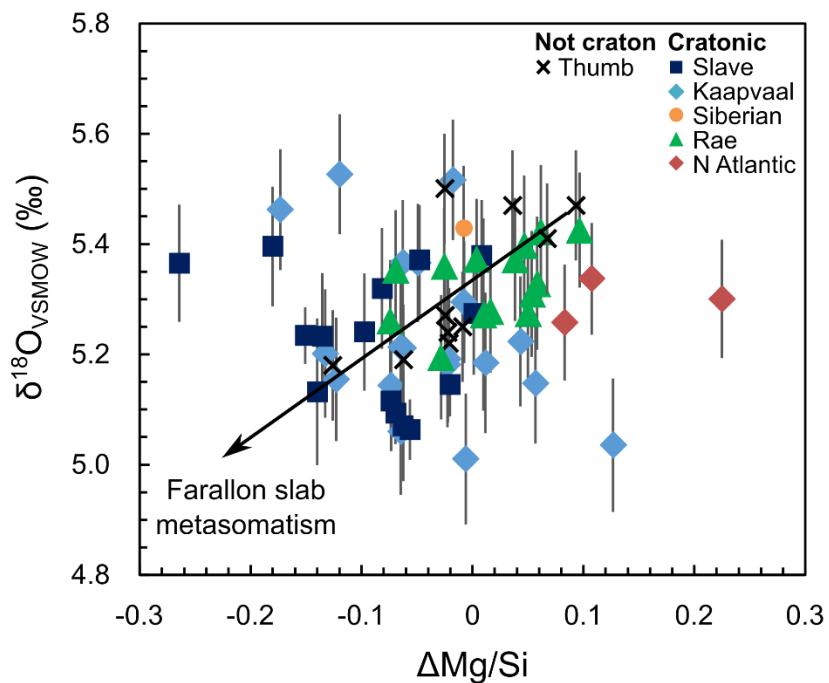


Figure A2. Oxygen isotope compositions for olivines from subcratonic and noncratonic peridotites (this study and Matthey et al. 1994) compared with bulk rock Si enrichment ( $\Delta\text{Mg/Si}$ ). Error bars are  $2\sigma$ . No correlations between Si enrichment (negative  $\Delta\text{Mg/Si}$ ) and  $\delta^{18}\text{O}$  exist in subcratonic samples, but one is visible for The Thumb xenoliths ( $r^2 = 0.52$ ; Canil and Lee 2009)

## Supplementary tables

Table A1.  $\delta^{18}\text{O}$  and major elements for cratonic olivine samples in this study.

Sample	Let28	Let29	M5	Let2	M12
<b>Locality</b>	Lesotho	Lesotho	Lesotho	Lesotho	Lesotho
<b>Craton</b>	Kaapvaal	Kaapvaal	Kaapvaal	Kaapvaal	Kaapvaal
<b>Eruption age</b>	Cretaceous	Cretaceous	Cretaceous	Cretaceous	Cretaceous
<b>Depth</b>	Spinel	Garnet	Spinel	Garnet	Garnet
<b>Lithology</b>	Harzburgite	Harzburgite	Lherzolite	Harzburgite	Lherzolite
<b><math>\delta^{18}\text{O}_{\text{VSMOW}}</math></b>	5.06	5.09	5.11	5.15	5.16
<b><math>\delta^{18}\text{O} \ 2\sigma</math></b>	0.05	0.06	0.05	0.12	0.12
<b>Isotopic reference</b>	This study	This study	This study	This study	This study
<b>Olivine Mg#</b>	92.9	92.5	91.9	93.3	92.2
<b>WR <math>\Delta\text{Mg/Si}</math></b>	-0.06	-0.07	-0.07	-0.02	n.a.
<b>Garnet Cr<sub>2</sub>O<sub>3</sub> (wt. %)</b>	n.a.	n.a.	n.a.	4.51	n.a.
<b>Garnet CaO (wt. %)</b>	n.a.	n.a.	n.a.	8.16	n.a.
<b>Elemental reference</b>	Simon et al., 2003	n.a.			

Table A1. continued

<b>Sample</b>	<b>LQ29</b>	<b>M9</b>	<b>M18/LQ2</b>	<b>LET 38</b>	<b>LQ1</b>
<b>Locality</b>	Lesotho	Lesotho	Lesotho	Letseng	Letseng
<b>Craton</b>	Kaapvaal	Kaapvaal	Kaapvaal	Kaapvaal	Kaapvaal
<b>Eruption age</b>	Cretaceous	Cretaceous	Cretaceous	Cretaceous	Cretaceous
<b>Depth</b>	Garnet	Garnet	Garnet	Garnet	Garnet
<b>Lithology</b>	Lherzolite	Lherzolite	Dunite	Lherzolite	Harzburgite
<b><math>\delta^{18}\text{O}_{\text{VSMOW}}</math></b>	5.22	5.23	5.27	5.23	5.27
<b><math>\delta^{18}\text{O} \ 2\sigma</math></b>	0.12	0.12	0.12	0.12	0.12
<b>Isotopic reference</b>	This study	This study	This study	This study	This study
<b>Olivine Mg#</b>	92.4	92.0	92.5	93.3	93.1
<b>WR <math>\Delta\text{Mg/Si}</math></b>	n.a.	-0.15	n.a.	-0.14	0.00
<b>Garnet Cr<sub>2</sub>O<sub>3</sub> (wt. %)</b>	n.a.	5.24	n.a.	5.07	n.a.
<b>Garnet CaO (wt. %)</b>	n.a.	5.04	n.a.	5.49	n.a.
<b>Elemental reference</b>	n.a.	Simon et al., 2003	n.a.	Simon et al., 2003	Pearson et al., 2004

Table A1. continued

<b>Sample</b>	<b>LET 49</b>	<b>PHN5273</b>	<b>FRB909</b>	<b>FRB1350</b>	<b>PHN 5267</b>
<b>Locality</b>	Letseng	Premier	Premier	Premier	Premier
<b>Craton</b>	Kaapvaal	Kaapvaal	Kaapvaal	Kaapvaal	Kaapvaal
<b>Eruption age</b>	Cretaceous	Proterozoic	Proterozoic	Proterozoic	Proterozoic
<b>Depth</b>	Garnet	Garnet	Garnet	Garnet/Spinel	Garnet
<b>Lithology</b>	Harzburgite	Harzburgite	Lherzolite	Lherzolite	Lherzolite
<b><math>\delta^{18}\text{O}_{\text{VSMOW}}</math></b>	5.38	5.13	5.15	5.24	5.28
<b><math>\delta^{18}\text{O}_{2\sigma}</math></b>	0.12	0.13	0.12	0.12	0.12
<b>Isotopic reference</b>	This study	This study	Mattey et al. 1994	This study	Mattey et al. 1994
<b>Olivine Mg#</b>	91.3	92.6	n.a.	91.7	n.a.
<b>WR <math>\Delta\text{Mg/Si}</math></b>	0.01	-0.14	n.a.	-0.10	n.a.
<b>Garnet Cr<sub>2</sub>O<sub>3</sub> (wt. %)</b>	n.a.	5.35	n.a.	2.07	3.54
<b>Garnet CaO (wt. %)</b>	n.a.	5.21	n.a.	5.43	4.93
<b>Elemental reference</b>	Pearson et al., 2004	Canil et al., 1994	n.a.	Canil et al., 1994	Luth et al., 1990

Table A1. continued

<b>Sample</b>	<b>PHN 5246</b>	<b>PHN5239</b>	<b>FRB909</b>	<b>PHN 5275</b>	<b>F866</b>
<b>Locality</b>	Premier	Premier	Premier	Premier	Finsch
<b>Craton</b>	Kaapvaal	Kaapvaal	Kaapvaal	Kaapvaal	Kaapvaal
<b>Eruption age</b>	Mesoproterozoic	Mesoproterozoic	Mesoproterozoic	Mesoproterozoic	Cretaceous
<b>Depth</b>	Garnet	Garnet	Garnet	Garnet	Garnet
<b>Lithology</b>	Lherzolite	Lherzolite	Lherzolite	Lherzolite	Harzburgite
<b><math>\delta^{18}\text{O}_{\text{VSMOW}}</math></b>	5.29	5.37	5.40	5.19	5.33
<b><math>\delta^{18}\text{O} \ 2\sigma</math></b>	0.12	0.12	0.12	0.12	0.12
<b>Isotopic reference</b>	Mattey et al. 1994	This study	This study	Mattey et al. 1994	This study
<b>Olivine Mg#</b>	n.a.	91.7	91.3	n.a.	93.1
<b>WR <math>\Delta\text{Mg/Si}</math></b>	n.a.	-0.05	-0.18	n.a.	n.a.
<b>Garnet Cr<sub>2</sub>O<sub>3</sub> (wt. %)</b>	n.a.	4.54	4.00	n.a.	n.a.
<b>Garnet CaO (wt. %)</b>	n.a.	4.95	4.73	n.a.	n.a.
<b>Elemental reference</b>	n.a.	Canil et al., 1994	Canil et al., 1994	n.a.	n.a.

Table A1. continued

Sample	F865	JJG 147	F556	JFL H1	JFL L1
<b>Locality</b>	Finsch	Finsch	Finsch	Jagersontein	Jagersontein
<b>Craton</b>	Kaapvaal	Kaapvaal	Kaapvaal	Kaapvaal	Kaapvaal
<b>Eruption age</b>	Cretaceous	Cretaceous	Cretaceous	Cretaceous	Cretaceous
<b>Depth</b>	Garnet	Garnet	Garnet	Garnet	Garnet
<b>Lithology</b>	Harzburgite	Harzburgite	Lherzolite	Harzburgite	Lherzolite
<b><math>\delta^{18}\text{O}_{\text{VSMOW}}</math></b>	5.07	5.15	5.37	5.07	5.23
<b><math>\delta^{18}\text{O} \ 2\sigma</math></b>	0.10	0.12	0.12	0.10	0.12
<b>Isotopic reference</b>	Mattey et al. 1994				
<b>Olivine Mg#</b>		n.a.		n.a.	n.a.
<b>WR <math>\Delta\text{Mg/Si}</math></b>	-0.06	n.a.	-0.26	n.a.	n.a.
<b>Garnet Cr<sub>2</sub>O<sub>3</sub> (wt. %)</b>	5.58	n.a.	7.44	n.a.	n.a.
<b>Garnet CaO (wt. %)</b>	4.91	n.a.	6.45	n.a.	n.a.
<b>Elemental reference</b>	Canil et al., 1994	n.a.	Canil et al., 1994	n.a.	n.a.

Table A1. continued

<b>Sample</b>	<b>KV9</b>	<b>FRB1434</b>	<b>K18-1</b>	<b>Opx-rich</b>	<b>UV 49/76</b>
<b>Locality</b>	Kaalvallei	Kimberly	Kimberly	Kimberly	Udachnaya
<b>Craton</b>	Kaapvaal	Kaapvaal	Kaapvaal	Kaapvaal	Siberia
<b>Eruption age</b>	Cretaceous	Cretaceous	Cretaceous	Cretaceous	Devonian
<b>Depth</b>	n.a.	Spinel	Garnet	Spinel	Garnet
<b>Lithology</b>	Harzburgite	Harzburgite	Harzburgite	Peridotite	Dunite
<b><math>\delta^{18}\text{O}_{\text{VSMOW}}</math></b>	5.13	5.32	5.32	5.16	5.30
<b><math>\delta^{18}\text{O} \ 2\sigma</math></b>	0.10	0.12	0.12	0.12	0.12
<b>Isotopic reference</b>	Mattey et al. 1994	This study	This study	This study	This study
<b>Olivine Mg#</b>	n.a.	93.1	92.2	92.9	92.9
<b>WR <math>\Delta\text{Mg/Si}</math></b>	n.a.	-0.08	n.a.	n.a.	n.a.
<b>Garnet Cr<sub>2</sub>O<sub>3</sub> (wt. %)</b>	n.a.	n.a.	n.a.	n.a.	n.a.
<b>Garnet CaO (wt. %)</b>	n.a.	n.a.	n.a.	n.a.	n.a.
<b>Elemental reference</b>	n.a.	Canil et al., 1994	n.a.	n.a.	n.a.

Table A1. continued

<b>Sample</b>	<b>UV 69/76</b>	<b>UV 70/76</b>	<b>UV 417/89</b>	<b>UV49/76</b>	<b>UV18-1</b>
<b>Locality</b>	Udachnaya	Udachnaya	Udachnaya	Udachnaya	Udachnaya
<b>Craton</b>	Siberia	Siberia	Siberia	Siberia	Siberia
<b>Eruption age</b>	Devonian	Devonian	Devonian	Devonian	Devonian
<b>Depth</b>	Spinel	Spinel	Garnet		Garnet
<b>Lithology</b>	Dunite	Dunite	Lherzolite	Dunite	Dunite
<b><math>\delta^{18}\text{O}_{\text{VSMOW}}</math></b>	5.37	5.41	5.43	5.19	5.27
<b><math>\delta^{18}\text{O } 2\sigma</math></b>	0.12	0.12	0.12	0.12	0.12
<b>Isotopic reference</b>	This study	This study	This study	Mattey et al. 1994	This study
<b>Olivine Mg#</b>	93.0	93.1	91.2	n.a.	92.6
<b>WR <math>\Delta\text{Mg/Si}</math></b>			-0.01	n.a.	n.a.
<b>Garnet Cr<sub>2</sub>O<sub>3</sub> (wt. %)</b>	12.70	10.80	1.34	n.a.	n.a.
<b>Garnet CaO (wt. %)</b>	3.10	1.69	4.38	n.a.	n.a.
<b>Elemental reference</b>	Boyd and Finnerty, 1980	Boyd and Finnerty, 1980	Canil et al., 1994	n.a.	n.a.

Table A1. continued

<b>Sample</b>	<b>UV 413/89</b>	<b>UV18-2</b>	<b>UV67/76</b>	<b>UV18-4</b>	<b>UV4776</b>
<b>Locality</b>	Udachnaya	Udachnaya	Udachnaya	Udachnaya	Udachnaya
<b>Craton</b>	Siberia	Siberia	Siberia	Siberia	Siberia
<b>Eruption age</b>	Devonian	Devonian	Devonian	Devonian	Devonian
<b>Depth</b>	Garnet	Garnet		Garnet	Spinel
<b>Lithology</b>	Lherzolite	Dunite	Harzburgite	Dunite	Dunite
<b><math>\delta^{18}\text{O}_{\text{VSMOW}}</math></b>	5.28	5.29	5.29	5.33	5.33
<b><math>\delta^{18}\text{O}_{2\sigma}</math></b>	0.12	0.12	0.12	0.12	0.12
<b>Isotopic reference</b>	Mattey et al. 1994	This study	This study	This study	This study
<b>Olivine Mg#</b>	n.a.	92.3	92.4	92.3	92.4
<b>WR <math>\Delta\text{Mg/Si}</math></b>	n.a.	n.a.	n.a.	n.a.	n.a.
<b>Garnet Cr<sub>2</sub>O<sub>3</sub> (wt. %)</b>	n.a.	n.a.	n.a.	n.a.	n.a.
<b>Garnet CaO (wt. %)</b>	n.a.	n.a.	n.a.	n.a.	n.a.
<b>Elemental reference</b>	n.a.	n.a.	n.a.	n.a.	n.a.

Table A1. continued

<b>Sample</b>	<b>UV18-3</b>	<b>477406c</b>	<b>126742B</b>	<b>126739</b>	<b>39670</b>
<b>Locality</b>	Udachnaya	NW Greenland	W Greenland	W Greenland	W Greenland
<b>Craton</b>	Siberia	N. Atlantic	N. Atlantic	N. Atlantic	N. Atlantic
<b>Eruption age</b>	Devonian	Neoproterozoic	Neoproterozoic	Neoproterozoic	Neoproterozoic
<b>Depth</b>	Garnet	Garnet/Spinel	Garnet	Garnet	Garnet
<b>Lithology</b>	Dunite	Wehrlite	Harzburgite	Harzburgite	Harzburgite
<b><math>\delta^{18}\text{O}_{\text{VSMOW}}</math></b>	5.35	5.40	5.27	5.30	5.31
<b><math>\delta^{18}\text{O } 2\sigma</math></b>	0.12	0.12	0.12	0.12	0.12
<b>Isotopic reference</b>	This study	This study	This study	This study	This study
<b>Olivine Mg#</b>	92.4	92.7	91.4	90.9	91.6
<b>WR <math>\Delta\text{Mg/Si}</math></b>	n.a.	n.a.	n.a.	n.a.	n.a.
<b>Garnet Cr<sub>2</sub>O<sub>3</sub> (wt. %)</b>	n.a.	n.a.	n.a.	n.a.	n.a.
<b>Garnet CaO (wt. %)</b>	n.a.	n.a.	n.a.	n.a.	n.a.
<b>Elemental reference</b>	n.a.	n.a.	n.a.	n.a.	n.a.

Table A1. continued

<b>Sample</b>	<b>G-06-06b</b>	<b>G-06-07d</b>	<b>G-06-04c</b>	<b>K13A3</b>	<b>K15A4</b>
<b>Locality</b>	SW Greenland	SW Greenland	SW Greenland	Batty Bay - Somerset Island	Batty Bay - Somerset Island
<b>Craton</b>	N. Atlantic	N. Atlantic	N. Atlantic	Rae	Rae
<b>Eruption age</b>	Neoproterozoic	Neoproterozoic	Neoproterozoic	Cretaceous	Cretaceous
<b>Depth</b>	Spinel	Spinel	Spinel	Spinel	Spinel
<b>Lithology</b>	Dunite	Dunite	Lherzolite	Lherzolite	Lherzolite
<b><math>\delta^{18}\text{O}_{\text{VSMOW}}</math></b>	5.26	5.30	5.34	5.20	5.27
<b><math>\delta^{18}\text{O } 2\sigma</math></b>	0.12	0.12	0.12	0.12	0.12
<b>Isotopic reference</b>	This study	This study	This study	This study	This study
<b>Olivine Mg#</b>	91.7	91.6	91.3	92.4	92.7
<b>WR <math>\Delta\text{Mg/Si}</math></b>	0.08	0.22	0.11	-0.03	0.01
<b>Garnet Cr<sub>2</sub>O<sub>3</sub> (wt. %)</b>	n.a.	n.a.	n.a.	n.a.	n.a.
<b>Garnet CaO (wt. %)</b>	n.a.	n.a.	n.a.	n.a.	n.a.
<b>Elemental reference</b>	Wittig et al., 2008	Wittig et al., 2008	Wittig et al., 2008	Irvine et al., 2003	Irvine et al., 2003

Table A1. continued

<b>Sample</b>	<b>K11A14</b>	<b>K12A1</b>	<b>K11A18</b>	<b>X07</b>	<b>N2B (PHA90)</b>
<b>Locality</b>	Batty Bay - Somerset Island	Batty Bay - Somerset Island	Batty Bay - Somerset Island	Nikos - Somerset Island	Nord
<b>Craton</b>	Rae	Rae	Rae	Rae	Rae
<b>Eruption age</b>	Cretaceous	Cretaceous	Cretaceous	Cretaceous	Cretaceous
<b>Depth</b>	Spinel	Spinel	Spinel	n.a.	Spinel
<b>Lithology</b>	Lherzolite	Lherzolite	Lherzolite	Harzburgite	Lherzolite
<b><math>\delta^{18}\text{O}_{\text{VSMOW}}</math></b>	5.27	5.31	5.43	5.26	5.33
<b><math>\delta^{18}\text{O}</math> 2<math>\sigma</math></b>	0.12	0.12	0.12	0.12	0.12
<b>Isotopic reference</b>	This study	This study	This study	This study	This study
<b>Olivine Mg#</b>	92.4	92.4	92.4	92.5	90.8
<b>WR <math>\Delta\text{Mg/Si}</math></b>	0.05	0.05	0.10	-0.07	0.06
<b>Garnet Cr<sub>2</sub>O<sub>3</sub> (wt. %)</b>	n.a.	n.a.	n.a.	n.a.	n.a.
<b>Garnet CaO (wt. %)</b>	n.a.	n.a.	n.a.	n.a.	n.a.
<b>Elemental reference</b>	Irvine et al., 2003	Irvine et al., 2003	Irvine et al., 2003	Irvine et al., 2003	Irvine et al., 2003

Table A1. continued

<b>Sample</b>	<b>N1C</b>	<b>JPN-9</b>	<b>JPN-3B</b>	<b>JP2-X2</b>	<b>JP3-X1</b>
<b>Locality</b>	Nord	JP - Somerset Island			
<b>Craton</b>	Rae	Rae	Rae	Rae	Rae
<b>Eruption age</b>	Cretaceous	Cretaceous	Cretaceous	Cretaceous	Cretaceous
<b>Depth</b>	Spinel	Garnet	Garnet	n.a.	Garnet
<b>Lithology</b>	Lherzolite	Lherzolite	Lherzolite	Lherzolite	Harzburgite
<b><math>\delta^{18}\text{O}_{\text{VSMOW}}</math></b>	5.40	5.28	5.35	5.36	5.37
<b><math>\delta^{18}\text{O} \ 2\sigma</math></b>	0.12	0.12	0.12	0.12	0.12
<b>Isotopic reference</b>	This study	This study	This study	This study	This study
<b>Olivine Mg#</b>	92.1	92.2	91.9	92.2	92.4
<b>WR <math>\Delta\text{Mg/Si}</math></b>	0.05	0.02	-0.07	-0.03	0.04
<b>Garnet Cr<sub>2</sub>O<sub>3</sub> (wt. %)</b>	n.a.	n.a.	n.a.	n.a.	7.21
<b>Garnet CaO (wt. %)</b>	n.a.	n.a.	n.a.	n.a.	6.18
<b>Elemental reference</b>	Irvine et al., 2003	Irvine et al., 2003	Irvine et al., 2003	Irvine et al., 2003	Irvine et al., 2003

Table A1. continued

Sample	JPN-4	JPS-6B	DDM_327	DDM_367	DDM_164
<b>Locality</b>	JP - Somerset Island	JP - Somerset Island	Diavik	Diavik	Diavik
<b>Craton</b>	Rae	Rae	Slave	Slave	Slave
<b>Eruption age</b>	Cretaceous	Cretaceous	Eocene	Eocene	Eocene
<b>Depth</b>	Garnet	Garnet	Garnet	Garnet	Garnet
<b>Lithology</b>	Lherzolite	Lherzolite	Lherzolite	Lherzolite	Lherzolite
<b><math>\delta^{18}\text{O}_{\text{VSMOW}}</math></b>	5.37	5.42	5.15	5.18	5.20
<b><math>\delta^{18}\text{O} \ 2\sigma</math></b>	0.12	0.12	0.12	0.12	0.12
<b>Isotopic reference</b>	This study	This study	This study	This study	This study
<b>Olivine Mg#</b>	91.9	91.9	90.4	91.4	92.7
<b>WR <math>\Delta\text{Mg/Si}</math></b>	0.00	0.06	-0.12	0.01	-0.13
<b>Garnet Cr<sub>2</sub>O<sub>3</sub> (wt. %)</b>	n.a.	n.a.	2.75	8.96	n.a.
<b>Garnet CaO (wt. %)</b>	n.a.	n.a.	4.8	6.53	n.a.
<b>Elemental reference</b>	Irvine et al., 2003	Irvine et al., 2003	Mather, 2012	Mather, 2012	Mather, 2012

Table A1. continued

<b>Sample</b>	<b>DDM_368</b>	<b>DDM_332</b>	<b>DDM_360</b>	<b>MX5023</b>	<b>DDM_339</b>
<b>Locality</b>	Diavik	Diavik	Diavik	Diavik	Diavik
<b>Craton</b>	Slave	Slave	Slave	Slave	Slave
<b>Eruption age</b>	Eocene	Eocene	Eocene	Eocene	Eocene
<b>Depth</b>	Garnet	Garnet	Garnet	Garnet	Garnet
<b>Lithology</b>	Lherzolite	Lherzolite	Lherzolite	Lherzolite	Lherzolite
<b><math>\delta^{18}\text{O}_{\text{VSMOW}}</math></b>	5.21	5.21	5.22	5.29	5.37
<b><math>\delta^{18}\text{O}</math> 2<math>\sigma</math></b>	0.12	0.12	0.12	0.12	0.12
<b>Isotopic reference</b>	This study	This study	This study	This study	This study
<b>Olivine Mg#</b>	91.7	91.8	91.2	92.6	89.8
<b>WR <math>\Delta\text{Mg/Si}</math></b>	-0.06	-0.06	0.04	-0.01	-0.06
<b>Garnet Cr<sub>2</sub>O<sub>3</sub> (wt. %)</b>	6.04	n.a.	2.73	n.a.	n.a.
<b>Garnet CaO (wt. %)</b>	5.82	n.a.	4.60	n.a.	n.a.
<b>Elemental reference</b>	Mather, 2012	Mather, 2012	Mather, 2012	Mather, 2012	Mather, 2012

Table A1. continued

<b>Sample</b>	<b>DDM_366</b>	<b>DDM_384</b>	<b>DDM_335</b>	<b>DDM_444</b>	<b>9-2</b>
<b>Locality</b>	Diavik	Diavik	Diavik	Diavik	Jericho
<b>Craton</b>	Slave	Slave	Slave	Slave	Slave
<b>Eruption age</b>	Eocene	Eocene	Eocene	Eocene	Jurassic
<b>Depth</b>	Garnet	Garnet	Garnet	Garnet	Garnet
<b>Lithology</b>	Lherzolite	Lherzolite	Lherzolite	Lherzolite	Lherzolite
<b><math>\delta^{18}\text{O}_{\text{VSMOW}}</math></b>	5.37	5.46	5.52	5.53	5.01
<b><math>\delta^{18}\text{O}</math> 2<math>\sigma</math></b>	0.12	0.12	0.12	0.12	0.12
<b>Isotopic reference</b>	This study				
<b>Olivine Mg#</b>	91.3	91.7	91.2	91.4	92.0
<b>WR <math>\Delta\text{Mg/Si}</math></b>		-0.17	-0.02	-0.12	-0.01
<b>Garnet Cr<sub>2</sub>O<sub>3</sub> (wt. %)</b>	6.70	n.a.	7.07	n.a.	3.56
<b>Garnet CaO (wt. %)</b>	5.60	n.a.	5.80	n.a.	5.42
<b>Elemental reference</b>	Mather, 2012	Mather, 2012	Mather, 2012	Mather, 2012	Kopylova et al., 1999

Table A1. continued

<b>Sample</b>	<b>39-23</b>	<b>28-15</b>	<b>22-1</b>	<b>53-10</b>	<b>10-12A</b>
<b>Locality</b>	Jericho	Jericho	Jericho	Jericho	Jericho
<b>Craton</b>	Slave	Slave	Slave	Slave	Slave
<b>Eruption age</b>	Jurassic	Jurassic	Jurassic	Jurassic	Jurassic
<b>Depth</b>	Spinel	Garnet/Spinel	Garnet/Spinel	Spinel	Spinel
<b>Lithology</b>	Peridotite	Peridotite	Lherzolite	Peridotite	Peridotite
<b><math>\delta^{18}\text{O}_{\text{VSMOW}}</math></b>	5.04	5.06	5.14	5.15	5.18
<b><math>\delta^{18}\text{O}</math> 2<math>\sigma</math></b>	0.12	0.11	0.12	0.12	0.12
<b>Isotopic reference</b>	This study				
<b>Olivine Mg#</b>	92.8	91.8	92.3	92.1	92.5
<b>WR <math>\Delta\text{Mg/Si}</math></b>	0.13	-0.06	-0.07	0.06	-0.02
<b>Garnet Cr<sub>2</sub>O<sub>3</sub> (wt. %)</b>	n.a.	n.a.	1.31	n.a.	n.a.
<b>Garnet CaO (wt. %)</b>	n.a.	n.a.	5.02	n.a.	n.a.
<b>Elemental reference</b>	Kopylova et al., 1999				

Table A1. continued

<b>Sample</b>	<b>25-4</b>	<b>LGS 40 (MX19)</b>	<b>JD1 (MX1)</b>	<b>26-11</b>
<b>Locality</b>	Jericho	Jericho	Jericho	Jericho
<b>Craton</b>	Slave	Slave	Slave	Slave
<b>Eruption age</b>	Jurassic	Jurassic	Jurassic	Jurassic
<b>Depth</b>	Garnet/Spinel	Spinel	Garnet	Garnet/Spinel
<b>Lithology</b>	Peridotite	Lherzolite	Lherzolite	Peridotite
<b><math>\delta^{18}\text{O}_{\text{VSMOW}}</math></b>	5.19	5.30	5.33	5.37
<b><math>\delta^{18}\text{O} \ 2\sigma</math></b>	0.12	0.12	0.12	0.12
<b>Isotopic reference</b>	This study	This study	This study	This study
<b>Olivine Mg#</b>	91.8	92.8	90.1	92.3
<b>WR <math>\Delta\text{Mg/Si}</math></b>	-0.02	n.a.	n.a.	-0.05
<b>Garnet Cr<sub>2</sub>O<sub>3</sub> (wt. %)</b>	5.27	n.a.	n.a.	3.74
<b>Garnet CaO (wt. %)</b>	6.29	n.a.	n.a.	5.50
<b>Elemental reference</b>	Kopylova et al., 1999	n.a.	n.a.	Irvine et al., 2003

Average  $\delta^{18}\text{O}$  is  $5.25 \text{ ‰} \pm 0.22 \text{ ‰}$  ( $2\sigma$ ). Fractionation-corrected, MORB-equivalent  $\delta^{18}\text{O}$  is  $5.45 \text{ ‰}$ . Whole rock is abbreviated WR.

Table A2.  $\delta^{18}\text{O}$  and major elements for cratonic Opx samples in this study.

Sample	$\delta^{18}\text{O}$ reference	Locality	Craton	Lithology	Opx Mg#	Opx $\delta^{18}\text{O}$	$2\sigma$	$\Delta\text{Mg/Si}$
PHN 5273	Mattey et al., 1994	Premier	Kaapvaal	harzburgite	92.6	5.70	0.2	-0.14
FRB 1350	Mattey et al., 1994	Premier	Kaapvaal	lherzolite	91.7	5.84	0.2	-0.10
F865	Mattey et al., 1994	Finsch	Kaapvaal	harzburgite	n.a.	5.63	0.2	-0.06
F866	Lowry et al., 1999	Finsch	Kaapvaal	harzburgite	94.1	5.76	0.2	n.a.
JJG 147	Lowry et al., 1999	Finsch	Kaapvaal	harzburgite	n.a.	5.63	0.2	n.a.
PHN 5239	this study	Premier	Kaapvaal	lherzolite	92.2	5.52	0.2	-0.05
08/81	this study	Obhazhennaya	Siberian	opx-pyroxenite	92.8	5.82	0.2	n.a.
GP402	this study	Kimberley	Kaapvaal	harzburgite	94.6	5.76	0.2	n.a.
GMM2002 /1	this study	Kimberley	Kaapvaal	lherzolite	93.9	5.97	0.2	n.a.
<b>Ave <math>\delta^{18}\text{O}</math></b>	<b>5.74</b>							
<b><math>2\sigma</math></b>	<b>0.27</b>							

Table A3.  $\delta^{18}\text{O}$  and major elements for non-cratonic fore-arc olivine samples

Sample	Locality	Lithology	Olivine $\delta^{18}\text{O}$	$2\sigma$	Olivine Mg#
GP02/108	Horoman peridotite massif, Japan	Harzburgite	5.31	0.20	91.3
DM18-1	Dun Mountain, New Zealand	Harzburgite	5.29	0.20	90.6

Table A4. pMELTS and  $\delta^{18}\text{O}$  mass balance modeling for melts interacting with harzburgite.

T °C	Melt (g)	Melt SiO <sub>2</sub> (g)	Opx (g)	Opx Mg#	Gt (g)	Gt Mg #	Ol (g)	Ol Mg#	$\delta^{18}\text{O}$ melt (‰)	$\delta^{18}\text{O}$ opx (‰)	$\delta^{18}\text{O}$ Ol (‰)	$\delta^{18}\text{O}$ Gt (‰)
Slab melt interacting with 1500 °C harzburgite*												
1365	100	66.1	0	n.a.	0	n.a.	0	n.a.	8.00	n.a.	n.a.	n.a.
1401	91	66.6	11	90.9	17	82.0	0	n.a.	7.75	7.25	n.a.	6.95
1430	85	64.2	27	90.9	0	n.a.	0	n.a.	7.46	6.96	n.a.	n.a.
1452	79	61.3	26	93.1	0	n.a.	0	n.a.	7.21	6.71	n.a.	n.a.
1466	75	57.7	24	94.2	0	n.a.	0	n.a.	6.91	6.72	n.a.	n.a.
1471	72	53.7	23	94.8	0	n.a.	0	n.a.	6.63	6.58	n.a.	n.a.
1468	70	49.4	21	94.8	0	n.a.	0	n.a.	6.36	6.46	n.a.	n.a.
1468	71	48.0	7	94.8	0	n.a.	13	94.0	6.20	6.36	5.86	n.a.
1470	72	48.0	0	94.8	0	n.a.	19	94.0	6.12	n.a.	5.77	n.a.
1471	72	48.0	0	n.a.	0	n.a.	19	94.0	6.06	n.a.	5.71	n.a.
1474	73	48.1	0	n.a.	0	n.a.	19	94.0	6.00	n.a.	5.66	n.a.
1476	74	48.1	0	n.a.	0	n.a.	19	94.0	5.97	n.a.	5.62	n.a.
1477	74	48.1	0	n.a.	0	n.a.	19	93.0	5.94	n.a.	5.59	n.a.
1479	75	48.1	0	n.a.	0	n.a.	19	93.0	5.91	n.a.	5.56	n.a.
1480	75	48.1	0	n.a.	0	n.a.	19	93.0	5.89	n.a.	5.55	n.a.
1481	76	48.1	0	n.a.	0	n.a.	19	93.0	5.88	n.a.	5.53	n.a.

Table A4. continued

T °C	Melt (g)	Melt SiO <sub>2</sub> (g)	Opx (g)	Opx Mg#	Gt (g)	Gt Mg #	Ol (g)	Ol Mg #	δ <sup>18</sup> O melt (‰)	δ <sup>18</sup> O opx (‰)	δ <sup>18</sup> O Ol (‰)	δ <sup>18</sup> O Gt (‰)
Slab melt interacting with 900 °C harzburgite*												
1365	100	66.1	0	n.a.	0	n.a.	0	n.a.	8.00	n.a.	n.a.	n.a.
1323	77	67.9	30	90.8	23	80.7	0	n.a.	7.86	7.36	n.a.	7.06
1271	59	64.6	47	91.9	1	82.4	0	n.a.	7.63	7.18	n.a.	6.83
1211	43	57.5	46	93.1	0	n.a.	0	n.a.	7.38	7.18	n.a.	n.a.
1140	31	45.7	38	93.7	0	n.a.	4	92.0	7.14	7.38	6.88	n.a.
1050	28	43.5	7	93.7	0	n.a.	26	93.0	6.56	6.87	6.37	n.a.
989	27	42.1	4	94.2	0	n.a.	27	93.0	6.16	6.53	5.96	n.a.
950	26	41.3	3	94.2	0	n.a.	28	93.0	6.53	6.93	6.33	n.a.
791	56	41.8	0	n.a.	0	n.a.	27	93.0	6.19	n.a.	5.99	n.a.
Fluxed harzburgitic melt interacting with 1300 °C harzburgite**												
1403	100	55.7	0	n.a	0.0	n.a	0.0	n.a	5.60	n.a.	n.a.	n.a.
1403	97	54.5	10	91.4	0.0	n.a	0.0	n.a	5.60	5.52	n.a.	n.a.
1403	94	53.3	10	91.4	0.0	n.a	0.0	n.a	5.60	5.56	n.a.	n.a.
1402	92	52.1	10	92.5	0.0	n.a	0.0	n.a	5.59	5.60	n.a.	n.a.
1400	89	50.7	10	92.5	0.0	n.a	0.0	n.a	5.58	5.63	n.a.	n.a.
1397	87	49.3	10	93.0	0.0	n.a	0.0	n.a	5.56	5.67	n.a.	n.a.
1395	85	47.9	9	93.0	0.0	n.a	0.0	n.a	5.54	5.70	n.a.	n.a.
1391	84	47.1	6	93.0	0.0	n.a	3	93.0	5.54	5.73	5.23	n.a.
1389	83	47.0	1	93.0	0.0	n.a	7	93.0	5.56	5.75	5.25	n.a.

pMELTS isenthalpic AFC output from Ghiorso et al. (2002). Harzburgite is 95 wt. % Fo93 and 5 wt. % clinoenstatite. Slab melt composition from Rapp et al. (1999). Water-fluxed depleted mantle melt from (Mitchell and Grove, 2015).  $\Delta^{18}\text{O}_{\text{crystals-melt}}$  from Eiler (2001). Initial oxygen fugacity set at QFM-1.

\*Initial slab melt  $\delta^{18}\text{O}$  is an average of the lava section of an ophiolite compilation model (Ickert et al. 2013). \*\*Starting  $\delta^{18}\text{O}$  calculated with 3 % slab derived H<sub>2</sub>O (8 ‰) and 97 % peridotite (5.5 ‰).

138

Table A5. Source data for oxygen isotopes of MORB

Sample	Reference	Locality	$\delta^{18}\text{O}$	$2\sigma$
Naudure ND 51	Eiler et al., 2000	Pacific Ocean	5.47	0.04
Naudure DR21-4	Eiler et al., 2000	Pacific Ocean	5.41	0.08
Searise1 DR5-102	Eiler et al., 2000	Pacific Ocean	5.43	0.04
Searise 1 Dr04	Eiler et al., 2000	Pacific Ocean	5.61	0.04
CHEPR 60	Eiler et al., 2000	Pacific Ocean	5.43	0.12
CY 82 27-1	Eiler et al., 2000	Pacific Ocean	5.51	0.06
Clipperton DR01	Eiler et al., 2000	Pacific Ocean	5.51	0.18
Venture #32	Eiler et al., 2000	Pacific Ocean	5.67	0.06
Searise 2 DR07	Eiler et al., 2000	Pacific Ocean	5.49	0.16
CYP 78 18-62	Eiler et al., 2000	Pacific Ocean	5.45	0.06
CYP 78 18-65	Eiler et al., 2000	Pacific Ocean	5.54	0.06
CYP 78 04-06	Eiler et al., 2000	Pacific Ocean	5.37	0.02
CYP 78 06-10	Eiler et al., 2000	Pacific Ocean	5.42	0.06
Ridelente DR10	Eiler et al., 2000	Atlantic Ocean	5.50	0.08
CH77 DR05 105a	Eiler et al., 2000	Atlantic Ocean	5.40	0.02
Mapco CH98 DR12	Eiler et al., 2000	Atlantic Ocean	5.41	0.04
Mapco CH98 DR11	Eiler et al., 2000	Atlantic Ocean	5.45	0.04
Mapco CH98 DR10	Eiler et al., 2000	Atlantic Ocean	5.49	0.10
EW 9309 25D	Eiler et al., 2000	Atlantic Ocean	5.81	0.08

Table A5. continued

Sample	Reference	Locality	$\delta^{18}\text{O}$	$2\sigma$
EW 9309 15D	Eiler et al., 2000	Atlantic Ocean	5.47	0.02
MD57 D13-7	Eiler et al., 2000	Indian Ocean	5.41	0.08
MD 57 D'10-1	Eiler et al., 2000	Indian Ocean	5.46	0.06
MD 57 D'10-4	Eiler et al., 2000	Indian Ocean	5.61	0.02
MD 57 D8-1	Eiler et al., 2000	Indian Ocean	5.57	0.12
MD 23 site 4	Eiler et al., 2000	Indian Ocean	5.49	0.10
MD 37 07-04-D1	Eiler et al., 2000	Indian Ocean	5.45	0.10
MD 34 D3	Eiler et al., 2000	Indian Ocean	5.47	0.02
MD 34 D4	Eiler et al., 2000	Indian Ocean	5.64	0.02
D1-2	Cooper et al., 2009	Pacific Ocean	5.38	0.03
D2-19	Cooper et al., 2009	Pacific Ocean	5.55	0.08
D3-4	Cooper et al., 2009	Pacific Ocean	5.43	0.1
D4-1	Cooper et al., 2009	Pacific Ocean	5.34	0.1
D5-5	Cooper et al., 2009	Pacific Ocean	5.42	0.05
MOA8801-017-026	Cooper et al., 2009	Pacific Ocean	5.31	0.01
D7-3	Cooper et al., 2009	Indian Ocean	5.45	0.02
D7-7	Cooper et al., 2009	Indian Ocean	5.55	0.03
D8-8	Cooper et al., 2009	Indian Ocean	5.36	0.02
D9-1	Cooper et al., 2009	Indian Ocean	5.51	0.07
D11-6	Cooper et al., 2009	Indian Ocean	5.38	0.03
D10-10	Cooper et al., 2009	Indian Ocean	5.71	0.01

Table A5. continued

Sample	Reference	Locality	$\delta^{18}\text{O}$	$2\sigma$
MOA8801-027-058	Cooper et al., 2009	Indian Ocean	5.64	0.04
BMRG05-30-4	Cooper et al., 2009	Indian Ocean	5.37	0.19
MOA8801-022-013	Cooper et al., 2009	Indian Ocean	5.49	0.11
MOA8801-023-001	Cooper et al., 2009	Indian Ocean	5.4	0.05
D01.A	Cooper et al., 2004	Mid Atlantic Ridge	5.34	0.01
D03.A	Cooper et al., 2004	Mid Atlantic Ridge	5.33	0.01
D02.A	Cooper et al., 2004	Mid Atlantic Ridge	5.61	0.08
D55.A	Cooper et al., 2004	Mid Atlantic Ridge	5.5	0.01
D55.B	Cooper et al., 2004	Mid Atlantic Ridge	5.34	0.01
D04.B	Cooper et al., 2004	Mid Atlantic Ridge	5.45	0.07
RC151.A	Cooper et al., 2004	Mid Atlantic Ridge	5.41	0.01
D05.B	Cooper et al., 2004	Mid Atlantic Ridge	5.46	0.01
RC150	Cooper et al., 2004	Mid Atlantic Ridge	5.36	0.03
RC149	Cooper et al., 2004	Mid Atlantic Ridge	5.56	0.03
D07.A	Cooper et al., 2004	Mid Atlantic Ridge	5.21	0.01
RC11	Cooper et al., 2004	Mid Atlantic Ridge	5.52	0.01
D53.A	Cooper et al., 2004	Mid Atlantic Ridge	5.5	0.01
D52-3	Cooper et al., 2004	Mid Atlantic Ridge	5.47	0.05
D08.A	Cooper et al., 2004	Mid Atlantic Ridge	5.45	0.05
D50-4	Cooper et al., 2004	Mid Atlantic Ridge	5.57	0.01
RC144	Cooper et al., 2004	Mid Atlantic Ridge	5.46	0.04

Table A5. continued

Sample	Reference	Locality	$\delta^{18}\text{O}$	$2\sigma$
D09.A	Cooper et al., 2004	Mid Atlantic Ridge	5.22	n.a.
D44.A	Cooper et al., 2004	Mid Atlantic Ridge	5.39	0.02
D44-3	Cooper et al., 2004	Mid Atlantic Ridge	5.32	n.a.
RC136-1	Cooper et al., 2004	Mid Atlantic Ridge	5.54	0.01
RC20	Cooper et al., 2004	Mid Atlantic Ridge	5.57	0.02
RC133	Cooper et al., 2004	Mid Atlantic Ridge	5.55	0.02
D41.A	Cooper et al., 2004	Mid Atlantic Ridge	5.43	0.03
D40-1	Cooper et al., 2004	Mid Atlantic Ridge	5.37	0.03
D40-2	Cooper et al., 2004	Mid Atlantic Ridge	5.57	0.05
D40-3	Cooper et al., 2004	Mid Atlantic Ridge	5.52	0.08
D40-4	Cooper et al., 2004	Mid Atlantic Ridge	5.69	0.06
D40-5	Cooper et al., 2004	Mid Atlantic Ridge	5.6	0.07
D40-6	Cooper et al., 2004	Mid Atlantic Ridge	5.61	0.16
D40-7	Cooper et al., 2004	Mid Atlantic Ridge	5.73	0.06
D10.A	Cooper et al., 2004	Mid Atlantic Ridge	5.4	0.06
D10.B	Cooper et al., 2004	Mid Atlantic Ridge	5.46	0.01
D11-6	Cooper et al., 2004	Mid Atlantic Ridge	5.48	0.01
D12.A	Cooper et al., 2004	Mid Atlantic Ridge	5.5	0.02
RC128-1	Cooper et al., 2004	Mid Atlantic Ridge	5.56	n.a.
RC120-1	Cooper et al., 2004	Mid Atlantic Ridge	5.43	0.07
RC30	Cooper et al., 2004	Mid Atlantic Ridge	5.33	0.03
RC119	Cooper et al., 2004	Mid Atlantic Ridge	5.44	0.11

Table A5. continued

Sample	Reference	Locality	$\delta^{18}\text{O}$	$2\sigma$
D13.A	Cooper et al., 2004	Mid Atlantic Ridge	5.34	0.04
D14.A	Cooper et al., 2004	Mid Atlantic Ridge	5.38	0.01
D38.A	Cooper et al., 2004	Mid Atlantic Ridge	5.49	0
RC103-1	Cooper et al., 2004	Mid Atlantic Ridge	5.45	0.04
RC104	Cooper et al., 2004	Mid Atlantic Ridge	5.41	0.05
D15.A	Cooper et al., 2004	Mid Atlantic Ridge	5.49	n.a.
RC105	Cooper et al., 2004	Mid Atlantic Ridge	5.48	0.07
RC107	Cooper et al., 2004	Mid Atlantic Ridge	5.44	0.03
RC108-1	Cooper et al., 2004	Mid Atlantic Ridge	5.44	0.06
RC110	Cooper et al., 2004	Mid Atlantic Ridge	5.58	0.01
RC111-1	Cooper et al., 2004	Mid Atlantic Ridge	5.43	0.09
RC112-1	Cooper et al., 2004	Mid Atlantic Ridge	5.43	0.13
RC113-1	Cooper et al., 2004	Mid Atlantic Ridge	5.56	0.06
D35.A	Cooper et al., 2004	Mid Atlantic Ridge	5.43	0.06
D17.A	Cooper et al., 2004	Mid Atlantic Ridge	5.45	0.01
D33-2	Cooper et al., 2004	Mid Atlantic Ridge	5.34	n.a.
D19-1A	Cooper et al., 2004	Mid Atlantic Ridge	5.52	0.06
D21.B	Cooper et al., 2004	Mid Atlantic Ridge	5.51	n.a.
RC59	Cooper et al., 2004	Mid Atlantic Ridge	5.38	0.01
D30.A	Cooper et al., 2004	Mid Atlantic Ridge	5.50	n.a.
D22.A	Cooper et al., 2004	Mid Atlantic Ridge	5.66	0.06
RC87	Cooper et al., 2004	Mid Atlantic Ridge	5.49	0.03

Table A5. continued

<b>Sample</b>	<b>Reference</b>	<b>Locality</b>	$\delta^{18}\text{O}$	$2\sigma$
D29.A	Cooper et al., 2004	Mid Atlantic Ridge	5.4	0.02
D27.A	Cooper et al., 2004	Mid Atlantic Ridge	5.47	0.08
RC82-1	Cooper et al., 2004	Mid Atlantic Ridge	5.23	0.03
D26.A	Cooper et al., 2004	Mid Atlantic Ridge	5.45	0.02
RC74	Cooper et al., 2004	Mid Atlantic Ridge	5.53	0.07
RC73	Cooper et al., 2004	Mid Atlantic Ridge	5.54	0.05
RC72	Cooper et al., 2004	Mid Atlantic Ridge	5.66	0.05
<b>Average</b>			<b>5.46</b>	

n.a. indicates not available.

Table A6. Source data for oxygen isotopes of eclogite xenoliths

Sample	Reference	Locality	Mineral/WR	$\delta^{18}\text{O}$	$2\sigma$
JJG 2104	Appleyard, 2000	Rietfontein	Gt	6.84	n.a.
JJG 2104	Appleyard, 2000	Rietfontein	Gt	5.95	n.a.
CMA 4	Appleyard, 2000	Rietfontein	Gt	5.58	n.a.
CMA 4	Appleyard, 2000	Rietfontein	Gt	5.82	n.a.
CMA 14	Appleyard, 2000	Rietfontein	Gt	5.99	n.a.
CMA 14	Appleyard, 2000	Rietfontein	Gt	5.61	n.a.
Gtfn 43.2	Appleyard, 2000	Rietfontein	Gt	5.24	n.a.
Gtfn 55.1	Appleyard, 2000	Rietfontein	Gt	5.16	n.a.
80-A2	Barth et al., 2001	West africa	Gt	5.75	0.02
81-3	Barth et al., 2001	West africa	Gt	5.27	0.01
81-4	Barth et al., 2001	West africa	Gt	5.05	0.01
81-5	Barth et al., 2001	West africa	Gt	5.57	0.04
81-7	Barth et al., 2001	West africa	Gt	5.59	0.00
81-8	Barth et al., 2001	West africa	Gt	5.15	0.10
81-10a	Barth et al., 2001	West africa	Gt	5.72	0.06
81-18	Barth et al., 2001	West africa	Gt	5.95	n.a.
81-21	Barth et al., 2001	West africa	Gt	6.09	0.08
86-6	Barth et al., 2001	West africa	Gt	5.95	0.01
86-13	Barth et al., 2001	West africa	Gt	5.51	0.01
86-14	Barth et al., 2001	West africa	Gt	5.68	0.00
86-34	Barth et al., 2001	West africa	Gt	5.38	0.06
86-36	Barth et al., 2001	West africa	Gt	5.97	0.01
56-56	Barth et al., 2001	West africa	Gt	5.33	0.01
86-71a	Barth et al., 2001	West africa	Gt	4.86	0.03

Table A6. continued

Sample	Reference	Locality	Mineral/WR	$\delta^{18}\text{O}$	$2\sigma$
91-2	Barth et al., 2001	West africa	Gt	5.70	0.02
91-4	Barth et al., 2001	West africa	Gt	4.68	0.02
91.7	Barth et al., 2001	West africa	Gt	5.43	0.04
91-11	Barth et al., 2001	West africa	Gt	4.93	n.a.
91-13	Barth et al., 2001	West africa	Gt	5.47	n.a.
91-20	Barth et al., 2001	West africa	Gt	5.76	n.a.
91-22	Barth et al., 2001	West africa	Gt	6.11	n.a.
91-23	Barth et al., 2001	West africa	Gt	6.10	n.a.
91-58	Barth et al., 2001	West africa	Gt	6.78	n.a.
86-12	Barth et al., 2001	West africa	Gt	4.85	n.a.
86-70	Barth et al., 2001	West africa	Gt	5.27	n.a.
86-1	Barth et al., 2001	West africa	Gt	4.73	n.a.
86-3	Barth et al., 2001	West africa	Gt	4.97	n.a.
86-4	Barth et al., 2001	West africa	Gt	5.09	n.a.
85-74b	Barth et al., 2001	West africa	Gt	5.35	n.a.
M84	Beard et al., 1996	Mir kimberlite	WR	5.85	n.a.
M772	Beard et al., 1996	Mir kimberlite	WR	5.71	n.a.
M2385	Beard et al., 1996	Mir kimberlite	WR	5.93	n.a.
M29	Beard et al., 1996	Mir kimberlite	WR	6.17	n.a.
M65	Beard et al., 1996	Mir kimberlite	WR	6.15	n.a.
M70	Beard et al., 1996	Mir kimberlite	WR	7.39	n.a.
M704	Beard et al., 1996	Mir kimberlite	WR	7.41	n.a.
M180	Beard et al., 1996	Mir kimberlite	WR	5.44	n.a.
M432	Beard et al., 1996	Mir kimberlite	WR	5.80	n.a.

Table A6. continued

Sample	Reference	Locality	Mineral/WR	$\delta^{18}\text{O}$	$2\sigma$
M69	Beard et al., 1996	Mir kimberlite	WR	5.88	n.a.
M54	Beard et al., 1996	Mir kimberlite	WR	4.80	n.a.
M83	Beard et al., 1996	Mir kimberlite	WR	4.82	n.a.
M86	Beard et al., 1996	Mir kimberlite	WR	4.28	n.a.
M84	Beard et al., 1996	Mir kimberlite	Cpx	5.90	n.a.
M772	Beard et al., 1996	Mir kimberlite	Cpx	5.37	n.a.
M2385	Beard et al., 1996	Mir kimberlite	Cpx	5.64	n.a.
M29	Beard et al., 1996	Mir kimberlite	Cpx	6.00	n.a.
M65	Beard et al., 1996	Mir kimberlite	Cpx	6.52	n.a.
M70	Beard et al., 1996	Mir kimberlite	Cpx	7.13	n.a.
M704	Beard et al., 1996	Mir kimberlite	Cpx	7.09	n.a.
M180	Beard et al., 1996	Mir kimberlite	Cpx	5.19	n.a.
M60/1214	Beard et al., 1996	Mir kimberlite	Cpx	5.13	n.a.
M53/1165	Beard et al., 1996	Mir kimberlite	Cpx	6.02	n.a.
M432	Beard et al., 1996	Mir kimberlite	Cpx	5.78	n.a.
M69	Beard et al., 1996	Mir kimberlite	Cpx	5.39	n.a.
M54	Beard et al., 1996	Mir kimberlite	Cpx	4.67	n.a.
M84	Beard et al., 1996	Mir kimberlite	Gt	5.77	n.a.
M772	Beard et al., 1996	Mir kimberlite	Gt	4.85	n.a.
M2385	Beard et al., 1996	Mir kimberlite	Gt	5.18	n.a.
M29	Beard et al., 1996	Mir kimberlite	Gt	5.97	n.a.
M65	Beard et al., 1996	Mir kimberlite	Gt	6.66	n.a.
M70	Beard et al., 1996	Mir kimberlite	Gt	7.18	n.a.
M704	Beard et al., 1996	Mir kimberlite	Gt	6.89	n.a.

Table A6. continued

Sample	Reference	Locality	Mineral/WR	$\delta^{18}\text{O}$	$2\sigma$
M180	Beard et al., 1996	Mir kimberlite	Gt	4.90	n.a.
M60/1214	Beard et al., 1996	Mir kimberlite	Gt	5.36	n.a.
M53/1165	Beard et al., 1996	Mir kimberlite	Gt	5.50	n.a.
M432	Beard et al., 1996	Mir kimberlite	Gt	5.40	n.a.
M69	Beard et al., 1996	Mir kimberlite	Gt	5.34	n.a.
M54	Beard et al., 1996	Mir kimberlite	Gt	4.20	n.a.
M83	Beard et al., 1996	Mir kimberlite	Gt	4.98	n.a.
M86	Beard et al., 1996	Mir kimberlite	Gt	3.09	n.a.
XM3	Deines et al., 1991	Orapa, Botswana	Cpx	8.30	n.a.
XM4	Deines et al., 1991	Orapa, Botswana	Cpx	6.00	n.a.
XM5	Deines et al., 1991	Orapa, Botswana	Cpx	5.70	n.a.
XM6	Deines et al., 1991	Orapa, Botswana	Cpx	6.20	n.a.
XM8	Deines et al., 1991	Orapa, Botswana	Cpx	5.70	n.a.
XM9	Deines et al., 1991	Orapa, Botswana	Cpx	5.80	n.a.
XM10	Deines et al., 1991	Orapa, Botswana	Cpx	6.00	n.a.
XM11	Deines et al., 1991	Orapa, Botswana	Cpx	5.50	n.a.
XM13	Deines et al., 1991	Orapa, Botswana	Cpx	6.50	n.a.
XM15	Deines et al., 1991	Orapa, Botswana	Cpx	5.30	n.a.
XM16	Deines et al., 1991	Orapa, Botswana	Cpx	6.20	n.a.
XM17	Deines et al., 1991	Orapa, Botswana	Cpx	4.60	n.a.
XM18	Deines et al., 1991	Orapa, Botswana	Cpx	5.50	n.a.
XM19	Deines et al., 1991	Orapa, Botswana	Cpx	4.60	n.a.
XM22	Deines et al., 1991	Orapa, Botswana	Cpx	5.30	n.a.
XM23	Deines et al., 1991	Orapa, Botswana	Cpx	5.40	n.a.

Table A6. continued

Sample	Reference	Locality	Mineral/WR	$\delta^{18}\text{O}$	$2\sigma$
XM24	Deines et al., 1991	Orapa, Botswana	Cpx	5.90	n.a.
XM25	Deines et al., 1991	Orapa, Botswana	Cpx	6.00	n.a.
XM27	Deines et al., 1991	Orapa, Botswana	Cpx	5.40	n.a.
XM28	Deines et al., 1991	Orapa, Botswana	Cpx	5.70	n.a.
XM29	Deines et al., 1991	Orapa, Botswana	Cpx	5.30	n.a.
XM31	Deines et al., 1991	Orapa, Botswana	Cpx	6.60	n.a.
XM32	Deines et al., 1991	Orapa, Botswana	Cpx	6.00	n.a.
XM3	Deines et al., 1991	Orapa, Botswana	Gt	7.90	n.a.
XM4	Deines et al., 1991	Orapa, Botswana	Gt	6.40	n.a.
XM5	Deines et al., 1991	Orapa, Botswana	Gt	5.90	n.a.
XM6	Deines et al., 1991	Orapa, Botswana	Gt	6.20	n.a.
XM7	Deines et al., 1991	Orapa, Botswana	Gt	6.10	n.a.
XM8	Deines et al., 1991	Orapa, Botswana	Gt	3.90	n.a.
XM9	Deines et al., 1991	Orapa, Botswana	Gt	5.70	n.a.
XM10	Deines et al., 1991	Orapa, Botswana	Gt	5.80	n.a.
XM11	Deines et al., 1991	Orapa, Botswana	Gt	5.90	n.a.
XM13	Deines et al., 1991	Orapa, Botswana	Gt	7.00	n.a.
XM14	Deines et al., 1991	Orapa, Botswana	Gt	6.80	n.a.
XM15	Deines et al., 1991	Orapa, Botswana	Gt	5.50	n.a.
XM17	Deines et al., 1991	Orapa, Botswana	Gt	5.50	n.a.
XM18	Deines et al., 1991	Orapa, Botswana	Gt	6.20	n.a.
XM19	Deines et al., 1991	Orapa, Botswana	Gt	5.20	n.a.
XM21	Deines et al., 1991	Orapa, Botswana	Gt	5.60	n.a.
XM22	Deines et al., 1991	Orapa, Botswana	Gt	6.10	n.a.

Table A6. continued

Sample	Reference	Locality	Mineral/WR	$\delta^{18}\text{O}$	$2\sigma$
XM23	Deines et al., 1991	Orapa, Botswana	Gt	5.80	n.a.
XM25	Deines et al., 1991	Orapa, Botswana	Gt	6.20	n.a.
XM26	Deines et al., 1991	Orapa, Botswana	Gt	8.10	n.a.
XM27	Deines et al., 1991	Orapa, Botswana	Gt	6.00	n.a.
XM28	Deines et al., 1991	Orapa, Botswana	Gt	5.90	n.a.
XM29	Deines et al., 1991	Orapa, Botswana	Gt	6.20	n.a.
XM30	Deines et al., 1991	Orapa, Botswana	Gt	9.20	n.a.
XM31	Deines et al., 1991	Orapa, Botswana	Gt	6.50	n.a.
XM32	Deines et al., 1991	Orapa, Botswana	Gt	6.30	n.a.
XM33	Deines et al., 1991	Orapa, Botswana	Gt	6.10	n.a.
XM34	Deines et al., 1991	Orapa, Botswana	Gt	5.80	n.a.
JJG889	Deines et al., 1991	Orapa, Botswana	Gt	7.20	n.a.
JJG890	Deines et al., 1991	Orapa, Botswana	Gt	5.00	n.a.
JJG891	Deines et al., 1991	Orapa, Botswana	Gt	7.80	n.a.
JJG892	Deines et al., 1991	Orapa, Botswana	Gt	6.60	n.a.
JJG894	Deines et al., 1991	Orapa, Botswana	Gt	5.80	n.a.
JJG895	Deines et al., 1991	Orapa, Botswana	Gt	4.70	n.a.
XM3	Deines et al., 1991	Orapa, Botswana	WR	8.10	n.a.
XM4	Deines et al., 1991	Orapa, Botswana	WR	6.20	n.a.
XM5	Deines et al., 1991	Orapa, Botswana	WR	5.80	n.a.
XM6	Deines et al., 1991	Orapa, Botswana	WR	6.20	n.a.
XM8	Deines et al., 1991	Orapa, Botswana	WR	4.80	n.a.
XM9	Deines et al., 1991	Orapa, Botswana	WR	5.75	n.a.
XM10	Deines et al., 1991	Orapa, Botswana	WR	5.90	n.a.

Table A6. continued

Sample	Reference	Locality	Mineral/WR	$\delta^{18}\text{O}$	$2\sigma$
XM11	Deines et al., 1991	Orapa, Botswana	WR	5.70	n.a.
XM13	Deines et al., 1991	Orapa, Botswana	WR	6.75	n.a.
XM15	Deines et al., 1991	Orapa, Botswana	WR	5.40	n.a.
XM16	Deines et al., 1991	Orapa, Botswana	WR	6.20	n.a.
XM17	Deines et al., 1991	Orapa, Botswana	WR	5.05	n.a.
XM18	Deines et al., 1991	Orapa, Botswana	WR	5.85	n.a.
XM19	Deines et al., 1991	Orapa, Botswana	WR	4.90	n.a.
XM22	Deines et al., 1991	Orapa, Botswana	WR	5.70	n.a.
XM23	Deines et al., 1991	Orapa, Botswana	WR	5.60	n.a.
XM25	Deines et al., 1991	Orapa, Botswana	WR	6.10	n.a.
XM27	Deines et al., 1991	Orapa, Botswana	WR	5.70	n.a.
XM28	Deines et al., 1991	Orapa, Botswana	WR	5.80	n.a.
XM29	Deines et al., 1991	Orapa, Botswana	WR	5.75	n.a.
XM31	Deines et al., 1991	Orapa, Botswana	WR	6.55	n.a.
XM32	Deines et al., 1991	Orapa, Botswana	WR	6.15	n.a.
4	Garlick et al., 1971	Roberts Victor	Cpx	6.80	n.a.
7	Garlick et al., 1971	Roberts Victor	Cpx	6.40	n.a.
50	Garlick et al., 1971	Roberts Victor	Cpx	6.10	n.a.
63	Garlick et al., 1971	Roberts Victor	Cpx	6.80	n.a.
64	Garlick et al., 1971	Roberts Victor	Cpx	7.20	n.a.
71	Garlick et al., 1971	Roberts Victor	Cpx	7.00	n.a.
15	Garlick et al., 1971	Roberts Victor	Cpx	6.00	n.a.
44	Garlick et al., 1971	Roberts Victor	Cpx	6.40	n.a.
8A	Garlick et al., 1971	Roberts Victor	Cpx	5.30	n.a.

Table A6. continued

Sample	Reference	Locality	Mineral/WR	$\delta^{18}\text{O}$	$2\sigma$
22	Garlick et al., 1971	Roberts Victor	Cpx	4.30	n.a.
26	Garlick et al., 1971	Roberts Victor	Cpx	3.20	n.a.
30	Garlick et al., 1971	Roberts Victor	Cpx	4.30	n.a.
47	Garlick et al., 1971	Roberts Victor	Cpx	3.20	n.a.
54	Garlick et al., 1971	Roberts Victor	Cpx	2.50	0.10
61	Garlick et al., 1971	Roberts Victor	Cpx	3.40	n.a.
4a	Garlick et al., 1971	Roberts Victor	Gt	8.00	0.10
38	Garlick et al., 1971	Roberts Victor	Gt	6.20	n.a.
64	Garlick et al., 1971	Roberts Victor	Gt	6.60	n.a.
71	Garlick et al., 1971	Roberts Victor	Gt	6.50	n.a.
13	Garlick et al., 1971	Roberts Victor	Gt	5.80	n.a.
53	Garlick et al., 1971	Roberts Victor	Gt	5.40	n.a.
65	Garlick et al., 1971	Roberts Victor	Gt	6.80	n.a.
6	Garlick et al., 1971	Roberts Victor	Gt	3.80	n.a.
8A	Garlick et al., 1971	Roberts Victor	Gt	5.30	n.a.
26	Garlick et al., 1971	Roberts Victor	Gt	3.20	n.a.
37	Garlick et al., 1971	Roberts Victor	Gt	3.10	n.a.
41	Garlick et al., 1971	Roberts Victor	Gt	2.20	0.10
47	Garlick et al., 1971	Roberts Victor	Gt	3.30	n.a.
54	Garlick et al., 1971	Roberts Victor	Gt	2.60	0.30
64	Garlick et al., 1971	Roberts Victor	WR	6.90	n.a.
71	Garlick et al., 1971	Roberts Victor	WR	6.75	n.a.
8A	Garlick et al., 1971	Roberts Victor	WR	5.30	n.a.
26	Garlick et al., 1971	Roberts Victor	WR	3.20	n.a.

Table A6. continued

Sample	Reference	Locality	Mineral/WR	$\delta^{18}\text{O}$	$2\sigma$
54	Garlick et al., 1971	Roberts Victor	WR	2.55	n.a.
65	Jacob et al., 1994	Udachnaya	Cpx	7.38	0.08
91	Jacob et al., 1994	Udachnaya	Cpx	7.26	0.07
55	Jacob et al., 1994	Udachnaya	Cpx	7.07	0.08
77	Jacob et al., 1994	Udachnaya	Cpx	6.24	0.03
29	Jacob et al., 1994	Udachnaya	Cpx	5.59	0.06
43	Jacob et al., 1994	Udachnaya	Cpx	5.69	0.10
65	Jacob et al., 1994	Udachnaya	Gt	6.96	0.03
91	Jacob et al., 1994	Udachnaya	Gt	6.94	0.08
55	Jacob et al., 1994	Udachnaya	Gt	6.71	0.17
77	Jacob et al., 1994	Udachnaya	Gt	5.97	0.06
29	Jacob et al., 1994	Udachnaya	Gt	5.28	0.03
43	Jacob et al., 1994	Udachnaya	Gt	5.19	0.09
84	Jacob et al., 1994	Udachnaya	Gt	5.42	0.07
68	Jacob et al., 1994	Udachnaya	Gt	5.58	0.04
65	Jacob et al., 1994	Udachnaya	WR	7.17	0.08
91	Jacob et al., 1994	Udachnaya	WR	7.10	0.07
55	Jacob et al., 1994	Udachnaya	WR	6.89	0.08
77	Jacob et al., 1994	Udachnaya	WR	6.11	0.03
29	Jacob et al., 1994	Udachnaya	WR	5.44	0.06
43	Jacob et al., 1994	Udachnaya	WR	5.44	0.10
79197	Malkovets et al., 2003	Grib kimberlite	Gt	5.64	n.a.
94/210	Malkovets et al., 2003	Grib kimberlite	Gt	5.64	n.a.
102/236	Malkovets et al., 2003	Grib kimberlite	Gt	5.40	n.a.

Table A6. continued

Sample	Reference	Locality	Mineral/WR	$\delta^{18}\text{O}$	$2\sigma$
73/230	Malkovets et al., 2003	Grib kimberlite	Gt	5.40	n.a.
93/265	Malkovets et al., 2003	Grib kimberlite	Gt	4.27	n.a.
102/254	Malkovets et al., 2003	Grib kimberlite	Gt	4.29	n.a.
441/3	Malkovets et al., 2003	Grib kimberlite	Gt	4.05	n.a.
437-1	Neal et al., 1990	Bellsbank kimberlite	WR	5.60	n.a.
437-2	Neal et al., 1990	Bellsbank kimberlite	WR	5.10	n.a.
438-2	Neal et al., 1990	Bellsbank kimberlite	WR	3.30	n.a.
438-3	Neal et al., 1990	Bellsbank kimberlite	WR	4.00	n.a.
438-7	Neal et al., 1990	Bellsbank kimberlite	WR	3.00	n.a.
2791-21	Neal et al., 1990	Bellsbank kimberlite	WR	2.90	n.a.
437-5	Neal et al., 1990	Bellsbank kimberlite	WR	3.40	n.a.
437-7	Neal et al., 1990	Bellsbank kimberlite	WR	4.00	n.a.
2791-34	Neal et al., 1990	Bellsbank kimberlite	WR	4.70	n.a.
HRV-272	Ongley et al., 1987	Roberts Victor	Cpx	6.30	n.a.
HRV-201	Ongley et al., 1987	Roberts Victor	Cpx	4.00	n.a.
HRV-187	Ongley et al., 1987	Roberts Victor	Cpx	5.70	n.a.
RV-102	Ongley et al., 1987	Roberts Victor	Cpx	5.50	n.a.
HRV-93	Ongley et al., 1987	Roberts Victor	Cpx	7.00	n.a.
R-52	Ongley et al., 1987	Roberts Victor	Cpx	6.90	n.a.
R-19	Ongley et al., 1987	Roberts Victor	Cpx	6.90	n.a.
HRV-15	Ongley et al., 1987	Roberts Victor	Cpx	6.10	n.a.
R-13	Ongley et al., 1987	Roberts Victor	Cpx	6.40	n.a.
R-11	Ongley et al., 1987	Roberts Victor	Cpx	7.40	n.a.
R-7	Ongley et al., 1987	Roberts Victor	Cpx	6.40	n.a.

Table A6. continued

Sample	Reference	Locality	Mineral/WR	$\delta^{18}\text{O}$	$2\sigma$
RV(W)	Ongley et al., 1987	Roberts Victor	Cpx	7.20	n.a.
HRV-272	Ongley et al., 1987	Roberts Victor	Gt	6.10	n.a.
HRV-201	Ongley et al., 1987	Roberts Victor	Gt	3.80	n.a.
HRV-187	Ongley et al., 1987	Roberts Victor	Gt	6.40	n.a.
RV-102	Ongley et al., 1987	Roberts Victor	Gt	5.40	n.a.
HRV-93	Ongley et al., 1987	Roberts Victor	Gt	7.00	n.a.
R-52	Ongley et al., 1987	Roberts Victor	Gt	6.70	n.a.
R-19	Ongley et al., 1987	Roberts Victor	Gt	6.80	n.a.
HRV-15	Ongley et al., 1987	Roberts Victor	Gt	5.90	n.a.
R-13	Ongley et al., 1987	Roberts Victor	Gt	6.10	n.a.
R-11	Ongley et al., 1987	Roberts Victor	Gt	7.10	n.a.
R-7	Ongley et al., 1987	Roberts Victor	Gt	6.40	n.a.
RV(W)	Ongley et al., 1987	Roberts Victor	Gt	6.90	n.a.
HRV-272	Ongley et al., 1987	Roberts Victor	WR	6.20	n.a.
HRV-201	Ongley et al., 1987	Roberts Victor	WR	3.90	n.a.
HRV-187	Ongley et al., 1987	Roberts Victor	WR	6.10	n.a.
RV-102	Ongley et al., 1987	Roberts Victor	WR	5.50	n.a.
HRV-93	Ongley et al., 1987	Roberts Victor	WR	7.00	n.a.
R-52	Ongley et al., 1987	Roberts Victor	WR	6.90	n.a.
R-19	Ongley et al., 1987	Roberts Victor	WR	6.80	n.a.
HRV-15	Ongley et al., 1987	Roberts Victor	WR	6.00	n.a.
R-13	Ongley et al., 1987	Roberts Victor	WR	6.30	n.a.
R-11	Ongley et al., 1987	Roberts Victor	WR	7.20	n.a.
R-7	Ongley et al., 1987	Roberts Victor	WR	6.40	n.a.

Table A6. continued

Sample	Reference	Locality	Mineral/WR	$\delta^{18}\text{O}$	$2\sigma$
RV(W)	Ongley et al., 1987	Roberts Victor	WR	7.00	n.a.
KE1	Schmickler et al., 2004	Kuruman kimberlite	Cpx	5.19	0.01
Z267	Schmickler et al., 2004	Kuruman kimberlite	Cpx	5.21	0.05
Z469	Schmickler et al., 2004	Kuruman kimberlite	Cpx	5.34	0.05
Z291	Schmickler et al., 2004	Kuruman kimberlite	Cpx	5.19	0.08
Z257	Schmickler et al., 2004	Kuruman kimberlite	Cpx	5.30	0.03
Z239	Schmickler et al., 2004	Kuruman kimberlite	Cpx	5.39	0.10
KE1	Schmickler et al., 2004	Kuruman kimberlite	Gt	5.18	0.03
Z267	Schmickler et al., 2004	Kuruman kimberlite	Gt	5.27	0.06
Z469	Schmickler et al., 2004	Kuruman kimberlite	Gt	5.45	0.05
Z291	Schmickler et al., 2004	Kuruman kimberlite	Gt	5.22	0.05
Z257	Schmickler et al., 2004	Kuruman kimberlite	Gt	5.35	0.03
Z239	Schmickler et al., 2004	Kuruman kimberlite	Gt	5.47	0.02

$\Delta$ clinopyroxene-garnet  $\approx 0$  (Beard et al. 1996). Garnet, clinopyroxene, and whole rock abbreviated as Gt, Cpx, and WR, respectively.

Table A7. Source data for oxygen isotopes of serpentinite

Sample	Reference	Locality	$\delta^{18}\text{O}$	$2\sigma$
1.4	Agrinier et al., 1988	Hess Deep, East Pacific Ridge	4.00	n.a.
9.6	Agrinier et al., 1988	Hess Deep, East Pacific Ridge	4.30	n.a.
9.7	Agrinier et al., 1988	Hess Deep, East Pacific Ridge	4.30	n.a.
9.9	Agrinier et al., 1988	Hess Deep, East Pacific Ridge	3.60	n.a.
D274	Agrinier et al., 1988	Xigaze	5.70	0.15
D72	Agrinier et al., 1988	Xigaze	4.40	0.15
X487	Agrinier et al., 1988	Xigaze	5.90	0.15
X492	Agrinier et al., 1988	Xigaze	4.50	0.15
X571	Agrinier et al., 1988	Xigaze	4.30	0.15
X636'	Agrinier et al., 1988	Xigaze	7.80	0.15
X640	Agrinier et al., 1988	Xigaze	2.80	0.15
X678	Agrinier et al., 1988	Xigaze	6.20	0.15
X685	Agrinier et al., 1988	Xigaze	6.40	0.15
X735	Agrinier et al., 1988	Xigaze	4.70	0.15
X766	Agrinier et al., 1988	Xigaze	4.60	0.15
1268A	Alt et al., 2007	Mid-Atlantic Ridge fracture zone	5.90	0.20
1268A	Alt et al., 2007	Mid-Atlantic Ridge fracture zone	3.70	0.20
1268A	Alt et al., 2007	Mid-Atlantic Ridge fracture zone	12.10	0.20
1268A	Alt et al., 2007	Mid-Atlantic Ridge fracture zone	3.60	0.20
1268A	Alt et al., 2007	Mid-Atlantic Ridge fracture zone	4.80	0.20
1268A	Alt et al., 2007	Mid-Atlantic Ridge fracture zone	5.90	0.20
1268A	Alt et al., 2007	Mid-Atlantic Ridge fracture zone	5.00	0.20
1268A	Alt et al., 2007	Mid-Atlantic Ridge fracture zone	5.60	0.20
1268A	Alt et al., 2007	Mid-Atlantic Ridge fracture zone	4.10	0.20

Table A7. continued

Sample	Reference	Locality	$\delta^{18}\text{O}$	$2\sigma$
1268A	Alt et al., 2007	Mid-Atlantic Ridge fracture zone	4.40	0.20
1268A	Alt et al., 2007	Mid-Atlantic Ridge fracture zone	4.60	0.20
1268A	Alt et al., 2007	Mid-Atlantic Ridge fracture zone	3.40	0.20
1268A	Alt et al., 2007	Mid-Atlantic Ridge fracture zone	2.90	0.20
1268A	Alt et al., 2007	Mid-Atlantic Ridge fracture zone	4.40	0.20
1268A	Alt et al., 2007	Mid-Atlantic Ridge fracture zone	2.60	0.20
1270B	Alt et al., 2007	Mid-Atlantic Ridge fracture zone	4.80	0.20
1270C	Alt et al., 2007	Mid-Atlantic Ridge fracture zone	4.00	0.20
1270C	Alt et al., 2007	Mid-Atlantic Ridge fracture zone	4.10	0.20
1270D	Alt et al., 2007	Mid-Atlantic Ridge fracture zone	5.20	0.20
1270D	Alt et al., 2007	Mid-Atlantic Ridge fracture zone	4.90	0.20
1270D	Alt et al., 2007	Mid-Atlantic Ridge fracture zone	3.20	0.20
1272A	Alt et al., 2007	Mid-Atlantic Ridge fracture zone	7.30	0.20
1272A	Alt et al., 2007	Mid-Atlantic Ridge fracture zone	7.60	0.20
1272A	Alt et al., 2007	Mid-Atlantic Ridge fracture zone	7.50	0.20
1272A	Alt et al., 2007	Mid-Atlantic Ridge fracture zone	8.10	0.20
1272A	Alt et al., 2007	Mid-Atlantic Ridge fracture zone	6.10	0.20
1272A	Alt et al., 2007	Mid-Atlantic Ridge fracture zone	7.10	0.20
1274A	Alt et al., 2007	Mid-Atlantic Ridge fracture zone	6.40	0.20
1274A	Alt et al., 2007	Mid-Atlantic Ridge fracture zone	5.80	0.20
1274A	Alt et al., 2007	Mid-Atlantic Ridge fracture zone	7.40	0.20
1274A	Alt et al., 2007	Mid-Atlantic Ridge fracture zone	7.40	0.20
1274A	Alt et al., 2007	Mid-Atlantic Ridge fracture zone	6.00	0.20
1274A	Alt et al., 2007	Mid-Atlantic Ridge fracture zone	4.80	0.20

Table A7. continued

Sample	Reference	Locality	$\delta^{18}\text{O}$	$2\sigma$
1274A	Alt et al., 2007	Mid-Atlantic Ridge fracture zone	5.40	0.20
1274A	Alt et al., 2007	Mid-Atlantic Ridge fracture zone	5.70	0.20
1274A	Alt et al., 2007	Mid-Atlantic Ridge fracture zone	5.40	0.20
1274A-3-1, 111–120	Barnes et al., 2009	Mid-Atlantic Ridge fracture zone	6.40	n.a.
1274A-6-2, 128–135	Barnes et al., 2009	Mid-Atlantic Ridge fracture zone	5.80	n.a.
1274A-10-1, 3–10	Barnes et al., 2009	Mid-Atlantic Ridge fracture zone	7.40	n.a.
1274A-14-1, 30–36	Barnes et al., 2009	Mid-Atlantic Ridge fracture zone	7.40	n.a.
1274A-16-1, 44–52	Barnes et al., 2009	Mid-Atlantic Ridge fracture zone	6.00	n.a.
1274A-17-1, 121–129	Barnes et al., 2009	Mid-Atlantic Ridge fracture zone	4.80	n.a.
1274A-18-1, 83–93	Barnes et al., 2009	Mid-Atlantic Ridge fracture zone	5.40	n.a.
1274A-22-1, 24–32	Barnes et al., 2009	Mid-Atlantic Ridge fracture zone	5.70	n.a.
1274A-27-2, 5–11	Barnes et al., 2009	Mid-Atlantic Ridge fracture zone	5.40	n.a.
1272A-13-2, 14–21	Barnes et al., 2009	Mid-Atlantic Ridge fracture zone	7.30	n.a.
1272A-16-1, 82–89	Barnes et al., 2009	Mid-Atlantic Ridge fracture zone	7.60	n.a.
1272A-21-1, 27–37	Barnes et al., 2009	Mid-Atlantic Ridge fracture zone	7.50	n.a.
1272A-24-1, 104–112	Barnes et al., 2009	Mid-Atlantic Ridge fracture zone	8.10	n.a.
1272A-26-1, 50–57	Barnes et al., 2009	Mid-Atlantic Ridge fracture zone	6.10	n.a.
1272A-26-3, 59–68	Barnes et al., 2009	Mid-Atlantic Ridge fracture zone	7.10	n.a.
1270B-7-1, 18–22	Barnes et al., 2009	Mid-Atlantic Ridge fracture zone	4.80	n.a.
1270C-2-1, 40–46	Barnes et al., 2009	Mid-Atlantic Ridge fracture zone	4.00	n.a.
1270C-3-1, 12–15	Barnes et al., 2009	Mid-Atlantic Ridge fracture zone	4.10	n.a.
1270D-1-1, 69–73	Barnes et al., 2009	Mid-Atlantic Ridge fracture zone	5.20	n.a.
1270D-3-2, 39–47	Barnes et al., 2009	Mid-Atlantic Ridge fracture zone	4.90	n.a.

Table A7. continued

Sample	Reference	Locality	$\delta^{18}\text{O}$	$2\sigma$
1270D-6-1, 58–63	Barnes et al., 2009	Mid-Atlantic Ridge fracture zone	3.20	n.a.
1268A-2-1, 10–14	Barnes et al., 2009	Mid-Atlantic Ridge fracture zone	5.90	n.a.
1268A-2-2, 108–115	Barnes et al., 2009	Mid-Atlantic Ridge fracture zone	3.70	n.a.
1268A-3-1, 29–38	Barnes et al., 2009	Mid-Atlantic Ridge fracture zone	12.10	n.a.
1268A-4-1, 26–32	Barnes et al., 2009	Mid-Atlantic Ridge fracture zone	3.60	n.a.
1268A-4-3, 26–35	Barnes et al., 2009	Mid-Atlantic Ridge fracture zone	4.80	n.a.
1268A-8-1, 28–35	Barnes et al., 2009	Mid-Atlantic Ridge fracture zone	5.90	n.a.
1268A-10-1, 58–64	Barnes et al., 2009	Mid-Atlantic Ridge fracture zone	5.00	n.a.
1268A-11-1, 78–85	Barnes et al., 2009	Mid-Atlantic Ridge fracture zone	5.60	n.a.
1268A-13-1, 46–55	Barnes et al., 2009	Mid-Atlantic Ridge fracture zone	4.10	n.a.
1268A-17-2, 131–138	Barnes et al., 2009	Mid-Atlantic Ridge fracture zone	4.40	n.a.
1268A-18-3, 100–110	Barnes et al., 2009	Mid-Atlantic Ridge fracture zone	4.60	n.a.
1268A-19-1, 34–43	Barnes et al., 2009	Mid-Atlantic Ridge fracture zone	3.40	n.a.
1268A-19-3, 6–13	Barnes et al., 2009	Mid-Atlantic Ridge fracture zone	2.90	n.a.
1268A-20-2, 121–127	Barnes et al., 2009	Mid-Atlantic Ridge fracture zone	4.40	n.a.
1268A-24-2, 13–20	Barnes et al., 2009	Mid-Atlantic Ridge fracture zone	2.60	n.a.
3639-1254C	Boschi et al., 2008	Atlantis Massif	3.30	0.15
3639-1254R	Boschi et al., 2008	Atlantis Massif	1.70	0.15
3639-1355	Boschi et al., 2008	Atlantis Massif	4.70	0.15
3642-1309	Boschi et al., 2008	Atlantis Massif	3.50	0.15
3645-1159C	Boschi et al., 2008	Atlantis Massif	2.60	0.15
3645-1159R	Boschi et al., 2008	Atlantis Massif	2.90	0.15

Table A7. continued

Sample	Reference	Locality	$\delta^{18}\text{O}$	$2\sigma$
3646-1000	Boschi et al., 2008	Atlantis Massif	3.80	0.15
3647-1416	Boschi et al., 2008	Atlantis Massif	4.50	0.15
3648-1403	Boschi et al., 2008	Atlantis Massif	5.60	0.15
3651-1252	Boschi et al., 2008	Atlantis Massif	3.20	0.15
3652-1226	Boschi et al., 2008	Atlantis Massif	6.70	0.15
3863-1419	Boschi et al., 2008	Atlantis Massif	4.40	0.15
3863-1425	Boschi et al., 2008	Atlantis Massif	2.80	0.15
3872-1136	Boschi et al., 2008	Atlantis Massif	4.50	0.15
3873-1124	Boschi et al., 2008	Atlantis Massif	2.00	0.15
3873-1344	Boschi et al., 2008	Atlantis Massif	3.20	0.15
3877-1158	Boschi et al., 2008	Atlantis Massif	3.30	0.15
3877-1344	Boschi et al., 2008	Atlantis Massif	4.30	0.15
3877-1406	Boschi et al., 2008	Atlantis Massif	2.70	0.15
3881-1132A	Boschi et al., 2008	Atlantis Massif	4.10	0.15
D3-18	Boschi et al., 2008	Atlantis Massif	3.00	0.15
D3-27	Boschi et al., 2008	Atlantis Massif	3.00	0.15
D3-34	Boschi et al., 2008	Atlantis Massif	3.50	0.15
D3-46	Boschi et al., 2008	Atlantis Massif	2.10	0.15
D3-6	Boschi et al., 2008	Atlantis Massif	4.10	0.15
D4-3m	Boschi et al., 2008	Atlantis Massif	3.80	0.15
D4-3s	Boschi et al., 2008	Atlantis Massif	2.00	0.15
D4-4	Boschi et al., 2008	Atlantis Massif	3.10	0.15
38492	Cocker et al., 1982	Macquarie	4.90	0.15
38498	Cocker et al., 1982	Macquarie	3.20	0.15

Table A7. continued

Sample	Reference	Locality	$\delta^{18}\text{O}$	$2\sigma$
ET 1/7	Früh-Green et al., 2001	Erro-Tobbio peridotite, Italian Alps	6.90	n.a.
ET 10/5	Früh-Green et al., 2001	Erro-Tobbio peridotite, Italian Alps	7.40	n.a.
ET 11/4	Früh-Green et al., 2001	Erro-Tobbio peridotite, Italian Alps	6.40	n.a.
ET 3/1	Früh-Green et al., 2001	Erro-Tobbio peridotite, Italian Alps	7.40	n.a.
ET 4/3	Früh-Green et al., 2001	Erro-Tobbio peridotite, Italian Alps	5.70	n.a.
ET9/4A	Früh-Green et al., 2001	Erro-Tobbio peridotite, Italian Alps	8.10	n.a.
ETA 10	Früh-Green et al., 2001	Erro-Tobbio peridotite, Italian Alps	6.40	n.a.
ETA 20	Früh-Green et al., 2001	Erro-Tobbio peridotite, Italian Alps	7.80	n.a.
ETA 42	Früh-Green et al., 2001	Erro-Tobbio peridotite, Italian Alps	4.20	n.a.
ETA 43	Früh-Green et al., 2001	Erro-Tobbio peridotite, Italian Alps	5.30	n.a.
ETA 44	Früh-Green et al., 2001	Erro-Tobbio peridotite, Italian Alps	6.20	n.a.
ETA 46	Früh-Green et al., 2001	Erro-Tobbio peridotite, Italian Alps	7.90	n.a.
ETA 50	Früh-Green et al., 2001	Erro-Tobbio peridotite, Italian Alps	6.50	n.a.
ETA 51	Früh-Green et al., 2001	Erro-Tobbio peridotite, Italian Alps	6.70	n.a.
ETA 9	Früh-Green et al., 2001	Erro-Tobbio peridotite, Italian Alps	6.50	n.a.
ETA 90	Früh-Green et al., 2001	Erro-Tobbio peridotite, Italian Alps	7.00	n.a.
ETF 1	Früh-Green et al., 2001	Erro-Tobbio peridotite, Italian Alps	5.80	n.a.
ETF 10	Früh-Green et al., 2001	Erro-Tobbio peridotite, Italian Alps	6.20	n.a.
ETF 11	Früh-Green et al., 2001	Erro-Tobbio peridotite, Italian Alps	3.80	n.a.
ETF 2	Früh-Green et al., 2001	Erro-Tobbio peridotite, Italian Alps	6.40	n.a.
ETF 3	Früh-Green et al., 2001	Erro-Tobbio peridotite, Italian Alps	6.70	n.a.
ETF 4	Früh-Green et al., 2001	Erro-Tobbio peridotite, Italian Alps	5.60	n.a.
ETF 5	Früh-Green et al., 2001	Erro-Tobbio peridotite, Italian Alps	6.40	n.a.
ETF 6	Früh-Green et al., 2001	Erro-Tobbio peridotite, Italian Alps	5.40	n.a.

Table A7. continued

Sample	Reference	Locality	$\delta^{18}\text{O}$	$2\sigma$
ETF 7	Früh-Green et al., 2001	Erro-Tobbio peridotite, Italian Alps	6.20	n.a.
ETF 8	Früh-Green et al., 2001	Erro-Tobbio peridotite, Italian Alps	6.10	n.a.
ETF 9	Früh-Green et al., 2001	Erro-Tobbio peridotite, Italian Alps	5.70	n.a.
CY-0B2	Vibetti et al., 1989	Troodos	-0.50	0.15
CY-B15	Vibetti et al., 1989	Troodos	1.20	0.15
CY-B17	Vibetti et al., 1989	Troodos	2.20	0.15
CY-WXO	Vibetti et al., 1989	Troodos	-0.90	0.15

Not available (n.a.).

## Appendix B – Supplementary material for Kankan inclusions

### Supplementary figures

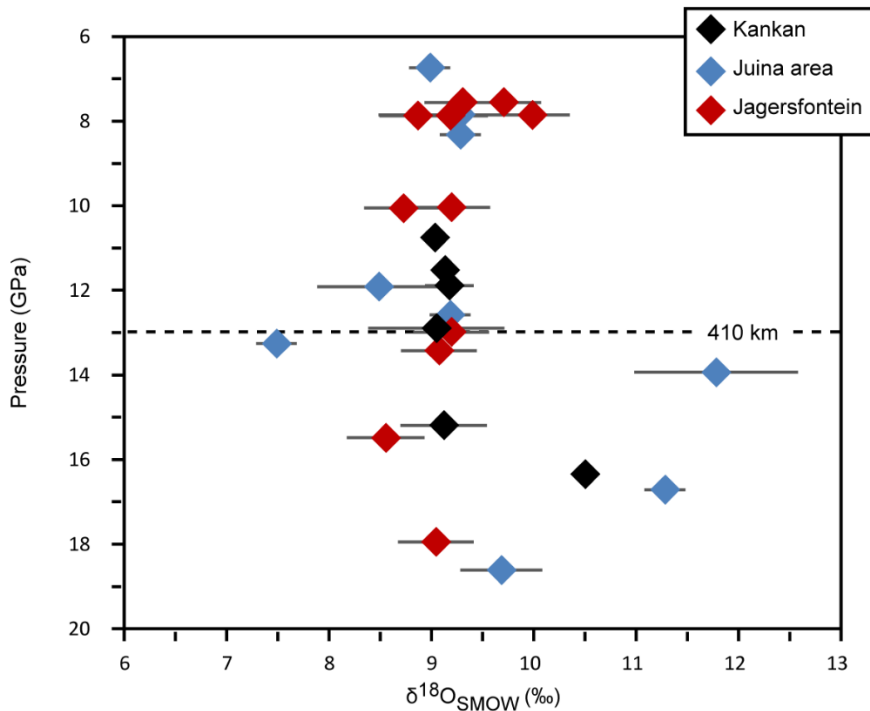


Figure B1. Oxygen isotopes for majoritic garnet inclusions versus depth. Majoritic inclusions include those from the Juina area (Brazil; Burnham et al. 2015), Jagersfontein (S. Africa; Ickert et al. 2015), and Kankan (Guinea). Pressure estimates calculated after Beyer and Frost (2017). Error bars are  $2\sigma$

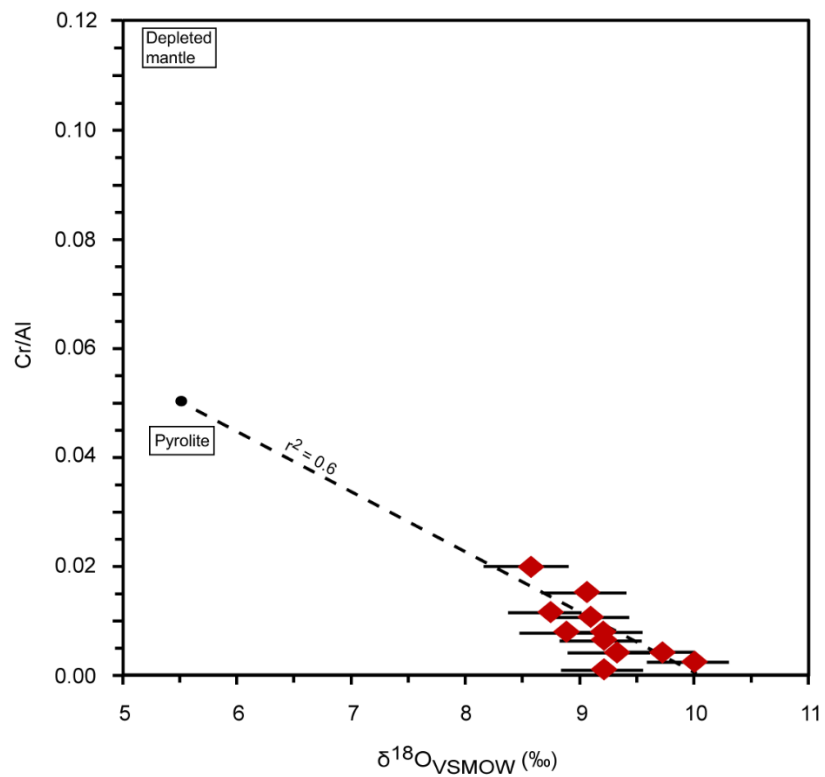


Figure B2. Oxygen isotopes versus Cr/Al of Jagersfontein majoritic garnets. A linear regression ( $r^2 = 0.6$ ) intersects a 5.5 ‰ mantle assimilate with a Cr/Al content of ~0.05, whereas primitive mantle has a Cr/Al of 0.04 (Ringwood 1975) and mildly depleted mantle has a Cr/Al of 0.10 (McDonough and Rudnick 1998). Error bars are  $2\sigma$ .

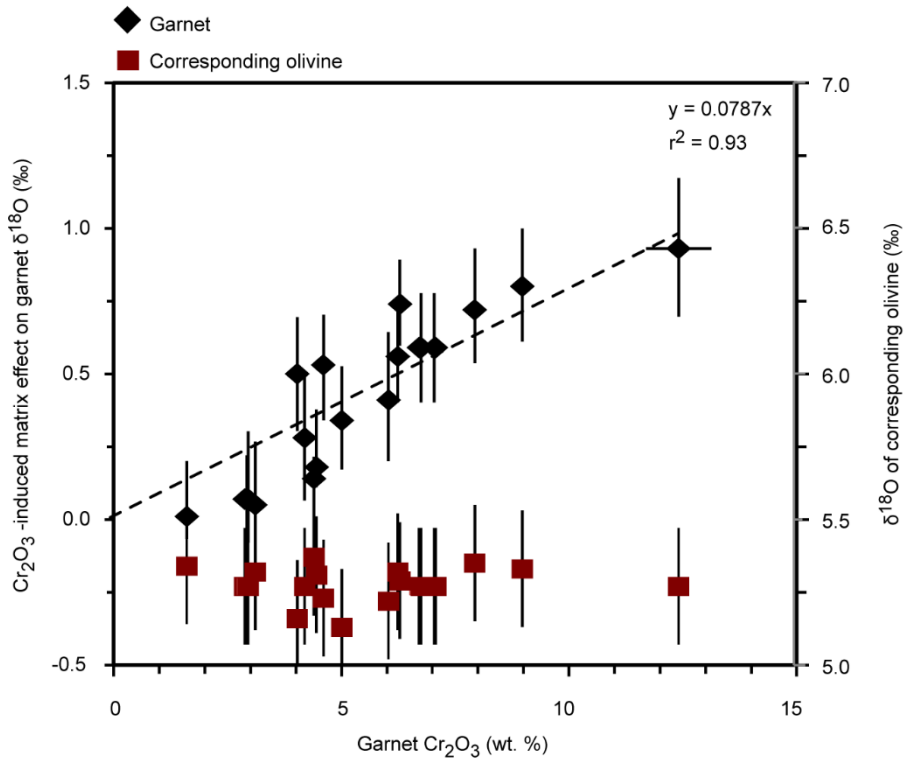


Figure B3. Ion probe δ<sup>18</sup>O calibration for Cr-rich garnets. Coexisting garnets and olivines from peridotitic mantle xenoliths were analyzed on the ion probe to determine the instrumental fractionation associated with Cr<sub>2</sub>O<sub>3</sub> content of garnets. The deviation of the measured garnet δ<sup>18</sup>O, after Ca# matrix-correction (Ickert and Stern 2013), from equilibrium with associated olivine is plotted, versus the Cr<sub>2</sub>O<sub>3</sub> contents of the garnets. As all the olivines have SIMS-measured δ<sup>18</sup>O within error of mantle, we assume isotopic equilibrium between garnet and olivine, and contend that the trend of SIMS-measured δ<sup>18</sup>O with Cr<sub>2</sub>O<sub>3</sub> content is a matrix effect. The trendline indicates the correction of the δ<sup>18</sup>O values to a hypothetical Cr-free garnet. Errors are 2σ.

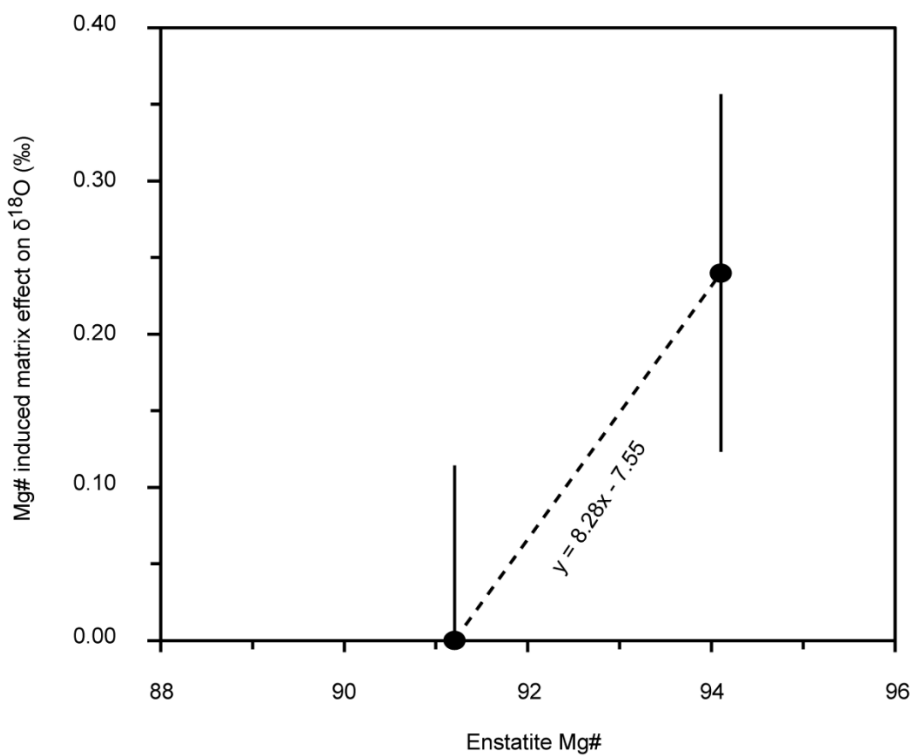


Figure B4. Ion probe  $\delta^{18}\text{O}$  calibration for enstatite Mg#. Instrumental mass fractionation with enstatite Mg# was assessed using reference material S0170 (Mg# of 91.2; laser fluorination  $\delta^{18}\text{O}$  of +5.64 ‰) and S0444 (Mg# of 94.1; laser fluorination  $\delta^{18}\text{O}$  of +5.76 (Lowry et al. 1999). Error bars incorporate 0.10 ‰ analytical uncertainty in laser fluorination measurements.

## Supplementary tables

Table B1. Mineral assemblages of analyzed Kankan diamonds. Abbreviations include lherzolitic (lherz), eclogitic (eclo), websteritic (web), majoritic (Maj), clinopyroxene (Cpx), garnet (Gt), olivine (Ol), walststromite (Wal), ferropericlase (FPer), and enstatite (Opx). Opx here are those that have low NiO and are interpreted as being lower mantle “former bridgemanite”. EPMA and  $\delta^{18}\text{O}$  are data produced during this study,  $\delta^{13}\text{C}$  is sourced from Stachel et al. (2002); Palot et al. (2014).

Sample	KK-26	KK-65	KK-86	KK-96	KK-78	KK-101	KK-97a	KK-97b
Type	Lherz Gt	Lherz Gt	Eclo Gt	Web Gt	Lherz Gt	Eclo Gt	Maj Gt*	Maj Gt*
Other inclusions	Ol	Cpx, Opx, Ol	n.a.	Cpx	Ol	n.a.	n.a.	n.a.
Formation (GPa/km)	<250 km	<250 km	<250 km	<250 km	<250 km	<250 km	12 GPa**	12 GPa**
$\delta^{13}\text{C}$ (‰)	-4.50	-2.21	-4.96	-5.37	-3.61	-5.78	-1.54	-1.54
$\delta^{13}\text{C}$ 2σ (‰)	0.05	0.05	0.05	0.05	0.05	0.05	0.05	0.05
$\delta^{18}\text{O}$ (‰)	5.72	5.34	3.83	5.29	5.33	6.09	9.05	9.15
$\delta^{18}\text{O}$ 2σ (‰)	0.24	0.22	0.07	0.20	0.29	0.21	0.08	0.10
$\text{SiO}_2$ (wt. %)	41.77	41.02	39.08	40.71	40.94	39.93	40.89	41.08
$\text{TiO}_2$ (wt. %)	0.28	bdl	0.74	0.50	bdl	0.40	1.66	1.60
$\text{Al}_2\text{O}_3$ (wt. %)	18.28	17.27	21.12	22.36	18.09	22.72	19.77	19.33
$\text{Cr}_2\text{O}_3$ (wt. %)	5.51	8.22	0.04	0.05	7.26	bdl	0.05	0.04
$\text{FeO}$ (wt. %)	7.09	6.06	21.17	15.33	6.43	13.00	12.68	12.34
$\text{MnO}$ (wt. %)	0.31	0.28	0.41	0.32	0.31	0.23	0.28	0.28
$\text{NiO}$ (wt. %)	bdl	bdl	bdl	bdl	bdl	bdl	bdl	bdl
$\text{MgO}$ (wt. %)	20.87	19.52	8.00	14.59	19.41	10.87	10.01	bdl
$\text{CaO}$ (wt. %)	5.13	6.86	9.43	5.54	6.47	12.18	14.49	14.58
$\text{Na}_2\text{O}$ (wt. %)	bdl	bdl	0.21	0.24	bdl	0.16	0.55	0.63
$\text{K}_2\text{O}$ (wt. %)	bdl	bdl	bdl	bdl	bdl	bdl	bdl	bdl
Total (wt. %)	99.24	99.23	100.20	99.64	98.91	99.51	100.39	99.88

Table B1. continued

<b>Sample</b>	<b>KK-61</b>	<b>KK-81</b>	<b>KK-1</b>	<b>KK-5</b>	<b>KK-044c</b>	<b>KK-103</b>
<b>Type</b>	Maj Gt *	Maj Gt *	Maj Gt *	Maj Gt *	Opx	Opx
<b>Other inclusions</b>	n.a.	Cpx	Opx	n.a.	FPer, Wal, Ol	FPer
<b>Formation (GPa/km)</b>	12 GPa**	15 GPa**	13 GPa**	16 GPa**	>660 km	>660 km
<b><math>\delta^{13}\text{C}</math> (‰)</b>	-0.35	-3.13	0.89	-0.91	-4.10	-3.88
<b><math>\delta^{13}\text{C}</math> 2σ (‰)</b>	0.05	0.05	0.05	0.05	0.05	0.05
<b><math>\delta^{18}\text{O}</math> (‰)</b>	9.19	9.14	9.06	10.52	5.78	5.33
<b><math>\delta^{18}\text{O}</math> 2σ (‰)</b>	0.24	0.42	0.67	0.07	0.20	0.17
<b>SiO<sub>2</sub> (wt. %)</b>	42.92	43.78	42.43	43.68	56.83	56.44
<b>TiO<sub>2</sub> (wt. %)</b>	1.37	1.22	1.48	0.07	0.06	0.05
<b>Al<sub>2</sub>O<sub>3</sub> (wt. %)</b>	17.89	17.27	17.19	20.56	1.09	1.18
<b>Cr<sub>2</sub>O<sub>3</sub> (wt. %)</b>	0.14	0.08	0.04	0.06	0.36	0.37
<b>FeO (wt. %)</b>	12.77	11.08	12.78	12.22	3.48	3.67
<b>MnO (wt. %)</b>	0.38	0.27	0.25	0.36	0.11	0.11
<b>NiO (wt. %)</b>	bdl	0.02	bdl	0.02	bdl	0.03
<b>MgO (wt. %)</b>	16.89	15.08	10.92	16.24	37.27	37.07
<b>CaO (wt. %)</b>	6.48	9.15	14.67	4.60	0.06	0.06
<b>Na<sub>2</sub>O (wt. %)</b>	0.48	1.02	0.69	1.26	bdl	bdl
<b>K<sub>2</sub>O (wt. %)</b>	bdl	bdl	bdl	bdl	0.01	bdl
<b>Total (wt. %)</b>	99.32	98.97	100.46	99.07	99.28	98.98

Table B1. continued

<b>Sample</b>	<b>KK-045</b>	<b>KK-044e</b>	<b>KK-203</b>
<b>Type</b>	Opx	Opx	Opx
<b>Other inclusions</b>	Sanidine	FPer, Wal, Ol	FPer, Ol, Cpx
<b>Formation (GPa/km)</b>	>660 km	>660 km	>660 km
<b><math>\delta^{13}\text{C}</math> (‰)</b>	-3.50	-4.10	-3.86
<b><math>\delta^{13}\text{C}</math> 2σ (‰)</b>	0.05	0.05	0.79
<b><math>\delta^{18}\text{O}</math> (‰)</b>	5.53	5.63	5.29
<b><math>\delta^{18}\text{O}</math> 2σ (‰)</b>	0.12	0.19	0.17
<b>SiO<sub>2</sub> (wt. %)</b>	56.81	56.71	57.94
<b>TiO<sub>2</sub> (wt. %)</b>	bdl	0.06	bdl
<b>Al<sub>2</sub>O<sub>3</sub> (wt. %)</b>	0.96	1.10	0.36
<b>Cr<sub>2</sub>O<sub>3</sub> (wt. %)</b>	0.29	0.36	0.38
<b>FeO (wt. %)</b>	3.36	3.47	2.70
<b>MnO (wt. %)</b>	0.12	0.11	0.10
<b>NiO (wt. %)</b>	bdl	bdl	bdl
<b>MgO (wt. %)</b>	37.11	37.10	37.99
<b>CaO (wt. %)</b>	0.03	0.05	0.08
<b>Na<sub>2</sub>O (wt. %)</b>	0.04	bdl	bdl
<b>K<sub>2</sub>O (wt. %)</b>	bdl	bdl	bdl
<b>Total (wt. %)</b>	98.72	98.96	99.55

\*Majoritic garnet defined here as  $\geq$  to 3.04 Si (pfu). \*\*Depth of formation for majorites calculated using Beyer and Frost (2017) (Beyer and Frost 2017). n.a. indicates not applicable, and bdl indicates values below the detection limit (0.018% SiO<sub>2</sub>, 0.020% TiO<sub>2</sub>, 0.019% Al<sub>2</sub>O<sub>3</sub>, 0.022% Cr<sub>2</sub>O<sub>3</sub>, 0.014% FeO, 0.016% NiO, 0.014% MnO, 0.011% MgO, 0.006% CaO, 0.026% Na<sub>2</sub>O, 0.006% K<sub>2</sub>O).

Table B2. The Mg# of bridgmanite and ferropericlase for experiments and natural inclusions in diamond. The Mg# of Kankan bridgmanite and ferropericlase fall between those produced in Fo91 and Fo89 experiments (Katsura and Ito 1996), and overlap mineralogical Mg# estimates (91-93 and 84-87 for bridgmanite and ferropericlase, respectively) for pyrolite with a Mg# of 90 (Wood 2000). This suggests the lower mantle Kankan inclusions are derived from a lithology similar to that of pyrolite with a Mg# of ~90 (Ringwood 1975).

	Fo91 starting material (Katsura and Ito 1996)	Fo89 starting material (Katsura and Ito 1996)	Kankan Mg# average	Kankan Mg# $2\sigma$
Bridgmanite	95.5	94.7	95.0	2.5
Ferropericlase	87.0	86.3	86.7	1.4

Table B3. Standards utilized for EPMA analyses. Secondary standards included the Gore garnet from New York, Fo90 from San Carlos, and enstatite H131709 from the Harvard collection.

Element	Analyzing crystals	Standard
Si $k\alpha$	LTAP	Fo90.5 olivine from Harvard
Ti $k\alpha$	PET	$\text{TiO}_2$ rutile from MTI
Al $k\alpha$	TAP	Frank Smith pyrope garnet
Cr $k\alpha$	PET	$\text{Cr}_2\text{O}_3$ chromium oxide from Alfa Aesar
Fe $k\alpha$	LLIF	$\text{Fe}_2\text{SiO}_4$ fayalite from Rockport, MA
Ni $k\alpha$	LLIF	Ni nickel from Alfa Aesar
Mn $k\alpha$	LLIF	$(\text{Mn},\text{Fe})_3\text{Al}_2\text{Si}_3\text{O}_{12}$ spessartine from Navegadora Mine, Brazil
Mg $k\alpha$	LTAP	Fo90.5 olivine from Harvard
Ca $k\alpha$	LPET	Plagioclase (labradorite) from Oregon, USNM 115900
Na $k\alpha$	TAP	$\text{NaAlSi}_3\text{O}_8$ albite from Virginia, Harvard 131705
K $k\alpha$	LPET	$\text{KAlSi}_3\text{O}_8$ sanidine from Itrongay, Madagascar

Table B4. Source data for eclogitic garnet inclusion Mg#. Compiled by TS.

Sample	Mg#	Reference			
U33/1-D3	50.0	Anand et al., 2004	APP-F92C	62.3	Appleyard et al., 2004
APP-F12A	59.5	Appleyard et al., 2004	APP-F96A	36.3	Appleyard et al., 2004
APP-F23A	39.0	Appleyard et al., 2004	APP-F96B	36.4	Appleyard et al., 2004
APP-F23B	39.4	Appleyard et al., 2004	APP-F9A	46.0	Appleyard et al., 2004
APP-F27A	40.5	Appleyard et al., 2004	v133	74.0	Aulbach, 1999
APP-F29A	42.4	Appleyard et al., 2004	v156b+c	72.1	Aulbach, 1999
APP-F29B	42.4	Appleyard et al., 2004	v157a	57.8	Aulbach, 1999
APP-F29C	42.5	Appleyard et al., 2004	v158a	58.8	Aulbach, 1999
APP-F33B	39.0	Appleyard et al., 2004	v160b	62.8	Aulbach, 1999
APP-F33C	37.9	Appleyard et al., 2004	v176a	63.4	Aulbach, 1999
APP-F37A	42.9	Appleyard et al., 2004	v176b	63.7	Aulbach, 1999
APP-F37B	43.2	Appleyard et al., 2004	v176c	60.2	Aulbach, 1999
APP-F46A	48.3	Appleyard et al., 2004	v178ab	52.4	Aulbach, 1999
APP-F53A	43.8	Appleyard et al., 2004	v180a	55.2	Aulbach, 1999
APP-F59B	40.8	Appleyard et al., 2004	v180b	55.5	Aulbach, 1999
APP-F59C	41.1	Appleyard et al., 2004	v180c	55.3	Aulbach, 1999
APP-F5A	39.9	Appleyard et al., 2004	v181b	62.1	Aulbach, 1999
APP-F5B	40.7	Appleyard et al., 2004	v53a	62.4	Aulbach, 1999
APP-F5C	40.4	Appleyard et al., 2004	v53b	63.6	Aulbach, 1999
APP-F71B	34.3	Appleyard et al., 2004	v53e	63.3	Aulbach, 1999
APP-F77A	48.7	Appleyard et al., 2004	v55	54.7	Aulbach, 1999
APP-F77B	49.4	Appleyard et al., 2004	v56+56b	63.6	Aulbach, 1999
APP-F90A	34.5	Appleyard et al., 2004	v61	54.2	Aulbach, 1999
			A115-1	49.5	Banas, 2006
			A115-2	48.9	Banas, 2006
			A128	46.7	Banas, 2006

Table B4. continued

Sample	Mg#	Reference			
1168-4	50.4	Bulanova, 1995	00007	48.6	Davies et al., 2004
1168-7	56.1	Bulanova, 1995	000129	57.4	Davies et al., 2004
d5	65.3	Daniels & Gurney, 1989	000155	48.4	Davies et al., 2004
d6	57.8	Daniels & Gurney, 1989	000175	43.8	Davies et al., 2004
d7	45.8	Daniels & Gurney, 1989	000177	48.4	Davies et al., 2004
d8	46.3	Daniels & Gurney, 1989	000177	49.6	Davies et al., 2004
D1334A	70.9	Daniels and Gurney, 1999	000199	55.6	Davies et al., 2004
D1336C	47.1	Daniels and Gurney, 1999	000200	55.4	Davies et al., 2004
D1336D	49.1	Daniels and Gurney, 1999	00042	48.1	Davies et al., 2004
D1351B	53.1	Daniels and Gurney, 1999	00052	41.9	Davies et al., 2004
D1367A	81.5	Daniels and Gurney, 1999	00052	38.6	Davies et al., 2004
DD103C	52.8	Daniels and Gurney, 1999	Ash-102A	53.9	Davies et al., 2004b
DD136-1	46.3	Daniels and Gurney, 1999	Ash-108A	56.7	Davies et al., 2004b
DD143A	65.5	Daniels and Gurney, 1999	Ash-111C	44.1	Davies et al., 2004b
DK12-2	49.1	Daniels and Gurney, 1999	058 (2)	63.7	De Stefano et al., 2009
97 22I	47.7	Davies et al., 1998	076G (1)	56.1	De Stefano et al., 2009
97 23A(1)	60.4	Davies et al., 1998	076G (2)	56.0	De Stefano et al., 2009
97 23A(2)	59.6	Davies et al., 1998	076G (3)	56.3	De Stefano et al., 2009
97 23J	49.5	Davies et al., 1998	171G (1)	53.1	De Stefano et al., 2009
97 29	52.7	Davies et al., 1998	280X (1)	57.1	De Stefano et al., 2009
98 28	53.0	Davies et al., 1998	284X (2)	72.9	De Stefano et al., 2009
98 28	47.0	Davies et al., 1998	284X (3)	72.3	De Stefano et al., 2009
98 29	55.4	Davies et al., 1998	284X (4)	72.7	De Stefano et al., 2009
98 33	51.4	Davies et al., 1998	284X (5)	72.7	De Stefano et al., 2009
			284X (6)	73.4	De Stefano et al., 2009
			284X (7)	73.3	De Stefano et al., 2009

Table B4. continued

Sample	Mg#	Reference			
298R (1)	69.7	De Stefano et al., 2009	lk 26a	57.0	Deines and Harris, 2004
298R (5)	59.5	De Stefano et al., 2009	lk 45a	60.7	Deines and Harris, 2004
302Q (1)	58.0	De Stefano et al., 2009	lk 46a	74.1	Deines and Harris, 2004
302Q (2)	57.8	De Stefano et al., 2009	lk 47a	53.5	Deines and Harris, 2004
302Q (4)	58.5	De Stefano et al., 2009	lk 47b	53.1	Deines and Harris, 2004
344X (1)	76.1	De Stefano et al., 2009	lk 48a	56.4	Deines and Harris, 2004
344X (2)	75.9	De Stefano et al., 2009	lk 48b	56.1	Deines and Harris, 2004
344X (3)	76.1	De Stefano et al., 2009	lk 49b	50.0	Deines and Harris, 2004
344X (4)	77.0	De Stefano et al., 2009	lk 50a	52.3	Deines and Harris, 2004
344X (5)	75.0	De Stefano et al., 2009	lk 50c	53.2	Deines and Harris, 2004
344X (6)	76.3	De Stefano et al., 2009	lk 51a	55.5	Deines and Harris, 2004
363R (1)	73.1	De Stefano et al., 2009	lk 51b	52.8	Deines and Harris, 2004
377X (1)	57.6	De Stefano et al., 2009	lk 47b	53.1	Deines and Harris, 2004
377X (2)	58.4	De Stefano et al., 2009	lk 52a	65.1	Deines and Harris, 2004
377X (3)	57.8	De Stefano et al., 2009	lk 53a	65.0	Deines and Harris, 2004
384R (1)	71.4	De Stefano et al., 2009	lk 54a	59.0	Deines and Harris, 2004
384R	72.0	De Stefano et al., 2009	lk 55a	52.6	Deines and Harris, 2004
393G	57.4	De Stefano et al., 2009	lk 56a	57.7	Deines and Harris, 2004
395G	61.2	De Stefano et al., 2009	lk 56b	57.8	Deines and Harris, 2004
401P(I)	76.4	De Stefano et al., 2009	lk 57a	52.5	Deines and Harris, 2004
405X	58.8	De Stefano et al., 2009	lk 63a	59.9	Deines and Harris, 2004
611 (1)	57.3	De Stefano et al., 2009	lk 63b	59.9	Deines and Harris, 2004
611 (2)	75.8	De Stefano et al., 2009	lk 64a	49.9	Deines and Harris, 2004
611 (3)	57.3	De Stefano et al., 2009	lk 65a	48.6	Deines and Harris, 2004
			lk 69a	53.2	Deines and Harris, 2004
			lk 70a	49.9	Deines and Harris, 2004

Table B4. continued

Sample	Mg#	Reference			
lk 70b	50.6	Deines and Harris, 2004	a005	53.0	GSC, Open File 2124
lk 71a	50.4	Deines and Harris, 2004	a008c	67.7	GSC, Open File 2124
lk 73b	59.3	Deines and Harris, 2004	a008r	66.8	GSC, Open File 2124
lk 75a	65.8	Deines and Harris, 2004	a009	47.7	GSC, Open File 2124
lk 76a	66.3	Deines and Harris, 2004	a010c	65.9	GSC, Open File 2124
lk 77a	43.9	Deines and Harris, 2004	a010r	66.0	GSC, Open File 2124
lk 78a	48.8	Deines and Harris, 2004	a014	52.5	GSC, Open File 2124
lk 78b	46.9	Deines and Harris, 2004	a015	45.1	GSC, Open File 2124
lk 78e	48.7	Deines and Harris, 2004	a017a	69.5	GSC, Open File 2124
lk 79a	52.8	Deines and Harris, 2004	a017b	63.2	GSC, Open File 2124
ddmi-166a	68.6	Donnelly, 2006	a018	37.9	GSC, Open File 2124
ddmi-166b	69.4	Donnelly, 2006	a019	41.1	GSC, Open File 2124
ddmi-166c	69.6	Donnelly, 2006	a022	54.7	GSC, Open File 2124
ddmi-205a	63.6	Donnelly, 2006	a023	70.1	GSC, Open File 2124
ddmi-205b	63.2	Donnelly, 2006	a025	57.2	GSC, Open File 2124
ddmi-208b	69.3	Donnelly, 2006	a027	36.5	GSC, Open File 2124
ddmi-208c	69.5	Donnelly, 2006	a028	38.5	GSC, Open File 2124
100L-105	44.8	GSC, Open File 2124	a029a	40.2	GSC, Open File 2124
100L-106	50.5	GSC, Open File 2124	a032a	48.4	GSC, Open File 2124
100L-154	43.5	GSC, Open File 2124	a032b	50.5	GSC, Open File 2124
100L-19	44.8	GSC, Open File 2124	a034	60.5	GSC, Open File 2124
100L-6	50.5	GSC, Open File 2124	a036r	42.6	GSC, Open File 2124
a001	58.5	GSC, Open File 2124	a038c	55.3	GSC, Open File 2124
004	45.0	GSC, Open File 2124	a038r	55.7	GSC, Open File 2124
			a039c	73.0	GSC, Open File 2124
			a039r	72.6	GSC, Open File 2124

Table B4. continued

Sample	Mg#	Reference			
a041	44.7	GSC, Open File 2124	a058r	52.3	GSC, Open File 2124
a042c	60.2	GSC, Open File 2124	a059c	49.8	GSC, Open File 2124
a042r	61.1	GSC, Open File 2124	a059r	50.4	GSC, Open File 2124
a043	54.3	GSC, Open File 2124	a061	69.9	GSC, Open File 2124
a044c	46.7	GSC, Open File 2124	a062c	49.7	GSC, Open File 2124
a044r	47.4	GSC, Open File 2124	a062r	50.7	GSC, Open File 2124
a045c	56.8	GSC, Open File 2124	a063	43.7	GSC, Open File 2124
a045r	59.7	GSC, Open File 2124	a064	52.7	GSC, Open File 2124
a046c	59.0	GSC, Open File 2124	a065	61.0	GSC, Open File 2124
a046r	59.7	GSC, Open File 2124	a066	51.5	GSC, Open File 2124
a047r	61.3	GSC, Open File 2124	a069c	44.1	GSC, Open File 2124
a049c	48.5	GSC, Open File 2124	a069r	43.4	GSC, Open File 2124
a049r	49.3	GSC, Open File 2124	a070c	50.2	GSC, Open File 2124
a050c	54.2	GSC, Open File 2124	a070r	50.3	GSC, Open File 2124
a050r	53.6	GSC, Open File 2124	a074c	54.9	GSC, Open File 2124
a051c	62.2	GSC, Open File 2124	a074r	55.9	GSC, Open File 2124
a051r	62.2	GSC, Open File 2124	a075c	39.5	GSC, Open File 2124
a053	47.8	GSC, Open File 2124	a075r	41.8	GSC, Open File 2124
a054c	46.1	GSC, Open File 2124	a077c	53.5	GSC, Open File 2124
a054r	46.0	GSC, Open File 2124	a077r	53.5	GSC, Open File 2124
a055	45.2	GSC, Open File 2124	a078	33.7	GSC, Open File 2124
a057c	52.6	GSC, Open File 2124	a079	43.1	GSC, Open File 2124
a057r	52.9	GSC, Open File 2124	a080	40.8	GSC, Open File 2124
a058c	51.8	GSC, Open File 2124	a081	45.5	GSC, Open File 2124
			a083c	51.3	GSC, Open File 2124
			a083r	50.8	GSC, Open File 2124

Table B4. continued

Sample	Mg#	Reference			
a084c	52.2	GSC, Open File 2124	a128	61.5	GSC, Open File 2124
a084r	53.2	GSC, Open File 2124	a132	49.5	GSC, Open File 2124
a086	46.5	GSC, Open File 2124	a133	38.5	GSC, Open File 2124
a087	60.2	GSC, Open File 2124	a134	41.5	GSC, Open File 2124
a088	60.2	GSC, Open File 2124	a135	62.4	GSC, Open File 2124
a089	51.5	GSC, Open File 2124	a140	70.6	GSC, Open File 2124
a101	68.4	GSC, Open File 2124	a141	53.5	GSC, Open File 2124
a105	60.6	GSC, Open File 2124	a142	58.6	GSC, Open File 2124
a106	59.1	GSC, Open File 2124	a144	67.3	GSC, Open File 2124
a107	42.9	GSC, Open File 2124	a145	38.6	GSC, Open File 2124
a108	47.8	GSC, Open File 2124	ST-29	63.0	GSC, Open File 2124
a109	68.4	GSC, Open File 2124	ST-29	61.0	GSC, Open File 2124
a110	55.9	GSC, Open File 2124	BR 2286L	59.3	GSC, Open File 2124
a111	71.4	GSC, Open File 2124	PC1	46.6	GSC, Open File 2124
a113	72.6	GSC, Open File 2124	GC001B	63.1	Chinn, 1995
a114	70.5	GSC, Open File 2124	GC002B	48.3	Chinn, 1995
a118	66.0	GSC, Open File 2124	GC004B	47.2	Chinn, 1995
a119	47.2	GSC, Open File 2124	GC007F	46.1	Chinn, 1995
a120	45.9	GSC, Open File 2124	GC009C	40.4	Chinn, 1995
a121	52.2	GSC, Open File 2124	GC009E	43.4	Chinn, 1995
a122	61.2	GSC, Open File 2124	GC012D	42.6	Chinn, 1995
a125	54.4	GSC, Open File 2124	GC014G	58.3	Chinn, 1995
a126	43.3	GSC, Open File 2124	GC014K	56.6	Chinn, 1995
a127	62.4	GSC, Open File 2124	GC020B	49.2	Chinn, 1995
			GC034C	44.2	Chinn, 1995
			GC034E	49.9	Chinn, 1995

Table B4. continued

Sample	Mg#	Reference				
GC035A	45.6	Chinn, 1995	a031	56.9	Jaques et al., 1989	
GC040A	44.2	Chinn, 1995	a031	58.8	Jaques et al., 1989	
GC041D	44.6	Chinn, 1995	a033	46.6	Jaques et al., 1989	
GC053A	71.1	Chinn, 1995	a036c	42.7	Jaques et al., 1989	
GC055C	43.8	Chinn, 1995	a047c	61.4	Jaques et al., 1989	
GC084B	42.1	Chinn, 1995	a052c	49.9	Jaques et al., 1989	
GC094A	55.6	Chinn, 1995	a052r	51.0	Jaques et al., 1989	
GC097A	42.0	Chinn, 1995	a068	51.6	Jaques et al., 1989	
GC132A	46.9	Chinn, 1995	a116	34.9	Jaques et al., 1989	
GC166A	56.7	Chinn, 1995	a130	66.1	Jaques et al., 1989	
GC309A	55.0	Chinn, 1995	a136	53.4	Jaques et al., 1989	
GC443B	54.1	Chinn, 1995	Guan-014	52.2	Kaminsky et al., 2000	
GC538A	60.4	Chinn, 1995	Guan-024	47.5	Kaminsky et al., 2000	
GC551A	59.1	Chinn, 1995	Guan-037a	47.3	Kaminsky et al., 2000	
GC564A	59.9	Chinn, 1995	Guan-043	51.0	Kaminsky et al., 2000	
GC600A	45.2	Chinn, 1995	Guan-051a	53.2	Kaminsky et al., 2000	
GC717C	40.1	Chinn, 1995	Guan-051b	49.1	Kaminsky et al., 2000	
e4/13	62.9	Jaques et al., 1989	Guan-052	52.6	Kaminsky et al., 2000	
e4/17	52.4	Jaques et al., 1989	Guan-053	48.5	Kaminsky et al., 2000	
e4/6	49.0	Jaques et al., 1989	Guan-012	50.6	Kaminsky et al., 2000	
e4/7	67.2	Jaques et al., 1989	Guan-004	51.4	Kaminsky et al., 2000	
a016	59.2	Jaques et al., 1989	Guan-006a	60.5	Kaminsky et al., 2000	
a029b	41.3	Jaques et al., 1989	Guan-1448	52.7	Kaminsky et al., 2000	
a030	35.7	Jaques et al., 1989	Guan-1504	55.7	Kaminsky et al., 2000	
			Guan-1810	53.8	Kaminsky et al., 2000	
			Guan-1877	50.8	Kaminsky et al., 2000	

Table B4. continued

Sample	Mg#	Reference			
Guan-1991	52.2	Kaminsky et al., 2000	U36B	58.6	Laiginhas, 2008
Guan-2138	48.8	Kaminsky et al., 2000	U36C	58.7	Laiginhas, 2008
Guan-2212	48.5	Kaminsky et al., 2000	U38A	60.1	Laiginhas, 2008
Guan-2214	55.0	Kaminsky et al., 2000	U38B	59.3	Laiginhas, 2008
Guan-2220	57.1	Kaminsky et al., 2000	U42A	50.5	Laiginhas, 2008
Guan-V-14	50.7	Kaminsky et al., 2000	U43A	49.7	Laiginhas, 2008
Guan-V-16	51.3	Kaminsky et al., 2000	U43B	49.3	Laiginhas, 2008
Guan-V-18	48.3	Kaminsky et al., 2000	U44A	46.6	Laiginhas, 2008
Guan-V-18	54.0	Kaminsky et al., 2000	U44B	46.6	Laiginhas, 2008
Guan-V-19	52.7	Kaminsky et al., 2000	U46A	54.1	Laiginhas, 2008
Guan-V-24	46.7	Kaminsky et al., 2000	U47A	71.7	Laiginhas, 2008
Guan-V-25	41.9	Kaminsky et al., 2000	U47B	73.2	Laiginhas, 2008
Guan-V-26	51.8	Kaminsky et al., 2000	U48A	56.8	Laiginhas, 2008
Guan-V-26	51.3	Kaminsky et al., 2000	U48B	54.5	Laiginhas, 2008
Guan-V-27	46.2	Kaminsky et al., 2000	U48C	50.5	Laiginhas, 2008
Guan-V-30	61.4	Kaminsky et al., 2000	U49A	60.8	Laiginhas, 2008
Guan-V-32	61.0	Kaminsky et al., 2000	U50A	67.9	Laiginhas, 2008
Guan-V-6	61.7	Kaminsky et al., 2000	U51A	61.0	Laiginhas, 2008
Guan-V-7	59.9	Kaminsky et al., 2000	U51B	59.0	Laiginhas, 2008
Guan-V-9	50.7	Kaminsky et al., 2000	U51C	59.4	Laiginhas, 2008
U34A	52.5	Laiginhas, 2008	U52A	47.9	Laiginhas, 2008
U35C	55.9	Laiginhas, 2008	U52B	47.2	Laiginhas, 2008
U35D	56.3	Laiginhas, 2008	U52C	48.3	Laiginhas, 2008
U36A	58.5	Laiginhas, 2008	U52D	48.2	Laiginhas, 2008

Table B4. continued

Sample	Mg#	Reference			
U52E	48.2	Laiginhas, 2008	U62B	54.6	Laiginhas, 2008
U53A	51.7	Laiginhas, 2008	U68A	56.2	Laiginhas, 2008
U53B	52.5	Laiginhas, 2008	U71A	47.7	Laiginhas, 2008
U53C	51.7	Laiginhas, 2008	U73A	58.2	Laiginhas, 2008
U54F	47.9	Laiginhas, 2008	U74B	49.6	Laiginhas, 2008
U54G	47.7	Laiginhas, 2008	U75D	54.7	Laiginhas, 2008
U54H	47.9	Laiginhas, 2008	U76B	43.4	Laiginhas, 2008
U55A	49.1	Laiginhas, 2008	U77B	49.8	Laiginhas, 2008
U56E	48.8	Laiginhas, 2008	U79A	53.8	Laiginhas, 2008
U56F	48.4	Laiginhas, 2008	U80A	52.1	Laiginhas, 2008
U57A	52.7	Laiginhas, 2008	U81B	46.3	Laiginhas, 2008
U57B	48.7	Laiginhas, 2008	U82C	45.8	Laiginhas, 2008
U58A	55.7	Laiginhas, 2008	U83A	53.2	Laiginhas, 2008
U58B	55.7	Laiginhas, 2008	U84A	49.5	Laiginhas, 2008
U58C	55.2	Laiginhas, 2008	U85A	44.4	Laiginhas, 2008
U58D	54.3	Laiginhas, 2008	U86C	48.5	Laiginhas, 2008
U58E	54.7	Laiginhas, 2008	Nam-11	60.9	Leost et al., 2003
U58F	55.8	Laiginhas, 2008	Nam-114	50.7	Leost et al., 2003
U59B	60.9	Laiginhas, 2008	Nam-13	46.4	Leost et al., 2003
U59C	61.0	Laiginhas, 2008	Nam-14	57.8	Leost et al., 2003
U59D	61.6	Laiginhas, 2008	Nam-19	48.8	Leost et al., 2003
U60A	57.1	Laiginhas, 2008	Nam-20	47.9	Leost et al., 2003
U61A	49.0	Laiginhas, 2008	Nam-202b	9.0	Leost et al., 2003
U62A	55.6	Laiginhas, 2008	Nam-203b	48.3	Leost et al., 2003
			Nam-218a	63.0	Leost et al., 2003
			Nam-21a	54.9	Leost et al., 2003

Table B4. continued

Sample	Mg#	Reference			
Nam-22b	48.7	Leost et al., 2003	Nam-98b	61.6	Leost et al., 2003
Nam-26	60.1	Leost et al., 2003	HM006a	48.8	Mc Kenna et al., 2004
Nam-34b	49.2	Leost et al., 2003	HM006b	50.2	Mc Kenna et al., 2004
Nam-35	36.3	Leost et al., 2003	HM006c	49.8	Mc Kenna et al., 2004
Nam-38b	56.4	Leost et al., 2003	HM1B2a	55.0	Mc Kenna et al., 2004
Nam-41	47.8	Leost et al., 2003	llt 02a	62.5	McDade and Harris, 1999
Nam-42	67.0	Leost et al., 2003	llt 11b	64.0	McDade and Harris, 1999
Nam-44	57.2	Leost et al., 2003	a4-05	79.9	Moore and Gurney, 1989
Nam-47	65.2	Leost et al., 2003	a6-01	59.7	Moore and Gurney, 1989
Nam-5	54.1	Leost et al., 2003	A1-18	67.9	Moore et al., 1991
Nam-56	46.0	Leost et al., 2003	A5-03	76.6	Moore et al., 1991
Nam-59	42.1	Leost et al., 2003	A6-01	59.7	Moore et al., 1991
Nam-63	56.1	Leost et al., 2003	40188	55.8	Otter, M. L., 1989
Nam-68	44.9	Leost et al., 2003	40193	66.2	Otter, M. L., 1989
Nam-74a	50.2	Leost et al., 2003	a22	43.5	Otter, M. L., 1989
Nam-79	58.5	Leost et al., 2003	a37	44.3	Otter, M. L., 1989
Nam-80	54.3	Leost et al., 2003	a46	44.4	Otter, M. L., 1989
Nam-80B	75.5	Leost et al., 2003	a46	41.1	Otter, M. L., 1989
Nam-81	54.9	Leost et al., 2003	a73	65.0	Otter, M. L., 1989
Nam-86b	56.2	Leost et al., 2003	28	71.7	Phillips et al., 2004
Nam-89b	65.6	Leost et al., 2003	106	39.2	Phillips et al., 2004
Nam-95	50.6	Leost et al., 2003	245	50.5	Phillips et al., 2004
Nam-96	66.5	Leost et al., 2003	333	64.3	Phillips et al., 2004
Nam-97	49.5	Leost et al., 2003	341	55.2	Phillips et al., 2004
			341	54.8	Phillips et al., 2004

Table B4. continued

Sample	Mg#	Reference			
342	48.5	Phillips et al., 2004	541	53.1	Phillips et al., 2004
342	47.7	Phillips et al., 2004	541	52.6	Phillips et al., 2004
343	48.8	Phillips et al., 2004	542	61.0	Phillips et al., 2004
344	57.1	Phillips et al., 2004	542	60.9	Phillips et al., 2004
346	47.6	Phillips et al., 2004	543	51.5	Phillips et al., 2004
348	56.4	Phillips et al., 2004	544	71.6	Phillips et al., 2004
349	55.1	Phillips et al., 2004	545	61.5	Phillips et al., 2004
351	59.0	Phillips et al., 2004	546	38.7	Phillips et al., 2004
355	59.0	Phillips et al., 2004	546	38.9	Phillips et al., 2004
361	41.6	Phillips et al., 2004	547	56.5	Phillips et al., 2004
379	55.0	Phillips et al., 2004	348-1b	56.4	Phillips et al., 2004
414	49.1	Phillips et al., 2004	379-1b	55.0	Phillips et al., 2004
414	48.4	Phillips et al., 2004	J011	52.5	Richardson et al., 1998
415	58.8	Phillips et al., 2004	J012	62.1	Richardson et al., 1998
444	49.2	Phillips et al., 2004	J033	44.1	Richardson et al., 1998
468	61.3	Phillips et al., 2004	J053	51.9	Richardson et al., 1998
513	62.4	Phillips et al., 2004	J068	44.6	Richardson et al., 1998
513	62.6	Phillips et al., 2004	J076	62.4	Richardson et al., 1998
538	49.5	Phillips et al., 2004	22A	43.9	Richardson et al., 2004
538	49.6	Phillips et al., 2004	KLD-4(-1)	55.1	Schulze et al., 2008
539	60.5	Phillips et al., 2004	KLD-4(-2)	55.6	Schulze et al., 2008
540	58.1	Phillips et al., 2004	KLD-5	72.3	Schulze et al., 2008
540	58.2	Phillips et al., 2004	9-1	51.1	Shatsky et al., 2015
541	52.5	Phillips et al., 2004	1-8	45.2	Shatsky et al., 2015
			1-9	47.2	Shatsky et al., 2015
			9-3_1	44.3	Shatsky et al., 2015

Table B4. continued

Sample	Mg#	Reference			
9-3_2	44.6	Shatsky et al., 2015	HI-70	45.1	Shatsky et al., 2015
HH-22	54.2	Shatsky et al., 2015	HI-72	61.2	Shatsky et al., 2015
HH-7	47.5	Shatsky et al., 2015	HI-74	44.8	Shatsky et al., 2015
HH-9	39.9	Shatsky et al., 2015	HI-80_1	36.8	Shatsky et al., 2015
HI-122	40.0	Shatsky et al., 2015	HI-80_2	36.4	Shatsky et al., 2015
HI-136	46.2	Shatsky et al., 2015	HI-80_3	36.9	Shatsky et al., 2015
HI-147	50.1	Shatsky et al., 2015	HI-80_4	37.4	Shatsky et al., 2015
HI-150_1	48.2	Shatsky et al., 2015	HI-84_1	63.3	Shatsky et al., 2015
HI-150_2	45.6	Shatsky et al., 2015	IST-49	47.8	Shatsky et al., 2015
HI-150_3	45.5	Shatsky et al., 2015	1	48.7	Shatsky et al., 2015
HI-19	51.2	Shatsky et al., 2015	7	57.5	Shatsky et al., 2015
HI-23	53.6	Shatsky et al., 2015	21	57.3	Shatsky et al., 2015
HI-29	76.7	Shatsky et al., 2015	38	53.8	Shatsky et al., 2015
HI-34	48.4	Shatsky et al., 2015	41	54.2	Shatsky et al., 2015
HI-41_1	45.4	Shatsky et al., 2015	45	41.4	Shatsky et al., 2015
HI-41_2	45.7	Shatsky et al., 2015	48	40.0	Shatsky et al., 2015
HI-441	56.2	Shatsky et al., 2015	49	48.1	Shatsky et al., 2015
HI-442	56.9	Shatsky et al., 2015	50	51.0	Shatsky et al., 2015
HI-47	68.8	Shatsky et al., 2015	51	39.4	Shatsky et al., 2015
HI-5	61.8	Shatsky et al., 2015	54	46.4	Shatsky et al., 2015
HI-50_1	61.7	Shatsky et al., 2015	58	49.0	Shatsky et al., 2015
HI-50_2	61.4	Shatsky et al., 2015	60	45.9	Shatsky et al., 2015
HI-541	61.1	Shatsky et al., 2015	62	45.8	Shatsky et al., 2015
HI-542	61.3	Shatsky et al., 2015	63	51.4	Shatsky et al., 2015
			71	45.5	Shatsky et al., 2015
			75	47.9	Shatsky et al., 2015

Table B4. continued

Sample	Mg#	Reference			
77	46.5	Shatsky et al., 2015	103_2	54.6	Shatsky et al., 2015
79	56.4	Shatsky et al., 2015	105_1	46.8	Shatsky et al., 2015
82	49.7	Shatsky et al., 2015	105_2	46.5	Shatsky et al., 2015
83	66.6	Shatsky et al., 2015	106_1	66.4	Shatsky et al., 2015
84	48.0	Shatsky et al., 2015	106_2	66.4	Shatsky et al., 2015
96	58.3	Shatsky et al., 2015	106_3	66.4	Shatsky et al., 2015
98	52.6	Shatsky et al., 2015	106_4	66.3	Shatsky et al., 2015
104	61.9	Shatsky et al., 2015	106_5	66.1	Shatsky et al., 2015
107	50.5	Shatsky et al., 2015	106_6	66.4	Shatsky et al., 2015
116	52.4	Shatsky et al., 2015	106_7	66.0	Shatsky et al., 2015
119	43.7	Shatsky et al., 2015	106_8	66.2	Shatsky et al., 2015
121	54.1	Shatsky et al., 2015	106_9	66.8	Shatsky et al., 2015
124	66.5	Shatsky et al., 2015	111_1	55.0	Shatsky et al., 2015
130	67.4	Shatsky et al., 2015	111_2	54.6	Shatsky et al., 2015
132	53.3	Shatsky et al., 2015	113_1	47.7	Shatsky et al., 2015
134	56.4	Shatsky et al., 2015	113_2	47.9	Shatsky et al., 2015
135	45.0	Shatsky et al., 2015	113_3	47.2	Shatsky et al., 2015
136	70.8	Shatsky et al., 2015	114_1	47.1	Shatsky et al., 2015
138	45.0	Shatsky et al., 2015	114_10	46.3	Shatsky et al., 2015
140	45.4	Shatsky et al., 2015	114_11	46.6	Shatsky et al., 2015
148	66.0	Shatsky et al., 2015	114_2	46.8	Shatsky et al., 2015
157	37.3	Shatsky et al., 2015	114_3	47.2	Shatsky et al., 2015
158	54.9	Shatsky et al., 2015	114_4	46.9	Shatsky et al., 2015
103_1	64.2	Shatsky et al., 2015	114_5	47.3	Shatsky et al., 2015
			114_6	47.5	Shatsky et al., 2015
			114_7	46.7	Shatsky et al., 2015

Table B4. continued

Sample	Mg#	Reference			
114_8	46.3	Shatsky et al., 2015	15_5	51.5	Shatsky et al., 2015
114_9	47.0	Shatsky et al., 2015	15_6	52.8	Shatsky et al., 2015
118_1	54.1	Shatsky et al., 2015	154_1	64.0	Shatsky et al., 2015
118_2	54.2	Shatsky et al., 2015	154_2	63.9	Shatsky et al., 2015
118_3	54.4	Shatsky et al., 2015	18_1	40.6	Shatsky et al., 2015
12_1	58.0	Shatsky et al., 2015	18_2	40.5	Shatsky et al., 2015
12_2	57.6	Shatsky et al., 2015	18_3	40.3	Shatsky et al., 2015
120_1	48.5	Shatsky et al., 2015	2_1	58.8	Shatsky et al., 2015
120_2	48.5	Shatsky et al., 2015	2_2	58.3	Shatsky et al., 2015
126_1	56.4	Shatsky et al., 2015	20_1	64.1	Shatsky et al., 2015
126_2	57.4	Shatsky et al., 2015	20_3	64.1	Shatsky et al., 2015
127_1	47.0	Shatsky et al., 2015	20_4	64.1	Shatsky et al., 2015
127_2	49.5	Shatsky et al., 2015	20_5	63.5	Shatsky et al., 2015
139_1	67.5	Shatsky et al., 2015	20_6	63.7	Shatsky et al., 2015
139_2	67.2	Shatsky et al., 2015	20_7	63.9	Shatsky et al., 2015
141_1	47.8	Shatsky et al., 2015	22_1	55.3	Shatsky et al., 2015
141_2	48.6	Shatsky et al., 2015	22_2	55.6	Shatsky et al., 2015
145_1	59.5	Shatsky et al., 2015	27_1	54.3	Shatsky et al., 2015
145_2	59.5	Shatsky et al., 2015	27_2	53.5	Shatsky et al., 2015
145_3	59.4	Shatsky et al., 2015	27_3	55.4	Shatsky et al., 2015
15_1	52.7	Shatsky et al., 2015	3_1	45.4	Shatsky et al., 2015
15_2	52.3	Shatsky et al., 2015	37_1	60.7	Shatsky et al., 2015
15_3	53.1	Shatsky et al., 2015	37_2	62.7	Shatsky et al., 2015
15_4	51.9	Shatsky et al., 2015	44_1	46.7	Shatsky et al., 2015
			44_2	46.6	Shatsky et al., 2015
			47_1	42.3	Shatsky et al., 2015

Table B4. continued

Sample	Mg#	Reference			
47_2	42.6	Shatsky et al., 2015	66_1	40.5	Shatsky et al., 2015
47_3	41.1	Shatsky et al., 2015	66_2	41.2	Shatsky et al., 2015
49_2	45.7	Shatsky et al., 2015	66_3	41.5	Shatsky et al., 2015
5_1	41.8	Shatsky et al., 2015	67_1	47.5	Shatsky et al., 2015
5_2	42.3	Shatsky et al., 2015	67_2	47.8	Shatsky et al., 2015
52_1	49.3	Shatsky et al., 2015	68_1	43.4	Shatsky et al., 2015
52_2	49.5	Shatsky et al., 2015	68_2	44.1	Shatsky et al., 2015
52_3	48.6	Shatsky et al., 2015	68_3	43.8	Shatsky et al., 2015
53_1	42.7	Shatsky et al., 2015	68_4	42.8	Shatsky et al., 2015
53_2	44.3	Shatsky et al., 2015	76_1	45.8	Shatsky et al., 2015
55_1	46.7	Shatsky et al., 2015	76_2	45.7	Shatsky et al., 2015
55_2	46.4	Shatsky et al., 2015	76_3	45.8	Shatsky et al., 2015
55_3	50.2	Shatsky et al., 2015	76_4	45.1	Shatsky et al., 2015
56_1	39.4	Shatsky et al., 2015	78_1	65.3	Shatsky et al., 2015
56_2	38.1	Shatsky et al., 2015	78_2	65.3	Shatsky et al., 2015
57_2	43.8	Shatsky et al., 2015	79_6	55.5	Shatsky et al., 2015
59_1	61.7	Shatsky et al., 2015	79_7	55.7	Shatsky et al., 2015
59_2	63.0	Shatsky et al., 2015	79_8	57.4	Shatsky et al., 2015
61_1	65.0	Shatsky et al., 2015	8_2	50.7	Shatsky et al., 2015
61_2	65.5	Shatsky et al., 2015	80_1	41.2	Shatsky et al., 2015
61_3	64.4	Shatsky et al., 2015	80_2	41.4	Shatsky et al., 2015
61_4	64.4	Shatsky et al., 2015	AGN-29	45.8	Sobolev et al. 1989
64_1	49.4	Shatsky et al., 2015	AGN-31	47.4	Sobolev et al. 1989
64_2	48.8	Shatsky et al., 2015	AGN-34	52.1	Sobolev et al. 1989
			AGN-37	56.8	Sobolev et al. 1989
			AGN-37	56.8	Sobolev et al. 1989

Table B4. continued

Sample	Mg#	Reference			
AGN-38	55.7	Sobolev et al. 1989	AGS-14	44.7	Sobolev et al. 1989
AGN-38	55.6	Sobolev et al. 1989	AGS-15	36.1	Sobolev et al. 1989
AGN-41	58.0	Sobolev et al. 1989	AGS-16	61.1	Sobolev et al. 1989
AGN-42	47.3	Sobolev et al. 1989	AGS-16	61.9	Sobolev et al. 1989
AGN-43	55.2	Sobolev et al. 1989	AGS-19	52.1	Sobolev et al. 1989
AGN-45	64.4	Sobolev et al. 1989	AGS-21	58.7	Sobolev et al. 1989
AGN-46	64.1	Sobolev et al. 1989	AGS-23	52.5	Sobolev et al. 1989
AGN-48	60.4	Sobolev et al. 1989	AGS-24	42.3	Sobolev et al. 1989
AGN-49	55.7	Sobolev et al. 1989	AGS-25	49.1	Sobolev et al. 1989
AGN-49	54.1	Sobolev et al. 1989	AGS-26	54.4	Sobolev et al. 1989
AGN-50	63.6	Sobolev et al. 1989	Argy_Sob-1	61.1	Sobolev et al. 1989
AGN-51	62.3	Sobolev et al. 1989	Argy_Sob-2	61.1	Sobolev et al. 1989
AGN-52	54.2	Sobolev et al. 1989	AGN-52	51.8	Sobolev et al. 1989
AGN-53	60.2	Sobolev et al. 1989	AGN-53	58.8	Sobolev et al. 1989
AGS-03	62.6	Sobolev et al. 1989	KGR-10	64.2	Sobolev et al. 1989
AGS-03	62.3	Sobolev et al. 1989	KGR-11	57.5	Sobolev et al. 1989
AGS-03	63.0	Sobolev et al. 1989	KGR-16	51.4	Sobolev et al. 1989
AGS-05	54.0	Sobolev et al. 1989	KGR-16	53.5	Sobolev et al. 1989
AGS-06	43.0	Sobolev et al. 1989	KGR-21	50.0	Sobolev et al. 1989
AGS-10	61.1	Sobolev et al. 1989	1//1	49.5	Sobolev et al. 1997
AGS-10	61.6	Sobolev et al. 1989	1//15	48.1	Sobolev et al. 1997
AGS-11	52.6	Sobolev et al. 1989	1//2	44.4	Sobolev et al. 1997
AGS-12	63.8	Sobolev et al. 1989	1//3	45.3	Sobolev et al. 1997
AGS-13	53.5	Sobolev et al. 1989	2//10	56.2	Sobolev et al. 1997
			2//12	45.0	Sobolev et al. 1997
			K-1-11	42.1	Sobolev et al. 1997

Table B4. continued

Sample	Mg#	Reference			
K-200	46.1	Sobolev et al. 1997	E-105	49.7	Sobolev et al. 1999
K-220	51.5	Sobolev et al. 1997	E-146	37.3	Sobolev et al. 1999
Po-15	42.4	Sobolev et al. 1997	E-19	65.8	Sobolev et al. 1999
Po-16	45.9	Sobolev et al. 1997	E-21	67.6	Sobolev et al. 1999
Po-20	68.9	Sobolev et al. 1997	E-30	65.1	Sobolev et al. 1999
Po-20	47.3	Sobolev et al. 1997	E-36	56.2	Sobolev et al. 1999
Po-35	43.4	Sobolev et al. 1997	E-56	64.7	Sobolev et al. 1999
Po-38	57.5	Sobolev et al. 1997	E-65	44.5	Sobolev et al. 1999
Po-42	44.7	Sobolev et al. 1997	D-35	67.1	Sobolev et al. 1999
Po-79	60.6	Sobolev et al. 1997	D-49	74.0	Sobolev et al. 1999
M-742 -1	50.1	Sobolev et al. 1998	D-92	69.5	Sobolev et al. 1999
M-742 -14	49.6	Sobolev et al. 1998	M-52	47.0	Sobolev et al. 1999
M-742 -15	54.7	Sobolev et al. 1998	K-95	50.0	Sobolev et al. 1999
M-742 -24a	49.2	Sobolev et al. 1998	AL-1	45.2	Sobolev et al. 2004
M-742 -28	55.4	Sobolev et al. 1998	AL-2	67.8	Sobolev et al. 2004
M-742 -29	49.2	Sobolev et al. 1998	Km-94/49	59.9	Sobolev et al. 2004
M-742 -3	49.5	Sobolev et al. 1998	Im-3	64.4	Sobolev et al. 2004
M-742 -9	56.5	Sobolev et al. 1998	ST-203/00	59.5	Sobolev et al. 2004
M-742 -A	56.4	Sobolev et al. 1998	STI-203/98	56.1	Sobolev et al. 2004
M-742 -B	50.1	Sobolev et al. 1998	Yum-31	29.2	Sobolev et al. 2004
Gm-100	48.7	Sobolev et al. 1998b	Mr-597	56.3	Sobolev et al. 2009
Gm-24	50.2	Sobolev et al. 1998b	Mr-835	45.4	Sobolev et al. 2009
Gm-24	48.8	Sobolev et al. 1998b	Sp-727	63.1	Sobolev et al. 2009
Gm-54	46.1	Sobolev et al. 1998b	Ud-10/90	45.6	Sobolev et al. 2009
			Ud-10/90	45.4	Sobolev et al. 2009
			G36-59	63.4	Stachel & Harris 1997

Table B4. continued

Sample	Mg#	Reference			
KK-18a	49.5	Stachel et al. 2000a	JF-41A	74.5	Tappert et al. 2005a
KK-18b	50.7	Stachel et al. 2000a	JF-41B	74.5	Tappert et al. 2005a
KK-86	41.1	Stachel et al. 2000a	JF-48A	67.7	Tappert et al. 2005a
KK-97	58.8	Stachel et al. 2000a	JF-48B	67.3	Tappert et al. 2005a
PA-63a	70.9	Tappert et al. 2005b	JF-51A	63.5	Tappert et al. 2005a
PA-64a	48.4	Tappert et al. 2005b	JF-51B	65.0	Tappert et al. 2005a
PA-65a	56.9	Tappert et al. 2005b	JF-52A	59.9	Tappert et al. 2005a
PA-65b	57.3	Tappert et al. 2005b	JF-53A	55.1	Tappert et al. 2005a
PA-71a	44.5	Tappert et al. 2005b	JF-53C	54.8	Tappert et al. 2005a
PA-71b	44.2	Tappert et al. 2005b	JF-56A	50.1	Tappert et al. 2005a
PA-73a	47.1	Tappert et al. 2005b	JF-59A	55.7	Tappert et al. 2005a
PA-74a	45.1	Tappert et al. 2005b	JF-61B	51.2	Tappert et al. 2005a
JF-04B	51.6	Tappert et al. 2005a	JF-63A	56.5	Tappert et al. 2005a
JF110A	54.9	Tappert et al. 2005a	JF-63B	56.2	Tappert et al. 2005a
JF-13A	61.1	Tappert et al. 2005a	JF-66A	66.8	Tappert et al. 2005a
JF-13B	61.4	Tappert et al. 2005a	JF-67A	62.3	Tappert et al. 2005a
JF-13C	61.5	Tappert et al. 2005a	JF-68A	71.6	Tappert et al. 2005a
JF-15A	63.9	Tappert et al. 2005a	JF-69A	62.9	Tappert et al. 2005a
JF-15B	64.1	Tappert et al. 2005a	JF-76A	53.0	Tappert et al. 2005a
JF-20B	65.1	Tappert et al. 2005a	JF-76B	52.5	Tappert et al. 2005a
JF-31A	61.0	Tappert et al. 2005a	BV34-A	37.3	Tappert et al. 2006
JF-34A	67.0	Tappert et al. 2005a	BV34-B	37.8	Tappert et al. 2006
JF-38A	68.2	Tappert et al. 2005a	CA14-A	64.1	Tappert et al. 2006
JF-40A	65.7	Tappert et al. 2005a	CA14-B	64.6	Tappert et al. 2006
			M-46	42.5	Taylor et al. 1996

Table B4. continued

Sample	Mg#	Reference			
U-41/3	40.7	Taylor et al. 1996	AP96	49.4	Viljoen et al. 2010
U-65/3 (a)	56.2	Taylor et al. 1996	AP97	66.8	Viljoen et al. 2010
U-65/3 (b)	56.3	Taylor et al. 1996	AP98	62.9	Viljoen et al. 2010
U-66/3	56.1	Taylor et al. 1996	APP-F12A	59.5	Viljoen et al. 2010
AP100	61.3	Viljoen et al. 2010	APP-F23A	39.0	Viljoen et al. 2010
AP101A	65.8	Viljoen et al. 2010	APP-F23B	39.4	Viljoen et al. 2010
AP102A	59.2	Viljoen et al. 2010	APP-F33B	39.0	Viljoen et al. 2010
AP104	68.2	Viljoen et al. 2010	APP-F37B	43.2	Viljoen et al. 2010
AP106A	51.9	Viljoen et al. 2010	APP-F46A	48.3	Viljoen et al. 2010
AP108A	68.1	Viljoen et al. 2010	APP-F53A	43.8	Viljoen et al. 2010
AP109	58.8	Viljoen et al. 2010	APP-F59C	41.1	Viljoen et al. 2010
AP112	69.9	Viljoen et al. 2010	APP-F5A	39.9	Viljoen et al. 2010
AP113	49.0	Viljoen et al. 2010	APP-F71B	34.3	Viljoen et al. 2010
AP114	61.1	Viljoen et al. 2010	APP-F77A	48.7	Viljoen et al. 2010
AP117	60.8	Viljoen et al. 2010	APP-F90A	34.5	Viljoen et al. 2010
AP125	56.4	Viljoen et al. 2010	APP-F92C	62.3	Viljoen et al. 2010
AP127	74.5	Viljoen et al. 2010	APP-F96A	36.3	Viljoen et al. 2010
AP85	48.1	Viljoen et al. 2010	APP-F9A	46.0	Viljoen et al. 2010
AP86	62.0	Viljoen et al. 2010	17_13a	41.9	Westerlund and Gurney 2004
AP90	62.6	Viljoen et al. 2010	17_13a2	42.2	Westerlund and Gurney 2004
AP91	40.9	Viljoen et al. 2010	17_2a	58.3	Westerlund and Gurney 2004
AP92	55.7	Viljoen et al. 2010	17_2b	58.2	Westerlund and Gurney 2004
AP93	68.7	Viljoen et al. 2010	17_3	55.0	Westerlund and Gurney 2004
AP94	62.0	Viljoen et al. 2010			

Table B4. continued

Sample	Mg#	Reference		P5_2e	55.4	Westerlund and Gurney 2004
17_3/2	54.5	Westerlund and Gurney 2004		P5_2e(e)	55.1	Westerlund and Gurney 2004
50W_2c	51.7	Westerlund and Gurney 2004		P5_2f	55.4	Westerlund and Gurney 2004
950W_2b	52.3	Westerlund and Gurney 2004		P5_2f(e)	54.8	Westerlund and Gurney 2004
950W_2c	50.9	Westerlund and Gurney 2004		P5_2g	55.6	Westerlund and Gurney 2004
A_10b	53.1	Westerlund and Gurney 2004		P5_2g(e)	55.2	Westerlund and Gurney 2004
A_10b/2	53.7	Westerlund and Gurney 2004		P5_2h	62.3	Westerlund and Gurney 2004
P3/1_2	53.2	Westerlund and Gurney 2004		P5_2h/2	62.1	Westerlund and Gurney 2004
P3_1	52.7	Westerlund and Gurney 2004		P5_2i	62.5	Westerlund and Gurney 2004
P5_1a	50.7	Westerlund and Gurney 2004		P5_2i(e)	62.5	Westerlund and Gurney 2004
P5_1a/2	50.7	Westerlund and Gurney 2004		P5_2j	55.5	Westerlund and Gurney 2004
P5_2a	56.3	Westerlund and Gurney 2004		P5_2j/2	55.2	Westerlund and Gurney 2004
P5_2a(e)	56.3	Westerlund and Gurney 2004		P5_3a	41.2	Westerlund and Gurney 2004
P5_2b	56.6	Westerlund and Gurney 2004		P5_3b	42.3	Westerlund and Gurney 2004
P5_2c	49.8	Westerlund and Gurney 2004		P5_3d	41.7	Westerlund and Gurney 2004
P5_2d	56.3	Westerlund and Gurney 2004		P5_3d/2	41.1	Westerlund and Gurney 2004
P5_2d/2	56.1	Westerlund and Gurney 2004		P5_3e	41.5	Westerlund and Gurney 2004

Table B4. continued

Sample	Mg#	Reference	P8_2c	55.6	Westerlund and Gurney 2004
P5_3e/2	42.1	Westerlund and Gurney 2004	M1_1	44.4	Westerlund and Gurney 2004
P6_1a	52.3	Westerlund and Gurney 2004	M1_1/2	44.7	Westerlund and Gurney 2004
P6_1a/2	54.2	Westerlund and Gurney 2004	M1_2a	51.2	Westerlund and Gurney 2004
P6_1b	54.1	Westerlund and Gurney 2004	M1_2a(e)	51.4	Westerlund and Gurney 2004
P6_1c	53.6	Westerlund and Gurney 2004	M1_2b	51.2	Westerlund and Gurney 2004
P6_1d	52.0	Westerlund and Gurney 2004	M1_2c	51.0	Westerlund and Gurney 2004
P6_1d/2	50.2	Westerlund and Gurney 2004	M1_2d	49.9	Westerlund and Gurney 2004
P7_13a	39.9	Westerlund and Gurney 2004	M1_2d/2	58.4	Westerlund and Gurney 2004
P7_13a/2	41.7	Westerlund and Gurney 2004	M1_2e	50.9	Westerlund and Gurney 2004
P7_13b	40.9	Westerlund and Gurney 2004	MDA_1a	52.1	Westerlund and Gurney 2004
P7_13b/2	41.4	Westerlund and Gurney 2004	MDA_1b	53.5	Westerlund and Gurney 2004
P7_4	51.0	Westerlund and Gurney 2004	MDA_1b/2	54.0	Westerlund and Gurney 2004
P7_4/2	53.3	Westerlund and Gurney 2004	MDA_1c	52.4	Westerlund and Gurney 2004
P8_2a	64.4	Westerlund and Gurney 2004	MDA_1c/2	52.7	Westerlund and Gurney 2004
P8_2a/2	65.0	Westerlund and Gurney 2004	Blow_3b	64.3	Westerlund and Gurney 2004
P8_2acf_aver	63.0	Westerlund and Gurney 2004	Blow_3b/2	63.9	Westerlund and Gurney 2004

Table B4. continued

Sample	Mg#	Reference		
Blow_6	71.6	Westerlund and Gurney 2004	bz37-3	62.2 Wilding 1990
SB_2ag_aver	66.0	Westerlund and Gurney 2004	bz39-1	55.6 Wilding 1990
TB_14a	56.9	Westerlund and Gurney 2004	bz42-1	54.5 Wilding 1990
TB_14b	56.2	Westerlund and Gurney 2004	bz44-1	59.1 Wilding 1990
TB_5	54.3	Westerlund and Gurney 2004	bz47-3	56.3 Wilding 1990
bz1-1	62.2	Wilding 1990	bz5-4	65.0 Wilding 1990
bz11-1	54.3	Wilding 1990	bf-148a	61.3 Wilding 1990
bz12	58.3	Wilding 1990		70.0 Wilding et al. 1994
bz121-5	57.0	Wilding 1990		
bz123-2	54.6	Wilding 1990		
bz124-1	64.8	Wilding 1990		
bz125-2	53.3	Wilding 1990		
bz126-1	72.4	Wilding 1990		
bz128-1	70.6	Wilding 1990		
bz130-2	77.6	Wilding 1990		
bz13-3	65.1	Wilding 1990		
bz14-1	63.2	Wilding 1990		
bz-2	68.2	Wilding 1990		
bz-24	62.1	Wilding 1990		
bz32	61.5	Wilding 1990		
bz34-4	59.1	Wilding 1990		

Table B5. Source data for peridotitic garnet inclusion Mg#. Compiled by TS.

Sample	Mg#	Reference			
v167b	86.8	Aulbach, 1999	Kms-10 (1)	81.9	Logvinova et al. 2005
v169a	87.8	Aulbach, 1999	Kms-10 (1)	81.9	Logvinova et al. 2005
v197ab	85.0	Aulbach, 1999	Kms-10 (2)	82.8	Logvinova et al. 2005
5a	82.5	Barashkov & Zudin 1997	Kms-10 (2)	82.8	Logvinova et al. 2005
5b	82.9	Barashkov & Zudin 1997	Kms-10 (3)	82.6	Logvinova et al. 2005
d1	85.1	Daniels & Gurney, 1989	Kms-10 (3)	82.6	Logvinova et al. 2005
d1	84.7	Daniels & Gurney, 1989	KW 49a	85.6	Motsamai, 2019
D1304A	84.6	Daniels & Gurney, 1999	SL-00/133	82.9	Pokhilenko et al., 2004
DO2700216	86.7	Davies et al., 2004	14_5	82.2	Shatsky et al., 2015
Ash-K10	84.6	Davies et al., 2004b	40	83.8	Shatsky et al., 2015
Ash-105C	83.2	Davies et al., 2004b	65	84.4	Shatsky et al., 2015
ddmi-199a	83.4	Donnelly, 2006	70	84.5	Shatsky et al., 2015
ddmi-199b	84.0	Donnelly, 2006	143	82.0	Shatsky et al., 2015
CHL 17	83.6	Harris, 1994	72_1	70.7	Shatsky et al., 2015
CHL 43a	83.0	Harris, 1994	72_2	70.6	Shatsky et al., 2015
CHL 51	84.3	Harris, 1994	72_3	70.7	Shatsky et al., 2015
Nam-217Bb	76.4	Harris, 1994	72_4	71.1	Shatsky et al., 2015
Nam-24	84.6	Harris, 1994	Ud-5	83.0	Sobolev et al., 1997
e4/12	83.8	Jaques et al., 1989	Po-71	82.3	Sobolev et al., 1997
e4-e226	84.0	Jaques et al., 1989	MT-85	84.2	Sobolev et al., 1997
Guan-V-12	65.5	Kaminsky et al., 2000	Km-68/23	84.6	Sobolev et al., 2004
Guan-V-36	85.0	Kaminsky et al., 2000	Km-69/23	85.6	Sobolev et al., 2004
Guan-V-36	84.4	Kaminsky et al., 2000	Im-21	86.5	Sobolev et al., 2004
			G102-102	77.5	Stachel and Harris, 1997
			G4-3	80.9	Stachel and Harris, 1997
			G50-82	83.6	Stachel and Harris, 1997

Table B5. continued

Sample	Mg#	Reference				
G50-85	83.0	Stachel and Harris, 1997	o5	85.6	Stachel et al., 2004	
MW11-19	86.7	Stachel et al., 1998a	o9	86.8	Stachel et al., 2004	
MW17-33	86.5	Stachel et al., 1998a	FLIN4-11	83.4	Tappert et al., 2009	
MW35-60	85.8	Stachel et al., 1998a	20	82.9	Phillips et al., 2004	
MW39-67	83.0	Stachel et al., 1998a	218	85.0	Phillips et al., 2004	
MW5-10	84.6	Stachel et al., 1998a	321	85.7	Phillips et al., 2004	
MW82-113	86.5	Stachel et al., 1998a	374	85.4	Phillips et al., 2004	
MW83-115	84.1	Stachel et al., 1998a	448	86.1	Phillips et al., 2004	
KK-26b	84.2	Stachel et al., 2000a	474	86.2	Phillips et al., 2004	
KK-26b	84.2	Stachel et al., 2000a	512	85.9	Phillips et al., 2004	
KK-65d	85.4	Stachel et al., 2000a	218-1a	85.0	Phillips et al., 2004	
KK-78c	84.8	Stachel et al., 2000a	448-1a	86.1	Phillips et al., 2004	
PA-11a	84.7	Stachel et al., 2003	AP54	82.8	Viljoen et al., 2014	
PA-11b	84.8	Stachel et al., 2003	AP60	86.3	Viljoen et al., 2014	
PA-19a (I)	85.8	Stachel et al., 2003	AP61	85.0	Viljoen et al., 2014	
PA-23a	85.9	Stachel et al., 2003	AP69	81.8	Viljoen et al., 2014	
PA-40b	86.1	Stachel et al., 2003	AP73	83.8	Viljoen et al., 2014	
PA-60b	85.6	Stachel et al., 2003	AP74	74.6	Viljoen et al., 2014	
j11	85.7	Stachel et al., 2004	P108	84.8	Viljoen et al., 2014	
j12	86.3	Stachel et al., 2004	P147	82.8	Viljoen et al., 2014	
j13	86.3	Stachel et al., 2004	P174	85.6	Viljoen et al., 2014	
j37	86.1	Stachel et al., 2004	P71	82.7	Viljoen et al., 2014	
j7	85.6	Stachel et al., 2004	P81	71.8	Viljoen et al., 2014	
j9	85.9	Stachel et al., 2004	P97	79.4	Viljoen et al., 2014	
			L12	86.6	Wang et al., 2000	
			L24-1	85.4	Wang et al., 2000	

Table B5. continued

<b>Sample</b>	<b>Mg#</b>	<b>Reference</b>
S03(2)	83.3	Wang et al., 2000
S06-2	83.5	Wang et al., 2000
S06-3	84.1	Wang et al., 2000

Table B6. Source data for  $\delta^{18}\text{O}$  and  $\delta^{13}\text{C}$  in AOC carbonate.

Sample	$\delta^{18}\text{O}$	$\delta^{13}\text{C}$	Reference
\	29.1	-2.7	Alt and Teagle 2003
\	29.5	0.2	Alt and Teagle 2003
\	29.3	-1.5	Alt and Teagle 2003
\	28.2	0.9	Alt and Teagle 2003
\	28.0	0.9	Alt and Teagle 2003
\	28.3	0.9	Alt and Teagle 2003
\	29.1	1.1	Alt and Teagle 2003
\	27.5	-0.2	Alt and Teagle 2003
\	27.8	0.0	Alt and Teagle 2003
\	26.6	0.5	Alt and Teagle 2003
\	27.1	0.9	Alt and Teagle 2003
\	26.9	0.6	Alt and Teagle 2003
\	27.9	0.7	Alt and Teagle 2003
40R-1 85-91	28.6	-3.6	Alt et al. 1992
41R-1 26-31	29.9	-5.2	Alt et al. 1992
41R-1 88-94	30.2	-4.5	Alt et al. 1992
43R-2 21-27	29.0	-0.4	Alt et al. 1992
5R-1 103-105	27.9	1.9	Alt et al. 1992
R-2 87- 89	27.3	0.3	Alt et al. 1992
5R-3 38- 43	29.5	0.7	Alt et al. 1992

5R-3 125-131	30.4	1.3	Alt et al. 1992
5R-3 125-131	30.0	1.4	Alt et al. 1992
8R-2 78- 80	27.7	0.3	Alt et al. 1992
8R-1 65- 67	28.2	1.1	Alt et al. 1992
4-5 91- 92	13.1	-9.0	Furnes et al. 1999
24-3 73- 94	14.4	-14.9	Furnes et al. 1999
24-3 73- 94	20.8	-12.0	Furnes et al. 1999
28-4 16- 17	19.6	-13.6	Furnes et al. 1999
48-2 123-124	30.7	-13.1	Furnes et al. 1999
48-2 123-124	25.1	-14.6	Furnes et al. 1999
62-2 23- 25	31.7	-12.6	Furnes et al. 1999
64-1 27- 28	30.9	-11.0	Furnes et al. 1999
208R-1 30-32	24.9	-13.7	Furnes et al. 1999
213R-1 45-47	19.4	-17.0	Furnes et al. 1999
222R-1 2-4	23.9	-8.8	Furnes et al. 1999
245B-1 36-38	33.9	4.7	Furnes et al. 1999
21-4 90- 92	24.1	-7.3	Furnes et al. 1999

Table B6. continued

Sample	$\delta^{18}\text{O}$	$\delta^{13}\text{C}$	Reference				
21-4 90-92	25.1	-10.3	Furnes et al. 1999	6-2 125-126	33.6	2.7	Furnes et al. 2001
35-1 109-111	23.2	-10.7	Furnes et al. 1999	1-1 40-41	22.3	-3.1	Furnes et al. 2001
10-2 14-15	19.6	-9.2	Furnes et al. 2001	2-1 4-5	20.3	-3.6	Furnes et al. 2001
37-1 112-113	28.8	1.0	Furnes et al. 2001	2-1 4-5	19.7	-4.9	Furnes et al. 2001
35-1 109-111	23.2	-10.7	Furnes et al. 1999	2-1 7-8	29.1	-1.8	Furnes et al. 2001
10-2 14-15	19.6	-9.2	Furnes et al. 2001	2-2 21-22	22.0	-7.8	Furnes et al. 2001
37-1 112-113	28.8	1.0	Furnes et al. 2001	2-2 21-22	19.9	-12.4	Furnes et al. 2001
39-1 52-53	24.7	-2.5	Furnes et al. 2001	3-1 94-95	24.8	-3.2	Furnes et al. 2001
41-1 2-3	22.3	-4.2	Furnes et al. 2001	4-1 87-88	21.0	-6.8	Furnes et al. 2001
42-2 58-59	23.4	-4.2	Furnes et al. 2001	5-1 136-137	12.1	-14.0	Furnes et al. 2001
21-1 3-4	33.5	2.0	Furnes et al. 2001	7-1 10-11	19.1	-8.3	Furnes et al. 2001
21-1 32-33	35.7	3.0	Furnes et al. 2001	8-2 5-6	21.7	-7.3	Furnes et al. 2001
25-2 40-41	35.2	2.7	Furnes et al. 2001	10-1 56-57	18.3	-6.9	Furnes et al. 2001
25-3 36-37	35.3	2.6	Furnes et al. 2001	11-1 89-90	8.8	-16.3	Furnes et al. 2001
32-1 60-61	26.7	-5.4	Furnes et al. 2001	14-1 8-9	23.2	-6.2	Furnes et al. 2001
2-1 3-4	32.4	2.6	Furnes et al. 2001	17-2 26-27	27.4	-1.3	Furnes et al. 2001
2-1 53-54	36.5	4.6	Furnes et al. 2001	17-3 64-65	10.8	-16.0	Furnes et al. 2001
2-2 50-51	29.6	-0.9	Furnes et al. 2001	17-3 109-110	21.4	-4.1	Furnes et al. 2001
2-3 50-51	29.6	-1.5	Furnes et al. 2001	17-4 54-55	22.4	-1.5	Furnes et al. 2001
2-5 96-97	33.4	3.0	Furnes et al. 2001	20-1 135-136	35.6	2.4	Furnes et al. 2001
4-1 134-135	28.0	-2.2	Furnes et al. 2001	20-4 114-115	23.4	-2.6	Furnes et al. 2001
6-1 86-87	20.1	-4.9	Furnes et al. 2001	20-5 72-73	26.3	-3.1	Furnes et al. 2001
				21-2 44-45	21.2	-3.3	Furnes et al. 2001
				21-2 44-45	19.3	-13.4	Furnes et al. 2001

Table B6. continued

Sample	$\delta^{18}\text{O}$	$\delta^{13}\text{C}$	Reference	100R-1 133-	18.1	-16.9	Li et al. 2019
23-1 92-93	22.0	-4.9	Furnes et al. 2001	134			
14R-1 28-29	18.8	-3.4	Furnes et al. 2001	10-03W 28-	27.5	-0.8	Li et al. 2019
14R-1 39-40	33.2	1.5	Furnes et al. 2001	30			
15R-1 53-55	33.0	4.2	Furnes et al. 2001	13-01W 18-	30.2	2.7	Li et al. 2019
16R-1 40-41	18.1	-4.4	Furnes et al. 2001	21			
33R-1 6-7	16.8	-6.0	Furnes et al. 2001	13-05W 85-	18.7	1.6	Li et al. 2019
35R-1 32-33	19.79	-8.7	Furnes et al. 2001	86			
45-3 93-95	30.32	0.9	Furnes et al. 2001	14-01W 37-	17	-3.4	Li et al. 2019
3-1 113-114	27.42	0.5	Furnes et al. 2001	39			
3-4 6-7	28.56	0.3	Furnes et al. 2001	15-01W 49-	25.9	-0.5	Li et al. 2019
4-1 140-141	34.12	1.5	Furnes et al. 2001	51			
7-2 93-94	24.81	-8.9	Furnes et al. 2001	15-03W 99-	26.6	-1.5	Li et al. 2019
9-1 128-129	19.59	-8.6	Furnes et al. 2001	100			
15-2 35-36	20.06	-3.2	Furnes et al. 2001	16-01W 88-	30.1	2.8	Li et al. 2019
18-1 8-9	23.82	-1.3	Furnes et al. 2001	90			
214R-2 101-102	13.1	-19.2	Li et al. 2019	16-03W	31	2.6	Li et al. 2019
223R-3 24-25	12.5	-19.8	Li et al. 2019	116-118			
230R-2 45-46	13.1	-21.4	Li et al. 2019	15R-1 63-64	20.3	-8.2	Li et al. 2019
234R-1 30-31	14.3	-22.6	Li et al. 2019	130R-2 49-50	15.5	-23.1	Li et al. 2019
2R-1 86-87	19.3	-19.6	Li et al. 2019	136R-1 74-75	11.4	-11.0	Li et al. 2019
6R-5 99-100	17.2	-15.1	Li et al. 2019	169R-3 53-54	16.6	-22.0	Li et al. 2019
32R-2 8-9	24.5	-9.0	Li et al. 2019	173R-1 12-13	13.5	-24.1	Li et al. 2019
				181R-1 63-64	13.1	-20.3	Li et al. 2019
				189R-1 70-71	14.6	-17.5	Li et al. 2019
				196R-1 35-36	14.2	-20.9	Li et al. 2019

Table B6. continued

Sample	$\delta^{18}\text{O}$	$\delta^{13}\text{C}$	Reference	G3-1	19.1	-21.1	Li et al. 2019
65R-3 22-23	17.3	-19.2	Li et al. 2019	G7-1	24.6	-1.0	Li et al. 2019
75R-1 112-113	21	-7.0	Li et al. 2019	G1-1	17.1	-15.0	Li et al. 2019
92R-1 95-96	18.1	-18.3	Li et al. 2019	1D-1-10W 69-73	22.7	-4.7	Li et al. 2019
11-02W 59-60	29.3	3.3	Li et al. 2019	7D-1-10W 70-73	20.2	-11.2	Li et al. 2019
12-02W 72-75	30.6	3.5	Li et al. 2019	10D-2-2bW 17-21	32.3	-0.8	Li et al. 2019
12-04W 128-133	25.3	-3.5	Li et al. 2019	16R-5-1cW 40-43	30.1	-0.7	Li et al. 2019
10-01W 57-58	30.6	2.0	Li et al. 2019	23R-2-1bW 29-32	20.4	-4.6	Li et al. 2019
10-02W 103-105	29.0	1.2	Li et al. 2019	37R-1-2bW 22-25	22.2	-3.9	Li et al. 2019
11-01W 30-33	28.7	2.2	Li et al. 2019	52R-4-4aW 60-61	22.8	-0.6	Li et al. 2019
12R-5 37-38	25.7	-5.7	Li et al. 2019	19R-2 15-17	26.8	0.0	Li et al. 2019
4R-2 74-77	25.9	-7.7	Li et al. 2019	20R-2 28-31	19.9	-3.6	Li et al. 2019
5R-1 48-50	29.0	-3.1	Li et al. 2019	22R-2 75-78	21.2	-10.6	Li et al. 2019
7R-1 56-58	17.4	10.9	Li et al. 2019	2R-1 37-40	31.6	1.6	Li et al. 2019
10R-1 102-104	33.4	2.2	Li et al. 2019	5R-4 12-13	23.6	-6.4	Li et al. 2019
20R-1 51-54	26.1	-8.7	Li et al. 2019	8R-1 118-119	24.1	-5.4	Li et al. 2019
25R-1 40-43	28.6	-5.8	Li et al. 2019	10R-3 74-75	19.9	-6.8	Li et al. 2019
G2-1	17.6	-5.9	Li et al. 2019	16R-7 42-45	21.8	-2.3	Li et al. 2019
G4-1	19.8	-13.0	Li et al. 2019	1R-1 44-45	22.8	6.4	Li et al. 2019
G6-1	21.1	-7.9	Li et al. 2019	12R-1 112-115	12.8	6.3	Li et al. 2019
G5-1	17.8	-8.2	Li et al. 2019	19R-2 18-21	30.0	-1.8	Li et al. 2019

Table B6. continued

Sample	$\delta^{18}\text{O}$	$\delta^{13}\text{C}$	Reference				et al. 2013
2R-1 19-22	27.6	-2.3	Li et al. 2019	\	30.7	0.6	Schwarzenbach et al. 2013
6R-1 43-45	22.5	-10.8	Li et al. 2019	\	31.0	0.6	Schwarzenbach et al. 2013
11R-1 38-41	24.5	-4.9	Li et al. 2019	\	30.4	0.8	Schwarzenbach et al. 2013
16R-2 61-63	28.8	-7.9	Li et al. 2019	\	31.0	1.7	Schwarzenbach et al. 2013
69R-3-5cW 82-85	20.3	-14.4	Li et al. 2019	\	29.7	0.1	Schwarzenbach et al. 2013
80R-62W-17	18.6	-4.7	Li et al. 2019	\	31.2	1.1	Schwarzenbach et al. 2013
90R-1-2W 105-107	17.8	-17.4	Li et al. 2019	\	31.1	2.3	Schwarzenbach et al. 2013
95R-1-7W 105-109	31.8	1.7	Li et al. 2019	\	30.8	0.5	Schwarzenbach et al. 2013
108R-2-1cW 36-37	17.6	-7.8	Li et al. 2019	\	29.5	0.6	Schwarzenbach et al. 2013
122R-2-1bW 11-15	27.9	-1.6	Li et al. 2019	\	30.8	-0.3	Schwarzenbach et al. 2013
130R-4-8bW 116-119	15.8	-6.1	Li et al. 2019	\	29.7	-1.5	Schwarzenbach et al. 2013
138R-3-1W 61-64	17.7	-9.8	Li et al. 2019	\	30.0	-0.2	Schwarzenbach et al. 2013
149R-7-2W 18-121	18.4	-9.9	Li et al. 2019	\	30.4	1.9	Schwarzenbach et al. 2013
180R-5- 4W38-40	16.7	-5.0	Li et al. 2019	\	30.0	1.9	Schwarzenbach et al. 2013
200R-4-1bW 37-38	16.6	-6.1	Li et al. 2019	\	29.9	1.9	Schwarzenbach et al. 2013
\	30.9	-0.4	Schwarzenbach et al. 2013	\	29.6	1.6	Schwarzenbach et al. 2013
\	30.6	0.8	Schwarzenbach et al. 2013	\	31.0	0.4	Schwarzenbach

Table B6. continued

Sample	$\delta^{18}\text{O}$	$\delta^{13}\text{C}$	Reference				
\	29.8	1.1	Schwarzenbach et al. 2013	11R-1 73-75	16.1	-8.9	Torsvik et al. 1998
\	29.7	0.3	Schwarzenbach et al. 2013	11R-1 73-75	16.4	-7.7	Torsvik et al. 1998
\	29.9	-1.1	Schwarzenbach et al. 2013	11R-1 111-113	23.5	-6.3	Torsvik et al. 1998
\	30.1	-1.1	Schwarzenbach et al. 2013	11R-1 111-113	22.4	-9.6	Torsvik et al. 1998
\	26.8	-1.1	Schwarzenbach et al. 2013	12R-2 7-9	23.8	-2.2	Torsvik et al. 1998
\	29.8	1.1	Schwarzenbach et al. 2013	12R-1 76-80	26.1	-6.4	Torsvik et al. 1998
\	30.4	1.6	Schwarzenbach et al. 2013	12R-1 76-80	12.4	-15.5	Torsvik et al. 1998
\	30.2	1.5	Schwarzenbach et al. 2013	14R-2 28-30	26.6	-6.5	Torsvik et al. 1998
\	27.9	-2.0	Schwarzenbach et al. 2013	14R-2 58-60	21.8	0.7	Torsvik et al. 1998
2R-1 47-49	24.1	-6.0	Torsvik et al. 1998	16R-1 31-32	22.9	-6.4	Torsvik et al. 1998
5R-2 39-41	21.8	-2.5	Torsvik et al. 1998	16R-3 89-91	25.4	-2.7	Torsvik et al. 1998
6R-3 30-34	16.2	-8.5	Torsvik et al. 1998	18R-1 75-77	23.4	-7.5	Torsvik et al. 1998
7R-1 58-60	24.2	-1.7	Torsvik et al. 1998	21R-3 25-27	29.4	-5.2	Torsvik et al. 1998
9R-1 17-21	23.4	-5.4	Torsvik et al. 1998	22R-4 31-33	21.8	-3.7	Torsvik et al. 1998
9R-1 17-21	27.1	-11.9	Torsvik et al. 1998	24R-1 18-19	24.1	-1.5	Torsvik et al. 1998
9R-1 90-92	19.1	-9.6	Torsvik et al. 1998	25R-2 130-132	24.3	-8.0	Torsvik et al. 1998
9R-1 90-92	17.5	-6.4	Torsvik et al. 1998	27R-1 114-117	19.1	-10.9	Torsvik et al. 1998
10R-1 40-46	23.4	-9.0	Torsvik et al. 1998	27R-1 1414-117	18.0	-10.9	Torsvik et al. 1998
10R-1 40-46	22.6	-4.3	Torsvik et al. 1998	27R-1 108-111	28.8	-11.6	Torsvik et al. 1998
				28R-1 23-26	22.0	-12.5	Torsvik et al. 1998
				28R-1 23-26	17.0	-10.9	Torsvik et al. 1998
				30R-1 61-63	23.9	-5.0	Torsvik et al. 1998
				30R-1 61-63	21.7	-7.0	Torsvik et al. 1998

Table B6. continued

Sample	$\delta^{18}\text{O}$	$\delta^{13}\text{C}$	Reference
6R-2 39-45	8.3	-11.5	Torsvik et al. 1998
17R-3 11-15	20.9	-1.9	Torsvik et al. 1998
17R-3 11-15	13.0	-11.5	Torsvik et al. 1998
9R-1 125- 130	23.5	-11.6	Torsvik et al. 1998
9R-1 125- 130	18.3	-9.4	Torsvik et al. 1998
11R-1 0-3	11.7	-13.1	Torsvik et al. 1998
11R-1 0-3	24.3	-0.2	Torsvik et al. 1998
14R-2 111- 112	24.5	-5.4	Torsvik et al. 1998
26R-3 43-46	20.3	-7.0	Torsvik et al. 1998
26R-3 43-46	22.2	-7.1	Torsvik et al. 1998
29R-2 4-6	22.3	-7.4	Torsvik et al. 1998

Table B7. Source data for mantle eclogite xenoliths  
 $\delta^{18}\text{O}$ .

Sample	$\delta^{18}\text{O}$	Reference			
79/197	5.6	Malkovets et al. 2003	9115	6.8	Ustinov et al. 1987
94/210	5.6	Malkovets et al. 2003	9202	5.6	Ustinov et al. 1987
102/236	5.4	Malkovets et al. 2003	9203	6.2	Ustinov et al. 1987
73/230	5.4	Malkovets et al. 2003	55	6.7	Jacob et al. 1994
93/265	4.3	Malkovets et al. 2003	65.00	7.0	Jacob et al. 1994
102/254	4.3	Malkovets et al. 2003	77.00	6.0	Jacob et al. 1994
441/3	4.1	Malkovets et al. 2003	91	6.9	Jacob et al. 1994
Ob-33	6.4	Ustinov et al. 1987	29	5.3	Jacob et al. 1994
Ob-75	6.8	Ustinov et al. 1987	43	5.2	Jacob et al. 1994
Ob-44	6.4	Ustinov et al. 1987	68	5.6	Jacob et al. 1994
Ob-140	7.0	Ustinov et al. 1987	84	5.4	Jacob et al. 1994
Ob-311	5.4	Ustinov et al. 1987	U-1	6.8	Snyder 1995
Ob-149	6.3	Ustinov et al. 1987	U-79	5.8	Snyder 1995
Ob-28	7.0	Ustinov et al. 1987	U-86	4.6	Snyder 1995
Ob-50	6.9	Ustinov et al. 1987	U-237	5.0	Snyder 1995
Ob-151	9.0	Ustinov et al. 1987	U-281	5.0	Snyder 1995
O-82/91	7.8	(Taylor et al. 2003)	Ud-107	12.4	Shatsky et al. 2016
O-423	6.1	(Taylor et al. 2003)	Ud-111-02	7.1	Shatsky et al. 2016
O-501	7.1	(Taylor et al. 2003)	Ud-172-02	6.8	Shatsky et al. 2016
O-926	5.6	(Taylor et al. 2003)	Ud-208-02	5.5	Shatsky et al. 2016
O-927	6.3	Taylor et al. 2003	UDR	5.3	Shatsky et al. 2016
O-1073	6.5	Taylor et al. 2003	M-84	5.8	Beard et al. 1996
O-1103	6.4	Taylor et al. 2003	M-772	4.9	Beard et al. 1996
			M-2385	5.2	Beard et al. 1996
			M-29	6.0	Beard et al. 1996
			M-65	6.7	Beard et al. 1996

Table B7. continued

Sample	$\delta^{18}\text{O}$	Reference			
M-704	6.9	Beard et al. 1996	N-19	5.5	Spetsius et al. 2008
M-180	4.9	Beard et al. 1996	N-20	6.4	Spetsius et al. 2008
M-60/1214	5.4	Beard et al. 1996	N-21	6.5	Spetsius et al. 2008
M-53/1165	5.5	Beard et al. 1996	N-22	5.3	Spetsius et al. 2008
M-432	5.4	Beard et al. 1996	N-23	6.3	Spetsius et al. 2008
M-69	5.3	Beard et al. 1996	N-24	6.6	Spetsius et al. 2008
M-54	4.2	Beard et al. 1996	N-25	6.4	Spetsius et al. 2008
M-83	5.0	Beard et al. 1996	N-26	6.8	Spetsius et al. 2008
M-86	3.1	Beard et al. 1996	N-27	6.2	Spetsius et al. 2008
N-3	6.4	Spetsius et al. 2008	N-28	6.6	Spetsius et al. 2008
N-4	6.7	Spetsius et al. 2008	N-30	6.4	Spetsius et al. 2008
N-5	6.3	Spetsius et al. 2008	N-31	5.4	Spetsius et al. 2008
N-6	6.5	Spetsius et al. 2008	N-32	6.2	Spetsius et al. 2008
N-7	6.7	Spetsius et al. 2008	N-33	6.6	Spetsius et al. 2008
N-8	6.4	Spetsius et al. 2008	N-34	6.8	Spetsius et al. 2008
N-9	6.5	Spetsius et al. 2008	N-35	6.6	Spetsius et al. 2008
N-11	6.6	Spetsius et al. 2008	N-36	6.4	Spetsius et al. 2008
N-12	6.5	Spetsius et al. 2008	N-38	5.5	Spetsius et al. 2008
N-13	6.7	Spetsius et al. 2008	N-42	6.8	Spetsius et al. 2008
N-14	5.5	Spetsius et al. 2008	N-44	6.5	Spetsius et al. 2008
N-15	5.4	Spetsius et al. 2008	N-45	6.3	Spetsius et al. 2008
N-16	6.2	Spetsius et al. 2008	N-48	6.4	Spetsius et al. 2008
N-17	5.4	Spetsius et al. 2008	N-49	6.7	Spetsius et al. 2008
N-18	6.4	Spetsius et al. 2008	N-50	6.6	Spetsius et al. 2008
			N-51	7.2	Spetsius et al. 2008
			N-54	7.1	Spetsius et al. 2008

Table B7. continued

Sample	$\delta^{18}\text{O}$	Reference			
N-55	6.5	Spetsius et al. 2008	N-84	4.8	Spetsius et al. 2008
N-56	6.6	Spetsius et al. 2008	N-85	6.6	Spetsius et al. 2008
N-58	6.9	Spetsius et al. 2008	N-87	4.7	Spetsius et al. 2008
N-59	6.7	Spetsius et al. 2008	N-88	6.2	Spetsius et al. 2008
N-60	7.0	Spetsius et al. 2008	N-89	6.3	Spetsius et al. 2008
N-61	6.9	Spetsius et al. 2008	N-90	6.4	Spetsius et al. 2008
N-62	7.0	Spetsius et al. 2008	N-91	6.4	Spetsius et al. 2008
N-63	6.4	Spetsius et al. 2008	N-93	6.8	Spetsius et al. 2008
N-64	5.3	Spetsius et al. 2008	N-94	6.7	Spetsius et al. 2008
N-65	6.8	Spetsius et al. 2008	N-96	6.2	Spetsius et al. 2008
N-66	6.0	Spetsius et al. 2008	N-99	5.0	Spetsius et al. 2008
N-67	6.6	Spetsius et al. 2008	N-100	5.1	Spetsius et al. 2008
N-68	6.7	Spetsius et al. 2008	N-101	6.9	Spetsius et al. 2008
N-69	6.8	Spetsius et al. 2008	N-102	6.9	Spetsius et al. 2008
N-72	6.5	Spetsius et al. 2008	N-103	6.7	Spetsius et al. 2008
N-73	6.8	Spetsius et al. 2008	N-104	8.6	Spetsius et al. 2008
N-74	6.7	Spetsius et al. 2008	N-105	6.7	Spetsius et al. 2008
N-75	6.3	Spetsius et al. 2008	N-106	6.3	Spetsius et al. 2008
N-76	6.6	Spetsius et al. 2008	N-107	6.3	Spetsius et al. 2008
N-39	6.6	Spetsius et al. 2008	N-110	6.0	Spetsius et al. 2008
N-78	6.7	Spetsius et al. 2008	N-111	5.9	Spetsius et al. 2008
N-79	7.2	Spetsius et al. 2008	N-112	6.6	Spetsius et al. 2008
N-80	6.6	Spetsius et al. 2008	N-113	6.8	Spetsius et al. 2008
N-81	6.5	Spetsius et al. 2008	N-117	6.8	Spetsius et al. 2008
			N-118	6.2	Spetsius et al. 2008
			N-119	6.4	Spetsius et al. 2008

Table B7. continued

Sample	$\delta^{18}\text{O}$	Reference			
N-120	6.8	Spetsius et al. 2008	N10	7.1	Riches et al. 2010
N-121	5.3	Spetsius et al. 2008	N11	6.6	Riches et al. 2010
N-124	6.9	Spetsius et al. 2008	N13	6.5	Riches et al. 2010
N-126	6.3	Spetsius et al. 2008	N14	5.5	Riches et al. 2010
N-127	6.8	Spetsius et al. 2008	N16	6.2	Riches et al. 2010
N-131	6.6	Spetsius et al. 2008	N18	6.4	Riches et al. 2010
N-132	6.7	Spetsius et al. 2008	N20	6.4	Riches et al. 2010
N-133	6.6	Spetsius et al. 2008	N26	6.8	Riches et al. 2010
N-135	6.4	Spetsius et al. 2008	N28	6.6	Riches et al. 2010
N-136	6.2	Spetsius et al. 2008	N30	6.4	Riches et al. 2010
N-140	6.1	Spetsius et al. 2008	N35	6.6	Riches et al. 2010
N-141	6.5	Spetsius et al. 2008	N36	6.4	Riches et al. 2010
N-143	6.6	Spetsius et al. 2008	N38	5.5	Riches et al. 2010
N-145	6.4	Spetsius et al. 2008	N42	6.8	Riches et al. 2010
N-157	5.5	Spetsius et al. 2008	N44	6.5	Riches et al. 2010
N-147†	6.0	Riches et al. 2010	N45	6.3	Riches et al. 2010
N104	8.6	Riches et al. 2010	N47†	6.0	Riches et al. 2010
N109	5.6	Riches et al. 2010	N49	6.7	Riches et al. 2010
N129	7.3	Riches et al. 2010	N50	6.6	Riches et al. 2010
N3	6.4	Riches et al. 2010	N59	6.7	Riches et al. 2010
N4	6.7	Riches et al. 2010	N60	7.0	Riches et al. 2010
N6	6.5	Riches et al. 2010	N62	7.0	Riches et al. 2010
N8†	6.4	Riches et al. 2010	N65	6.8	Riches et al. 2010
N9	6.5	Riches et al. 2010	N67	6.6	Riches et al. 2010
			N68	6.7	Riches et al. 2010
			N69	6.8	Riches et al. 2010

Table B7. continued

Sample	$\delta^{18}\text{O}$	Reference			
N72	6.5	Riches et al. 2010	K3	5.3	Pernet-Fisher et al. 2014
N73	6.8	Riches et al. 2010	K4	5.4	Pernet-Fisher et al. 2014
N74	6.7	Riches et al. 2010	K5a	5.4	Pernet-Fisher et al. 2014
N77†*	5.4	Riches et al. 2010	K5b	5.4	Pernet-Fisher et al. 2014
N79	7.2	Riches et al. 2010	K6	5.2	Pernet-Fisher et al. 2014
N84*	4.8	Riches et al. 2010	K7	5.5	Pernet-Fisher et al. 2014
N8*†	6.4	Riches et al. 2010	K8	5.5	Pernet-Fisher et al. 2014
N17*	5.4	Riches et al. 2010	K11	5.4	Pernet-Fisher et al. 2014
N31	5.4	Riches et al. 2010	K12	5.3	Pernet-Fisher et al. 2014
N77†*	5.4	Riches et al. 2010	K13	5.2	Pernet-Fisher et al. 2014
N87	4.7	Riches et al. 2010	35-2	5.7	Smart et al. 2014
N121*	5.3	Riches et al. 2010	Mx8A	5.6	Smart et al. 2014
K1a	6.2	Pernet-Fisher et al. 2014	Jd6fn	5.2	Smart et al. 2014
K1b	6.2	Pernet-Fisher et al. 2014	53-11	5.7	Smart et al. 2014
K9b	7.0	Pernet-Fisher et al. 2014	44-9	5.6	Smart et al. 2014
K10	6.8	Pernet-Fisher et al. 2014	55-7	5.6	Smart et al. 2014
K14a	8.1	Pernet-Fisher et al. 2014	1-1	5.6	Smart et al. 2014
K15a	6.7	Pernet-Fisher et al. 2014	10-13	6.3	Smart et al. 2014
K2a	5.3	Pernet-Fisher et al. 2014	Jde02*	5.3	Smart et al. 2014
K2b	5.3	Pernet-Fisher et al. 2014	Jde03*	5.5	Smart et al. 2014
			Jde07*	5.5	Smart et al. 2014

Table B7. continued

Sample	$\delta^{18}\text{O}$	Reference				
Jde25*	6.6	Smart et al. 2014	64	6.6	MacGregor & Manton 1986	
Jde15*	6.6	Smart et al. 2014	71	6.5	MacGregor & Manton 1986	
VIC0608	5.2	Smit et al. 2014	13	5.8	MacGregor & Manton 1986	
VIC0502	7.0	Smit et al. 2014	44	5.4	MacGregor & Manton 1986	
VIC0504	6.3	Smit et al. 2014	53	5.4	MacGregor & Manton 1986	
VIC0604	5.5	Smit et al. 2014	65	3.8	MacGregor & Manton 1986	
VIC0703	5.4	Smit et al. 2014	6	3.8	MacGregor & Manton 1986	
VIC0704	6.3	Smit et al. 2014	8A	5.3	MacGregor & Manton 1986	
VIC0705	5.1	Smit et al. 2014	22	3.2	MacGregor & Manton 1986	
VIC1104	5.9	Smit et al. 2014	26	3.2	MacGregor & Manton 1986	
VIC1305	5.0	Smit et al. 2014	30	3.1	MacGregor & Manton 1986	
VIC0101	5.5	Smit et al. 2014	37	3.1	MacGregor & Manton 1986	
VIC0107	5.8	Smit et al. 2014	41	2.2	MacGregor & Manton 1986	
VIC0201	5.6	Smit et al. 2014	47	3.3	MacGregor & Manton 1986	
VIC0302	5.8	Smit et al. 2014	54	2.6	MacGregor & Manton 1986	
VIC0506	5.4	Smit et al. 2014	BD1934	5.8	Jagoutz et al. 1984	
VIC0607	5.3	Smit et al. 2014	BD1191	3.8	Jagoutz et al. 1984	
VIC0707	5.5	Smit et al. 2014	BD1175	6.9	Jagoutz et al. 1984	
VIC1601	5.6	Smit et al. 2014	BD3699	6.9	Jagoutz et al. 1984	
4	8.0	MacGregor & Manton 1986	HRV272	6.1	Ongley et al. 1987	
4A	8.0	MacGregor & Manton 1986	HRV201	3.8	Ongley et al. 1987	
7	6.2	MacGregor & Manton 1986	HRV187	6.4	Ongley et al. 1987	
38	6.2	MacGregor & Manton 1986	RV-102	5.4	Ongley et al. 1987	
63	6.6	MacGregor & Manton 1986	HRV-93	7.0	Ongley et al. 1987	
			R-52	6.7	Ongley et al. 1987	
			R-19	6.8	Ongley et al. 1987	

Table B7. continued

Sample	$\delta^{18}\text{O}$	Reference			
HRV-15	5.9	Ongley et al. 1987	BD1175	6.0	Jacob et al. 2005
R-13	6.1	Ongley et al. 1987	BD3699	6.5	Jacob et al. 2005
R-11	7.1	Ongley et al. 1987	RV-1	6.8	Jacob et al. 2005
R-7	6.4	Ongley et al. 1987	DEJ-5	3.4	Jacob et al. 2005
RV(W)	6.9	Ongley et al. 1987	HRV-247	5.9	Jacob et al. 2005
SRV-1	5.0	Caporuscio 1990	RV07-1	6.7	Gréau et al. 2011
SRV-4	5.5	Caporuscio 1990	RV07-2	5.0	Gréau et al. 2011
XM-37	6.7	Caporuscio 1990	RV07-3	7.3	Gréau et al. 2011
13-64-1	5.9	Schulze et al. 2000	RV07-7	4.2	Gréau et al. 2011
13-64-3	6.1	Schulze et al. 2000	RV07-11	5.6	Gréau et al. 2011
13-64-6	5.9	Schulze et al. 2000	RV07-13	6.4	Gréau et al. 2011
13-64-100	5.3	Schulze et al. 2000	RV07-16	4.1	Gréau et al. 2011
13-64-103	5.9	Schulze et al. 2000	RV07-17	6.3	Gréau et al. 2011
13-64-104	5.9	Schulze et al. 2000	RV07-18	6.2	Gréau et al. 2011
13-64-107	5.6	Schulze et al. 2000	RV07-20	5.4	Gréau et al. 2011
13-64-109	5.7	Schulze et al. 2000	RV07-22	5.9	Gréau et al. 2011
13-64-121	6.0	Schulze et al. 2000	RV07-29a	5.3	Gréau et al. 2011
13-64-122	7.0	Schulze et al. 2000	RV07-9a	6.5	Gréau et al. 2011
13-64-125	5.9	Schulze et al. 2000	RV73-12	3.5	Gréau et al. 2011
13-64-133	6.8	Schulze et al. 2000	RV07-8	3.9	Gréau et al. 2011
13-64-136	6.3	Schulze et al. 2000	a15	7.8	Huang et al. 2013
13-64-137	6.1	Schulze et al. 2000	a4	7.8	Huang et al. 2013
13-64-138	6.7	Schulze et al. 2000	b1	7.5	Huang et al. 2013
BD1191	3.1	Jacob et al. 2005	b2	7.6	Huang et al. 2013
			b20	7.3	Huang et al. 2013
			b3	7.5	Huang et al. 2013

Table B7. continued

Sample	$\delta^{18}\text{O}$	Reference			
b4	7.7	Huang et al. 2013	e9-1	7.8	Huang et al. 2013
b5	7.4	Huang et al. 2013	f10	7.9	Huang et al. 2013
b6	7.8	Huang et al. 2013	f12	7.5	Huang et al. 2013
c10	8.0	Huang et al. 2013	f15	8.0	Huang et al. 2013
c12	7.9	Huang et al. 2013	f18	7.2	Huang et al. 2013
c13	7.8	Huang et al. 2013	f2	8.2	Huang et al. 2013
c14	7.7	Huang et al. 2013	f20	7.7	Huang et al. 2013
c15	7.7	Huang et al. 2013	f21	7.2	Huang et al. 2013
c16	7.4	Huang et al. 2013	f22	7.6	Huang et al. 2013
c25	7.7	Huang et al. 2013	f23	7.5	Huang et al. 2013
c8	7.9	Huang et al. 2013	f4	8.2	Huang et al. 2013
e10	7.8	Huang et al. 2013	f7	8.2	Huang et al. 2013
e11	7.8	Huang et al. 2013	f8	8.1	Huang et al. 2013
e13	7.8	Huang et al. 2013	g18	7.1	Huang et al. 2013
e14	7.9	Huang et al. 2013	g20	7.1	Huang et al. 2013
e16	7.7	Huang et al. 2013	g8	7.8	Huang et al. 2013
e18	7.1	Huang et al. 2013	h2	8.2	Huang et al. 2013
e2	8.1	Huang et al. 2013	h22	6.5	Huang et al. 2013
e20	7.2	Huang et al. 2013	h4	8.1	Huang et al. 2013
e3	7.8	Huang et al. 2013	h7	7.9	Huang et al. 2013
e4	7.5	Huang et al. 2013	a19	7.3	Huang et al. 2013
e5	7.7	Huang et al. 2013	a5	7.2	Huang et al. 2013
e6-2	7.6	Huang et al. 2013	b16	6.7	Huang et al. 2013
e7	7.7	Huang et al. 2013	b18	6.7	Huang et al. 2013
			b19	7.0	Huang et al. 2013
			c11	7.3	Huang et al. 2013

Table B7. continued

Sample	$\delta^{18}\text{O}$	Reference			
c26	7.0	Huang et al. 2013	a2	6.9	Huang et al. 2013
c28	6.8	Huang et al. 2013	a20	6.8	Huang et al. 2013
c29	7.4	Huang et al. 2013	a6	6.3	Huang et al. 2013
c30	6.8	Huang et al. 2013	a8	6.6	Huang et al. 2013
c34	6.9	Huang et al. 2013	f14	7.0	Huang et al. 2013
c7	7.1	Huang et al. 2013	f16	7.2	Huang et al. 2013
e19	7.0	Huang et al. 2013	f17	5.9	Huang et al. 2013
e8	7.5	Huang et al. 2013	f24	6.9	Huang et al. 2013
f13	7.1	Huang et al. 2013	f9	7.1	Huang et al. 2013
f3	7.6	Huang et al. 2013	a12	6.8	Huang et al. 2013
h1	7.5	Huang et al. 2013	a3	7.0	Huang et al. 2013
h10	6.6	Huang et al. 2013	a7	6.4	Huang et al. 2013
h17	7.0	Huang et al. 2013	a9	6.3	Huang et al. 2013
h19	6.4	Huang et al. 2013	c18	6.5	Huang et al. 2013
h21	6.6	Huang et al. 2013	c20	6.6	Huang et al. 2013
h3	7.8	Huang et al. 2013	c6	6.8	Huang et al. 2013
h6	8.1	Huang et al. 2013	d1	6.5	Huang et al. 2013
h9	7.6	Huang et al. 2013	d10	6.8	Huang et al. 2013
a1	6.7	Huang et al. 2013	d11	6.0	Huang et al. 2013
a11	6.6	Huang et al. 2013	d13	6.4	Huang et al. 2013
a13	6.9	Huang et al. 2013	d15	6.4	Huang et al. 2013
a14	6.7	Huang et al. 2013	d16	6.5	Huang et al. 2013
a17	6.7	Huang et al. 2013	d17	7.0	Huang et al. 2013
a18	6.6	Huang et al. 2013	d18	6.6	Huang et al. 2013
			d19	6.1	Huang et al. 2013
			d2	6.4	Huang et al. 2013

Table B7. continued

Sample	$\delta^{18}\text{O}$	Reference		
d20	6.3	Huang et al. 2013	g8	6.9 Huang et al. 2013
d3	6.5	Huang et al. 2013	g9	6.7 Huang et al. 2013
d4	6.3	Huang et al. 2013	h5	7.1 Huang et al. 2013
d5	6.7	Huang et al. 2013	RV07-03	6.0 Huang et al. 2016
d6	6.6	Huang et al. 2013	RV07-09	8.5 Huang et al. 2016
d7	6.5	Huang et al. 2013	RV07-13	8.0 Huang et al. 2016
d8	6.6	Huang et al. 2013	RV07-20	6.5 Huang et al. 2016
d9	6.8	Huang et al. 2013	RVF6	9.1 Huang et al. 2016
f11	6.6	Huang et al. 2013	RVF8	6.3 Huang et al. 2016
f19	5.9	Huang et al. 2013	RV07-07	6.7 Huang et al. 2016
f5	7.2	Huang et al. 2013	RV07-11	6.5 Huang et al. 2016
g1	5.9	Huang et al. 2013	RV07-14	6.2 Huang et al. 2016
g10	6.6	Huang et al. 2013	RV07-16	6.3 Huang et al. 2016
g11	6.6	Huang et al. 2013	RV07-18	6.1 Huang et al. 2016
g12	6.7	Huang et al. 2013	RV07-19	6.2 Huang et al. 2016
g13	6.6	Huang et al. 2013	RV07-22	8.3 Huang et al. 2016
g14	6.3	Huang et al. 2013	RV07-29	6.5 Huang et al. 2016
g15	6.6	Huang et al. 2013	RV07-08	2.9 Huang et al. 2016
g2	5.7	Huang et al. 2013	RV07-30	2.5 Huang et al. 2016
g3	5.9	Huang et al. 2013	RV07-31	2.8 Huang et al. 2016
g4	6.1	Huang et al. 2013	RV07-33	2.6 Huang et al. 2016
g5	5.9	Huang et al. 2013	RV07-34	2.3 Huang et al. 2016
g6	6.1	Huang et al. 2013	09RV09**	6.5 Huang et al. 2016
g7	6.4	Huang et al. 2013	SBB-2H	3.6 Caporuscio 1990
			SBB-3H	4.6 Caporuscio 1990
			SBB-7P	5.8 Caporuscio 1990

Table B7. continued

Sample	$\delta^{18}\text{O}$	Reference			
SBB-25	6.0	Caporuscio 1990	370	5.2	Viljoen et al. 2005
SBB-34	6.8	Caporuscio 1990	379	5.4	Viljoen et al. 2005
SBB-37	6.1	Caporuscio 1990	45	6.0	Viljoen et al. 2005
SBB-39	7.2	Caporuscio 1990	109	5.8	Viljoen et al. 2005
SBB-61	6.0	Caporuscio 1990	372	5.3	Viljoen et al. 2005
437-1	5.6	Neal et al., 1990	171	5.6	Viljoen et al. 2005
437-2	5.3	Neal et al., 1990	295	5.2	Viljoen et al. 2005
438-2	3.4	Neal et al., 1990	381	5.2	Viljoen et al. 2005
438-3	4.1	Neal et al., 1990	410	5.0	Viljoen et al. 2005
2791-21	2.8	Neal et al., 1990	412	5.5	Viljoen et al. 2005
437-5	3.9	Neal et al., 1990	413	4.8	Viljoen et al. 2005
437-7	4.4	Neal et al., 1990	415	5.2	Viljoen et al. 2005
2791-34	4.3	Neal et al., 1990	325	5.1	Viljoen et al. 2005
BE1	3.5	Shu et al. 2016	349	5.6	Viljoen et al. 2005
BE6	3.8	Shu et al. 2016	306	5.0	Viljoen et al. 2005
BE11	2.5	Shu et al. 2016	BE1	3.5	Viljoen et al. 2005
BE13	4.6	Shu et al. 2016	307	4.4	Viljoen et al. 2005
BBm	4.4	Shu et al. 2016	BE6	3.8	Jacob et al. 2009
BBs	4.6	Shu et al. 2016	BE11	2.5	Jacob et al. 2009
BBu	2.9	Shu et al. 2016	BE13	4.6	Jacob et al. 2009
BBw	4.5	Shu et al. 2016	BBm	4.4	Aulbach et al. 2017
JJG 546	2.8	Lowry et al. 1999	BBs	4.6	Aulbach et al. 2017
JJG 1146	3.4	Lowry et al. 1999	BBu	2.9	Aulbach et al. 2017
369	4.9	Viljoen et al. 2005	BBw	4.5	Aulbach et al. 2017
			JJG 546	2.8	Aulbach et al. 2017
			JJG 1146	3.4	Aulbach et al. 2017
			369	4.9	Aulbach et al. 2017

Table B7. continued

Sample	$\delta^{18}\text{O}$	Reference	KEC 81-21	6.1	Barth et al., 2001
57	5.3	Aulbach et al. 2017	KEC 86-6	6.0	Barth et al., 2001
60	5.8	Aulbach et al. 2017	KEC 86-13	5.5	Barth et al., 2001
152	5.7	Aulbach et al. 2017	KEC 86-14	5.7	Barth et al., 2001
81	5.6	Aulbach et al. 2017	KEC 86-34	5.4	Barth et al., 2001
201	5.8	Aulbach et al. 2017	KEC 86-36	6.0	Barth et al., 2001
KE1	5.2	Schmickler et al., 2004	KEC 86-56	5.3	Barth et al., 2001
Z267	5.3	Schmickler et al., 2004	KEC 86-71A	4.9	Barth et al., 2001
Z469	5.5	Schmickler et al., 2004	K 91-2	5.7	Barth et al., 2001
Z291	5.2	Schmickler et al., 2004	K 91-4	4.7	Barth et al., 2001
Z257	5.4	Schmickler et al., 2004	K 91-7	5.4	Barth et al., 2001
Z239	5.5	Schmickler et al., 2004	K 91-11	4.9	Barth et al., 2001
JJG2104	6.4	Appleyard et al. 2007	K 91-13	5.5	Barth et al., 2001
CMA4	5.7	Appleyard et al. 2007	K 91-20	5.8	Barth et al., 2001
CMA14	5.8	Appleyard et al. 2007	K 91-22	6.1	Barth et al., 2001
Rtnf43.2	5.2	Appleyard et al. 2007	K 91-23	6.1	Barth et al., 2001
Rtnf55.1	5.2	Appleyard et al. 2007	K 91-58	6.8	Barth et al., 2001
KEC 80-A2	5.8	Barth et al., 2001	KEC 86-12	4.9	Barth et al., 2001
KEC 81-3	5.3	Barth et al., 2001	KEC 86-70	5.3	Barth et al., 2001
KEC 81-4	5.1	Barth et al., 2001	KEC 86-1	4.7	Barth et al., 2001
KEC 81-5	5.6	Barth et al., 2001	KEC 86-3	5.0	Barth et al., 2001
KEC 81-7	5.6	Barth et al., 2001	KEC 86-4	5.1	Barth et al., 2001
KEC 81-8	5.2	Barth et al., 2001	KEC 85-74B	5.4	Barth et al., 2001
KEC 81-10A	5.7	Barth et al., 2001	KEC 86-90	5.3	Barth et al. 2002
KEC 81-18	6.0	Barth et al., 2001	KEC 80-B1	5.7	Barth et al. 2002
			KEC 81-2	5.5	Barth et al. 2002

Table B7. continued

Sample	$\delta^{18}\text{O}$	Reference			
KEC 81-11	5.5	Barth et al. 2002	XM15	5.5	Deines et al., 1991
KEC 86-2	5.6	Barth et al. 2002	XM17	5.5	Deines et al., 1991
KEC 86-8	5.5	Barth et al. 2002	XM18	6.2	Deines et al., 1991
KEC 86-15	5.2	Barth et al. 2002	XM19	5.2	Deines et al., 1991
KEC 86-60	5.2	Barth et al. 2002	XM21	5.6	Deines et al., 1991
KEC 86-73A	5.7	Barth et al. 2002	XM22	6.1	Deines et al., 1991
KEC 86-90	5.3	Barth et al. 2002	XM23	5.8	Deines et al., 1991
KEC 86-107	5.4	Barth et al. 2002	XM25	6.2	Deines et al., 1991
K91-6	5.1	Barth et al. 2002	XM26	8.1	Deines et al., 1991
K91-10	5.2	Barth et al. 2002	XM27	6.0	Deines et al., 1991
K91-16	5.4	Barth et al. 2002	XM28	5.9	Deines et al., 1991
K91-46	5.5	Barth et al. 2002	XM29	6.2	Deines et al., 1991
KEC 86-19	4.8	Barth et al. 2002	XM30	9.2	Deines et al., 1991
XM3	7.9	Deines et al., 1991	XM31	6.5	Deines et al., 1991
XM4	6.4	Deines et al., 1991	XM32	6.3	Deines et al., 1991
XM5	5.9	Deines et al., 1991	XM33	6.1	Deines et al., 1991
XM6	6.2	Deines et al., 1991	XM34	5.8	Deines et al., 1991
XM7	6.1	Deines et al., 1991	JJG889	7.2	Deines et al., 1991
XM8	3.9	Deines et al., 1991	JJG890	5.0	Deines et al., 1991
XM9	5.7	Deines et al., 1991	JJG891	7.8	Deines et al., 1991
XM10	5.8	Deines et al., 1991	JJG892	6.6	Deines et al., 1991
XM11	5.9	Deines et al., 1991	JJG894	5.8	Deines et al., 1991
XM13	7.0	Deines et al., 1991	JJG895	4.7	Deines et al., 1991
XM14	6.8	Deines et al., 1991	XM3	7.9	Viljoen et al. 1996
			XM5	5.9	Viljoen et al. 1996
			XM23	5.8	Viljoen et al. 1996

Table B7. continued

Sample	$\delta^{18}\text{O}$	Reference			
XM26	8.1	Viljoen et al. 1996	793	6.7	Aulbach et al. 2017
XM31	6.5	Viljoen et al. 1996	798	5.3	Aulbach et al. 2017
JJG889	7.2	Viljoen et al. 1996	800	8.4	Aulbach et al. 2017
JJG891	7.8	Viljoen et al. 1996	OE10	5.3	Aulbach et al. 2017
Ec4	7.2	Viljoen et al. 1996	OE14	5.7	Aulbach et al. 2017
EcB	6.1	Viljoen et al. 1996	OE15	5.3	Aulbach et al. 2017
XM11	5.9	Viljoen et al. 1996	OE16	5.4	Aulbach et al. 2017
XM18	6.2	Viljoen et al. 1996	OE17	7.1	Aulbach et al. 2017
Ec8	5.8	Viljoen et al. 1996	OE18	7.0	Aulbach et al. 2017
Ec11	6.0	Viljoen et al. 1996	OE19	5.8	Aulbach et al. 2017
EcC	5.8	Viljoen et al. 1996	OE2	5.3	Aulbach et al. 2017
665	5.9	Aulbach et al. 2017	OE23	5.3	Aulbach et al. 2017
697	5.9	Aulbach et al. 2017	OE24	6.2	Aulbach et al. 2017
720	5.9	Aulbach et al. 2017	OE25	5.4	Aulbach et al. 2017
732	5.6	Aulbach et al. 2017	OE26	5.0	Aulbach et al. 2017
737	5.4	Aulbach et al. 2017	OE3	5.5	Aulbach et al. 2017
748	5.5	Aulbach et al. 2017	OE33	7.0	Aulbach et al. 2017
750	5.4	Aulbach et al. 2017	OE34	5.6	Aulbach et al. 2017
766	7.7	Aulbach et al. 2017	OE38	5.7	Aulbach et al. 2017
777	6.6	Aulbach et al. 2017	OE39	5.0	Aulbach et al. 2017
778	5.0	Aulbach et al. 2017	OE43	7.3	Aulbach et al. 2017
779	5.1	Aulbach et al. 2017	OE50	5.3	Aulbach et al. 2017
784	5.4	Aulbach et al. 2017	OE51	5.5	Aulbach et al. 2017
792	5.9	Aulbach et al. 2017	OE52	5.8	Aulbach et al. 2017
			OE54	5.4	Aulbach et al. 2017
			OE55	6.1	Aulbach et al. 2017

Table B7. continued

Sample	$\delta^{18}\text{O}$	Reference			
OE57	5.6	Aulbach et al. 2017	13-128-38	6.6	Schulze et al. 2003
OE59	5.5	Aulbach et al. 2017	13-128-39	9.3	Schulze et al. 2003
OE62	5.3	Aulbach et al. 2017	13-128-40	8.1	Schulze et al. 2003
OE63	5.5	Aulbach et al. 2017	13-128-45	6.4	Schulze et al. 2003
OE64	4.8	Aulbach et al. 2017	488585A	6.1	Tappe et al. 2011
OE65	5.6	Aulbach et al. 2017	488585C	6.4	Tappe et al. 2011
OE67	6.3	Aulbach et al. 2017	592572A	5.9	Tappe et al. 2011
OE7	7.0	Aulbach et al. 2017	592572F	6.3	Tappe et al. 2011
OE75	5.3	Aulbach et al. 2017	KL2-1	5.3	Dongre et al. 2015
OE8	5.0	Aulbach et al. 2017	KL2-4	6.5	Dongre et al. 2015
OE82	6.0	Aulbach et al. 2017	KL2-5	5.4	Dongre et al. 2015
OE83	5.6	Aulbach et al. 2017	KL2-7	n.m.	Dongre et al. 2015
OE86	5.4	Aulbach et al. 2017	KL2-8	5.5	Dongre et al. 2015
OE92	5.7	Aulbach et al. 2017	KL2-9	5.6	Dongre et al. 2015
13-128-1	6.4	Schulze et al. 2003	KL2-10	5.8	Dongre et al. 2015
13-128-2	5.7	Schulze et al. 2003	KL2-20	5.4	Dongre et al. 2015
13-128-3	5.3	Schulze et al. 2003	KL2-37	5.4	Dongre et al. 2015
13-128-4	6.1	Schulze et al. 2003	KL2-44	6.7	Dongre et al. 2015
13-128-5	5.7	Schulze et al. 2003	KL2-48	5.7	Dongre et al. 2015
13-128-6	5.6	Schulze et al. 2003	KL2-49	5.3	Dongre et al. 2015
13-128-19	5.2	Schulze et al. 2003	KL2-50	5.4	Dongre et al. 2015
13-128-24	7.0	Schulze et al. 2003	KL2-61	5.6	Dongre et al. 2015
13-128-27	6.3	Schulze et al. 2003	P3-25	5.5	Dongre et al. 2015
13-128-29	6.1	Schulze et al. 2003	KL2-2	6.3	Dongre et al. 2015
			KL2-24	7.8	Dongre et al. 2015
			KL2-33	7.4	Dongre et al. 2015

Table B7. continued

Sample	$\delta^{18}\text{O}$	Reference
KL2-36	7.3	Dongre et al. 2015
KL2-52	7.7	Dongre et al. 2015
KL2-54	7.6	Dongre et al. 2015
KL2-56	7.7	Dongre et al. 2015
KL2-57	7.5	Dongre et al. 2015
KL2-60	7.6	Dongre et al. 2015

Table B8. Source data for  $\delta^{18}\text{O}$  of eclogitic and majoritic garnet inclusions in diamonds

Sample	$\delta^{18}\text{O}$	$2\sigma$	Reference	
ColN-23	9.00	0.20	Burnham et al. 2015	dam08A
Ju5-119	9.30	0.80	Burnham et al. 2015	dam09
RC1-2	9.30	0.20	Burnham et al. 2015	dam10
ColN18-1	8.50	0.60	Burnham et al. 2015	dam11
ColN18-2	9.20	0.20	Burnham et al. 2015	dam12
ColN-10	7.50	0.20	Burnham et al. 2015	dam14
Ju5-82	11.80	0.80	Burnham et al. 2015	dam15
Ju5-83	11.30	0.20	Burnham et al. 2015	dam16
Ju5-32	9.70	0.40	Burnham et al. 2015	dam19A
JF-37A	9.32	0.37	Ickert et al. 2015	dam19B
JF-37B	9.72	0.37	Ickert et al. 2015	dam76
JF-09	10.00	0.37	Ickert et al. 2015	dam88
JF-01A	8.88	0.37	Ickert et al. 2015	7(1)
JF-01B	9.20	0.37	Ickert et al. 2015	7(7)
JF-58B	9.21	0.38	Ickert et al. 2015	7(11)
JF-44B	8.74	0.38	Ickert et al. 2015	12(2)
JF-42A	9.21	0.37	Ickert et al. 2015	12(4)
JF-39A	9.09	0.37	Ickert et al. 2015	12(5)
JF-55A	8.57	0.38	Ickert et al. 2015	12(6)
JF-22A	9.06	0.37	Ickert et al. 2015	12(7)
dam03	4.82	0.25	Ickert et al. 2013	7(2)
dam05	8.76	0.23	Ickert et al. 2013	7(4)
dam07	4.71	0.25	Ickert et al. 2013	a017b
				a018
				a034
				a052r

Table B8. continued

Sample	$\delta^{18}\text{O}$	2 $\sigma$	Reference				
a054r	7.20	0.2	Schulze et al. 2013	9_3	8.1	0.6	Zedgenizov et al. 2016
a059c	7.10	0.2	Schulze et al. 2013	MT-77	6.5	0.3	Zedgenizov et al. 2016
a068	7.40	0.2	Schulze et al. 2013	MT-141	6.7	0.3	Zedgenizov et al. 2016
a069c	7.70	0.2	Schulze et al. 2013	HI-136	7.7	0.3	Zedgenizov et al. 2016
a075c	7.30	0.2	Schulze et al. 2013	MT-63	7.1	0.3	Zedgenizov et al. 2016
a077c	7.50	0.3	Schulze et al. 2013	MT-120	7.6	0.8	Zedgenizov et al. 2016
a078	7.40	0.2	Schulze et al. 2013	MT-51	6.5	0.2	Zedgenizov et al. 2016
a111	6.00	0.6	Schulze et al. 2013	MT-119	8.5	0.3	Zedgenizov et al. 2016
a116	7.80	0.3	Schulze et al. 2013	MT-126	4.8	0.6	Zedgenizov et al. 2016
a121	7.50	0.2	Schulze et al. 2013				
a134	7.90	0.2	Schulze et al. 2013				
a136	7.00	0.2	Schulze et al. 2013				
a145	5.70	0.2	Schulze et al. 2013				
MT-136	7.2	0.5	Zedgenizov et al. 2016				
MT-78	6.6	0.4	Zedgenizov et al. 2016				
MT-124	5.9	0.2	Zedgenizov et al. 2016				
HI-44	5.7	0.1	Zedgenizov et al. 2016				
MT-130	6.4	0.3	Zedgenizov et al. 2016				
MT-103	6.7	0.3	Zedgenizov et al. 2016				
MT-158	7.4	0.6	Zedgenizov et al. 2016				
MT-59	7.1	0.3	Zedgenizov et al. 2016				
MT-157	9.6	0.6	Zedgenizov et al. 2016				
MT-58	7.5	0.2	Zedgenizov et al. 2016				
MT-138	8.1	0.3	Zedgenizov et al. 2016				

Table B9. Source data for  $\delta^{13}\text{C}$  and  $\delta^{15}\text{N}$  of eclogitic and superdeep diamonds.

Sample	$\delta^{13}\text{C}$	$\delta^{15}\text{N}$	Reference
S5304a	-10.91	-2.29	Bulbuc BSc Unpubl
S5304b	-4.47	-2.20	Bulbuc BSc Unpubl
S5309	-9.46	-2.11	Bulbuc BSc Unpubl
333	-5.64	-9.60	Cartigny et al. 1997
343	-5.41	-5.00	Cartigny et al. 1997
346	-4.31	-2.25	Cartigny et al. 1997
or011	-10.31	-1.85	Cartigny et al. 1997
028	-4.89	-1.40	Cartigny et al. 1997
351	-4.76	-1.25	Cartigny et al. 1997
or012	-6.78	-0.40	Cartigny et al. 1997
361	-4.84	0.05	Cartigny et al. 1997
or007	-17.97	0.30	Cartigny et al. 1997
349	-4.50	1.60	Cartigny et al. 1997
or010	-14.25	2.30	Cartigny et al. 1997
344	-5.34	4.05	Cartigny et al. 1997
or009	-6.35	4.40	Cartigny et al. 1997
545	-5.22	-6.15	Cartigny et al. 1997; Melton et al. 2013
468	-4.53	-5.25	Cartigny et al. 1997; Melton et al. 2013
G036	-2.12	-3.20	Cartigny et al. 1997; Melton et al. 2013
547	-5.46	-0.60	Cartigny et al. 1997; Melton et al. 2013
Nam020	-5.10	-8.50	Cartigny et al. 2004
Nam096	-3.74	-7.50	Cartigny et al. 2004
Nam081	-6.66	-2.70	Cartigny et al. 2004
Nam041	-6.89	-0.20	Cartigny et al. 2004
Nam011	-4.42	1.20	Cartigny et al. 2004
Nam035	-5.37	3.30	Cartigny et al. 2004
Nam114	-26.93	4.00	Cartigny et al. 2004
Nam056	-29.26	6.70	Cartigny et al. 2004
jw-010	-5.68	-8.50	Cartigny et al. 1998
jw-057	-8.61	-8.00	Cartigny et al. 1998
jw-050	-6.58	-7.60	Cartigny et al. 1998
jw-058	-7.79	-7.40	Cartigny et al. 1998
jw-051	-9.38	-6.70	Cartigny et al. 1998
jw-009	-5.65	-6.70	Cartigny et al. 1998
jw-004	-12.06	-6.30	Cartigny et al. 1998
jw-013	-12.24	-5.80	Cartigny et al. 1998
jw-003	-5.19	-5.80	Cartigny et al. 1998
jw-060	-10.92	-5.50	Cartigny et al. 1998
jw-049	-6.67	-5.50	Cartigny et al. 1998
jw-015	-10.83	-5.40	Cartigny et al. 1998
jw-048	-17.39	-5.30	Cartigny et al. 1998
jw-053	-4.96	-5.20	Cartigny et al. 1998
jw-008	-5.18	-4.80	Cartigny et al. 1998
jw-054	-6.41	-4.20	Cartigny et al. 1998
jw-005	-7.08	-2.90	Cartigny et al. 1998
jw-002	-15.20	-1.90	Cartigny et al. 1998

Table B9. continued

Sample	$\delta^{13}\text{C}$	$\delta^{15}\text{N}$	Reference	DP-16 (2)	-3.50	-4.87	Howell et al. 2020 Stachel (in prep)
jw-001	-21.13	-1.60	Cartigny et al. 1998	DP-3	-5.55	-0.60	Howell et al. 2020 Stachel (in prep)
PA-64	-5.10	-2.10	Cartigny et al. 2009	DP-4 "core"	-6.20	-0.66	Howell et al. 2020 Stachel (in prep)
PA-74	-4.37	-2.00	Cartigny et al. 2009	DP-4 "rim"	-5.75	-0.69	Howell et al. 2020 Stachel (in prep)
PA-73	-5.45	-1.70	Cartigny et al. 2009	DP-5	-6.32	-0.23	Howell et al. 2020 Stachel (in prep)
Aust046 "core"	-10.55	14.72	Howell et al. 2020 Stachel (in prep)	DP-6 "core"	-6.60	0.16	Howell et al. 2020 Stachel (in prep)
Aust046 "rim"	-10.06	7.87	Howell et al. 2020 Stachel (in prep)	DP-6 "middle"	-5.08	0.36	Howell et al. 2020 Stachel (in prep)
ddmi037 "rim"	-4.53	-4.57	Howell et al. 2020 Stachel (in prep)	DP-6 "rim"	-5.70	-1.37	Howell et al. 2020 Stachel (in prep)
ddmi078	-5.33	-4.98	Howell et al. 2020 Stachel (in prep)	DP-9	-5.72	-0.03	Howell et al. 2020 Stachel (in prep)
ddmi093	-5.19	-4.82	Howell et al. 2020 Stachel (in prep)	E20 "core"	-9.76	10.79	Howell et al. 2020 Stachel (in prep)
ddmi127	-5.26	-4.98	Howell et al. 2020 Stachel (in prep)	JWR1 core	-4.58	-1.46	Howell et al. 2020 Stachel (in prep)
ddmi186	-4.73	-13.14	Howell et al. 2020 Stachel (in prep)	JWR1 middle	-2.36	-4.98	Howell et al. 2020 Stachel (in prep)
ddmi196	-5.08	-4.84	Howell et al. 2020 Stachel (in prep)	JWR1 rim	-4.69	-8.52	Howell et al. 2020 Stachel (in prep)
ddmi205	-4.71	-5.15	Howell et al. 2020 Stachel (in prep)	JWR10	-4.97	-5.45	Howell et al. 2020 Stachel (in prep)
ddmi208	-4.54	6.03	Howell et al. 2020 Stachel (in prep)	JWR13 middle	-17.01	4.56	Howell et al. 2020 Stachel (in prep)
DP-13 "core"	-5.27	-0.02	Howell et al. 2020 Stachel (in prep)	JWR13 rim	-5.09	-6.73	Howell et al. 2020 Stachel (in prep)
DP-13 "rim"	-5.19	-1.59	Howell et al. 2020 Stachel (in prep)	JWR16	-5.41	-4.56	Howell et al. 2020 Stachel (in prep)
DP-16	-5.85	-4.00	Howell et al. 2020 Stachel (in prep)				

Table B9. continued

Sample	$\delta^{13}\text{C}$	$\delta^{15}\text{N}$	Reference	JWR3	-6.07	0.49	Howell et al. 2020; Stachel (in prep)
JWR19	-6.20	0.99	Howell et al. 2020; Stachel (in prep)	JWR3	-4.84	-7.10	Howell et al. 2020; Stachel (in prep)
JWR2	-5.49	-1.75	Howell et al. 2020; Stachel (in prep)	JWR6	-4.53	-3.80	Howell et al. 2020; Stachel (in prep)
JWR21 core	-5.84	-4.22	Howell et al. 2020; Stachel (in prep)	JWR6	-5.23	2.76	Howell et al. 2020; Stachel (in prep)
JWR21 middle	-6.33	-2.10	Howell et al. 2020; Stachel (in prep)	JWR6	-5.23	2.76	Howell et al. 2020; Stachel (in prep)
JWR21 rim	-4.81	-6.74	Howell et al. 2020; Stachel (in prep)	JWR7	-13.06	-2.29	Howell et al. 2020; Stachel (in prep)
JWR22 core	-7.33	7.41	Howell et al. 2020; Stachel (in prep)	JWR7	-4.97	-6.02	Howell et al. 2020; Stachel (in prep)
JWR22 middle	-3.83	-3.85	Howell et al. 2020; Stachel (in prep)	JWR9	-4.64	-	Howell et al. 2020; Stachel (in prep)
JWR22 rim	-5.11	-8.08	Howell et al. 2020; Stachel (in prep)	JWR9	-5.13	6.27	Howell et al. 2020; Stachel (in prep)
JWR24 (1)	-6.27	1.75	Howell et al. 2020; Stachel (in prep)	ORS-1	-6.19	9.30	Howell et al. 2020; Stachel (in prep)
JWR24 (2)	-6.23	-3.21	Howell et al. 2020; Stachel (in prep)	ORS-10	-6.06	-1.38	Howell et al. 2020; Stachel (in prep)
JWR24 (3)	-5.80	3.82	Howell et al. 2020; Stachel (in prep)	ORS-11 (1)	-7.63	1.66	Howell et al. 2020; Stachel (in prep)
JWR25	-5.23	-2.23	Howell et al. 2020; Stachel (in prep)	ORS-11 (2)	-7.84	-0.24	Howell et al. 2020; Stachel (in prep)
JWR26 core	-3.95	1.06	Howell et al. 2020; Stachel (in prep)	ORS-12	-4.93	-8.07	Howell et al. 2020; Stachel (in prep)
JWR26 rim	-5.23	-5.91	Howell et al. 2020; Stachel (in prep)	ORS-14	-12.11	1.77	Howell et al. 2020; Stachel (in prep)
JWR27 core	-5.33	-4.97	Howell et al. 2020; Stachel (in prep)	ORS-15 core	-11.92	8.18	Howell et al. 2020; Stachel (in prep)
JWR27 rim	-4.62	-1.57	Howell et al. 2020; Stachel (in prep)	ORS-15 middle	-11.56	-1.87	Howell et al. 2020; Stachel (in prep)

Table B9. continued

Sample	$\delta^{13}\text{C}$	$\delta^{15}\text{N}$	Reference				
ORS-15 rim	-5.05	-7.06	Howell et al. 2020; Stachel (in prep)	U25A	-17.48	1.04	Laiginhas 2008
ORS-16	-10.33	-6.82	Howell et al. 2020; Stachel (in prep)	U42A	-6.12	0.72	Laiginhas 2008
ORS-22 middle	-4.71	-0.10	Howell et al. 2020; Stachel (in prep)	U47A	-18.93	2.23	Laiginhas 2008
ORS-22 rim	-9.03	-2.06	Howell et al. 2020; Stachel (in prep)	U53A	-8.28	2.32	Laiginhas 2008
ORS-23 rim	-5.15	-3.46	Howell et al. 2020; Stachel (in prep)	U72F	-6.77	4.42	Laiginhas 2008
ORS-30B	-10.05	-6.43	Howell et al. 2020; Stachel (in prep)	U75D	-5.36	1.83	Laiginhas 2008
ORS-30C (1)	-10.02	-4.65	Howell et al. 2020; Stachel (in prep)	U81B	-4.24	-6.90	Laiginhas 2008
ORS-30C (2)	-6.52	0.64	Howell et al. 2020; Stachel (in prep)	kv1-1	-4.90	-5.70	Palot et al. 2009
ORS-30C (2)	-10.63	8.35	Howell et al. 2020; Stachel (in prep)	kv1-2	-5.20	-6.20	Palot et al. 2009
ORS-31B	-5.07	-3.36	Howell et al. 2020; Stachel (in prep)	kv1-3	-6.00	-8.20	Palot et al. 2009
ORS-31C	-4.93	-2.75	Howell et al. 2020; Stachel (in prep)	kv1-4	-5.10	-6.70	Palot et al. 2009
ORS-5 core	-9.47	-2.70	Howell et al. 2020; Stachel (in prep)	kv1-5	-5.20	-6.80	Palot et al. 2009
ORS-5 rim	-6.75	-3.50	Howell et al. 2020; Stachel (in prep)	kv1-6	-5.20	-5.10	Palot et al. 2009
ORS-9 core	-6.01	2.42	Howell et al. 2020; Stachel (in prep)	kv1-8	-5.50	-7.80	Palot et al. 2009
ORS-9 rim	-8.42	9.90	Howell et al. 2020; Stachel (in prep)	kv2-1	-5.20	-6.70	Palot et al. 2009
U15A	-11.91	-3.23	Laiginhas 2008	kv2-10	-5.20	-8.90	Palot et al. 2009
				kv2-2	-4.90	-5.80	Palot et al. 2009
				kv2-3	-5.60	-8.60	Palot et al. 2009
				kv2-4	-5.50	-7.00	Palot et al. 2009
				kv2-5	-5.10	-7.90	Palot et al. 2009
				kv2-6	-5.20	-6.40	Palot et al. 2009
				kv2-8	-5.30	-6.30	Palot et al. 2009
				kv2-9	-5.00	-7.20	Palot et al. 2009
				kv3-1	-5.00	-6.60	Palot et al. 2009
				kv3-10	-5.20	-6.70	Palot et al. 2009

Table B9. continued

Sample	$\delta^{13}\text{C}$	$\delta^{15}\text{N}$	Reference	
kv3-2	-5.00	-6.20	Palot et al. 2009	KK80 -4.70 -7.00 Palot et al. 2012
kv3-3	-4.90	-6.20	Palot et al. 2009	KK-86 -4.80 -4.30 Palot et al. 2012
kv3-4	-5.30	-7.30	Palot et al. 2009	JW 01 -5.27 -2.61 Thomassot et al. 2009
kv3-5	-5.80	-8.10	Palot et al. 2009	JW 02 -5.56 -7.17 Thomassot et al. 2009
kv3-6	-5.10	-6.90	Palot et al. 2009	JW 03 -6.01 -5.44 Thomassot et al. 2009
kv3-8	-5.60	-6.70	Palot et al. 2009	JW 04 -5.38 -5.47 Thomassot et al. 2009
kv3-9	-4.20	-7.30	Palot et al. 2009	JW 05 -4.73 -7.55 Thomassot et al. 2009
kv4-1	-5.10	-7.70	Palot et al. 2009	JW 06 -6.46 -0.81 Thomassot et al. 2009
kv4-2	-5.00	-6.60	Palot et al. 2009	JW 07 -5.57 -6.61 Thomassot et al. 2009
kv4-3	-5.30	-6.90	Palot et al. 2009	JW 08 -4.87 -7.56 Thomassot et al. 2009
kv4-4	-5.30	-7.00	Palot et al. 2009	JW 09 -5.00 -6.09 Thomassot et al. 2009
kv4-5	-5.50	-7.00	Palot et al. 2009	JW 10 -5.81 2.66 Thomassot et al. 2009
kv4-6	-4.70	-6.40	Palot et al. 2009	JW 11 -5.67 -5.91 Thomassot et al. 2009
kv4-7	-5.40	-5.40	Palot et al. 2009	JW 12 -5.45 -0.87 Thomassot et al. 2009
kv4-8	-5.50	-8.90	Palot et al. 2009	JW 13 -3.09 -5.52 Thomassot et al. 2009
kv4-9	-5.60	-4.10	Palot et al. 2009	JW 14 -5.67 -8.85 Thomassot et al. 2009
KK03	-4.80	-4.70	Palot et al. 2012	JW 15 -6.50 -3.96 Thomassot et al. 2009
KK04	-0.80	8.50	Palot et al. 2012	JW 16 -4.92 -6.23 Thomassot et al. 2009
KK40	-5.10	-0.30	Palot et al. 2012	JW 17 -5.78 -4.95 Thomassot et al. 2009
KK67	-9.20	7.80	Palot et al. 2012	JW 18 -5.77 -7.05 Thomassot et al. 2009
KK68	-	-4.10 10.40	Palot et al. 2012	
KK75	-4.80	- 11.20	Palot et al. 2012	
KK77	-2.00	0.60	Palot et al. 2012	

Table B9. continued

Sample	$\delta^{13}\text{C}$	$\delta^{15}\text{N}$	Reference	JW95 05	-5.40	-5.08	Thomassot et al. 2009
JW 19	-18.73	0.89	Thomassot et al. 2009	JW95 06	-5.50	-7.32	Thomassot et al. 2009
JW 20	-6.17	1.93	Thomassot et al. 2009	JW95 07	-4.77	-7.80	Thomassot et al. 2009
JW 21	-2.00	-6.64	Thomassot et al. 2009	JW95 08	-4.86	-4.45	Thomassot et al. 2009
JW94 01	-7.37	-0.39	Thomassot et al. 2009	JW95 09	-5.67	-4.79	Thomassot et al. 2009
JW94 02	-5.78	-0.59	Thomassot et al. 2009	JW95 10	-6.35	1.40	Thomassot et al. 2009
JW94 03	-4.50	-0.28	Thomassot et al. 2009	JW95 11	-4.51	-9.77	Thomassot et al. 2009
JW94 04	-3.73	-8.74	Thomassot et al. 2009	JW95 11-2	-4.94	-6.11	Thomassot et al. 2009
JW94 05	-4.84	-0.24	Thomassot et al. 2009	JW95 12	-5.58	-6.37	Thomassot et al. 2009
JW94 06	-4.50	-4.41	Thomassot et al. 2009	JW95 12-2	-5.87	-8.00	Thomassot et al. 2009
JW94 07-2	-4.62	-4.73	Thomassot et al. 2009	JW95 14	-7.57	-5.30	Thomassot et al. 2009
JW94 08	-8.36	0.73	Thomassot et al. 2009	JW95 15	-5.98	-7.31	Thomassot et al. 2009
JW94 09	-5.30	-4.71	Thomassot et al. 2009	JW95 16	-3.42	-2.60	Thomassot et al. 2009
JW94 09-2	-4.84	-8.66	Thomassot et al. 2009	JW95 18	-8.38	-6.54	Thomassot et al. 2009
JW95 01	-5.44	-6.62	Thomassot et al. 2009	JW95 19	-4.61	-5.01	Thomassot et al. 2009
JW95 02	-4.68	-9.53	Thomassot et al. 2009	JW95 20	-4.57	-10.05	Thomassot et al. 2009
JW95 03	-8.38	-3.21	Thomassot et al. 2009	JW95 21	-5.23	-9.19	Thomassot et al. 2009

Table B9. continued

Sample	$\delta^{13}\text{C}$	$\delta^{15}\text{N}$	Reference	KK-75	-4.80	-	Palot et al. 2012
JW95 22	-5.67	1.67	Thomassot et al. 2009	KK-77	-2.00	0.60	Palot et al. 2012
JW95 24	-5.89	-7.10	Thomassot et al. 2009	KK-80	-4.70	-7.00	Palot et al. 2012
kv3-2	-5.00	-6.20	Palot et al. 2009	KK-086	-4.80	-4.30	Palot et al. 2012
kv3-3	-4.90	-6.20	Palot et al. 2009	KK-086	-4.80	-4.30	Palot et al. 2012
kv3-4	-5.30	-7.30	Palot et al. 2009	JW 01	-5.27	-2.61	Thomassot et al. 2009
kv3-5	-5.80	-8.10	Palot et al. 2009	JW 02	-5.56	-7.17	Thomassot et al. 2009
kv3-6	-5.10	-6.90	Palot et al. 2009	JW 03	-6.01	-5.44	Thomassot et al. 2009
kv3-8	-5.60	-6.70	Palot et al. 2009	JW 04	-5.38	-5.47	Thomassot et al. 2009
kv3-9	-4.20	-7.30	Palot et al. 2009	JW 05	-4.73	-7.55	Thomassot et al. 2009
kv4-1	-5.10	-7.70	Palot et al. 2009	JW 06	-6.46	-0.81	Thomassot et al. 2009
kv4-2	-5.00	-6.60	Palot et al. 2009	JW 07	-5.57	-6.61	Thomassot et al. 2009
kv4-3	-5.30	-6.90	Palot et al. 2009	JW 08	-4.87	-7.56	Thomassot et al. 2009
kv4-4	-5.30	-7.00	Palot et al. 2009	JW 09	-5.00	-6.09	Thomassot et al. 2009
kv4-5	-5.50	-7.00	Palot et al. 2009	JW 10	-5.81	2.66	Thomassot et al. 2009
kv4-6	-4.70	-6.40	Palot et al. 2009	JW 11	-5.67	-5.91	Thomassot et al. 2009
kv4-7	-5.40	-5.40	Palot et al. 2009	JW 12	-5.45	-0.87	Thomassot et al. 2009
kv4-8	-5.50	-8.90	Palot et al. 2009	JW 13	-3.09	-5.52	Thomassot et al. 2009
kv4-9	-5.60	-4.10	Palot et al. 2009				
KK-03	-4.80	-4.70	Palot et al. 2012				
KK-04	-0.80	8.50	Palot et al. 2012				
KK-40	-5.10	-0.30	Palot et al. 2012				
KK-67	-9.20	7.80	Palot et al. 2012				
KK-68	-10.40	-4.10	Palot et al. 2012				

Table B9. continued

Sample	$\delta^{13}\text{C}$	$\delta^{15}\text{N}$	Reference	JW94 09	-5.30	-4.71	Thomassot et al. 2009
JW 14	-5.67	-8.85	Thomassot et al. 2009	JW94 09-2	-4.84	-8.66	Thomassot et al. 2009
JW 15	-6.50	-3.96	Thomassot et al. 2009	JW95 01	-5.44	-6.62	Thomassot et al. 2009
JW 16	-4.92	-6.23	Thomassot et al. 2009	JW95 02	-4.68	-9.53	Thomassot et al. 2009
JW 17	-5.78	-4.95	Thomassot et al. 2009	JW95 03	-8.38	-3.21	Thomassot et al. 2009
JW 18	-5.77	-7.05	Thomassot et al. 2009	JW95 05	-5.40	-5.08	Thomassot et al. 2009
JW 19	- 18.73	0.89	Thomassot et al. 2009	JW95 06	-5.50	-7.32	Thomassot et al. 2009
JW 20	-6.17	1.93	Thomassot et al. 2009	JW95 07	-4.77	-7.80	Thomassot et al. 2009
JW 21	-2.00	-6.64	Thomassot et al. 2009	JW95 08	-4.86	-4.45	Thomassot et al. 2009
JW94 01	-7.37	-0.39	Thomassot et al. 2009	JW95 09	-5.67	-4.79	Thomassot et al. 2009
JW94 02	-5.78	-0.59	Thomassot et al. 2009	JW95 10	-6.35	1.40	Thomassot et al. 2009
JW94 03	-4.50	-0.28	Thomassot et al. 2009	JW95 11	-4.51	-9.77	Thomassot et al. 2009
JW94 04	-3.73	-8.74	Thomassot et al. 2009	JW95 11-2	-4.94	-6.11	Thomassot et al. 2009
JW94 05	-4.84	-0.24	Thomassot et al. 2009	JW95 12	-5.58	-6.37	Thomassot et al. 2009
JW94 06	-4.50	-4.41	Thomassot et al. 2009	JW95 12-2	-5.87	-8.00	Thomassot et al. 2009
JW94 07-2	-4.62	-4.73	Thomassot et al. 2009	JW95 14	-7.57	-5.30	Thomassot et al. 2009
JW94 08	-8.36	0.73	Thomassot et al. 2009	JW95 15	-5.98	-7.31	Thomassot et al. 2009

Table B9. continued

Sample	$\delta^{13}\text{C}$	$\delta^{15}\text{N}$	Reference
JW95 16	-3.42	-2.60	Thomassot et al. 2009
JW95 18	-8.38	-6.54	Thomassot et al. 2009
JW95 19	-4.61	-5.01	Thomassot et al. 2009
JW95 20	-4.57	-10.05	Thomassot et al. 2009
JW95 21	-5.23	-9.19	Thomassot et al. 2009
JW95 22	-5.67	1.67	Thomassot et al. 2009
JW95 24	-5.89	-7.10	Thomassot et al. 2009
JW95 25	-4.95	-7.98	Thomassot et al. 2009
JW95 26	-6.98	8.26	Thomassot et al. 2009
B2K4-1	-5.65	-3.31	Xia 2018
B2K4-14	-5.47	-3.28	Xia 2018
B4WK2- 2	-16.85	0.99	Xia 2018
N2K4-5	-4.13	-3.55	Xia 2018
N2K4-8 core	-4.93	-3.35	Xia 2018
N2K4-8 rim	-4.90	-0.56	Xia 2018
N5K2-5	-6.53	-0.57	Xia 2018

## **Appendix C – Supplementary material for blue diamonds**

### **C1 Supplementary information**

#### **C1.1 Isotopic and spectroscopic zoning of blue diamonds**

Dislocation networks, which are ubiquitous in strained superdeep Type II diamonds (Smith et al. 2018), are visible in the panchromatic cathodoluminescence imaging (350-850 nm CL) of blue diamonds (Fig. C2). While most samples do not show any zoning in their CL emission, ten samples have broad zones of higher emission (NL247-2, -9, -10, -12, -14, -15, -16, -17, -21, -22). Secondary ion mass spectrometry (SIMS) analyses determined that the low emission areas are on average  $\sim 0.2$  ppm B, which falls within the previously reported 0.1 to 8 ppm B range for blue diamonds (Gaillou et al. 2012). Transects across the CL boundaries to zones of high emission, reveal lower concentrations (Fig. C2;  $\sim 0.02$  ppm B), suggesting that the sampled panchromatic wavelengths that are dominated by nitrogen emitters may be neutralized by high concentrations of boron acceptors (Collins and Williams, 1971).

The carbon isotope signatures of multiple spots on individual cuts are generally statistically identical to each other. This extreme  $\delta^{13}\text{C}$  consistency within sample, even across distinct zones of B abundance (Fig. C2), is in accordance with diffusive studies that suggest that carbon isotopic heterogeneity will be significantly relaxed at lower mantle temperatures (Koga et al. 2003).

#### **C1.2 Impact of laser window on trace element blank**

In order to identify the impact of the closed-cell laser ablation procedure on the background of

the blue diamond trace elemental analyses, silica glass windows that top the ablation cell were analyzed for their trace element composition. Three distinct experiments with concentrated 90% HNO<sub>3</sub>:10% HF were completed: 1) The polished faces of two windows were rinsed with 2 mL, 2) 300 μL was placed on the polished faces of four windows for 10-20 minutes, 3) three windows were fully submerged in 5 mL of the solution for 10-20 minutes. These digestions allowed for the sampling of contamination sourced from the polished face of the window, as well as from the rough, unpolished sides of the window. Following collection, the solution was dried down at 100 °C and taken up in 1 mL dilute nitric acid with a 2000 ppt Ir internal standard for 30 hours at 120 °C. Subsequent analyses of trace elements were completed on a Thermo Scientific Element XR2 ICPMS with an APEX-Q high-efficiency sample introduction system. A 3-minute wash was run between every sample. Concentrations were calibrated using a 6-point weighted regression lines derived from 25,000x, 50,000x, 100,000x, 250,000x, 500,000x and 1,000,0000x dilutions of a synthetic rock multi-element standard solution. We fully propagate uncertainty and use a 7σ limit of quantification (LOQ).

Except for cerium, which has a median concentration of 0.48 ppb, nearly all trace elements were below the limit of quantification for the six experiments that sampled the polished face of windows by a 10-20 min. soak or rinse. The windows that were fully submerged in the solution show measurable LREE concentrations, with an extensively scratched and damaged window having the highest elemental concentrations (20\_6; Table C6). The contamination of these window by LREE is likely due to the initial polishing of the window by a La-Ce slurry. Despite extensive acid cleaning prior to ablation, this contamination appears to persist, especially in the unpolished regions of the window. While no acid touches the window during the procedure for

trace elemental analyses of blue diamonds, we postulate that contamination of the sample from the window may occur during the energetic fragmentation of the diamond during ablation. In fact, the average Ce/La ratio of the unpolished face dissolution (Ce/La = 3.7) closely matches the Ce/La ratio of 5 of our blue diamond analyses (Ce/La = 3.0 to 4.7). Following the results of this study, we have excluded Ce and La measurements that appear to show this contaminant signal and suggest that positive Ce anomalies reported in other diamond analyses (Krebs et al. 2019; Timmerman et al. 2019) are treated with caution. Figure 4.2 excludes all Ce and La values for Juina and blue diamonds that have a Ce/La ~ 3.

## C2 Supplementary figures

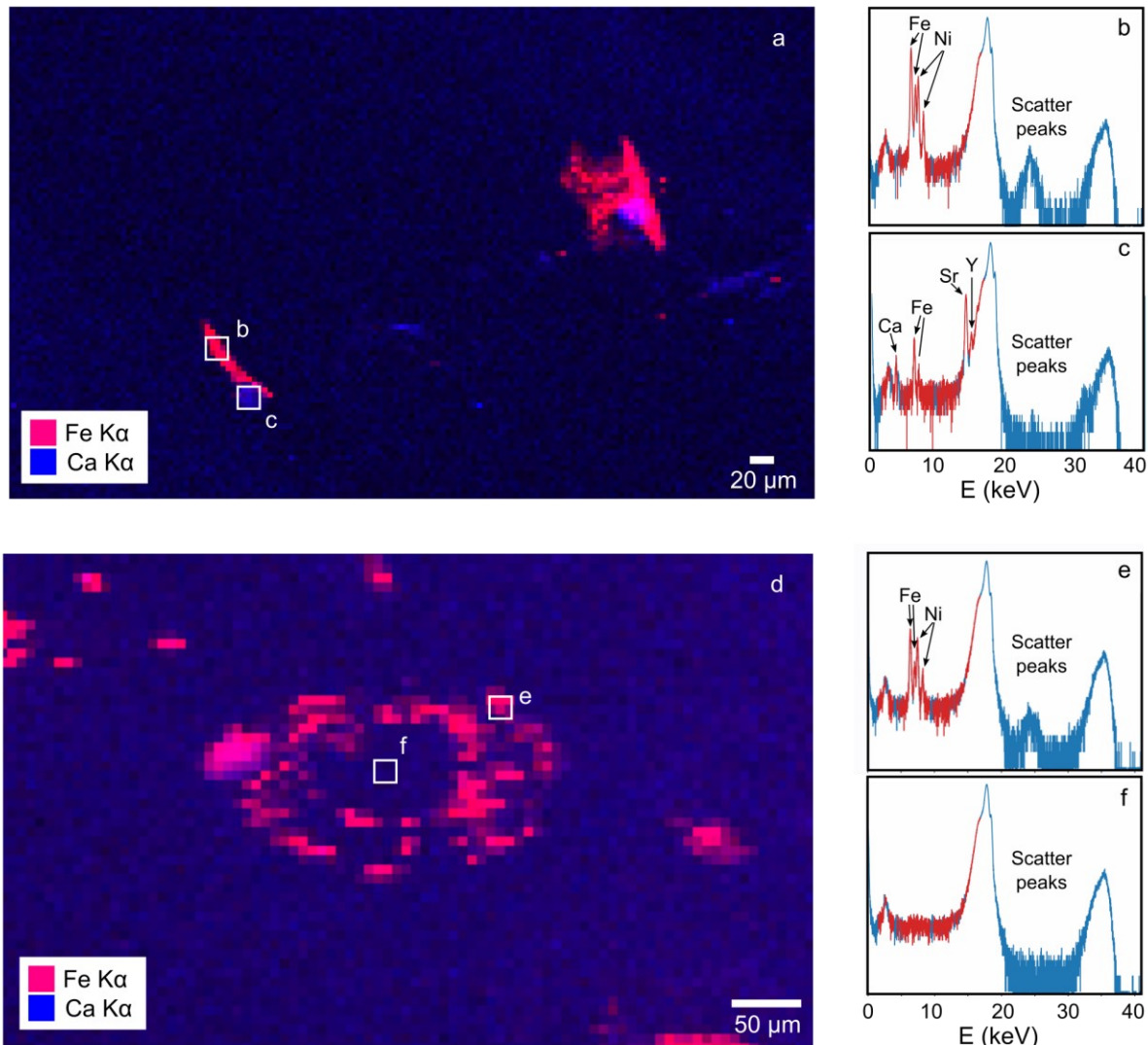


Figure C1.  $\mu$ XRF from GSECARS 13-IDE for diamonds Blue2 and NL247-2. (a) Image of Ca-silicate inclusion in diamond NL247-2 with Fe-Ni rich alloy rims. (b) Fe-Ni-rich rims around inclusion is visible in spectra. Peaks that are not identified are analytical background features due to Bremsstrahlung radiation and x-ray scattering. (c) Ca, Fe, Sr, and Y are visible in the spectra of the Ca-silicate inclusion. (d) Image of enstatite inclusion in Blue 2. The enstatite inclusion does not fluoresce, but it identifiable due to the Fe-Ni rich rim. (e) Fe and Ni peaks are visible around inclusion. (f) Enstatite inclusion shows no visible peaks in this range.

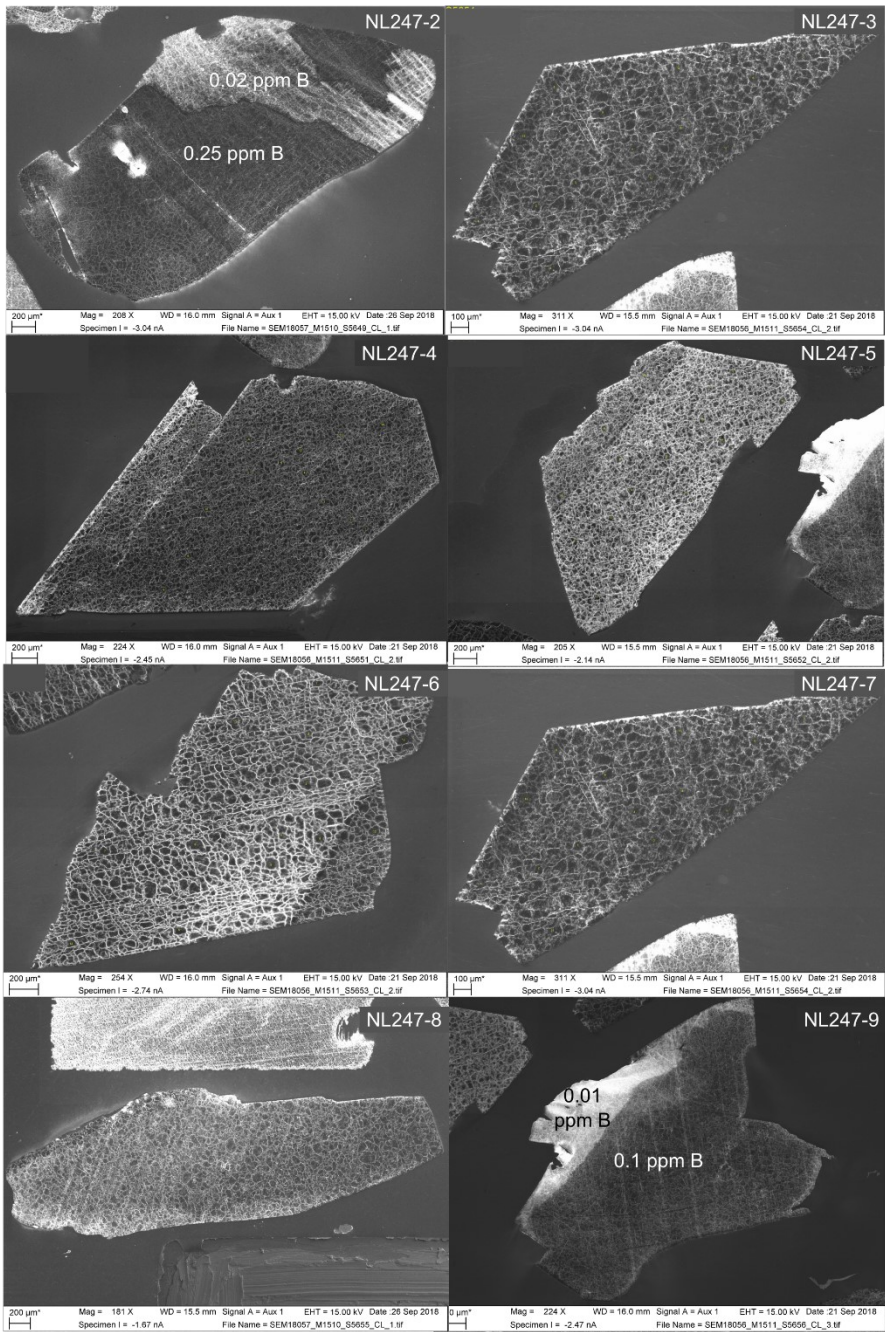


Figure C2. Panchromatic CL images of diamonds in study. CL emission of all diamonds in this study have dislocation networks that form after diamond deformation in the deep Earth. A few samples (NL247-2, NL247-9, NL247-14, NL247-15, NL247-16, NL247-17, NL247-21) show luminescence zoning that is inversely correlated with boron concentration. Where distinct zones are visible, boron concentrations are shown.

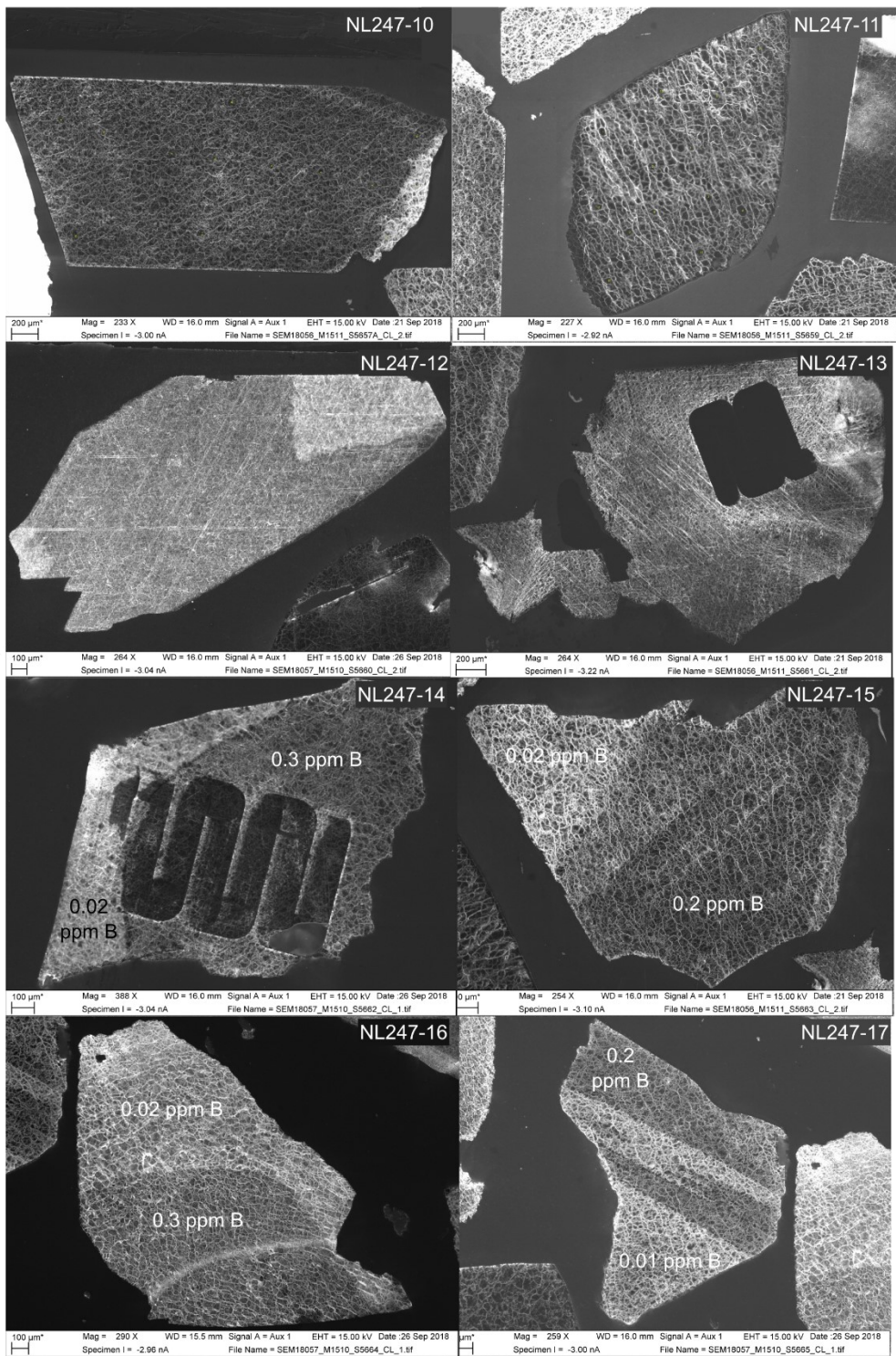


Figure C2. continued

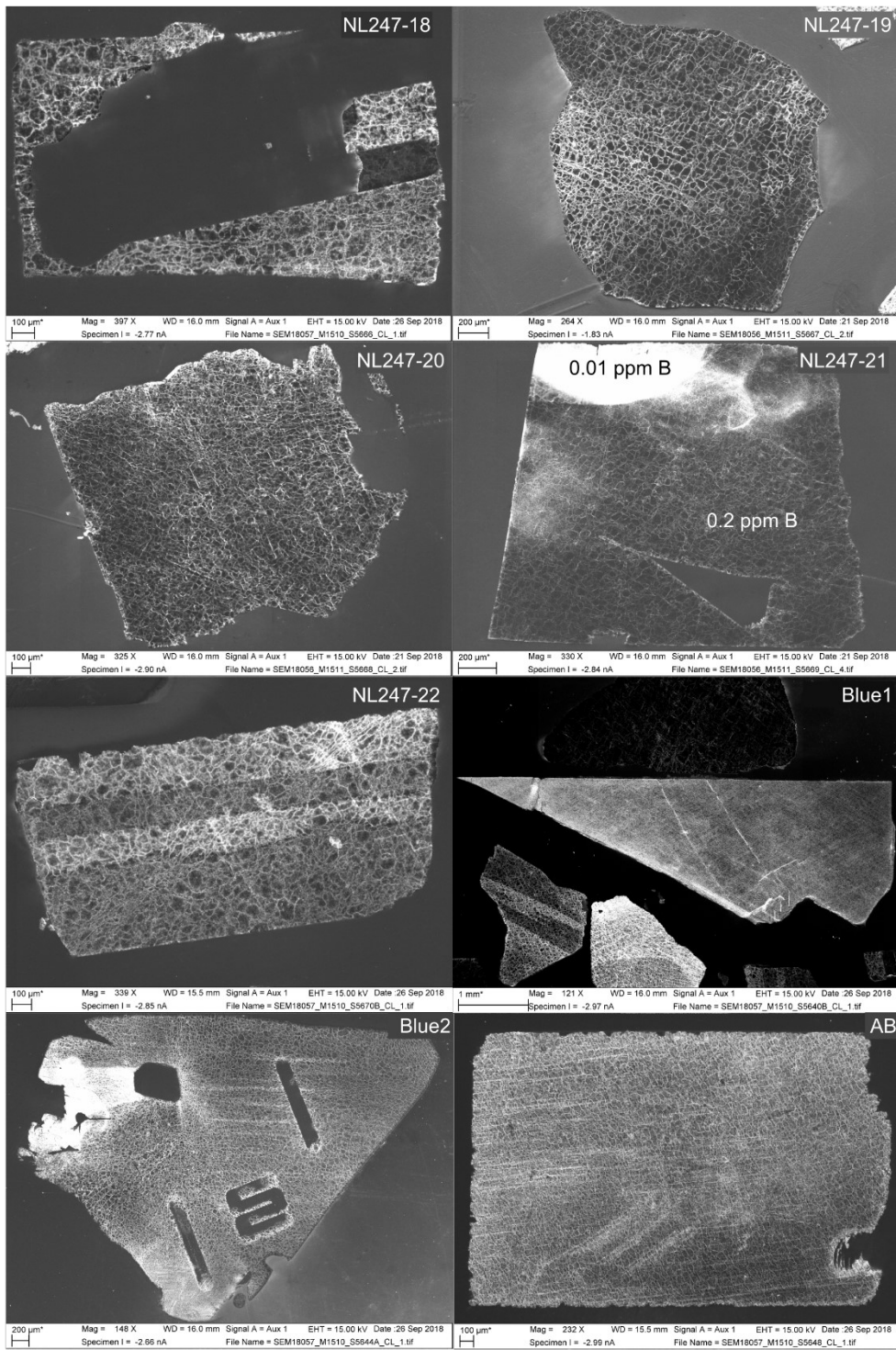


Figure C2. continued

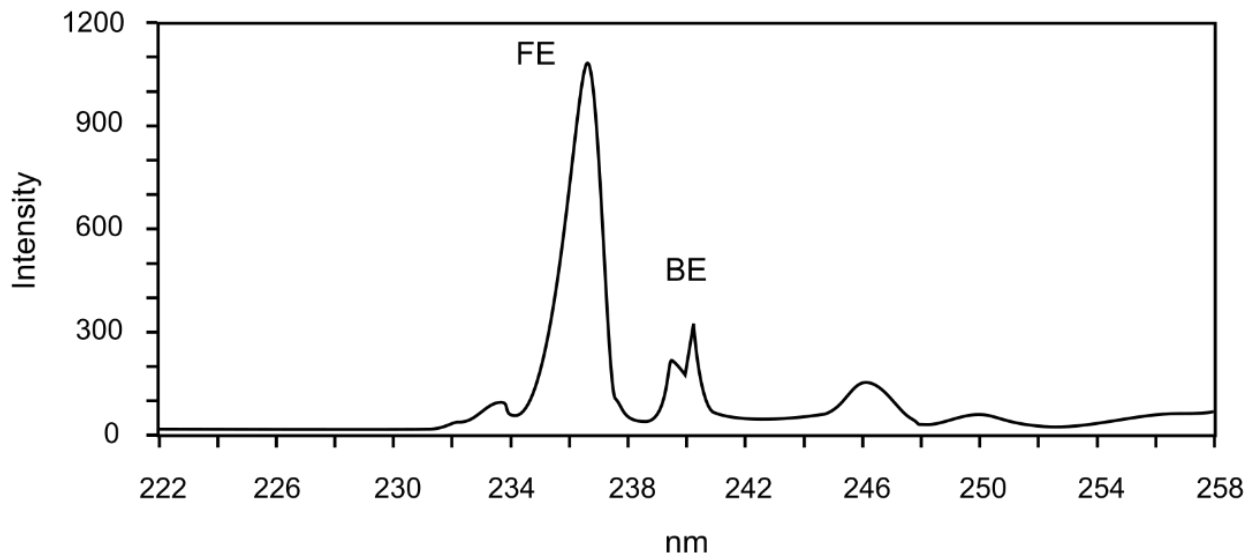


Figure C3. Hyperspectral CL spectra from NL247-20. The ratio between the neutral-boron bound exciton (BE) and the free-exciton (FE) intensities is proportional to boron concentration (Barjon et al. 2011). This sample was used to calibrate the ion probe analyses.

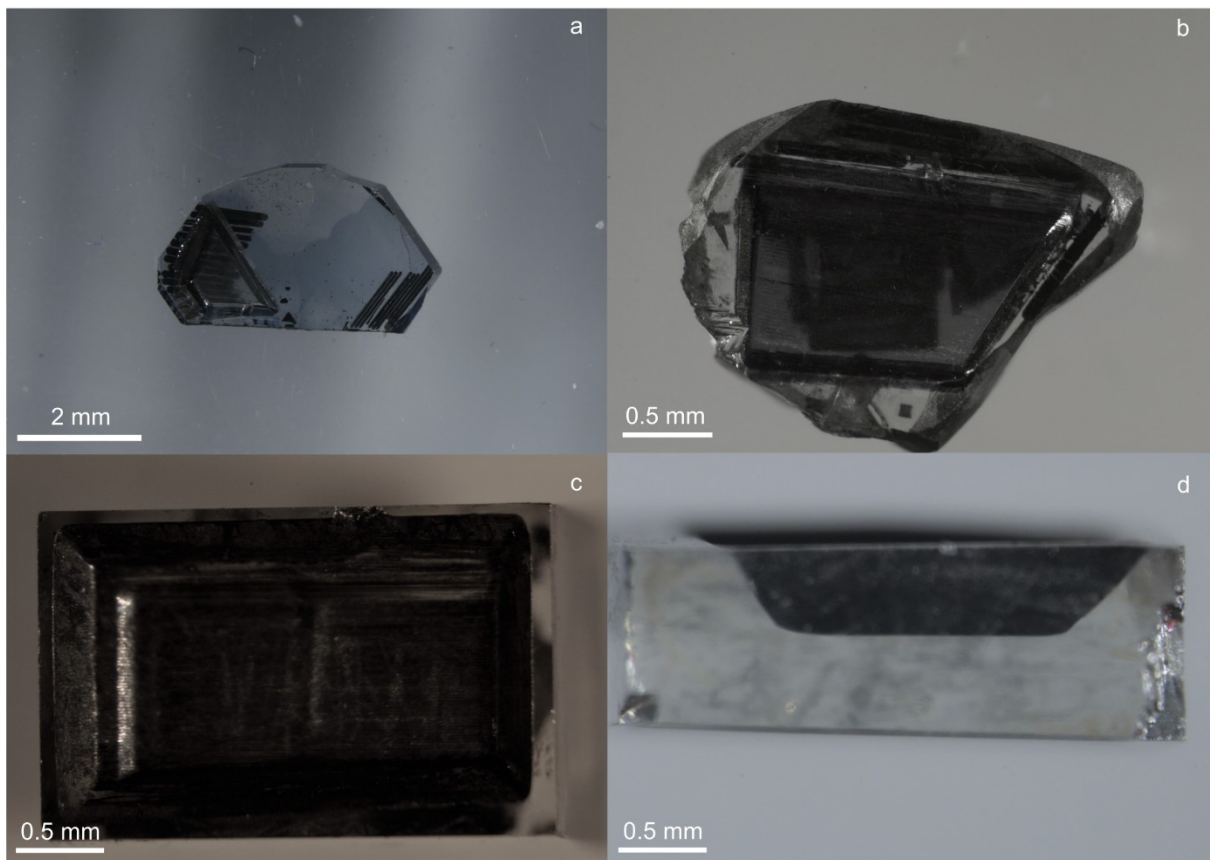


Figure C4. Typical ablation pits of diamonds (a) syn271, (b) Blue2, (c-d) AB. Ablation pit on left of syn271 is from this study, whereas the ablation lines on the back and right of the sample are from direct laser-ablation tests.

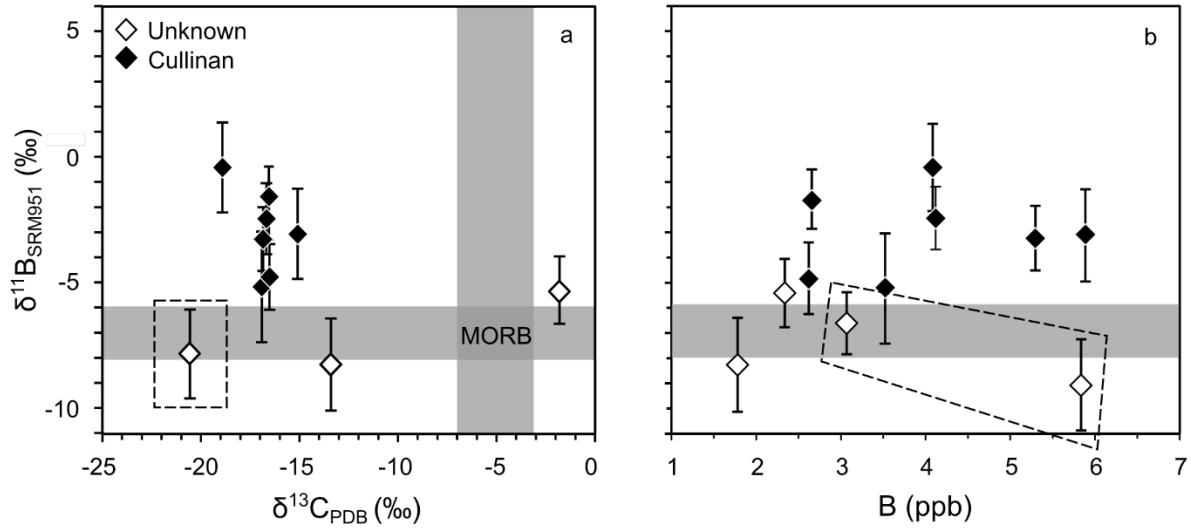


Figure C5. Boron and carbon isotope and concentration data for blue diamonds. (a)  $\delta^{11}\text{B}$  vs.  $\delta^{13}\text{C}$  of blue diamonds from Cullinan mine and those of uncertain origin. MORB is indicated in grey field (Marschall 2018), and an average of repeat analyses (AB) is indicated by checkered box. (b) Measured  $\delta^{11}\text{B}$  vs. the concentration of B in the solution. Repeat analyses on different sides of the same stone shown in checkered box.

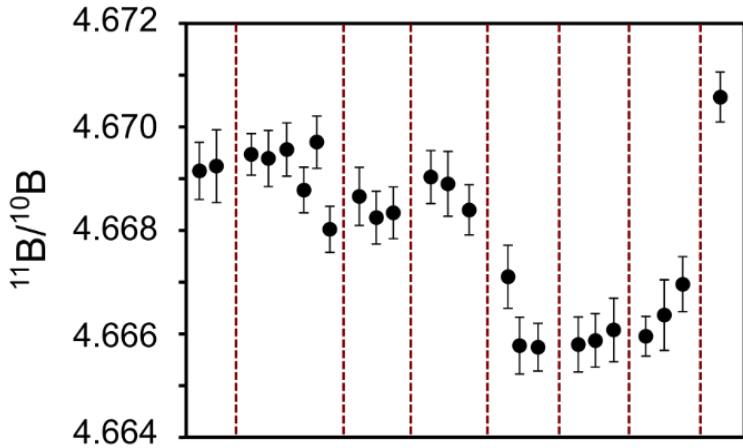


Figure C6.  $^{11}\text{B}/^{10}\text{B}$  measurements for a 50 ppb SRM 951 standard over a full day of analyses. Dotted red lines indicate sample measurements. Sample bracketing standard jumps are generally no greater than those between repeat analyses of SRM 951. The largest sample bracketing standard jump shown here is the last sample (0.75 ‰). The errors associated with these uncertainties is propagated into the total sample error.

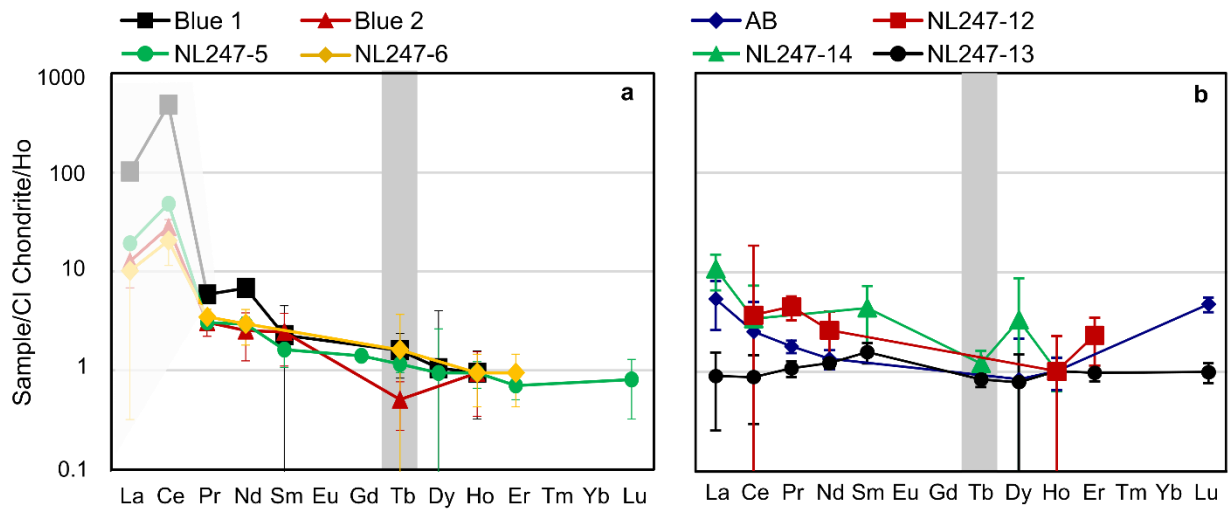


Figure C7. REE patterns for blue diamonds are split into two populations, those with Ce anomalies (**a**) and those with approximately flat slopes (**b**). La and Ce measurements in the first population are greyed out due to possible contamination. Measurements below limit of quantification ( $7\sigma$ ) are not plotted, but lines are interpolated.

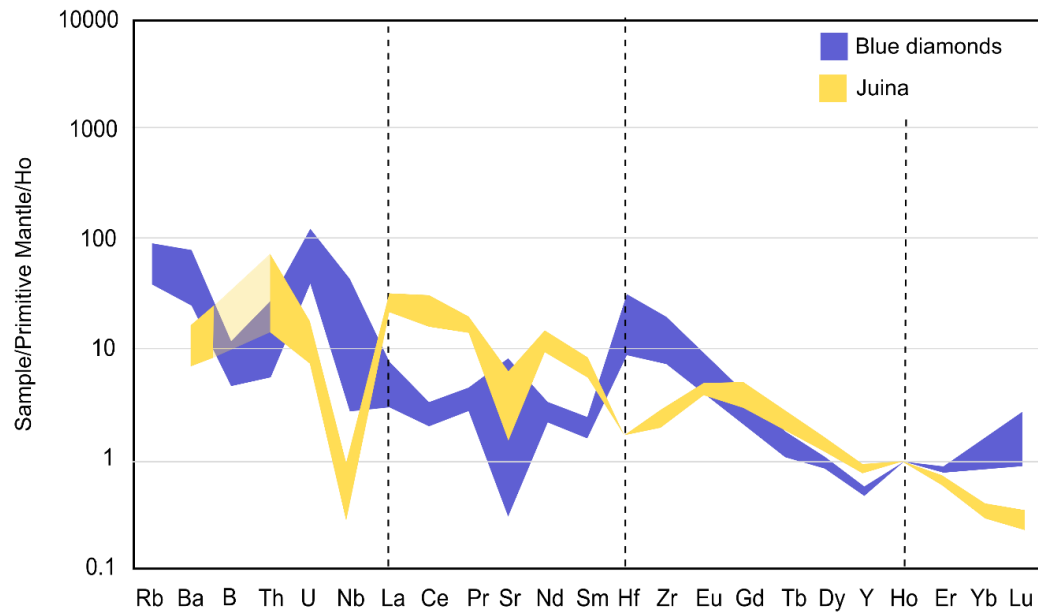


Figure C8. Trace element abundance of blue diamonds compared to those of Juina superdeep diamonds (Group III; Timmerman et al. 2019). All samples are normalized to primitive mantle and Ho (McDonough and Sun 1995). Dark colored fields indicate interquartile range. Lighter colors (e.g. B) are those not measured.

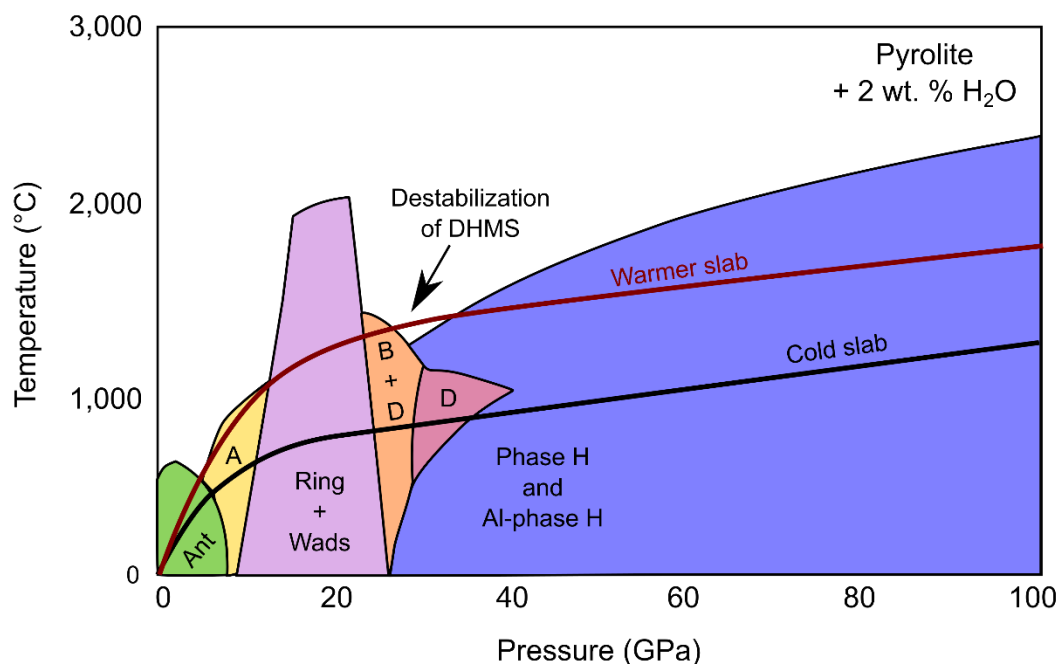


Figure C9. Stability of hydrous meta-peridotitic phases including antigorite (Ant), ringwoodite (Ring), wadsleyite (Wads), dense hydrous phases A, B, D, H, and aluminous phase H (Al-phase H). Overlaid on this phase diagram is the projection of a cold slab geotherm that would translate volatiles into the deep lower mantle and a warmer slab geotherm that would allow for DHMS destabilization in the uppermost lower mantle. Figure is modified from Nishi et al. (2014).

### C3 Supplementary tables

Table C1. Results for standards, including the biogenic standards (JCp-1 and JCt-1) and synthetic diamonds doped with iron borate - S107 and S271 (provided by David Fischer and DeBeers Group).

Sample	B (ppm)	Measured $\delta^{11}\text{B}$ (‰)	Known $\delta^{11}\text{B}$ (‰)	Type of sample	Comments
NIST 951	--	--	0	Certified reference (Gatanzaro et al. 1970)	
Jcp	47.7 (Farmer et al. 2016)	25.41 ± 0.20	24.30 (Farmer et al. 2016)	Coral ablation standard	$\delta^{11}\text{B}$ measured 09/2018
Jcp	47.7 (Farmer et al. 2016)	23.60 ± 0.20	24.30 (Farmer et al. 2016)	Coral ablation standard	$\delta^{11}\text{B}$ measured 09/2018
Jct	19.4 (Farmer et al. 2016)	18.55 ± 0.24	16.68 (Farmer et al. 2016)	Coral ablation standard	$\delta^{11}\text{B}$ measured 09/2018
s107	0.2-18.0	2.63 ± 0.28		Type IIb HPHT synthetic	$\delta^{11}\text{B}$ measured 10/2015
s107	0.2-18.0	2.83 ± 0.28		Type IIb HPHT synthetic	$\delta^{11}\text{B}$ measured 10/2015
s107	0.2-18.0	2.23 ± 0.29		Type IIb HPHT synthetic	$\delta^{11}\text{B}$ measured 11/2018
s107	0.2-18.0	2.57 ± 0.30		Type IIb HPHT synthetic	$\delta^{11}\text{B}$ measured 11/2018
s107	0.2-18.0	1.83 ± 0.13		Type IIb HPHT synthetic	$\delta^{11}\text{B}$ measured 09/2019
s107	0.2-18.0	3.73 ± 0.14		Type IIb HPHT synthetic	Measured 09/2019. Data rejected given extreme graphitization of sample
S271	0.2-18.0	2.72 ± 0.30		Type IIb HPHT synthetic	$\delta^{11}\text{B}$ measured 02/2020
S271	0.2-18.0	1.01 ± 0.39		Type IIb HPHT synthetic	Measured 02/2020. Data rejected – damp sample led to vapor phase during ablation.

The average  $\delta^{11}\text{B}$  of synthetic diamonds with and without rejected data are very similar ( $2.60 \pm 0.75$  ‰ and  $2.60 \pm 0.30$  ‰, respectively, for 2 sigma standard errors).

Table C2. Results on natural blue diamonds. Nitrogen and  $\delta^{13}\text{C}$  are analyzed by SIMS, whereas boron concentration was measured by FTIR, SIMS, and hyperspectral CL. Errors for SIMS and CL are  $2\sigma$  standard deviation from multiple spots, whereas FTIR is only 1 spot per sample. Higher B concentrations obtained by FTIR analyses correlates with the finding that the Hall Effect calibration for FTIR may overestimate B content by up to a factor of 2 (Howell et al. 2019). Date of  $\delta^{11}\text{B}$  analysis by closed-cell ablation and ICP-MS is indicated  $\delta^{11}\text{B}$  value.

Sample	N (ppm)	B (ppm) by FTIR*	B (ppm) by SIMS	$\delta^{13}\text{C}$ (‰)	$\delta^{11}\text{B}$ (‰)	Comment
1102084 25476	n.a.	$0.7 \pm 0.06$	n.a.	-1.8 (Smith et al. 2018)	$-5.4 \pm 1.3$ (02/2020)	Ferropericlose, olivine, nyerereite inclusion (Smith et al. 2018). Unknown origin
DVBT	n.a.	$0.6 \pm 0.04$	n.a.	-13.4 (Smith et al. 2018)	$-8.23 \pm 1.8$ (02/2020)	Breyite inclusion (Smith et al. 2018). Unknown origin
AB_1	$3.6 \pm 3.3$	$0.5 \pm 0.04$	$0.3 \pm 0.2$	$-20.6 \pm 0.2$	$-9.24 \pm 2$ (11/2018)	Unknown origin. Ablation on ‘front’ side of cube
AB_3	$3.6 \pm 3.3$	$0.5 \pm 0.04$	$0.3 \pm 0.2$	$-20.6 \pm 0.2$	$-6.6 \pm 1.3$ (02/2020)	Unknown origin. Ablation of the ‘side’ of the cube
Blue1	<0.35	$0.1 \pm 0.01$	$0.1 \pm 0.02$	$-15.1 \pm 0.1$	$-3.1 \pm 1.8$ (09/2019)	Cullinan diamond
Blue2	<0.35	$0.4 \pm 0.03$	$0.2 \pm 0.1$ **	$-18.9 \pm 1.5$	$0.5 \pm 1.8$ (11/2018)	Enstatite and Ca-silicate inclusions with Fe-Ni rims. Cullinan diamond
NL247- 2	<0.35	$0.2 \pm 0.02$	$0.1 \pm 0.2$	$-15.6 \pm 0.2$	n.a.	Ca-silicate inclusions. Cullinan diamond

Table C2. Continued

Sample	N (ppm)	FTIR B (ppm) *	SIMS B (ppm)	$\delta^{13}\text{C}$ (‰)	$\delta^{11}\text{B}$ (‰), (analysis date)	Comment
NL247-3	<0.35	0.2 ± 0.02	0.2 ± 0.1	-16.9 ± 0.1	-3.2 ± 1.3 (09/2019)	Type IIb Cullinan
NL247-4	<0.5	0.3 ± 0.03	0.2 ± 0.04	-16.8 ± 0.1	n.a.	Type IIb Cullinan
NL247-5	<0.5	n.a.	0.1 ± 0.2	-16.8 ± 0.1	n.a.	Type IIb Cullinan
NL247-6	<0.5	n.a.	0.05 ± 0.1	-16.7 ± 0.1	n.a.	Type IIb Cullinan
NL247-7	<0.5	n.a.	0.2 ± 0.1	-16.5 ± 0.1	n.a.	Type IIb Cullinan
NL247-8	<0.35	0.4 ± 0.03	0.2 ± 0.1	-16.9 ± 0.1	-5.2 ± 2.2 (09/2019)	Type IIb Cullinan
NL247-9	<0.5	n.a.	0.1 ± 0.1	-14.6 ± 0.4	n.a.	Type IIb Cullinan
NL247-10	<0.5	0.3 ± 0.02	0.1 ± 0.1	-16.6 ± 0.2	-1.7 ± 1.3 (02/2020)	Type IIb Cullinan
NL247-11	<0.5	n.a.	0.1 ± 0.1	-15.3 ± 0.1	n.a.	Type IIb Cullinan
NL247-12	<0.35	0.3 ± 0.03	n.a.	-15.3 ± 0.1	n.a.	Type IIb Cullinan
NL247-13	<0.5	0.4 ± 0.04	0.2 ± 0.1	-16.8 ± 0.1	n.a.	Type IIb Cullinan

Table C2. Continued

Sample	N (ppm)	FTIR B (ppm) *	SIMS B (ppm)	$\delta^{13}\text{C}$ (‰)	$\delta^{11}\text{B}$ (‰), (analysis date)	Comment
NL247-14	n.a.	$0.5 \pm 0.04$	$0.1 \pm 0.2$	$-15.9 \pm 0.2$	n.a.	Type IIb Cullinan
NL247-15	<0.5	$0.4 \pm 0.03$	$0.1 \pm 0.2$	$-16.6 \pm 0.3$	$-2.4 \pm 1.3$ (02/2020)	Type IIb Cullinan
NL247-16	n.a.	n.a.	$0.1 \pm 0.3$	$-16.8 \pm 0.22$	n.a.	Type IIb Cullinan
NL247-17	<0.35	n.a.	$0.1 \pm 0.2$	$-16.9 \pm 0.2$	n.a.	Type IIb Cullinan
NL247-18	n.a.	$0.4 \pm 0.03$	n.a.	$-16.4 \pm 0.2$	n.a.	Type IIb Cullinan
NL247-19	<0.5	$0.5 \pm 0.04$	$0.2 \pm 0.2$	$-16.5 \pm 0.2$	$-4.8 \pm 1.5$ (02/2020)	Type IIb Cullinan
NL247-20	<0.5	n.a.	$0.2 \pm 0.01$ **	$-15.7 \pm 0.2$	n.a.	Type IIb Cullinan
NL247-21	<0.5	n.a.	$0.2 \pm 0.2$	$-16.5 \pm 0.1$	n.a.	Type IIb Cullinan
NL247-22	n.a.	n.a.	n.a.	$-16.4 \pm 0.2$	n.a.	Type IIb Cullinan
NL247-23	$660 \pm 220$	n.a.	$0.002 \pm 0.006$	$-4.7 \pm 1.06$	n.a.	Type I Cullinan

\* FTIR data processing utilized the spreadsheet provided by Howell et al. (2019) \*\* Hyperspectral CL-calibrated standard. Abbreviations - not analyzed (n.a.) and below detection limit (bdl).

Table C3. Electron probe analysis of recovered olivine inclusion from Blue 2a. TiO<sub>2</sub>, Al<sub>2</sub>O<sub>3</sub>, Cr<sub>2</sub>O<sub>3</sub>, Na<sub>2</sub>O, K<sub>2</sub>O were measured as below detection limit.

	<b>SiO<sub>2</sub></b>	<b>FeO</b>	<b>NiO</b>	<b>MnO</b>	<b>MgO</b>	<b>CaO</b>	<b>Total</b>	<b>Mg#</b>
Blue 2a olivine	41.05	6.75	0.45	0.09	50.74	0.01	99.10	93.0

Table C4. Trace element abundances determined for blue diamonds. The concentrations are in ppb and are normalized to the weight loss during ablation; <LOD indicates below limit of detection (blank + 3 $\sigma$ ), and red font indicates below limit of quantification (blank +7 $\sigma$ ).

	NL247-2	2 $\sigma$	NL247-5	2 $\sigma$	NL247-6	2 $\sigma$	NL247-12	2 $\sigma$
Cs	<LOD	<LOD	9.03	0.50	1.65	0.06	0.720	0.076
Rb	<LOD	<LOD	8.70	2.95	0.333	0.422	<LOD	<LOD
Pb	0.264	0.366	2.03	0.450	0.475	0.068	0.700	0.104
Ba	2.32	3.49	34.44	1.78	3.17	0.21	7.11	0.52
Th	0.0048	0.0380	0.826	0.178	0.013	0.041	0.005	0.025
U	0.0191	0.0266	0.0967	0.0389	0.0448	0.0134	0.091	0.292
Nb	<LOD	<LOD	0.247	0.510	0.151	0.080	0.129	0.099
K	<LOD	<LOD	5682	7913	<LOD	<LOD	<LOD	<LOD
La	0.062	0.315	4.889	0.761	0.054	0.104	<LOD	<LOD
Ce	<LOD	<LOD	31.763	2.383	0.280	0.245	0.042	0.333
Pr	0.0098	0.0235	0.303	0.0560	0.0072	0.00280	0.00771	0.0042
Sr	0.179	4.920	2.65	17.15	<LOD	<LOD	<LOD	<LOD
Nd	0.034	0.064	1.439	0.500	0.030	0.024	0.022	0.024
Sm	0.0112	0.0191	0.222	0.151	0.006	0.010	0.009	0.009
Hf	<LOD	<LOD	1.311	0.614	0.184	0.067	0.0490	0.0750
Eu	<LOD	<LOD	<LOD	<LOD	<LOD	<LOD	<LOD	<LOD
Tb	0.00128	0.00269	0.0449	0.0160	0.00130	0.00332	<LOD	<LOD
Dy	0.00786	0.00912	0.249	0.130	<LOD	<LOD	0.005	0.005
Ho	0.00156	0.00391	0.0554	0.0331	0.00080	0.00103	0.00102	0.00255
Er	<LOD	<LOD	0.121	0.068	0.004	0.004	0.007	0.007

Table C4. continued

	NL247-2	$2\sigma$	NL247-5	$2\sigma$	NL247-6	$2\sigma$	NL247-12	$2\sigma$
<b>Yb</b>	<LOD	<LOD	<LOD	<LOD	<LOD	<LOD	<LOD	<LOD
<b>Lu</b>	0.001	0.002	0.0214	0.0257	<LOD	<LOD	<LOD	<LOD
<b>Zr</b>	0.756	3.41	52.4	10.3	5.76	2.05	<LOD	<LOD
<b>V</b>	<LOD	<LOD	<LOD	<LOD	<LOD	<LOD	<LOD	<LOD
<b>Sc</b>	<LOD	<LOD	<LOD	<LOD	36.7	1.49	18.0	1.26
<b>Zn</b>	<LOD	<LOD	<LOD	<LOD	<LOD	<LOD	<LOD	<LOD
<b>Cu</b>	17.2	21.8	129	27.5	44.0	9.4	<LOD	<LOD
<b>Ti</b>	<LOD	<LOD	431	42.6	145	82.1	<LOD	<LOD
<b>Mn</b>	0.62	2.18	22.50	3.89	0.72	0.54	<LOD	<LOD
<b>Fe</b>	20.9	73.4	563.6	219.3	49.1	31.6	<LOD	<LOD
<b>Co</b>	<LOD	<LOD	3.68	0.90	0.08	0.09	<LOD	<LOD
<b>Mg</b>	<LOD	<LOD	9252.50	458.35	<LOD	<LOD	<LOD	<LOD
<b>Ni</b>	2.60	1.13	22.7	1.27	3.47	0.36	<LOD	<LOD
<b>Cr</b>	0.07	3.64	101.2	14.4	6.78	1.96	<LOD	<LOD
<b>Ce/ La<sub>N</sub></b>	<LOD	<LOD	2.51*	0.04	2.02*	1.38	<LOD	<LOD

Table C4. continued

	NL247-13	$2\sigma$	NL247-14	$2\sigma$	Blue 1	$2\sigma$	Blue 2	$2\sigma$
Cs	2.25	0.11	3.27	0.17	1.32	0.09	0.714	0.086
Rb	<LOD	<LOD	<LOD	<LOD	0.260	0.596	1.18	1.39
Pb	0.264	0.098	1.288	0.208	1.591	0.125	1.454	0.227
Ba	1.90	0.06	16.34	0.70	2.85	0.18	7.53	0.61
Th	0.081	0.037	0.130	0.063	0.024	0.029	0.133	0.063
U	0.0310	0.0077	0.0926	0.0229	0.0430	0.0340	0.0346	0.0160
Nb	0.437	0.206	0.144	0.254	0.803	0.114	0.040	0.242
K	<LOD	<LOD	728	3658	<LOD	<LOD	517	3787
La	0.117	0.167	0.425	0.331	1.20	0.19	0.371	0.340
Ce	0.294	0.388	0.349	0.789	14.617	0.794	2.126	0.818
Pr	0.0545	0.0197	0.341	0.034	0.0270	0.0088	0.0354	0.0198
Sr	<LOD	<LOD	38.7	8.2	<LOD	<LOD	<LOD	<LOD
Nd	0.303	0.067	1.704	0.349	0.154	0.033	0.143	0.145
Sm	0.109	0.051	0.093	0.123	0.0144	0.0284	0.0388	0.0424
Hf	0.0905	0.0921	0.113	0.186	0.254	0.087	0.121	0.198
Eu	<LOD	<LOD	<LOD	<LOD	<LOD	<LOD	<LOD	<LOD
Tb	0.0164	0.0054	0.00730	0.00492	0.00285	0.00272	0.00227	0.00232
Dy	0.105	0.027	0.135	0.065	0.013	0.011	0.018	0.011
Ho	0.0300	0.00847	0.00924	0.00691	0.00255	0.00336	0.00640	0.00813
Er	0.085	0.030	0.024	0.024	0.011	0.008	<LOD	<LOD
Yb	<LOD	<LOD	<LOD	<LOD	<LOD	<LOD	<LOD	<LOD

Table C4. Continued

	NL247-13	$2\sigma$	NL247-14	$2\sigma$	Blue 1	$2\sigma$	Blue 2	$2\sigma$
<b>Lu</b>	0.0132	0.0060	<LOD	<LOD	<LOD	<LOD	0.003	0.003
<b>Zr</b>	2.66	2.22	5.05	4.60	7.15	2.04	4.07	4.64
<b>V</b>	<LOD	<LOD	<LOD	<LOD	<LOD	<LOD	<LOD	<LOD
<b>Sc</b>	<LOD	<LOD	<LOD	<LOD	9.24	1.33	<LOD	<LOD
<b>Zn</b>	<LOD	<LOD	4945	1995	<LOD	<LOD	6811	2224
<b>Cu</b>	18.7	4.2	76.5	14.9	1240	227	30.1	7.6
<b>Ti</b>	1188	222	161	195	3199	250	164	43.3
<b>Mn</b>	1.06	0.85	8.79	1.76	7.25	0.97	8.72	2.17
<b>Fe</b>	311	51.8	414	104	177	45.5	791	117
<b>Co</b>	1.75	0.30	3.13	0.59	2.32	0.23	4.81	0.49
<b>Mg</b>	<LOD	<LOD	<LOD	<LOD	<LOD	<LOD	<LOD	<LOD
<b>Ni</b>	66.63	3.04	15.15	1.28	6.74	0.45	33.19	2.03
<b>Cr</b>	4.70	2.99	95.26	7.63	9.15	4.76	8.08	6.28
<b>Ce/La<sub>N</sub></b>	0.97	1.17	0.32	1.28	4.71*	0.03	2.21*	0.40

Table C4. continued

	<b>AB</b>	<b>2σ</b>
<b>Cs</b>	0.025	0.010
<b>Rb</b>	1.39	0.43
<b>Pb</b>	0.946	0.117
<b>Ba</b>	13.36	0.65
<b>Th</b>	0.0097	0.0167
<b>U</b>	0.0283	0.0052
<b>Nb</b>	0.782	0.187
<b>K</b>	4267	1010
<b>La</b>	0.087	0.089
<b>Ce</b>	0.105	0.208
<b>Pr</b>	0.0114	0.0033
<b>Sr</b>	0.106	2.109
<b>Nd</b>	0.042	0.018
<b>Sm</b>	<b>0.0058</b>	<b>0.0033</b>
<b>Hf</b>	0.0939	0.0493
<b>Eu</b>	<LOD	<LOD
<b>Tb</b>	0.0106	0.00320
<b>Dy</b>	0.014	0.006
<b>Ho</b>	0.00378	0.00266
<b>Er</b>	<b>0.012</b>	<b>0.012</b>
<b>Yb</b>	<LOD	<LOD

Table C4. Continued

	<b>AB</b>	<b>2σ</b>
<b>Lu</b>	0.00799	0.00268
<b>Zr</b>	3.22	1.27
<b>V</b>	<LOD	<LOD
<b>Sc</b>	<LOD	<LOD
<b>Zn</b>	108337	19488
<b>Cu</b>	263.0	48.2
<b>Ti</b>	66.1	35.5
<b>Mn</b>	1.43	0.47
<b>Fe</b>	201	28.8
<b>Co</b>	57.58	3.00
<b>Mg</b>	<LOD	<LOD
<b>Ni</b>	11.19	0.85
<b>Cr</b>	150.6	7.0
<b>Ce/LaN</b>	0.47	1.25

\* La and Ce measurements with chondrite-normalized Ce/La ratios ~ 3 are rejected due to likely contaminated by ablation window (see Table C6).

Table C5. Limit of quantification (LOQ) and limit of detection (LOD). Values are ppt in solution.

	<b>LOD (3σ)</b>	<b>LOQ (7σ)</b>
<b>Cs</b>	0.0369	0.0698
<b>Rb</b>	0.271	0.478
<b>Pb</b>	0.0733	0.154
<b>Ba</b>	0.00516	0.0103
<b>Th</b>	0.00279	0.00564
<b>U</b>	0.0150	0.0291
<b>Ta</b>	0.00935	0.0199
<b>Nb</b>	0.01454	0.02908
<b>K</b>	93.4	130.3
<b>Mo</b>	0.108	0.216
<b>La</b>	0.000188	0.000375
<b>Ce</b>	0.0246	0.0490
<b>Pr</b>	0.00269	0.00539
<b>Sr</b>	0.0853	0.169
<b>Nd</b>	0.0145	0.0291
<b>Sm</b>	0.0129	0.0260
<b>Hf</b>	0.0509	0.100
<b>Eu</b>	0.0250	0.0510
<b>Tb</b>	0.000852	0.00171
<b>Dy</b>	0.0102	0.0204
<b>Ho</b>	0.00144	0.00289
<b>Er</b>	0.0267	0.0540
<b>Yb</b>	0.00071	0.00143

Table C5. continued

	<b>LOD (3<math>\sigma</math>)</b>	<b>LOQ (7<math>\sigma</math>)</b>
<b>Lu</b>	0.00243	0.00487
<b>Zr</b>	0.268	0.532
<b>V</b>	1.18	2.31
<b>Ca</b>	7.36	14.8
<b>Sc</b>	0.513	1.08
<b>Zn</b>	224	289
<b>Cu</b>	0.521	1.31
<b>Ti</b>	0.637	1.27
<b>Mn</b>	0.318	0.657
<b>Fe</b>	8.47	17.3
<b>Co</b>	0.242	0.458
<b>Mg</b>	4513	7338
<b>Ni</b>	0.544	1.08
<b>Cr</b>	0.115	0.230

Table C6. Results of trace element analyses of silica glass ablation windows. <LOD indicates below limit of detection (blank + 3 $\sigma$ ) and red font indicates below limit of quantification (LOQ = blank + 7 $\sigma$ ).

	<b>TPB_1</b>	<b>TPB_2</b>	<b>TPB_3</b>	<b>Rinse_4</b>	<b>Rinse_7</b>	<b>10_1</b>	<b>10_2</b>
Window quality	n.a.	n.a.	n.a.	scratches	laser damage	no scratches	no scratches
Experimental details	blank	blank	blank	rinse of polished face	rinse of polished face	10 min soak of polished face	10 min soak of polished face
Sr (ppb)	<LOD	4.2	<LOD	<LOD	<LOD	<LOD	<LOD
2 $\sigma$ abs.	<LOD	11.5	<LOD	<LOD	<LOD	<LOD	<LOD
Zr (ppb)	5.75	<LOD	<LOD	<LOD	3.52	<LOD	<LOD
2 $\sigma$ abs.	6.06	<LOD	<LOD	<LOD	6.28	<LOD	<LOD
La (ppb)	<LOD	0.001	<LOD	0.052	<LOD	<LOD	<LOD
2 $\sigma$ abs.	<LOD	0.236	<LOD	0.211	<LOD	<LOD	<LOD
Ce (ppb)	0.458	<LOD	<LOD	0.719	0.357	0.594	0.203
2 $\sigma$ abs.	0.118	<LOD	<LOD	0.115	0.153	0.074	0.061
Pr (ppb)	0.0041	<LOD	<LOD	0.0013	0.0139	<LOD	<LOD
2 $\sigma$ abs.	0.0172	<LOD	<LOD	0.0184	0.0247	<LOD	<LOD
Eu (ppb)	<LOD	<LOD	<LOD	<LOD	<LOD	<LOD	<LOD
2 $\sigma$ abs.	<LOD	<LOD	<LOD	<LOD	<LOD	<LOD	<LOD
Ho (ppb)	0.00216	<LOD	<LOD	<LOD	<LOD	<LOD	<LOD
2 $\sigma$ abs.	0.00504	<LOD	<LOD	<LOD	<LOD	<LOD	<LOD
Er (ppb)	0.0140	<LOD	<LOD	<LOD	<LOD	<LOD	<LOD
2 $\sigma$ abs.	0.0147	<LOD	<LOD	<LOD	<LOD	<LOD	<LOD
Lu (ppb)	0.00154	<LOD	<LOD	<LOD	0.00015	<LOD	<LOD
2 $\sigma$ abs.	0.00202	<LOD	<LOD	<LOD	0.00193	<LOD	<LOD

Table C6. continued

	<b>TPB_1</b>	<b>TPB_2</b>	<b>TPB_3</b>	<b>Rinse_4</b>	<b>Rinse_7</b>	<b>10_1</b>	<b>10_2</b>
Hf (ppb)	0.258	<LOD	<LOD	<LOD	<LOD	<LOD	<LOD
$2\sigma$ abs.	0.201	<LOD	<LOD	<LOD	<LOD	<LOD	<LOD
CeN/LaN	<LOD	<LOD	<LOD	<LOD	<LOD	<LOD	<LOD

Table C6. continued

	20_1	20_2	10_3	10_5	20_6	Unpolished face median	Polished face median
Window quality	no scratches	no scratches	laser damage	no scratches	scratched & damaged		
Experimental details	20 min soak of polished face	20 min soak of polished face	10 min soak of unpolished face	10 min soak of unpolished face	20 min soak of unpolished face		
Sr (ppb)	<LOD	2.42	<LOD	<LOD	23.1	<LOQ	<LOQ
2σ abs.	<LOD	4.92	<LOD	<LOD	2.40	<LOQ	<LOQ
Zr (ppb)	<LOD	<LOD	<LOD	<LOD	20.7	<LOQ	<LOQ
2σ abs.	<LOD	<LOD	<LOD	<LOD	2.24	<LOQ	<LOQ
La (ppb)	0.013	0.024	0.283	0.312	1.40	0.312	<LOQ
2σ abs.	0.093	0.125	0.047	0.044	0.12	0.047	<LOQ
Ce (ppb)	1.24	0.292	2.68	4.86	7.52	4.86	0.476
2σ abs.	0.10	0.070	0.15	0.35	0.61	0.35	0.086
Pr (ppb)	0.00512	0.00754	0.00902	0.0294	0.220	0.0294	<LOQ
2σ abs.	0.00765	0.01136	0.00362	0.0047	0.018	0.0047	<LOQ
Eu (ppb)	<LOD	<LOD	<LOD	<LOD	0.0512	<LOQ	<LOQ
2σ abs.	<LOD	<LOD	<LOD	<LOD	0.0326	<LOQ	<LOQ
Ho (ppb)	0.00048	0.00172	<LOD	<LOD	0.0143	<LOQ	<LOQ
2σ abs.	0.00226	0.00229	<LOD	<LOD	0.0019	<LOQ	<LOQ
Er (ppb)	<LOD	<LOD	<LOD	0.00040	0.0421	<LOQ	<LOQ
2σ abs.	<LOD	<LOD	<LOD	0.00305	0.0043	<LOQ	<LOQ
Lu (ppb)	0.00066	<LOD	0.000107	0.000136	0.00703	<LOQ	<LOQ
2σ abs.	0.00102	<LOD	0.000470	0.000361	0.00152	<LOQ	<LOQ

Table C6. continued

	20_1	20_2	10_3	10_5	20_6	Unpolished face median	Polished face median
Hf (ppb)	<LOD	<LOD	<LOD	<LOD	0.584	<LOQ	<LOQ
2σ abs.	<LOD	<LOD	<LOD	<LOD	0.058	<LOQ	<LOQ
Ce/LaN	<LOD	<LOD	3.67	6.02	2.08	3.67	<LOQ

Table C7. Standards, analysing crystals and detection limits for EPMA analyses.

<b>Element</b>	<b>Standard</b>	<b>Detection Limit (wt.%)</b>
<b>Si <math>\kappa</math></b>	Fo90.5 from Harvard	0.015
<b>Ca <math>\kappa</math></b>	Diopside from Wakefield	0.012
<b>Na <math>\kappa</math></b>	Albite 131705 from Virgina	0.018
<b>Fe <math>\kappa</math></b>	Fayalite from Rockport, MA	0.012
<b>Mn <math>\kappa</math></b>	Navegadora spessartine	0.012
<b>K <math>\kappa</math></b>	KAlSi <sub>3</sub> O <sub>8</sub> sanidine, Itrongay	0.005
<b>Ti <math>\kappa</math></b>	Rutile from MTI	0.008
<b>Mg <math>\kappa</math></b>	Fo90.5 from Harvard	0.010
<b>Al <math>\kappa</math></b>	Frank Smith pyrope garnet	0.012
<b>Cr <math>\kappa</math></b>	Chromium oxide, Alfa Aesar	0.020
<b>V <math>\kappa</math></b>	Vanadium from Alfa Aesar	0.007
<b>Ni <math>\kappa</math></b>	Nickel from Alfa Aesar	0.013
<b>Zn <math>\kappa</math></b>	Gahnite H111989	0.018

Table C8. Source data for  $\delta^{11}\text{B}$  of uncontaminated OIB (Marschall 2018).

Sample	$\delta^{11}\text{B}$	Reference			
PL2RC01	-10.6	Chaussidon & Marty 1995	HW11-2	-4.3	Tanaka & Nakamura 2005
PL224-14	-9.8	Chaussidon & Marty 1995	HW30	-3.3	Tanaka & Nakamura 2005
PL224-32	-10.0	Chaussidon & Marty 1995	HW35	-3.4	Tanaka & Nakamura 2005
PL225-03	-8.2	Chaussidon & Marty 1995	HW34	-3.0	Tanaka & Nakamura 2005
PL229-03	-10.1	Chaussidon & Marty 1995	HW33	-3.1	Tanaka & Nakamura 2005
PL29-29	-6.6	Chaussidon & Marty 1995	HW32	-3.5	Tanaka & Nakamura 2005
PL214-8	-11.4	Chaussidon & Marty 1995	HW31	-3.8	Tanaka & Nakamura 2005
PL226-7	-10.6	Chaussidon & Marty 1995	WAF-2	-5.3	Tanaka & Nakamura 2005
SO8463-1	-11.1	Chaussidon & Marty 1995	KOL43	-5.0	Tanaka & Nakamura 2005
SO8463-2	-9.4	Chaussidon & Marty 1995	KOL48	-5.2	Tanaka & Nakamura 2005
SO8463-3	-11.6	Chaussidon & Marty 1995	K89-6	-5.2	Tanaka & Nakamura 2005
SO8463-4	-9.8	Chaussidon & Marty 1995	D7-1	-5.4	Tanaka & Nakamura 2005
SO4764-2	-9.0	Chaussidon & Marty 1995	S500-1	-5.4	Tanaka & Nakamura 2005
HW1	-4.0	Tanaka & Nakamura 2005	S500-5B	-4.5	Tanaka & Nakamura 2005
HW2	-3.9	Tanaka & Nakamura 2005	S500-9A	-5.0	Tanaka & Nakamura 2005
HW24	-3.7	Tanaka & Nakamura 2005	WAF-36	-5.9	Tanaka & Nakamura 2005
HW21	-4.1	Tanaka & Nakamura 2005	WAF-39	-5.0	Tanaka & Nakamura 2005
HW6	-3.7	Tanaka & Nakamura 2005	KOL14	-4.2	Tanaka & Nakamura 2005
HW22	-3.6	Tanaka & Nakamura 2005	MH-11	-1.8	Tanaka & Nakamura 2005
HW27	-4.2	Tanaka & Nakamura 2005	PM1	0.9	Tanaka & Nakamura 2005
HW7-3	-3.8	Tanaka & Nakamura 2005	PM7	-0.3	Tanaka & Nakamura 2005
HW29	-3.7	Tanaka & Nakamura 2005	LK1	-2.5	Tanaka & Nakamura 2005
HW9	-4.6	Tanaka & Nakamura 2005	LK2	-3.6	Tanaka & Nakamura 2005
			LK3	-2.8	Tanaka & Nakamura 2005
			LK4	-2.2	Tanaka & Nakamura 2005

Table C8. continued

Sample	$\delta^{11}\text{B}$	Reference	3027y6921	et al. 2019
37_LP-1017-MI03_x-613y-546	-10.0	Walowski et al. 2019	60_LP-1002-MI14_x-4908y4569	-10.6 Walowski et al. 2019
38_LP-1017-MI01_x3630y1028	-9.8	Walowski et al. 2019	61_LP-1002-MI17_x-4431y1075	-8.6 Walowski et al. 2019
39_LP-1017-MI09_x509y-2318	-13.7	Walowski et al. 2019	62_LP-1002-MI22_x-6434y4260	-12.4 Walowski et al. 2019
40_LP-1017-MI16_x618y-3576	-11.2	Walowski et al. 2019	34_LP_1002_MI201_x-230y316	-10.3 Walowski et al. 2019
44_LP-1017-MI20_x573y-5935	-6.7	Walowski et al. 2019	37_LP_1002_MI206_x-1719y-2689	-11.1 Walowski et al. 2019
61_LP-1017-MI04_x-2809y-542	-11.1	Walowski et al. 2019	40_LP_1002_MI207b_x-1846y-4540	-10.8 Walowski et al. 2019
60_LP-1017-MI01-02enc_x3199y844	-9.6	Walowski et al. 2019	41_LP_1002_MI210_x-3513y-3465	-11.3 Walowski et al. 2019
36_LP-1017_MI06a_x5642y-1881	-8.9	Walowski et al. 2019	39_LP_1006_06_x-102y-2314	-9.1 Walowski et al. 2019
37_LP-1017_MI06b_x5505y-1828	-11.3	Walowski et al. 2019	40_LP_1006_05_x748y-5345	-8.1 Walowski et al. 2019
38_LP-1017_MI13_x4613y-4383	-9.4	Walowski et al. 2019	48_LP_1006_05b_x671y-5918	-7.0 Walowski et al. 2019
39_LP-1017_MI_18_x-2003y-4520	-9.2	Walowski et al. 2019	50_LP_1006_07_x-1335y-3589	-8.4 Walowski et al. 2019
42_LP-1017_MI_01re_x3535y922	-7.5	Walowski et al. 2019	51_LP_1006_09_x-896y-6100	-8.5 Walowski et al. 2019
48_LP-1002-MI02_x58y5015	-9.1	Walowski et al. 2019	41_LP_1025_10_x-274y3102	-8.5 Walowski et al. 2019
54_LP-1002-MI09_x-2128y7402	-10.3	Walowski et al. 2019	57_LP_1025_01_x3570y1435	-12.0 Walowski et al. 2019
57_LP-1002_MI08_x-	-10.9	Walowski	61_LP_1025_05_x1608y5279	-9.0 Walowski et al. 2019
			63_LP_1025_08a_x-1784y6154	-10.9 Walowski et al. 2019

Table C8. continued

Sample	$\delta^{11}\text{B}$	Reference	69y3067	et al. 2019
67_LP_1025_13_x-1230y2799	-9.2	Walowski et al. 2019	39_LP_1025_MI305b_x3587y3595	-8.1 Walowski et al. 2019
68_LP_1025_11_x-3177y6163	-8.0	Walowski et al. 2019	40_LP_1025_MI306_x5728y1767	-10.6 Walowski et al. 2019
69_LP_1025_17_x-3815y193	-12.5	Walowski et al. 2019	5_RPC_01_x2584y761.ais	-6.6 Walowski et al. 2019
70_LP_1025_15_x-3748y2692	-13.3	Walowski et al. 2019	6_RPC_02_x3792y1069.ai	-7.0 Walowski et al. 2019
42_LP_1025_MI201_x-1429y2460	-13.5	Walowski et al. 2019	7_RPC_03_x5322y1068.ai	-7.7 Walowski et al. 2019
45_LP_1025_MI202_x-2510y3161	-9.1	Walowski et al. 2019	8_RPC_06_x-2354y1643@1.ais	-8.3 Walowski et al. 2019
46_LP_1025_MI208a_x-1190y3942	-7.9	Walowski et al. 2019	9_RPC_07_x-3618y1568@2.ais	-6.8 Walowski et al. 2019
47_LP_1025_MI208b_x-1188y4175	-10.6	Walowski et al. 2019	11_RPC_08_x-5283y1260@4.ais	-8.0 Walowski et al. 2019
48_LP_1025_MI203_x-4501y2610	-9.1	Walowski et al. 2019	12_RPC_15_x-5530y-1738@5.ais	-6.5 Walowski et al. 2019
50_LP_1025_MI209_x-1141y5944	-11.5	Walowski et al. 2019	13_RPC_16_x-4212y-1426@6.ais	-6.4 Walowski et al. 2019
51_LP_1025_MI209bre_x-1445y7320	-10.1	Walowski et al. 2019	14_RPC_19_x640y-2513@7.ais	-7.6 Walowski et al. 2019
52_LP_1025_MI210a_x-3022y6436	-9.2	Walowski et al. 2019	15_RPCC_20_x4138y-1955@8.ais	-6.5 Walowski et al. 2019
53_LP_1025_MI210b_x-4293y6524	-10.4	Walowski et al. 2019	19_RPC_23_1_x-2408y-4381.ais	-8.6 Walowski et al. 2019
35_LP_1025_MI301_x3599y-2183	-8.4	Walowski et al. 2019	20_RPC_24_x1747y-4042.ais	-5.8 Walowski et al. 2019
37_LP_1025_MI302_x3244y-785	-10.6	Walowski et al. 2019	21_RPC_27_x4613y-5850.ais	-8.0 Walowski et al. 2019
38_LP_1025_MI305a_x37	-7.7	Walowski	22_RPC_28_x1234y-6570.ais	-6.9 Walowski et al. 2019

Table C8. continued

<b>Sample</b>	<b><math>\delta^{11}\text{B}</math></b>	<b>Reference</b>
23_RPC_29_x-1723y-6534.ais	-7.8	Walowski et al. 2019
71_RPC_113_x-2753y5623	-10.5	Walowski et al. 2019
72_RPC_113_2_x-2413y5602	-8.9	Walowski et al. 2019
73_RPC_112_x-798y5927	-8.2	Walowski et al. 2019
74_RPC_112_2x-932y6177	-10.5	Walowski et al. 2019
75_RPC_108_x4267y302_5	-7.6	Walowski et al. 2019
77_RPC_107_x2364y383_6	-9.1	Walowski et al. 2019
78_RPC_111_x402y5472	-10.6	Walowski et al. 2019
23_RPC_29_x-1723y-6534.ais	-7.8	Walowski et al. 2019
71_RPC_113_x-2753y5623	-10.5	Walowski et al. 2019
72_RPC_113_2_x-2413y5602	-8.9	Walowski et al. 2019
73_RPC_112_x-798y5927	-8.2	Walowski et al. 2019
74_RPC_112_2x-932y6177	-10.5	Walowski et al. 2019
75_RPC_108_x4267y302_5	-7.6	Walowski et al. 2019
77_RPC_107_x2364y383_6	-9.1	Walowski et al. 2019
78_RPC_111_x402y5472	-10.6	Walowski et al. 2019

Table C9. Source data for  $\delta^{11}\text{B}$  of uncontaminated carbonatite.

<b>Sample</b>	<b><math>\delta^{11}\text{B}</math></b>	<b>Reference</b>
13-2	1.13	Hulett et al. 2016
AMD-003	4.80	Hulett et al. 2016
BMR 056	-3.06	Hulett et al. 2016
MC117	1.51	Hulett et al. 2016
TAN 213	1.24	Hulett et al. 2016
OKA 4A	-2.23	Hulett et al. 2016
OKA 4B	1.03	Hulett et al. 2016
OKA 206	1.45	Hulett et al. 2016
OKA 203	0.68	Hulett et al. 2016
OKA 109	-3.02	Hulett et al. 2016
OKA 153	-0.88	Hulett et al. 2016
13-19	-6.33	Hulett et al. 2016
13-6	1.47	Hulett et al. 2016
13-1	-5.24	Hulett et al. 2016
13-29	-0.27	Hulett et al. 2016
13-27	-7.95	Hulett et al. 2016
13-11	-5.98	Hulett et al. 2016
MB-3a	-3.33	Çimen et al. 2018
MB-3b	-6.65	Çimen et al. 2018
MB-4B	-6.26	Çimen et al. 2018
MB-6	2.82	Çimen et al. 2018
MB-7	-7.34	Çimen et al. 2018
MB-8	3.89	Çimen et al. 2018

FIR-W	-3.98	Çimen et al. 2019
FIR-K	-2.47	Çimen et al. 2019
GUM	-8.67	Çimen et al. 2019
HW-CR	-6.36	Çimen et al. 2019
FLX	-8.38	Çimen et al. 2019
FEN-1	-7.12	Çimen et al. 2019
FEN-2	-9.79	Çimen et al. 2019
CHP-LK	-8.48	Çimen et al. 2019

Table C10. Source data for  $\delta^{11}\text{B}$  of meta-sediments and meta-AOC.

Sample	$\delta^{11}\text{B}$	Reference		
meta-AOC	-2.7	Peacock and Hervig 1999	meta-sed	-8.9 Nakano & Nakamura 2001
meta-AOC	-6.7	Peacock and Hervig 1999	meta-sed	-10.3 Nakano & Nakamura 2001
meta-AOC	-7.0	Peacock and Hervig 1999	meta-sed	-10.9 Peacock and Hervig 1999
meta-AOC	-7.2	Peacock and Hervig 1999	meta-sed	-6.7 Peacock and Hervig 1999
meta-AOC	-6.1	Peacock and Hervig 1999	meta-sed	-8.09 Pabst et al. 2012
meta-AOC	-3.0	Peacock and Hervig 1999	meta-sed	2.24 Pabst et al. 2012
meta-AOC	-2.45	Pabst et al. 2012	meta-sed	-7.04 Pabst et al. 2012
meta-AOC	-15.56	Pabst et al. 2012	meta-sed	-5.94 Pabst et al. 2012
meta-AOC	-10.17	Pabst et al. 2012	meta-sed	-0.59 Pabst et al. 2012
meta-sed	-11.9	Nakano & Nakamura 2001	meta-sed	-2.01 Pabst et al. 2012
meta-sed	-11.9	Nakano & Nakamura 2001	meta-sed	-7.02 Pabst et al. 2012
meta-sed	-11.7	Nakano & Nakamura 2001	meta-sed	-1.36 Pabst et al. 2012
meta-sed	-11.6	Nakano & Nakamura 2001	meta-sed	-8.45 Pabst et al. 2012
meta-sed	-9.0	Nakano & Nakamura 2001	meta-sed	-3.99 Pabst et al. 2012
meta-sed	-11.2	Nakano & Nakamura 2001	meta-sed	-9.17 Pabst et al. 2012
meta-sed	-10.2	Nakano & Nakamura 2001	meta-sed	-8.59 Pabst et al. 2012
meta-sed	-8.8	Nakano & Nakamura 2001	meta-sed	-7.00 Pabst et al. 2012
meta-sed	-14.2	Nakano & Nakamura 2001	meta-sed	-8.66 Pabst et al. 2012
meta-sed	-13.4	Nakano & Nakamura 2001	meta-sed	-8.71 Pabst et al. 2012
meta-sed	-11.8	Nakano & Nakamura 2001	meta-sed	-7.55 Pabst et al. 2012
meta-sed	-12.7	Nakano & Nakamura 2001	meta-sed	-12.83 Pabst et al. 2012
meta-sed	-10.8	Nakano & Nakamura 2001	meta-sed	-7.04 Pabst et al. 2012
meta-sed	-10.4	Nakano & Nakamura 2001	meta-sed	-6.41 Pabst et al. 2012
			meta-sed	-7.69 Pabst et al. 2012
			meta-sed	0.09 Pabst et al. 2012

Table C10. continued

Sample	$\delta^{11}\text{B}$	Reference	meta-sed	-13.96	Pabst et al. 2012
meta-sed	2.44	Pabst et al. 2012	meta-sed	4.86	Pabst et al. 2012
meta-sed	-5.32	Pabst et al. 2012	meta-sed	-5.72	Pabst et al. 2012
meta-sed	-0.86	Pabst et al. 2012	meta-sed	-7.77	Pabst et al. 2012
meta-sed	0.72	Pabst et al. 2012	meta-sed	-5.43	Pabst et al. 2012
meta-sed	-4.35	Pabst et al. 2012	meta-sed	-6.54	Pabst et al. 2012
meta-sed	-5.81	Pabst et al. 2012	meta-sed	-2.61	Pabst et al. 2012
meta-sed	-3.23	Pabst et al. 2012	meta-sed	-6.01	Pabst et al. 2012
meta-sed	1.56	Pabst et al. 2012	meta-sed	-7.40	Pabst et al. 2012
meta-sed	-0.66	Pabst et al. 2012	meta-sed	-6.98	Pabst et al. 2012
meta-sed	1.97	Pabst et al. 2012	meta-sed	-5.19	Pabst et al. 2012
meta-sed	2.11	Pabst et al. 2012	meta-sed	-4.41	Pabst et al. 2012
meta-sed	-0.66	Pabst et al. 2012	meta-sed	-3.96	Pabst et al. 2012
meta-sed	-6.07	Pabst et al. 2012	meta-sed	-5.89	Pabst et al. 2012
meta-sed	-7.62	Pabst et al. 2012	meta-sed	-9.30	Pabst et al. 2012
meta-sed	7.88	Pabst et al. 2012	meta-sed	-3.81	Pabst et al. 2012
meta-sed	2.20	Pabst et al. 2012	meta-sed	-4.89	Pabst et al. 2012
meta-sed	2.11	Pabst et al. 2012	meta-sed	-3.52	Pabst et al. 2012
meta-sed	1.92	Pabst et al. 2012	meta-sed	-1.96	Pabst et al. 2012
meta-sed	2.04	Pabst et al. 2012	meta-sed	-6.91	Pabst et al. 2012
meta-sed	-3.62	Pabst et al. 2012	meta-sed	-0.94	Pabst et al. 2012
meta-sed	-4.93	Pabst et al. 2012			
meta-sed	-7.70	Pabst et al. 2012			
meta-sed	-12.78	Pabst et al. 2012			